

NASA TECHNICAL  
MEMORANDUM

NASA TM X-53579

February 20, 1967

NASA TM X-53579

|                   |                               |            |
|-------------------|-------------------------------|------------|
| FACILITY FORM 602 | <b>N67-31300</b>              | _____      |
|                   | (ACCESSION NUMBER)            | (THRU)     |
|                   | <u>295</u>                    | <u>1</u>   |
|                   | (PAGES)                       | (CODE)     |
|                   | <u>TMX-53579</u>              | <u>31</u>  |
|                   | (NASA CR OR TMX OR AD NUMBER) | (CATEGORY) |

REVIEW OF THERMAL RADIATION FROM LIQUID AND  
SOLID PROPELLANT ROCKET EXHAUSTS

By William C. Rochelle  
Aero-Astroynamics Laboratory

NASA

*George C. Marshall  
Space Flight Center,  
Huntsville, Alabama*

## REVIEW OF THERMAL RADIATION FROM LIQUID AND SOLID PROPELLANT ROCKET EXHAUSTS

By

William C. Rochelle \*

George C. Marshall Space Flight Center  
Huntsville, Alabama

### ABSTRACT

A comprehensive review of the general theory of thermal radiation from liquid and solid propellant rocket exhausts is presented. More than 600 references are discussed and almost 500 equations describe the details of gaseous radiation, radiation from carbon particles, and radiation from aluminum oxide ( $\text{Al}_2\text{O}_3$ ) particles. The equation of radiation transfer is derived in detail, and solutions include the effects of scattering (Mie and Rayleigh), as well as emission and absorption. The analyses of spectral line broadening and band models are presented for gaseous radiation, and formation and sizes of carbon and  $\text{Al}_2\text{O}_3$  particles are discussed for particle radiation. Numerous methods of predicting gas and particle emissivities and radiative heating are critically analyzed, and the most accurate methods currently available are discussed in detail. Although the application of the general theory is directed toward radiation from the exhausts of the Saturn H-1, F-1, J-2 and RL-10 liquid propellant engines (for base heating) and of the solid propellant ullage and retro motors (for stage-separation heating), the basic theory applies to radiation from the exhaust of any liquid propellant engine or solid propellant motor.

\* Captain, U. S. Army

NASA-GEORGE C. MARSHALL SPACE FLIGHT CENTER

---

TECHNICAL MEMORANDUM X-53579

---

REVIEW OF THERMAL RADIATION FROM LIQUID  
AND SOLID PROPELLANT ROCKET EXHAUSTS

By

William C. Rochelle<sup>\*</sup>

<sup>\*</sup> Captain, U. S. Army

AEROPHYSICS DIVISION  
AERO-ASTRODYNAMICS LABORATORY  
RESEARCH AND DEVELOPMENT OPERATIONS

## ACKNOWLEDGEMENTS

The author would like to express his appreciation to Dr. Richard C. Farmer, Chief of the Base Heating Section, R-AERO-ATB at NASA/MSFC, for suggesting and encouraging the writing of this review of thermal radiation. The contributions made by the many MSFC contractors to this report are gratefully acknowledged. In particular the assistance of and discussions with the personnel at Aeronutronic (Philco-Ford) are appreciated. The author wishes to thank Mr. Homer B. Wilson and R. M. Huffaker of the MSFC Thermal Environment Branch, R-AERO-AT, Drs. Robert Goulard and Richard Hoglund of Purdue University, Dr. Tom J. Love of Oklahoma University, and Dr. R. P. Bobco of Hughes Aircraft for reading the rough draft and making numerous suggestions. Thanks are also extended to Mrs. Sara Hightower and Irene Dolan of MSFC and Mrs. Joan Barnett of RCA for editing the manuscript and to Miss Wanda Hensley of RCA for typing the manuscript. Finally, the author would like to express his deepest appreciation to Mrs. Essie Haywood of Thermal Environment Branch for typing the entire rough draft and for preparing all of the illustrations.

## TABLE OF CONTENTS

|   | Page |
|---|------|
| LIST OF SYMBOLS. . . . .  | x    |
| SUMMARY . . . . .   | 1    |
| INTRODUCTION. . . . .   | 1    |
| EQUATION OF RADIATION TRANSFER. . . . .                           | 6    |
| Spectral Intensity of Radiation . . . . .                         | 6    |
| Absorption . . . . .  | 8    |
| Emission . . . . .  | 10   |
| Local Thermodynamic Equilibrium . . . . .                         | 11   |
| Scattering. . . . .   | 14   |
| Formulation of the Equation of Radiation Transfer . . . . .       | 18   |
| Solutions to the Equation of Radiation Transfer . . . . .         | 22   |
| 1. Use of Monochromatic Effective Absorption Coefficient. . . . . | 22   |
| 2. Purely Absorbing Medium . . . . .                              | 23   |
| 3. Purely Scattering Medium . . . . .                             | 25   |
| 4. Plane-Parallel Case. . . . .                                   | 26   |
| GASEOUS RADIATION. . . . .  | 28   |
| Radiation from an Accelerated Charge . . . . .                    | 29   |
| Shape and Broadening of Spectral Lines . . . . .                  | 34   |
| 1. Natural-Line Broadening . . . . .                              | 37   |
| 2. Doppler Broadening . . . . .                                   | 38   |
| 3. Pressure Broadening . . . . .                                  | 39   |
| a. Collision broadening . . . . .                                 | 40   |
| b. Stark broadening . . . . .                                     | 41   |
| c. Statistical theory . . . . .                                   | 45   |
| d. Impact theory . . . . .  | 47   |
| Band Models . . . . .   | 48   |
| 1. Single-Line Model . . . . .                                    | 50   |
| 2. Elsasser Model . . . . .                                       | 54   |
| 3. Statistical Model . . . . .                                    | 57   |
| 4. Random Elsasser Model . . . . .                                | 59   |
| 5. Quasi-Random Model . . . . .                                   | 61   |
| Methods of Predicting Gaseous Radiation from Rocket Exhausts. . . | 63   |
| 1. Total Emissivity Method . . . . .                              | 64   |
| 2. Apparent Emissivity and Mean Path Length Method . . . . .      | 65   |
| 3. Spectral Absorption Coefficient Methods . . . . .              | 70   |

TABLE OF CONTENTS (Cont'd)

|  | Page       |
|--|------------|
| a. Weak-line or exact absorption coefficient method. . . . .   | 71         |
| b. Statistical band model method with Curtis-Godson<br>approximation . . . . .   | 73         |
| c. Generalized method with modified Curtis-Godson<br>approximation . . . . .   | 76         |
| <b>RADIATION FROM CARBON PARTICLES. . . . .</b>  | <b>79</b>  |
| Formation of Carbon Particles in Luminous Flames. . . . .  | 83         |
| 1. The C <sub>2</sub> , Atomic Carbon, and C <sub>3</sub> Condensation Theories. . . . .   | 85         |
| 2. The Hydrocarbon Polymerization-Condensation Theory. . . . .   | 86         |
| 3. The Acetylene Theory. . . . .   | 86         |
| 4. The Surface Decomposition Theory . . . . .  | 86         |
| 5. The Boudouard Reaction Theory . . . . .   | 87         |
| 6. "Vapor Pocket" Theory . . . . .   | 88         |
| 7. New Carbon Formation Theories. . . . .  | 88         |
| 8. Carbon Ionization Theories . . . . .  | 89         |
| Carbon Particle Size Determination. . . . .  | 91         |
| Dispersion Equation for Carbon . . . . .   | 94         |
| Rayleigh Scattering Theory . . . . .   | 100        |
| Methods of Predicting Carbon Absorption Coefficients and<br>Emissivities . . . . .   | 106        |
| 1. Rayleigh Theory Method . . . . .  | 106        |
| 2. Mie Theory Method. . . . .  | 108        |
| 3. Inverse Wavelength Method . . . . .   | 111        |
| 4. Experimental Methods. . . . .   | 117        |
| Radiant Heating Calculations for Luminous Flames and Rocket<br>Exhausts. . . . .   | 122        |
| <b>RADIATION FROM Al<sub>2</sub>O<sub>3</sub> PARTICLES . . . . .</b>  | <b>136</b> |
| Mie Theory of Scattering. . . . .  | 141        |
| 1. Determination of Mie Coefficients, a <sub>m</sub> and b <sub>m</sub> . . . . .  | 142        |
| 2. Determination of Scattering and Extinction Cross-Sections,<br>σ <sub>s</sub> and σ <sub>t</sub> , and Efficiency Factors, Q <sub>s</sub> and Q <sub>t</sub> . . . . . | 148        |
| 3. Limiting Case of Rayleigh Scattering. . . . .   | 154        |
| 4. Discussion of the Mie Theory Calculations . . . . .   | 155        |

## TABLE OF CONTENTS (Concluded)

|  | Page    |
|--|---------|
| Determination of $\text{Al}_2\text{O}_3$ Particle Sizes and Distributions . . . . .                    | 158     |
| 1. Combustion of Aluminum Powder to $\text{Al}_2\text{O}_3$ Particles . . . . .                        | 158     |
| 2. Experimental Determination of $\text{Al}_2\text{O}_3$ Particle Sizes<br>and Distributions . . . . . | 161     |
| 3. Theoretical Determination of $\text{Al}_2\text{O}_3$ Particle Sizes<br>and Distributions . . . . .  | 165     |
| Determination of $\text{Al}_2\text{O}_3$ Particle Cloud Emissivity . . . . .                           | 172     |
| 1. Inverse Wavelength Method . . . . .   | 172     |
| 2. Neutron-Scattering Analogy Method . . . . .   | 173     |
| 3. One-Dimensional Beam Approximation Method . . . . .   | 177     |
| Determination of $\text{Al}_2\text{O}_3$ Particle Cloud Effective Temperature . . . . .                | 184     |
| Radiation Calculations for Aluminized Solid Propellant Rocket<br>Exhausts . . . . .                    | 191     |
| <br>CONCLUSIONS AND RECOMMENDATIONS . . . . .  | <br>201 |
| <br>REFERENCES . . . . .   | <br>207 |

## LIST OF ILLUSTRATIONS

| Figure |   | Page |
|--------|---|------|
| 1.     | Sketch of Spectral Intensity of Radiation . . . . .   | 7    |
| 2.     | Sketch of Coordinate System for Radiation Scattered by<br>a Particle . . . . .  | 16   |
| 3.     | Sketch of Coordinate System for Plane-Parallel Case . . . . .   | 27   |
| 4.     | Energy Level Transitions for a Diatomic Molecule . . . . .  | 36   |
| 5.     | Ratio of Doppler to Lorentz Half-Widths as a Function of<br>Altitude or Pressure for H <sub>2</sub> O in 2.7- $\mu$ Band at Various<br>Temperatures . . . . . | 42   |
| 6.     | Ratio of Doppler to Lorentz Half-Widths as a Function of<br>Altitude or Pressure for CO <sub>2</sub> in 4.3- $\mu$ Band at Various<br>Temperatures . . . . .  | 43   |
| 7.     | Ladenberg-Reiche Function, Showing Straight-Line and<br>Square Root Approximation . . . . .   | 53   |
| 8.     | Elsasser Model . . . . .  | 54   |
| 9.     | Statistical Model . . . . .   | 55   |
| 10.    | Random Elsasser Model . . . . .   | 60   |
| 11.    | Sketch of Semi-Infinite Cylindrical Gas Body Used in<br>Apparent Emissivity and Mean Path Length Method . . . . .   | 66   |
| 12.    | Apparent Emissivities in the Base Plane of a Cylindrical<br>and a Conical Gray-Gas Body for H = 1 . . . . .   | 68   |
| 13.    | Comparison of Measured and Calculated Intensity for J-2<br>Engine Fired at Sea Level . . . . .  | 79   |
| 14.    | Comparison of Measured and Calculated Intensity Near the<br>Exit of a 1/45-Scale F-1 Engine Fired at CAL at 120,000<br>Feet . . . . .                         | 80   |

LIST OF ILLUSTRATIONS (Cont'd)

| Figure |  | Page |
|--------|--|------|
| 15.    | Spectrum of LOX/RP-1 Plume Showing Carbon Continuum. . . .   | 81   |
| 16.    | Spectrum of N <sub>2</sub> O <sub>4</sub> /UDMH Plume Showing Lack of Carbon Continuum . . . . .   | 82   |
| 17.    | Rocketdyne F-1 Hot Gas Sampler Showing 4.12-Inch Probe Immersion. . . . .  | 93   |
| 18.    | Anomalous Dispersion. . . . .  | 96   |
| 19.    | Polarization of Radiation Scattered by a Particle Cloud . . . . .  | 101  |
| 20.    | Rayleigh Scattering Diagram Showing Scattered Intensity, I <sub>θ</sub> as a Function of θ for Unpolarized Incident Radiation of Intensity, I <sub>0</sub> . . . . .   | 103  |
| 21.    | Extinction and Scattering Efficiency Factors for Carbon Particles as a Function of α for λ = 1.8μ . . . . .  | 110  |
| 22.    | Carbon Particle Emissivity as a Function of Wavelength for the Particle Size Distribution of Equation (297) . . . . .  | 112  |
| 23.    | Carbon Particle Emissivity as a Function of Wavelength for Particles of Various Radii. . . . .   | 112  |
| 24.    | Linear Absorption Coefficient for Clouds of Very Small Carbon Particles . . . . .  | 116  |
| 25.    | Values of $(\bar{\kappa}_{m, \lambda} \rho)_c$ for Carbon Particles Determined from Measurements on the GD/C 5.25:1 Area Ratio Motor . . . . .   | 123  |
| 26.    | Variation in Carbon Particle Temperatures Along the Axis of the Rocketdyne 2:1:8 Area Ratio Nozzle. . . . .  | 130  |
| 27.    | Flame Shield Design Levels for Incident Radiation, q <sub>R</sub> , Total Heat Flux, q <sub>T</sub> , Recovery Temperature, T <sub>r</sub> , and Wall Temperature, T <sub>W</sub> , on S-IB Flame Shield . . . . . | 132  |

LIST OF ILLUSTRATIONS (Cont'd)

| Figure |   | Page |
|--------|---|------|
| 28.    | Schematic of the S-IB Base Region . . . . .   | 133  |
| 29.    | S-IC Radiative Base Heating from F-1 Engines at Sea<br>Level . . . . .                                      | 134  |
| 30.    | Schematic of the S-IC Base Region . . . . .   | 135  |
| 31.    | S-IC Static Firing . . . . .  | 135  |
| 32.    | Radiative Intensity from Exhausts of S-II Ullage and S-IC<br>Retro Motors Fired at CAL . . . . .            | 138  |
| 33.    | First Stage Minuteman Plume at Sea Level . . . . .  | 139  |
| 34.    | S-II Ullage Rocket Plume at ~ 121,000 Feet in AEDC<br>J-4 Test Cell . . . . .                               | 140  |
| 35.    | S-IB Retrorocket Plume at ~ 200,000 Feet in CAL<br>Altitude Chamber . . . . .                               | 141  |
| 36.    | Total Efficiency Factor for Alumina as a Function of $\alpha$<br>for $\lambda = 2\mu$ . . . . .             | 157  |
| 37.    | Al <sub>2</sub> O <sub>3</sub> Particle Sizes Determined from Different Studies . . . . .                   | 162  |
| 38.    | Al <sub>2</sub> O <sub>3</sub> Particle Size Variation with Throat Radius as<br>Measured by AFRPL . . . . . | 162  |
| 39.    | Particle Size Distribution for Saturn S-II Ullage Rocket . . . . .  | 171  |
| 40.    | Apparent Emissivity for a Cloud of Particles in the Form<br>of a Slab or a Cylinder . . . . .               | 177  |
| 41.    | Normal and Hemispherical Emissivity of Planar Particle<br>Clouds of Finite Thickness . . . . .              | 179  |
| 42.    | Spectral Emissivity of Alumina Particles . . . . .  | 180  |

LIST OF ILLUSTRATIONS (Concluded)

| Figure |   | Page |
|--------|---|------|
| 43.    | Temperature Profiles for Saturn S-II Ullage Rocket<br>Motor at 175,000 Feet . . . . .   | 189  |
| 44.    | S-II Ullage Rocket Plume at 130,000 Feet Altitude<br>Showing Particle Limiting Streamlines ( $Al_2O_3$ ) . . . . .                        | 190  |
| 45.    | Sketch of Inside of J-4 Test Cell Showing Instrumentation<br>Locations . . . . .  | 198  |
| 46.    | Radiation Heating Rates for S-II Ullage Rocket Using<br>Model FF-1 Radiometer 6 Inches From Exit Plane . . . . .                          | 198  |
| 47.    | S-II Ullage Rocket Exhaust Spectral Heat Transfer Cal-<br>culations at 120,000 Feet, at a Position 6 Inches From<br>Nozzle Exit . . . . . | 199  |
| 48.    | HTL Copper Probe Used in AEDC S-II Ullage Rocket Tests . . .  | 199  |
| 49.    | Mounting Support for Copper Probe Used in S-II Ullage<br>Sea Level Tests . . . . .  | 200  |
| 50.    | Proposed Saturn V Vehicle with Four 120-Inch Strap-Ons . . . .  | 201  |

## LIST OF SYMBOLS

$a$  - split width per unit strength; also constant in equation (202);  
also parameter in equation (427)

$\bar{a}$  - fine structure parameter defined by equation (321)

$a_n$  - function of Gamma functions

$a_m$  - Mie coefficient

$a_\lambda$  - quantity in equation (333)

$A$  - area; also constant in equation (135); also exponent in  
equation (298); also quantity defined by equation (359)

$\vec{A}$  - arbitrary vector

$A(s_j, \nu, \theta, \phi)$  - integral defined by equation (209)

$A_c(i)$  - collision broadening parameter defined by equation (230)

$A_D(i)$  - Doppler broadening parameter defined by equation (231)

$A_e$  - nozzle exit area

$\bar{A}_{E,i}$  - average spectral absorptance of the  $i^{\text{th}}$  Elsasser band

$A_{nm}$  - Einstein spontaneous emission coefficient or Einstein  
spontaneous transition probability

$A_p$  - surface area of a particle

$\bar{A}_p$  - average particle area or projected area of a mass-mean  
particle size

$A_t$  - nozzle throat area

$A_\lambda$  or  $A_\nu$  - spectral absorptance

$\bar{A}_\lambda$  or  $\bar{A}_\nu$  - average spectral absorptance at the band center

## LIST OF SYMBOLS (Cont'd)

$C(\theta, \phi)$  - integral defined by equation (211)

$C_e$  - equilibrium concentration of oxide particle

$C_{H_2O}$  - concentration of water vapor

$C_{p_g}$  - specific heat at constant pressure of gas

$C_v$  - specific heat at constant volume of gas

$d$  - average spacing between spectral lines; also density of conducting material

$d( )$  - differential of ( )

$d_o$  - initial diameter of carbon particles

$d_1, d_2$  - optical collision diameters of a molecule

$d_m$  - parameter in equations (366) and (367)

$d_p$  - diameter of particle

$d_{p_o}$  - median diameter of particle

$d_{PL}$  - plume diameter

$d_t$  - nozzle throat diameter

$d_{\frac{1}{2}}, d_{43}, d_{30}, d_{32}$  - particle diameters defined by equations (409-412), respectively

$D$  - frequency interval; also parameter defined by equation (458)

$\vec{D}$  - dielectric displacement vector

$D(\phi)$  - integral defined by equation (212)

## LIST OF SYMBOLS (Cont'd)

- $A_1, A_2$  - atomic weights
- $b$  - constant in equations (124) and (202); also parameter in equations (425) and (427)
- $b_m$  - Mie coefficient
- $b_\lambda$  - quantity in equation (333)
- $B$  - quantity defined by equation (359)
- $\vec{B}$  - magnetic intensity vector
- $B(\nu, \theta, \phi)$  - integral defined by equation (210)
- $B_e$  - constant in equation (105)
- $B_{mn}$  or  $B_{nm}$  - Einstein absorption coefficient or Einstein transition probability
- $B_\lambda(T), B_\nu(T)$ ,  
or  $B(\nu_j, T_i)$  - Planck blackbody intensity
- $c$  - velocity of light
- $c_m$  - parameter in equations (364) and (365)
- $c_v$  - particle volume concentration
- $c_\lambda$  - exponent in equation (334)
- $C$  - constant of integration; also rate of carbon deposition; also specific heat of particle; also concentration of oxide particle in gas phase; also constant in equations (133), (298), and (442)
- $C_1$  - constant defined by equations (19) and (198) equal to  $c^2h$
- $C_2$  - constant defined by equations (19) and (198) equal to  $ch/k$

## LIST OF SYMBOLS (Cont'd)

- $D_c(i)$  - collision broadening parameter defined by equation (227)
- $D_D(i)$  - Doppler broadening parameter defined by equation (228)
- $D_e$  - constant in equation (105)
- $D_{ni}(\lambda_{ni}, T)$  - relative cumulative spectral radiance defined by equation (200)
- $e$  - electronic charge
- $E$  - constant in equation (204); also integral defined by equation (213)
- $\vec{E}$  - electric field vector
- $\vec{E}_0$  - applied electric field vector
- $E'$  - electric field at center of sphere
- $E_D$  - average electric field from surrounding dipoles
- $E_E$  - electron orbital energy
- $E_{ES}$  - electron spin energy
- $E_i$  - average electric field from surrounding ions
- $E_{IE}$  - interaction energy
- $E_m$  - energy of lower state
- $E_n$  - energy of higher state
- $E_{NS}$  - nuclear spin energy
- $E_q$  - average electric field from surrounding quadrupoles
- $E_R$  - rotational energy

## LIST OF SYMBOLS (Cont'd)

- $E_T$  - translational energy
- $E_V$  - vibrational energy
- $E_1$  - energy of ground state; also elliptical integral of the first kind
- $E_1(\ )$  - exponential integral defined by equation (451)
- $E_2$  - elliptical integral of the second kind
- $E_\lambda$  or  $E_\nu$  - spectral energy
- $E_\theta$  - electric field of a scattered wave
- $E_\omega$  - electric field defined by equation (100)
- $E_{||}, E_{o||}$  - parallel components of electric field
- $E_{\perp}, E_{o\perp}$  - perpendicular components of electric field
- $E_{k+1}$  - integroexponential function defined by equation (438)
- $f(r_p)$  - particle size distribution function
- $f(x)$  - Ladenberg-Reiche function or curve-of-growth defined by equation (148)
- $F$  - thrust of rocket engine; also shape or form factor defined by equations (188) and (194); also constant in equation (204)
- $\vec{F}_{ELASTIC}$  - elastic force
- $\vec{F}_{EXTERNAL}$  - external force
- $\vec{F}_{SELF}$  - self force
- $F(i)$  - quantity defined by equation (229)

## LIST OF SYMBOLS (Cont'd)

- $F(\lambda)$  - quantity defined by equation (305)
- $g$  - gravitational constant (acceleration due to gravity)
- $g_m$  - degeneracy or statistical weight of the  $m^{\text{th}}$  state
- $g_n$  - degeneracy or statistical weight of the  $n^{\text{th}}$  state
- $G$  - force constant
- $h$  - Planck's constant; also height of rocket nozzle exit as measured from the base plane
- $\hbar$  - modified Planck's constant, equal to  $h/2\pi$
- $H$  - non-dimensional parameter defined by equation (191)
- $\vec{H}$  - magnetic field vector
- $\vec{H}_\phi$  - average magnetic field corresponding to current element in dipole
- $H_m^{(1)}$  or  $H_m^{(2)}$  - Hankel function
- $i$  - complex number equal to  $(-1)^{\frac{1}{2}}$
- $i_1, i_2$  - components of intensity in equations (271) and (387)
- $I$  - intensity of scattered radiation
- $I_o$  - intensity of incident radiation; also intensity defined by equation (102)
- $I_{F\lambda}$  - spectral intensity of flame or rocket exhaust
- $I'_{F\lambda}$  - double path spectral intensity of flame or rocket exhaust
- $I_{G\lambda}$  - spectral intensity of continuous source or graybody

## LIST OF SYMBOLS (Cont'd)

- $I_{sp}$  - specific impulse of rocket engine  
 $I_{T\lambda}$  - spectral intensity transmitted through flame or rocket exhaust  
 $I_{\lambda}, I_{\nu},$  or  $I_{\lambda_{nm}}$  - spectral or radiant intensity  
 $I_{\theta}$  - intensity of scattered radiation in direction of  $\theta$  when incident radiation is unpolarized  
 $I_{\psi}$  - intensity of scattered radiation in direction of  $\psi$  when incident radiation is plane-polarized  
 $I_{\omega}$  - spectral intensity defined by equation (101)  
 $\text{Im}( )$  - imaginary part of ( )  
 $j_{e,\lambda}$  or  $j_{e,\nu}$  - effective emission coefficient  
 $j_{\lambda}, j_{\nu},$  or  $j_{\lambda_{nm}}$  - emission coefficient  
 $J$  - rotational quantum number; also backward scattered component of intensity  
 $\vec{J}$  - current density vector  
 $J_0, J_1, J_m$  - Bessel function  
 $J_{\lambda}$  or  $J_{\nu}$  - source function  
 $k$  - Boltzmann's constant; also parameter defined by equation (455); also wave number equal to  $2\pi/\lambda$   
 $k'$  - parameter defined by equation (459)  
 $k_1$  - propagation constant of conducting sphere  
 $k_2$  - propagation constant of surrounding medium

## LIST OF SYMBOLS (Cont'd)

- $K$  - quantity defined by equation (239); also normalizing constant defined by equation (419); also parameter equal to  $v_p/v_g$
- $K_D$  - ratio of actual drag coefficient to Stokes value
- $K_H$  - ratio of actual Nusselt number to Stokes value
- $K_m$  - quantity defined by equation (360)
- $K_1, K_2, K_3, K_4, K_5$  - constants in equation (235)
- $K_\lambda$  - non-dimensional absorption coefficient defined by equation (191)
- $\ell$  - direction cosine; also azimuthal quantum number; also path length
- $\ell(s)$  - scattering mean path
- $L$  - mean path length defined by equation (203); also quantity defined by equation (324)
- $m$  - direction cosine; also mass of medium; also mass per molecule; also exponent in equation (204); also mass flow after time  $t$ ; also ratio of absorption to total cross-section or ratio of absorption to total efficiency factor
- $m_a$  - mass of one atom of conducting material
- $m_e$  - mass of electron
- $m_\ell$  - magnetic quantum number
- $m_o$  - initial mass flow rate
- $m_s$  - spin quantum number
- $m_p$  - particle mass flow rate

## LIST OF SYMBOLS (Cont'd)

- $M$  - mass of particles per volume; also Mach number
- $M_1, M_2$  - molecular weights
- $M_o$  - mass of particles of unit atomic weight; also mass of median volume diameter particle
- $M_r, M_\theta, M_\phi$  - polar components of  $\vec{M}_\psi$
- $\vec{M}_u, \vec{M}_v$  - solutions to scalar wave equation
- $\vec{M}_\psi$  - solution to vector wave equation
- MW - molecular weight
- $\overline{MW}$  - effective molecular weight
- $n$  - direction cosine; also principal quantum number; also total number of molecules per unit volume; also number of spectral lines; also index of refraction
- $\vec{n}$  - vector normal to surface
- $n_1$  - real part of index of refraction
- $n_2$  - imaginary part of index of refraction
- $n_\lambda$  or  $n_\nu$  - index of refraction (same as  $n$  above)
- $N$  - density of perturbers; also total electron concentration
- $N(\nu)$  - probability defined by equation (164)
- $N_c$  - conduction electron concentration
- $N_e$  - free electron concentration (same as  $N_c$ )
- $N_k$  - bound electron concentration
- $N_m$  - number of atoms per unit volume in the state  $m$ ; also Bessel function

## LIST OF SYMBOLS (Cont'd)

- $N_n$  - number of atoms per unit volume in the state  $n$   
 $N_p$  - particle concentration  
 $N_r, N_\theta, N_\phi$  - polar components of  $\vec{N}_\psi$   
 $\vec{N}_u, \vec{N}_v$  - solutions to vector wave equation  
 $\dot{N}_{1 \rightarrow 2}$  - rate of particle collision  
 $p$  - induced dipole moment equal to  $\beta E_o$   
 $p(\cos\theta)$  or  
 $p(\theta, \phi; \theta', \phi')$  - phase function  
 $P$  - pressure or partial pressure  
 $\vec{P}$  - polarization vector  
 $P(S_i)$  - probability function defined by equation (165)  
 $P_a$  - pressure of absorbing gas  
 $P_b$  - pressure of non-absorbing, line broadening gas  
 $P_c$  - rocket chamber pressure  
 $P_e$  - equivalent pressure defined by equation (202)  
 $P_h^a$  - pressure of absorbing gas in zone  $h$   
 $P_h^b$  - pressure of non-absorbing, line broadening gas in zone  $h$   
 $P_m'$  - Legendre polynomial  
 $P_{O_2}$  - partial pressure of oxygen  
 $Pr$  - Prandtl number

## LIST OF SYMBOLS (Cont'd)

$P_{0,k}, P_{1,k}, P_{2,k}$  - probability function

$q$  - heat transfer rate; also quadrupole moment

$q_{\lambda}$  - spectral heat transfer rate

$Q_a$  - absorption efficiency factor

$Q_s$  - scattering efficiency factor

$Q_t$  - total or extinction efficiency factor

$Q_1, Q_2, Q_3$  - energies defined by equations (336), (337), and (339), respectively

$r$  - position of excited atom or molecule (separation distance of perturbing particle from emitting atom or molecule); also radial distance in base plane; also distance between differential area on confining surface and differential gas volume

$\vec{r}$  - distance from radiation field to accelerating charge

$r_e$  - radius of rocket nozzle exit

$r_{ij}$  - distance between  $i^{\text{th}}$  and  $j^{\text{th}}$  oscillator

$r_p$  - radius of particle

$r_{p_m}$  - mean radius of particle

$R$  - distance from dipole to scattered wave; also distance from spherical particle to point of observation; also non-dimensional parameter defined by equation (191); also carbon-to-hydrogen ratio; also gas constant; also path length from area being heated to volume of emitting particles; also distance from surface to particle of size  $n$

$R_c$  - distance from surface to edge of particle cloud

## LIST OF SYMBOLS (Cont'd)

Re - Reynolds number

Re( ) - real part of ( )

s - path length; also parameter in equation (425)

s' - path length

$\vec{s}$  - direction of emitted intensity

S - line strength; also non-dimensional parameter defined by equation (191)

S<sup>0</sup> - line strength at unit pressure

S<sub>1</sub>, S<sub>2</sub>, S<sub>3</sub>, S<sub>4</sub> - components of scattering matrix in equation (377)

$\vec{S}^*$  - Poynting vector

t - time

t<sub>E,i</sub> - weighted average of spectral transmissivity or transmittance for i<sup>th</sup> Elsasser band

t<sub>jν</sub> - spectral transmittance at frequency ν as a result of n<sub>j</sub> lines in frequency interval δ<sub>j</sub>

t<sub>λ</sub> or t<sub>ν</sub> - spectral transmissivity or transmittance

$\bar{t}_\lambda$  or  $\bar{t}_\nu$  - weighted average of spectral transmissivity or transmittance

T - temperature

$\bar{T}$  - effective plume temperature

T<sub>AW</sub> - adiabatic wall temperature

T<sub>b</sub> - boiling temperature of fuel

## LIST OF SYMBOLS (Cont'd)

$T_{BR}$  - brightness temperature

$T_c$  - rocket chamber temperature

$T_{eff}$  - effective temperature

$T_F$  - temperature of flame or rocket exhaust

$T_G$  - temperature of continuous source or graybody

$T_p$  - particle temperature

$\bar{T}_{p\text{eff}}$  - effective particle temperature

$u$  - product of density and path length taken at standard temperature and pressure; also solution of scalar wave equation

$\vec{u}$  - velocity vector of charged particle

$v$  - vibrational quantum number; also phase velocity equal to  $c/n$ ; also solution of scalar wave equation

$\vec{v}$  - velocity vector; also mean relative velocities of radiating and perturbing particles defined by equation (139)

$\vec{v}_g$  - gas velocity vector

$\vec{v}_p$  - particle velocity vector

$v_x$  - velocity in x-direction

$V$  - volume of spherical particle; also average volume of particles per unit volume of cloud

$V'$  - average volume of particles per unit volume of cloud

$V_p$  - volume of single particle

## LIST OF SYMBOLS (Cont'd)

- $V'_p$  - average particle volume
- $\overline{V}_{p_n}$  - number average particle volume
- $w$  - absorber concentration
- $W$  - integrated absorptance or equivalent width; also total energy scattered in all directions
- $W_a$  - absorbed energy
- $W_{E,i}$  - integrated absorptance or equivalent width of  $i^{\text{th}}$  Elsasser band
- $W_I$  - incident energy
- $W_p$  - weight fraction of particles in plume
- $W_S$  - scattered energy
- $W_{S.L.}$  - integrated absorptance or equivalent width of a single line
- $\overline{W}_{S.L.}$  - average value of integrated absorptance or equivalent width of a single line
- $W_t$  - total energy
- $x$  - parameter defined by equation (147); also distance along path from boundary of particle cloud; also position coordinate
- $\vec{x}$  - position coordinate vector
- $\vec{x}$  - velocity in x-direction
- $\vec{\ddot{x}}$  - acceleration in x-direction
- $\vec{\ddot{\ddot{x}}}$  - derivative of acceleration in x-direction

## LIST OF SYMBOLS (Cont'd)

- $\bar{x}_i$  - parameter defined by equation (220)
- $x_e$  - constant in equation (105)
- $x_o$  - amplitude
- $X$  - optical beam length defined by equation (187)
- $y$  - position coordinate; also quantity defined by equation (234)
- $y_e$  - constant in equation (105)
- $y_i$  - fraction of particles of the  $i^{\text{th}}$  size
- $Y_m$  - Neumann function
- $z$  - position coordinate; also parameter defined by equation (162); also path length; also axial distance downstream of nozzle throat
- $z_1$  - position coordinate
- $z'$  - position coordinate
- $Z$  - atomic number
- $\alpha$  - parameter equal to  $2\pi r_p/\lambda$ ; also accommodation coefficient; also fraction of radiation scattered in forward direction ( $\theta = 0$ )
- $\alpha_e$  - constant in equation (105)
- $\alpha_g$  - total absorptivity of gas stream
- $\alpha_\lambda$  or  $\alpha_\nu$  - spectral absorptivity
- $\beta$  - polarizability equal to  $ex/E$ ; also van der Waals constant; also band model parameter defined by equation (150); also polar angle in equations (191) and (195); also quantity defined by equation (310); also parameter equal to  $n\alpha$ ; also fraction of radiation scattered in backward direction ( $\theta = 180^\circ$ )

## LIST OF SYMBOLS (Cont'd)

- $\beta(\tau)$  - neutron blackness
- $\beta'$  - polar angle in equation (310)
- $\beta_e$  - constant in equation (105)
- $\beta_{m,\lambda}$  or  $\beta_{m,\nu}$  - mass extinction coefficient
- $\beta_\lambda$  or  $\beta_\nu$  - extinction coefficient
- $\gamma$  - dissipative or radiation damping function or natural half-width defined by equations (87) and (103); also parameter in equation (130); also rate of growth constant; also isentropic exponent
- $\bar{\gamma}$  - effective isentropic exponent
- $\gamma(\theta)$  - phase function
- $\gamma^0$  - half-width at unit pressure
- $\gamma_a^0$  - half-width at unit pressure for self-broadening
- $\gamma_b^0$  - half-width at unit pressure for foreign-gas broadening
- $\gamma_c$  - damping parameter pertaining to collision electrons
- $\gamma_{\text{COLL}}$  - collision frequency
- $\gamma_k$  - damping parameter pertaining to bound electrons
- $\gamma_{\text{TR}}$  - spontaneous transition probability
- $\Gamma$  - parameter defined by equation (116); also gamma function
- $\delta$  - average spacing between lines in random Elsasser band model; also density of solid graphite; also quantity defined by equation (311)

## LIST OF SYMBOLS (Cont'd)

- $\delta^{\bar{n}_k}$  - average spacing between lines in quasi-random band model  
 $\delta(\bar{S}-\bar{S})$  - Dirac delta probability function  
 $\Delta$  - shift in intensity maximum for van der Waals forces  
 $\epsilon$  - total emissivity; also dielectric constant  
 $\epsilon_a$  or  $\bar{\epsilon}_a$  - apparent emissivity of particle cloud  
 $\epsilon_{F\lambda}$  - spectral emissivity of flame or rocket exhaust  
 $\epsilon_{G\lambda}$  - spectral emissivity of continuous source (graybody)  
 $\epsilon_H$  - hemispherical emissivity of particle cloud  
 $\epsilon_N$  - normal emissivity of particle cloud  
 $\epsilon_o$  - dielectric constant in free space  
 $\epsilon_p$  - total hemispherical emissivity of particle  
 $\epsilon_{p_x}$  - total hemispherical emissivity of particle as a function of axial distance  $x$  from nozzle exit  
 $\epsilon_{p\lambda}$  - spectral hemispherical emissivity of particle  
 $\epsilon_\lambda$  or  $\epsilon_\nu$  - spectral emissivity  
 $\epsilon_\infty$  - particle cloud emissivity (normal or hemispherical) when  $\tau \rightarrow \infty$   
 $\zeta$  - parameter defined by equation (157)  
 $\zeta_m(z)$  - Riccati-Bessel function  
 $\eta$  - total phase shift; also correction factor used in equation (470)

## LIST OF SYMBOLS (Cont'd)

- $\bar{\eta}$  - quantity defined by equation (328)
- $\eta_m(z)$  - parameter defined by equation (373)
- $\theta$  or  $\theta'$  - polar angle between normal to surface and direction of radiant intensity; also angle between direction of propagation of incident and scattered radiation
- $\theta_o$  - polar angle from element of area being heated to emitting carbon particles in volume element
- $\Theta$  - scattering angle between incident intensity and scattered intensity whose cosine is defined by equation (34)
- $\kappa_{\text{eff}}$  - effective absorption coefficient
- $\kappa_{m,\lambda}$  or  $\kappa_{m,\nu}$  - mass absorption coefficient
- $\bar{\kappa}_{m,\lambda}$  - average mass absorption coefficient defined by equation (320)
- $\kappa_\lambda, \kappa_\nu$ , or  $\kappa_{\lambda_{mn}}$  - absorption coefficient
- $\bar{\kappa}_\gamma$  - average absorption coefficient equal to  $S/d$
- $\lambda$  - wavelength
- $\lambda_{mn}$  - wavelength corresponding to quantum transition from lower state  $m$  to higher state  $n$
- $\lambda_{nm}$  - wavelength corresponding to quantum transition from higher state  $n$  to lower state  $m$
- $\mu$  - cosine of  $\theta$ ; also dipole moment; also magnetic permeability
- $\mu'$  - cosine of  $\theta'$
- $\mu_g$  - gas viscosity

## LIST OF SYMBOLS (Cont'd)

- $\nu$  - frequency of vibration
- $\nu_0$  - resonant frequency of vibration
- $\nu_h$  - frequency at half intensity or natural half-width
- $\nu_{mn}$  - frequency corresponding to quantum transition from lower state m to higher state n
- $\nu_{nm}$  - frequency corresponding to quantum transition from higher state n to lower state m
- $\nu_{ST}$  - frequency corresponding to Stark broadening
- $\xi$  - exponent defined by equation (300)
- $\xi_i$  - parameter defined by equation (185)
- $\xi_m(z)$  - parameter defined by equation (374)
- $\pi$  - constant equal to 3.1416
- $\pi_m$  - parameter defined by equation (384)
- $\prod_{i=1}^n$  - product over  $i = 1$  to  $n$
- $\rho$  - density of medium; also closest approach parameter
- $\rho_c$  - density of carbon particles
- $\rho_e$  - charge density
- $\rho_g$  - gas density
- $\rho_{m_c}$  - mean carbon particle density
- $\rho_0$  - density of carbon in bulk form

## LIST OF SYMBOLS (Cont'd)

- $\rho_s$  - alumina bulk density
- $\rho_\lambda$  or  $\rho_\nu$  - spectral reflectivity or reflection coefficient
- $\rho_\infty$  - reflectivity when  $\tau \rightarrow \infty$
- $\sigma$  - ratio of half-widths caused by self-broadening; also complex conductivity
- $\sigma'$  - static conductivity
- $\sigma_a$  - absorption cross-section
- $\sigma_B$  - Stefan-Boltzmann constant defined by equation (28)
- $\sigma_g$  - parameter defined by equation (413)
- $\sigma_{m,\lambda}$  or  $\sigma_{m,\nu}$  - mass scattering coefficient
- $\sigma_s$  - scattering cross-section
- $\sigma_t$  - total or extinction cross-section equal to  $\sigma_a + \sigma_s$
- $\sigma_x$  - ratio of foreign-gas half-width to H<sub>2</sub>O half-width
- $\sigma_\lambda$  or  $\sigma_\nu$  - scattering coefficient
- $\langle \sigma_a \rangle$  - average absorption cross-section
- $\sum_{i=1}^n$  - summation from  $i = 1$  to  $n$
- $\tau$  - time constant or lifetime of excited state; also optical depth or thickness
- $\tau_{c,\lambda}$  - optical depth at center of plume
- $\tau_m$  - quantity defined by equation (385)

## LIST OF SYMBOLS (Concluded)

$\tau_\lambda, \tau_\nu$ , or  $\tau_\lambda'$  - optical depth or thickness (dimensionless)

$\phi$  - azimuthal angle; also carbon particle work function or ionization potential; also ratio of particle flow rate to gas flow rate

$\phi'$  - azimuthal angle

$\phi_0$  - azimuthal angle from element of area being heated to emitting carbon particles in volume element

$\chi$  - exponent defined by equation (300)

$\chi_m(z)$  - Riccati-Bessel function

$\psi$  - parameter defined by equation (111); also angle between propagation direction of scattered radiation and electric vector in direction of incident radiation

$\psi_m(z)$  - Riccati-Bessel function

$\psi'''$  - function defined in equation (301)

$\omega$  - solid angle; also circular frequency of vibration equal to  $2\pi\nu$

$\omega_e$  - equilibrium frequency based on equilibrium internuclear distance  $r_e$

$\omega_h$  - circular frequency at half intensity or natural half-width

$\omega_0$  - natural or resonant frequency of vibration equal to  $2\pi\nu_0$

$\omega'$  - solid angle

$\bar{\omega}_0$  or  $\bar{\omega}_n$  - albedo for single scattering

## REVIEW OF THERMAL RADIATION FROM LIQUID AND SOLID PROPELLANT ROCKET EXHAUSTS

### SUMMARY

A comprehensive review of the general theory of thermal radiation from liquid and solid propellant rocket exhausts is presented. More than 600 references are discussed and almost 500 equations describe the details of gaseous radiation, radiation from carbon particles, and radiation from aluminum oxide ( $\text{Al}_2\text{O}_3$ ) particles. The equation of radiation transfer is derived in detail, and solutions include the effects of scattering (Mie and Rayleigh), as well as emission and absorption. The analyses of spectral line broadening and band models are presented for gaseous radiation, and formation and sizes of carbon and  $\text{Al}_2\text{O}_3$  particles are discussed for particle radiation. Numerous methods of predicting gas and particle emissivities and radiative heating are critically analyzed, and the most accurate methods currently available are discussed in detail. Although the application of the general theory is directed toward radiation from the exhausts of the Saturn H-1, F-1, J-2 and RL-10 liquid propellant engines (for base heating) and of the solid propellant ullage and retro motors (for stage-separation heating), the basic theory applies to radiation from the exhaust of any liquid propellant engine or solid propellant motor.

### INTRODUCTION

Among the many problems which designers of modern rockets and missiles face today are the accurate predictions of radiation and convective heating from the exhausts from the large main-stage engines and the smaller ullage and retrorockets during stage separation. Excessive heating from the exhausts of the first-stage engines in the base region destroyed several of the early Atlas, Jupiter and Titan missiles during lift-off. On the other hand, too much insulation for the heat shield in the base region is not desirable because of the weight penalty this imposes. Thus, it would be advantageous to obtain the best possible means of predicting this base heating.

Heating in the base region from clustered engines is caused mainly by radiation at the low altitudes; however, at some intermediate altitude (25,000 to 50,000 feet) reverse flow begins to occur, and convective heating becomes the dominant mode of heating. For the solid propellant ullage and retro motors, impingement of the exhaust directly on the vehicle causes an additional heating problem because of the thermal and kinetic energy transfer from the hot particles to the surface. This report, however, is concerned only with the radiation

heating from these rocket exhausts. This includes the detailed analysis of the selective emission of the gases (emitting in certain spectral bands only), the near blackbody continuum emission of carbon particles found in exhausts of hydrocarbon-fueled engines, and the graybody continuum emission (plus scattering) associated with  $\text{Al}_2\text{O}_3$  particles found in the exhausts of solid propellant motors.

For the past several years the Thermal Environment Branch in the Aero-Astroynamics Laboratory at NASA/Marshall Space Flight Center (MSFC) has been analyzing, both theoretically and experimentally, the effects of heating to the base of the Saturn booster stages (S-I, S-IB, and S-IC) and upper stages (S-IV, S-II, and S-IVB) caused by the exhausts of the hydrocarbon-fueled H-1 and F-1 engines and the hydrogen-fueled RL-10 and J-2 engines. For the past two years this branch has been analyzing the effects of heating to various components and structures exposed to the exhausts of the Saturn solid propellant ullage (S-II and S-IVB) and retro motors (S-I, S-IB, S-IC, S-II, S-IVB, and Centaur). In recent months various presentations have been made and publications written by members of the Thermal Environment Branch and its associated contractors on the general subject of the thermal environment of the Saturn vehicles caused by the exhausts of both liquid and solid propellant rockets.

At the American Institute of Aeronautics and Astronautics (AIAA) Second Propulsion Joint Specialist Conference held at Colorado Springs, Colorado, in June 1966, Farmer et al. [1], Chu, Neimann, and Powers [2], and D'Attore, Nowak, and Thommen [3] presented analyses of flow fields from plumes of liquid propellant engines; Huffaker [4] and Carlson [5] presented, respectively, analyses of radiation from liquid and solid propellant exhausts; Rochelle [6] discussed experimental measurements and the theoretical correlations of heating (radiative, convective, and particle impingement) in Saturn solid rocket exhausts; and Hendershot [7] and Hopson and McAnelly [8]\* discussed base region thermal environments from the exhausts of clustered nozzles. Earlier this year, Payne and Jones [9] had an article published in the AIAA Journal which summarized the Saturn I base thermal environment from the exhausts of the H-1 engines to the S-I stage base region and from the exhausts of the RL-10 engines to the S-IV stage base region. Wilson [10,11] late in 1966 presented applications of the short-duration technique developed at Cornell Aeronautical Laboratory (CAL), under contract from this branch for predicting heating to the Saturn vehicles from exhausts of scale models of the Saturn liquid and solid propellant rockets.

---

\*Propulsion and Vehicle Engineering Laboratory, MSFC.

This report presents a comprehensive review of the general theory of radiation from rocket exhausts and discusses the most current methods available for predicting radiation heating as developed by this branch, its associated contractors, and other agencies. More than 600 documents have been reviewed, and nearly 500 equations are presented which pertain to the general theories of gaseous radiation, radiation from carbon particles, and radiation from  $Al_2O_3$  particles. This is believed to be the most comprehensive survey presented on this subject, although Beheshti and Thibbodeaux [12] and Robertson and Usher [13] have recently published summaries of various methods of predicting radiation from rocket exhausts. Several years ago Carpenter, Foreman, and Goldstein [14] presented a detailed review of rocket exhaust radiation and presented numerous references through the end of 1957.

Many Thermal Environment Branch contractors have contributed to the radiation programs mentioned in this report. For the gaseous radiation analysis some of these contractors include General Dynamics/Convair at San Diego, California; Rocketdyne at Canoga Park, California; Warner-Swasey at Flushing, New York; Brown Engineering at Huntsville, Alabama; and Hayes International at Birmingham, Alabama. Rocketdyne and General Dynamics/Convair have contributed extensively in the analysis of radiation from carbon particles. Aeronutronic at Newport Beach, California, has been chiefly responsible for the  $Al_2O_3$  particle theoretical radiation programs. Heat Technology Laboratory at Huntsville, Alabama, and Hayes International (using instrumentation from Hayes and from Block Engineering at Cambridge, Massachusetts) have been responsible for radiation measurements obtained from exhausts of both solid and liquid propellant rockets. The stage contractors - Boeing at Huntsville, Alabama, and New Orleans, Louisiana (S-IC stage); Chrysler at New Orleans, Louisiana (S-IB stage); North American at Downey, California (S-II stage); and Douglas at Huntington Beach, California (S-IVB stage), as well as MSFC's Propulsion and Vehicle Engineering (P&VE) Laboratory (and its contractors, Rocketdyne, United Technology Center at Sunnyvale, California, and the University of California at Berkeley, California) - have all made valuable contributions to the radiation heating problems associated with the Saturn vehicles. Lockheed at Huntsville, Alabama, has been responsible for the development of the flow-field (method-of-characteristics and thermochemical) programs used by MSFC and many contractors for the radiation analyses. Aeronutronic has combined the Lockheed single-phase program with its two-phase program to handle the radiation from the  $Al_2O_3$  particles.

Experimental programs sponsored by MSFC involving radiation measurements have been performed in altitude cells at Arnold Engineering Development Center (AEDC) at Tullahoma, Tennessee, for the S-II and S-IVB ullage and

S-IVB retro motors and J-2 engines (all full-scale), and scale models of H-1 engines (on the S-I and S-IB stage) with external flow. Experiments on radiant base heating from the exhausts of model F-1 engines (on the S-IC stage) have been performed at Lewis Research Center, Cleveland, Ohio, in transonic and supersonic wind tunnels (at altitude). Radiation measurements have also been made in altitude cells at Cornell Aeronautical Laboratory (CAL) at Buffalo, New York, which involved scale models of H-1, F-1, J-2, and RL-10 engines and S-II and S-IVB ullage and S-I, S-IB, S-IC, and S-II retro motors. Measurements of plume radiation have also been obtained in altitude cells at the Ordnance Aerophysics Laboratory (OAL) at Daingerfield, Texas, for the S-II ullage motors and at MSFC's Test Laboratory for the Centaur retro motors. Sea level radiation measurements have been obtained at MSFC's Test Laboratory for the J-2, H-1, and F-1 engines (including a static firing of the S-IC stage which has five F-1 engines), and total heating measurements were obtained at Rocketdyne at McGregor, Texas, on objects placed in an S-II ullage motor plume 20 inches from the nozzle exit.

This report is primarily concerned with the development of the theoretical aspects of radiation from rocket exhausts, although in various places experimental data (some of which are compared with the theoretical calculations) are discussed. In general, the radiation discussed here occurs in the infrared ( $\lambda > 0.8\mu$ ) portion of the spectrum, although occasionally radiation in the visible and ultraviolet will be discussed. The details of plume gas dynamics, while important in the analysis of radiation, are not discussed except for the effective particle temperatures (two-phase flow) associated with radiation from solid propellant rocket exhausts. Also, form factors are not discussed in detail, although references are included in various sections which describe their analysis.

The equation of transfer of radiation, including the process of absorption, emission, local thermodynamic equilibrium, and scattering, is derived first, and certain solutions to this equation based upon various simplifying assumptions are discussed. In the analysis of gaseous radiation, radiation from an accelerating charge as it relates to the Lorentz line shape (important in the analysis of band models) is discussed; the shape and broadening of spectral lines is then considered; various band models (such as single-line, Elsasser, statistical, random Elsasser, and quasi-random) are described; and, finally, various methods of predicting gaseous radiation from rocket exhausts are presented.

The next major section considers the analysis of radiation from carbon particles (such as found in exhausts of H-1 and F-1 engines). In this section, the formation of carbon particles in luminous flames (including rocket exhausts), the determination of carbon particle sizes and the carbon dispersion equation are analyzed; then, the Rayleigh scattering theory as it applies to scattering by carbon particles is developed. Various methods of predicting carbon absorption coefficients and emissivities are then described and finally calculations of radiant heating in luminous flames and rocket exhausts are discussed.

Radiation from  $\text{Al}_2\text{O}_3$  particles (such as found in exhausts of solid propellant motors) is analyzed and a detailed discussion of the Mie theory of scattering by these particles is given. Alumina ( $\text{Al}_2\text{O}_3$ ) particle sizes and distributions, including the combustion of aluminum powder to  $\text{Al}_2\text{O}_3$  particles, are then considered, and various methods of predicting the  $\text{Al}_2\text{O}_3$  particle cloud emissivity are described. The determination of  $\text{Al}_2\text{O}_3$  particle cloud effective temperature is discussed briefly. All of these items are then combined to analyze various methods of calculating radiation from aluminized rocket exhausts.

Since this report has been abstracted from a large number of sources and references, units of measure used by the authors are retained. Conversions to S. I. units are not made in order that the work of these authors be accurately presented and remain intact.

# EQUATION OF RADIATION TRANSFER

The fundamental equation of radiation transfer as it pertains to radiation from both gases and solid particles, such as carbon or  $\text{Al}_2\text{O}_3$ , is derived in this section. The spectral intensity is discussed, followed by a discussion of absorption, emission, local thermodynamic equilibrium, and scattering. The equation of transfer is derived, and solutions to this equation with certain simplifying assumptions are given.

This discussion is based upon a number of classic textbooks on radiation transfer theory and astrophysics, as well as on several recent documents which derive the equation of transfer and/or give some of its solutions. The textbooks consulted were Chandrasekhar [15,16], Busbridge [17], Kourganoff [18], Ambartsumyan [19], Hopf [20], Wooly and Stibbs [21], Sobolev [22], Rosseland [23], Pai [24], and Goody [25]. The documents consulted included Samuelson [26], Viskanta [27,28], Love [29], Love and Grosh [30], Viskanta and Grosh [31], Seay [32], Brown [33], Bartky and Bauer [34], Lai and Purgalis [35], deSoto [36], Goulard [37], Sampson [38], Tellep and Edwards [39], Hansen [40], Ueno et al. [41], and Churchill et al. [42]. Most, but not all, of these authors included the effects of scattering in their derivations of the equation of transfer. In the analysis to follow, the salient features in each of these derivations are put together to formulate the equation of transfer for use in rocket exhaust radiation applications.

## Spectral Intensity of Radiation

This section discusses the spectral intensity as it relates to the spectral energy  $dE_\lambda$  or spectral radiant heat transfer rate  $q_\lambda$ . The spectral energy  $dE_\lambda$  is defined as the radiant energy absorbed, emitted, or scattered in the wavelength interval  $(\lambda, \lambda + d\lambda)$ , in a time interval  $(t, t + dt)$ , passing through the solid angle  $d\omega$  and the unit area normal to the surface  $dA$ . This quantity is expressed as

$$dE_\lambda = I_\lambda \vec{n} \cdot \vec{s} d\omega dt dA d\lambda = I_\lambda \cos\theta d\omega dt dA d\lambda \quad (1)$$

The spectral heat transfer rate  $q_\lambda$  from a rocket exhaust, which is analogous to the integral of equation (1), is also related to the spectral intensity  $I_\lambda$  and can be written in the form

$$q_{\lambda}/A = \int_{\omega} I_{\lambda} \cos \theta d\omega \quad (2)$$

The total radiation heat transfer rate would then be the integral of  $q_{\lambda}/A$  over the entire spectrum. The spectral intensity  $I_{\lambda}$ , which is sometimes denoted by  $I_{\nu}$  (frequency dependent), is also called the specific intensity or monochromatic intensity and is usually written in units of Btu/ft<sup>2</sup>-sec-micron-steradian or watts/cm<sup>2</sup>-micron-steradian. This intensity at point P, in the direction  $\vec{s}$ , is related to the polar angle  $\theta$ , azimuthal angle  $\phi$ , element of solid angle  $d\omega$ , element of surface area  $dA$ , and normal to the surface area  $\vec{n}$ , as shown in Figure 1.

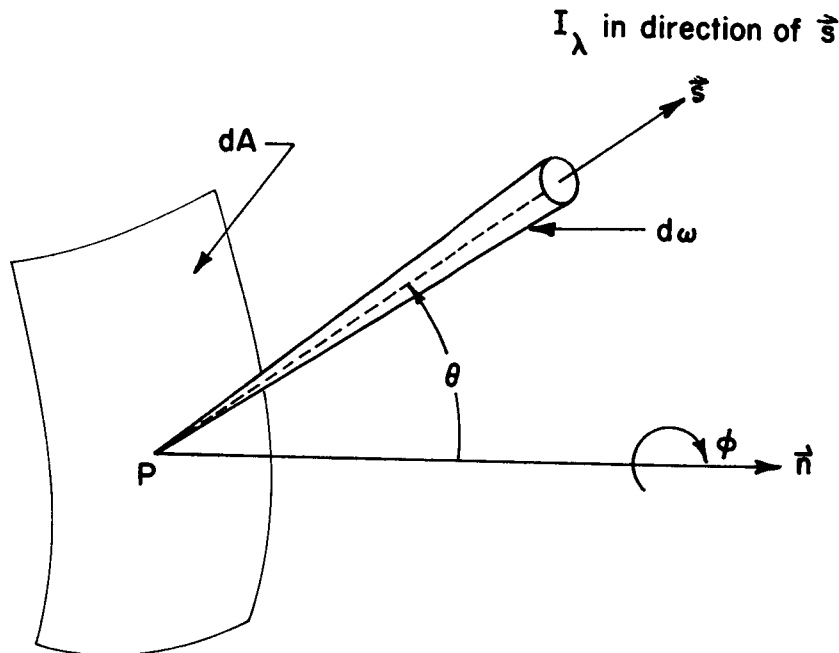


FIGURE 1. SKETCH OF SPECTRAL INTENSITY OF RADIATION

The spectral intensity is in general a function of wavelength  $\lambda$ , of time  $t$ , of solid angle  $\omega$ , (or direction cosines  $l$ ,  $m$ ,  $n$ ), and of position coordinates  $x$ ,  $y$ ,  $z$ , and thus can be written as

$$I_{\lambda} = I_{\lambda} (x, y, z; l, m, n; t) . \quad (3)$$

The integrated intensity  $I$  is merely the integral of the spectral intensity  $I_\lambda$  and can be written as

$$I = \int_0^\infty I_\lambda d\lambda . \quad (4)$$

## Absorption

As a pencil of radiation travels through matter (such as a rocket exhaust) it is usually weakened by absorption. If the decrease in spectral intensity is  $dI_\lambda$ , and the coefficient of absorption is  $\kappa_\lambda$ , then the following relation (experimentally proven) holds true:

$$dI_\lambda = -\kappa_\lambda I_\lambda ds , \quad (5)$$

where  $s$  represents the distance traversed along a pencil of radiation as shown by the vector  $\vec{s}$  in Figure 1. This expression is valid for both line and continuous absorption. The coefficient of absorption can also be expressed in terms of a mass absorption coefficient  $\kappa_{m,\lambda}$  as

$$\kappa_\lambda = \rho \kappa_{m,\lambda} , \quad (6)$$

where  $\rho$  is the density of a rocket exhaust at a particular point in the plume. Also, the notation  $\kappa_\nu$  for the frequency-dependent absorption coefficient is sometimes used. (See the section entitled "Gaseous Radiation," and subsection "Band Models.")

The absorption coefficient is a property of the particular rocket exhaust, and in general, depends upon temperature, pressure, and exhaust gas composition, in addition to wavelength and time (for non-steady-state conditions). The absorption defined in this section is designated as "true absorption," that is, absorption which may be converted into heat which may be emitted at another wavelength. Some authors prefer to consider another type of absorption as scattering, which is merely the redistribution of incident energy into another direction but at the same wavelength. Scattering is discussed in detail later in this section.

An example of "true absorption" is the absorption of radiation of frequency  $\nu_{mn}$  corresponding to a quantum transition from the lower state  $m$  to the higher state  $n$  of the atoms comprising the particular medium. This transition can be represented according to Bohr's Theory as

$$h\nu_{mn} = E_m - E_n, \quad (7)$$

where  $h$  is Planck's constant,  $\nu_{mn} = c/\lambda_{mn}$  (where  $c$  is the velocity of light), and  $E_m$  and  $E_n$  are energies of the higher and lower states, respectively.

A further coefficient,  $B_{mn}$ , which is associated with absorption, is known as the Einstein absorption coefficient or the Einstein transition probability and is defined in the following manner:

$$B_{mn} I_{\lambda_{mn}} \equiv \text{probability per unit time that an atom in state } m \text{ absorbs a photon of energy } h\nu_{mn} \text{ and goes to state } n \text{ with intensity } I_{\lambda_{mn}}.$$

By assuming a purely absorbing medium and integrating equation (5) with insertion of equation (6), a new quantity called the optical depth  $\tau_{\lambda}$  may be defined. The integration of equation (5) is known as Beer's equation and may be written as

$$I_{\lambda}(s) = I_{\lambda}(0) \exp\left(-\int_0^s \rho\kappa_{m,\lambda} ds\right), \quad (8)$$

where  $I_{\lambda}(s)$  is the intensity after the radiation has traveled a path  $s$  through the medium. Equation (5) is usually written in the form

$$I_{\lambda}(s) = I_{\lambda}(0) e^{-\tau_{\lambda}}, \quad (9)$$

where the optical depth of the medium is

$$\tau_{\lambda} = \int_0^s \rho\kappa_{m,\lambda} ds. \quad (10)$$

A more general relation for optical depth is derived in the subsection entitled "Scattering," where the effects of scattering are included.

## Emission

The process of emission of radiation from a medium such as a rocket exhaust can be characterized by an emission coefficient  $j_\lambda$ . This coefficient is defined as the spectral radiant energy rate  $dq_\lambda$ , emitted by an element of mass  $dm$  in the solid angle  $d\omega$  during the time interval  $(t, t + dt)$ , and in the wavelength interval  $(\lambda, \lambda + d\lambda)$ , and is given as

$$j_\lambda = \frac{dq_\lambda}{dm d\omega d\lambda} \quad (11)$$

The emission coefficient depends on the wavelength, location of unit volume, exhaust gas composition, temperature, and time (for non-steady-state conditions). In general, there are two types of emission processes: spontaneous emission and stimulated (or induced) emission.

The first type of emission occurs when atoms in a higher state,  $n$ , undergo a quantum transition to a lower state,  $m$ , emitting a quantum of energy,  $h\nu_{nm}$ . For this spontaneous emission, another emission coefficient,  $A_{nm}$ , can be defined. This coefficient is known as the Einstein spontaneous emission coefficient or Einstein spontaneous transition probability, and is defined as the probability per unit time that an atom in state  $n$  makes a transition to state  $m$ .

Stimulated emission (sometimes referred to as negative absorption) occurs when the transmitted intensity becomes greater than the incident intensity. This process occurs when a condition is artificially created in which the number of atoms per unit volume  $N_n$  in a higher-energy state exceeds the number of atoms per unit volume  $N_m$  in a lower-energy state. This is accomplished by adding energy either by absorption or collision. The stimulated emission then takes place when the atoms drop to the lower states and emit photons corresponding to an energy difference between the two states. When an atom in the state  $n$  has been exposed to radiation of intensity  $I_{\lambda_{nm}}$ , it is possible to define a stimulated emission transition probability per unit time as  $B_{nm}$ , such that

$$B_{nm} I_{\lambda_{nm}} \equiv \text{probability per unit time that the atom makes the } n \rightarrow m \text{ transition and emits energy in the direction of } I_{\lambda_{nm}} .$$

Stimulated emission is very important in the new science of lasers, which are discussed by Garbuny [43], Brown [44], and Lengyel [45]. Successful application of a laser requires the utilization of a system of molecules or atoms in excited states in such a manner that the stimulated emission processes (obtained through population inversion) are enhanced while the energy losses are kept low enough to produce an amplification greater than unity.

## Local Thermodynamic Equilibrium

Through the concept of local thermodynamic equilibrium (LTE), established by Kirchoff, it is possible to relate the emission coefficient  $j_\lambda$  to the absorption coefficient  $\kappa_\lambda$  and to the Planck blackbody intensity of radiation  $B_\lambda(T)$ . This quantity,  $B_\lambda(T)$ , will be derived in terms of the transition probabilities  $A_{nm}$ ,  $B_{nm}$ , and  $B_{mn}$ , defined above.

Kirchoff stated that, in general, any closed system which is not experiencing any change with time is in local thermodynamic equilibrium. That is, in the system the temperature is everywhere constant, and if the system contains more than one substance, it must also be in chemical equilibrium such that there can be no sudden change in internal structure. Furthermore, the system must be in mechanical equilibrium such that there can be no macroscopic movement within the system itself and also between the surroundings and the system.

Kirchoff also postulated that, if  $I_\lambda$  is the intensity at any point in the medium whose refractive index is  $n_\lambda$ , then  $I_\lambda/n_\lambda^2$  is a constant value throughout an enclosure containing the medium. He also stated that the quantity  $j_\lambda/(n_\lambda^2 \kappa_{m,\lambda})$ , which is constant throughout any one enclosure, is the same for the other enclosures at the same temperature and is a universal function of temperature. This relation is expressed by the Kirchoff Law

$$j_\lambda = n_\lambda^2 \kappa_{m,\lambda} B_\lambda(T) . \quad (12)$$

The Planck blackbody function  $B_\lambda(T)$  may be derived in terms of the Einstein transition probabilities  $A_{nm}$ ,  $B_{nm}$ , and  $B_{mn}$  in the following manner as discussed in a previous report [46]. A more detailed treatment of transition probabilities is found in the classic paper by Milne [47]. The total emission (sum of spontaneous plus stimulated) may be expressed as

$$j_{\lambda_{nm}} = \frac{N_n}{\rho} (A_{nm} + B_{nm} I_{\lambda_{nm}}) h \nu_{nm}, \quad (13)$$

where  $\rho$  = density of the medium and  $N_n$  = number of atoms per unit volume in the state  $n$ .

The absorption coefficient may be written as

$$\kappa_{\lambda_{nm}} = \frac{N_m}{\rho} B_{mn} h \nu_{nm}, \quad (14)$$

where  $N_m$  denotes the number of atoms per unit volume in the state  $m$ .

Since an equilibrium between energy states and radiation exists such that, per unit time, as many atoms are raised from state  $m$  to state  $n$  with the absorption of a photon as undergo transition from state  $n$  to state  $m$  with subsequent emission of a photon, it is possible to write

$$N_n (A_{nm} + B_{nm} I_{\lambda_{nm}}) = B_{mn} N_m I_{\lambda_{nm}}. \quad (15)$$

This implies that the processes  $n \rightarrow m$  and  $m \rightarrow n$  occur at equal rates.

The resulting equation for  $I_{\lambda_{nm}}$  is

$$I_{\lambda_{nm}} = \frac{A_{nm}}{B_{nm}} \frac{1}{[(N_m B_{mn}/N_n B_{nm}) - 1]}. \quad (16)$$

From Maxwell-Boltzmann statistics, the following relation applies:

$$\frac{N_m}{N_n} = \frac{g_m}{g_n} \exp \left\{ - [(E_n - E_m)/(kT)] \right\} = \frac{g_m}{g_n} \exp (ch/\lambda_{nm} kT), \quad (17)$$

where  $g_m$  and  $g_n$  are the degeneracies (or statistical weights) of the  $m$  and  $n$  states, respectively, and  $k$  is Boltzmann's constant.

By combining equations (16) and (17), the following equation for the blackbody radiation intensity is obtained:

$$I_{\lambda_{nm}} = \frac{A_{nm}}{B_{nm}} \frac{1}{(B_{nm} g_m / B_{nm} g_n) \exp (ch/\lambda_{nm} kT) - 1} = B_{\lambda_{nm}} (T) \quad (18)$$

Another expression for  $B_{\lambda_{nm}} (T)$  can be obtained from quantum statistics as

$$I_{\lambda_{nm}} = \frac{2c^2 h}{\lambda^5} \frac{1}{[\exp (ch/\lambda kT) - 1]} = \frac{2C_1}{\lambda^5} \frac{1}{[\exp (C_2/\lambda T) - 1]} = B_{\lambda_{nm}} (T) \quad (19)$$

Thus, it may be seen that

$$A_{nm} / B_{nm} = \frac{2c^2 h}{\lambda^5} \text{ and } \frac{B_{mn}}{B_{nm}} \frac{g_m}{g_n} = 1 . \quad (20)$$

By noting that  $\nu\lambda = c$  and

$$B_{\nu} (T) d\nu = - B_{\lambda} (T) d\lambda \text{ or } B_{\nu} (T) = \frac{\lambda^2}{c^2} B_{\lambda} (T) , \quad (21)$$

equation (19) can be written in terms of the frequency as

$$B_{\nu} (T) = \frac{2h\nu^3}{c[\exp (h\nu/kT) - 1]} . \quad (22)$$

Hence, equation (12) can be written as

$$j_{\lambda} = n_{\lambda}^2 \kappa_{m,\lambda} \left\{ \frac{2c^2 h}{\lambda^5} \frac{1}{[\exp (ch/\lambda kT) - 1]} \right\} \quad (23)$$

or in terms of the frequency,  $\nu$ , as

$$j_{\nu} = n_{\lambda}^2 \kappa_{m, \nu} \left\{ \frac{2h\nu^3}{c^2} \frac{1}{[\exp(h\nu/kT) - 1]} \right\} . \quad (24)$$

The Planck blackbody function behaves differently at the two extremes of the spectrum [ $\lambda \rightarrow \infty (\nu \rightarrow 0)$  or  $\lambda \rightarrow 0 (\nu \rightarrow \infty)$ ].

For the first case (Rayleigh-Jeans distribution):

$$B_{\lambda}(T) = 2kTc/\lambda^4 \quad \text{or} \quad B_{\nu}(T) = 2kT\nu^2/c^2 . \quad (25)$$

$\lambda \rightarrow \infty$   $\nu \rightarrow 0$

For the second case (Wein Distribution):

$$B_{\lambda}(T) = (2hc^2/\lambda^5) e^{-hc/\lambda kT} \quad \text{or} \quad B_{\nu}(T) = (2h\nu^3/c^2) e^{-h\nu/kT} . \quad (26)$$

$\lambda \rightarrow 0$   $\nu \rightarrow \infty$

By integrating equation (19) over wavelength or equation (22) over frequency, the following equation results for the intensity of blackbody radiation  $B(T)$ :

$$B(T) = \int_0^{\infty} B_{\lambda}(T) d\lambda = \frac{\sigma_B}{\pi} T^4 , \quad (27)$$

where  $\sigma_B$  is the Stefan-Boltzmann constant and is equal to

$$\sigma_B = \frac{2\pi^5}{15} \frac{k^4}{c^2 h^3} . \quad (28)$$

## Scattering

If there are particles in a medium (having a radius of the order of 100 Å or so), a pencil of radiation of intensity  $I_{\lambda}$  may be weakened not only by absorption, but also by scattering. This scattering phenomenon includes the combined effects of reflection, refraction, diffraction, and transmission of radiation by

the particles. In the exhaust of hydrocarbon-fueled rockets, scattering of radiation by carbon particles whose radii are much less than the wavelength of radiation is characterized by the Rayleigh theory of scattering. In the exhaust of aluminized solid propellant rockets, scattering of radiation by  $\text{Al}_2\text{O}_3$  particles whose radii are of the same order of magnitude as the wavelength of radiation is characterized by the Mie theory of scattering. These theories are described in detail in the sections entitled "Radiation from Carbon Particles" and "Radiation from  $\text{Al}_2\text{O}_3$  Particles," respectively.

The type of scattering considered in this section is single scattering. Problems in multiple scattering, briefly discussed in the section entitled "Radiation from  $\text{Al}_2\text{O}_3$  Particles," involve the scattering of a diffuse field of radiation by very large numbers of particles which in turn absorb and scatter radiant energy originating or scattered from other particles. Also, only coherent scattering, i. e. , scattering in which the absorbed quantum is re-emitted in the same wavelength, the re-emitted and absorbed quanta differing only in direction, is considered in this analysis.

A scattering coefficient  $\sigma_\lambda$  may be used to characterize a medium if, from a pencil of radiation incident on an element of volume of height  $ds$  and area  $dA$ , the amount of energy scattered from it in all directions is

$$\sigma_\lambda \int I_\lambda \cos \theta \, dA \, ds \, d\omega \, d\lambda \, dt , \quad (29)$$

in which a mass scattering coefficient  $\sigma_{m,\lambda}$  can be defined as

$$\sigma_\lambda = \rho \sigma_{m,\lambda} . \quad (30)$$

Since the mass of the element of volume is

$$dm = \rho \cos \theta \, dA \, ds , \quad (31)$$

expression (29) may be written in the form

$$\sigma_{m,\lambda} \int I_\lambda \, dm \, d\omega \, d\lambda \, dt . \quad (32)$$

The radiant energy scattered from a pencil of radiation will contribute to the radiant intensity in another direction. To assess fully the overall effects of scattering, it is necessary to account for the direction of scattering. In general, a phase function,  $p(\cos \Theta)$ , may be defined to account for the directional dependence of scattering. This function may be called a scattering function or an amplitude function and may be written differently [such as  $p(\theta, \phi; \theta', \phi')$ ] by various authors. The coordinate system for the phase function used in this analysis is shown in Figure 2.

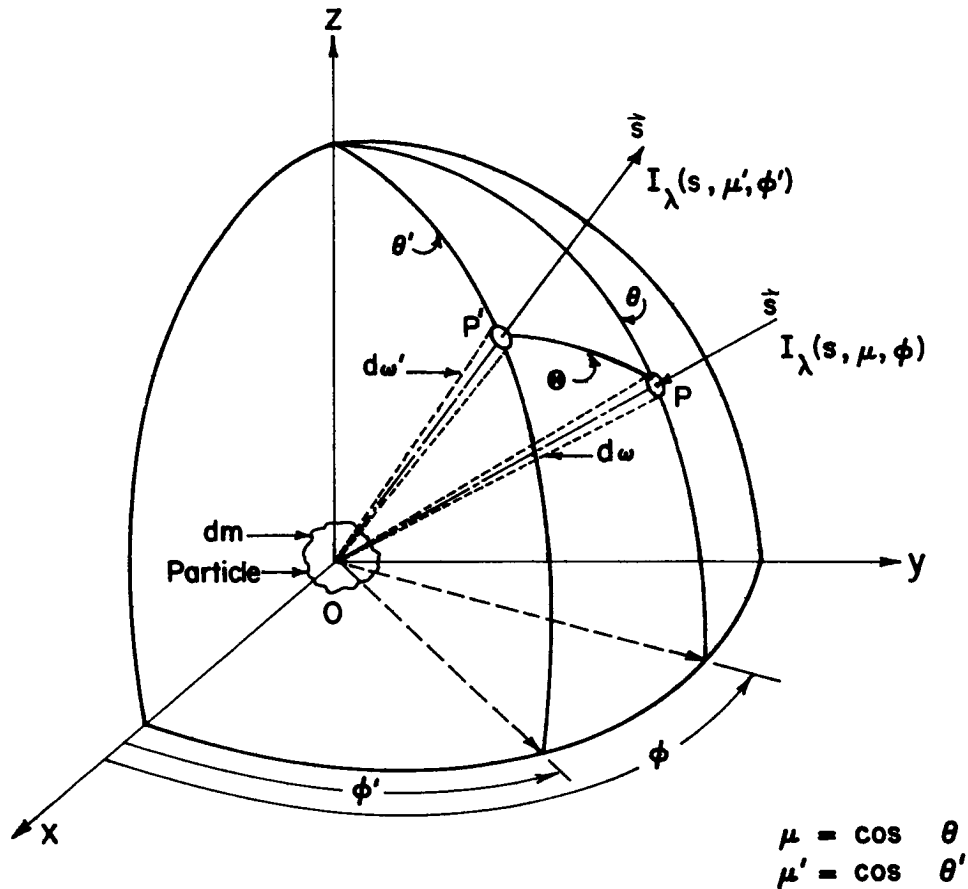


FIGURE 2. SKETCH OF COORDINATE SYSTEM FOR RADIATION SCATTERED BY A PARTICLE

The phase function will be represented in the following manner by observing Figure 2. The rate at which energy is scattered by the element of mass  $dm$  from a pencil of rays of intensity  $I_\lambda(s, \mu, \phi)$  in the direction  $(\mu, \phi)$  and having a solid angle  $d\omega$  with a wavelength interval  $d\lambda$  into a solid angle  $d\omega'$  in the polar direction  $\theta'$  and the azimuthal direction  $\phi'$ , is

$$\sigma_{m,\lambda} I_{\lambda}(s, \mu, \phi) p(\cos \Theta) \frac{d\omega'}{4\pi} d\lambda d\omega dm . \quad (33)$$

The angle  $\Theta$  is the scattering angle between the incident intensity  $I_{\lambda}(s, \mu, \phi)$  and the scattered intensity  $I_{\lambda}(s, \mu', \phi')$  whose cosine may be determined as

$$\cos \Theta = \cos \theta \cos \theta' + \sin \theta \sin \theta' \cos(\phi' - \phi) = \mu \mu' + (1 - \mu^2)^{\frac{1}{2}} (1 - \mu'^2)^{\frac{1}{2}} \cos(\phi' - \phi) \quad (34)$$

where  $\mu = \cos \theta$  and  $\mu' = \cos \theta'$ .

Furthermore, the quantity  $p(\cos \Theta) \frac{d\omega'}{4\pi}$  is a probability function which expresses the probability that a photon in the wavelength interval  $d\lambda$  incident on the element of mass  $dm$ , from a direction within the solid angle  $d\omega$ , characterized by angles  $\theta$  and  $\phi$ , will be deflected into a direction within the solid angle  $d\omega'$  characterized by the angles  $\theta'$  and  $\phi'$ .

The rate of loss of radiant energy from the pencil of rays caused by scattering in all directions may now be written as

$$\sigma_{m,\lambda} d\lambda dm d\omega I_{\lambda}(s, \mu, \phi) \int_0^{4\pi} p(\cos \Theta) \frac{d\omega'}{4\pi} \quad (35)$$

This formulation agrees with expression (32) if

$$\int_0^{4\pi} p(\cos \Theta) \frac{d\omega'}{4\pi} = 1; \quad (36)$$

that is, if the phase function is normalized to unity. However, it must be stated that equation (36) applies only for no absorption and for perfect isotropic scattering; i. e., the magnitude of the radiation intensity is independent of the scattering angle  $\Theta$ .

In the general case where both true absorption and scattering are present, equation (36) is less than unity. An albedo for single scattering  $\bar{\omega}_0$  may therefore be defined as the fraction of radiation lost from an incident pencil of radiation. Hence,  $1 - \bar{\omega}_0$  would be the remaining radiation transformed into other forms of energy or of radiation of other wavelengths. The albedo for single scattering is thus defined as

$$\int_0^{4\pi} p(\cos \Theta) \frac{d\omega'}{4\pi} = \bar{\omega}_o = \frac{\sigma_{m,\lambda}}{\beta_{m,\lambda}} \leq 1, \quad (37)$$

where a mass extinction coefficient  $\beta_{m,\lambda}$  has also been added. This monochromatic mass extinction coefficient is equal to the sum of the monochromatic mass absorption and scattering coefficients, as

$$\beta_{m,\lambda} = \kappa_{m,\lambda} + \sigma_{m,\lambda}. \quad (38)$$

For anisotropic scattering the phase function may be written in terms of the Rayleigh phase function (if the radii of the particles are very small compared to the wavelength) as

$$p(\cos \Theta) = 3/4 (1 + \cos^2 \Theta). \quad (39)$$

It may also be written in terms of the Mie coefficients if the radii of the particles are of the same order of magnitude as the wavelength (discussed in the section entitled "Radiation from  $Al_2O_3$  Particles"). The phase function may also be expanded in a Legendre polynomial series as

$$p(\cos \Theta) = \sum_{n=1}^{\infty} \bar{\omega}_n p_n(\cos \Theta), \quad (40)$$

such as used by Churchill et al. [48], Chu and Churchill [49], and Brown [33].

## Formulation of the Equation of Radiation Transfer

The results of the five previous sections will now be put together to form the equation of radiation transfer, which describes the radiation field in an isotropic medium. This medium absorbs, emits and scatters thermal radiation at a wavelength  $\lambda$ . In deriving this equation, it is necessary to consider four classes of photons, two of which are lost from the radiation field in the direction  $(\mu, \phi)$  by scattering and absorption, and two of which are gained by the radiation field in the direction  $(\mu', \phi')$  by scattering and emission. Figure 2 should be used for the following discussion.

The first class of photons considered is that made up of photons incident upon the element of mass  $dm$ , in time  $dt$ , and in the direction  $(\mu, \phi)$  contained in the solid angle  $d\omega$  which is singly scattered into the solid angle  $d\omega'$  in the direction  $(\mu', \phi')$  by interactions with particles in the mass element  $dm$ . The loss of radiant energy is given as in equation (35) with the change that the phase function  $p(\cos \Theta)$  will be written  $p(\mu, \phi; \mu', \phi')$ , denoting scattering through the angle between the directions  $(\mu, \phi)$  and  $(\mu', \phi')$ . Also, the solid angle  $d\omega'$  is set equal to  $\sin \theta' d\theta' d\phi'$ . Hence, the rate of loss of radiant energy caused by scattering may be written as

$$\frac{\sigma_{m,\lambda}}{4\pi} dm d\lambda d\omega I_{\lambda}(s, \mu, \phi) \int_0^{\pi} \int_0^{2\pi} p(\mu, \phi; \mu', \phi') \sin \theta' d\theta' d\phi' . \quad (41)$$

This relation may be simplified if equation (36) is used to choose a phase function such that

$$\frac{1}{4\pi} \int_0^{\pi} \int_0^{2\pi} p(\mu, \phi; \mu', \phi') \sin \theta' d\theta' d\phi' = 1 . \quad (42)$$

In this case, equation (41) may be written similarly to equation (32) as

$$\sigma_{m,\lambda} I_{\lambda}(s, \mu, \phi) dm d\lambda d\omega . \quad (43)$$

The second class of photons is that incident upon  $dm$  in time  $dt$  and direction  $(\mu, \phi)$  contained in the solid angle  $d\omega$  and absorbed by the individual particles in the mass element  $dm$ . The rate of loss of energy by absorption may be expressed similarly to equation (32), with the mass scattering coefficient being replaced by the mass absorption coefficient as

$$\kappa_{m,\lambda} I_{\lambda}(s, \mu, \phi) dm d\lambda d\omega . \quad (44)$$

The third class of photons considered is that incident on the mass element  $dm$ , in time  $dt$  and in the direction  $(\mu', \phi')$  contained in the solid angle  $d\omega'$ , which is singly scattered in the direction  $(\mu, \phi)$  into the solid angle  $d\omega$ . This change in energy is actually a gain whose rate of change may be expressed as

$$\frac{\sigma_{m,\lambda}}{4\pi} dm d\lambda d\omega \int_0^\pi \int_0^{2\pi} I_\lambda(s, \mu', \phi') p(\mu, \phi; \mu', \phi') \sin \theta' d\theta' d\phi'. \quad (45)$$

The fourth class of photons is that thermally emitted from the particles contained in the mass element  $dm$ , into the solid angle  $d\omega$  in the direction  $(\mu, \phi)$  during the time  $dt$ . This change in energy also represents a gain whose rate of change is expressed as

$$j_\lambda dm d\omega d\lambda. \quad (46)$$

Calculation of this contribution may be modified by considering the element of mass to be located in a perfectly insulated isothermal enclosure which is maintained at a constant equilibrium temperature,  $T$ . Since within the enclosure the radiation field is isotropic and is in equilibrium with its surroundings, the rate of energy which would be emitted from  $dm$  in the wavelength interval  $(\lambda, \lambda + d\lambda)$  and in the direction  $(\mu, \phi)$  contained in  $d\omega$ , upon an instantaneous removal of the enclosure walls, is

$$n_\lambda^2 \kappa_{m,\lambda} B_\lambda(T) dm d\lambda d\omega \quad (47)$$

where equation (12) has been used.

These four classes of photons or changes in energy may be summarized as follows: (1) scattering of a fraction of incident photons into  $d\omega'$ , or redirection of a fraction of incident energy into  $d\omega'$  (loss); (2) absorption of a fraction of incident photons coming from  $d\omega$  or decrease in incident energy (loss); (3) scattering of a fraction of incident photons into  $d\omega$  or redirection of a fraction of incident energy into  $d\omega$  (gain); and (4) emission of photons from the mass element  $dm$  into  $d\omega$  or increase in energy (gain).

The sum of the above changes in energy should be equated to the net change in radiant energy crossing a cylindrical element of cross-section  $dA$  and height  $ds$ . The net change in radiant energy crossing the faces normally in the wavelength interval  $(\lambda, \lambda + d\lambda)$ , in time  $dt$ , and confined to the element of solid angle  $d\omega$  is given by

$$\frac{dI_\lambda}{dt}(s, \mu, \phi) d\lambda d\omega dA dt. \quad (48)$$

The total derivative  $\frac{dI_\lambda}{dt}(s, \mu, \phi)$  may be written as

$$\frac{dI_\lambda}{dt}(s, \mu, \phi) = \frac{\partial I_\lambda}{\partial t}(s, \mu, \phi) + c \frac{\partial I_\lambda}{\partial s}(s, \mu, \phi) . \quad (49)$$

The quantity  $dm$  occurring in equations (43), (44), (45), and (47) may be written as  $dm = \rho ds dA$ , since in this case of radiation normal to the faces of a cylinder, the factor  $\cos \theta$ , appearing in equation (31), may be equated to unity. Also, the quantity  $ds$  may be written as  $c dt$ .

Thus, equation (49) may be set equal to the sum of equations (43), (44), (45), and (47), with the result as

$$\left[ \frac{\partial I_\lambda}{\partial t}(s, \mu, \phi) + c \frac{\partial I_\lambda}{\partial s}(s, \mu, \phi) \right] d\omega d\lambda dt dA = \left\{ -(\sigma_{m,\lambda} + \kappa_{m,\lambda}) I_\lambda(s, \mu, \phi) + n^2 \kappa_{m,\lambda} B_\lambda [T(s)] + \frac{\sigma_{m,\lambda}}{4\pi} \int_0^\pi \int_0^{2\pi} I_\lambda(s, \mu', \phi') p(\mu, \phi; \mu', \phi) \sin \theta' d\theta' d\phi' \right\} c d\omega d\lambda dt \rho dA . \quad (50)$$

Cancelling out the quantities  $c d\omega d\lambda dt dA$  and assuming steady-state conditions along the pencil of rays in the direction of the vector  $\vec{s}$ , the equation of transfer may finally be written as

$$\frac{dI_\lambda}{ds}(s, \mu, \phi) = -(\kappa_\lambda + \sigma_\lambda) I_\lambda(s, \mu, \phi) + n^2 \kappa_\lambda B_\lambda [T(s)] + \frac{\sigma_\lambda}{4\pi} \int_0^\pi \int_0^{2\pi} I_\lambda(s, \mu', \phi') p(\mu, \phi; \mu', \phi') \sin \theta' d\theta' d\phi' , \quad (51)$$

where the substitutions  $\kappa_\lambda = \rho \kappa_{m,\lambda}$  and  $\sigma_\lambda = \rho \sigma_{m,\lambda}$  have been made.

## Solutions to the Equation of Radiation Transfer

The final form of the equation of radiation transfer, equation (51), is an integro-differential equation, the solution of which is quite formidable unless certain simplifying assumptions are made. The following four simplifying assumptions are briefly discussed in this section: (1) use of monochromatic effective absorption coefficient, (2) purely absorbing medium, (3) purely scattering medium, and (4) plane-parallel case.

1. Use of Monochromatic Effective Absorption Coefficient. One simplifying assumption which may be helpful in solving equation (51) is to define a monochromatic effective emission coefficient,  $j_{e,\lambda}$ , as the radiant energy leaving the element of mass  $dm$  in the medium per unit solid angle, per unit wavelength, and per unit of time as

$$j_{e,\lambda}(s) = j_{\lambda}(s) + \frac{\sigma_{\lambda}(s)}{4\pi} \int_0^{\pi} \int_0^{2\pi} I_{\lambda}(s, \mu', \phi') p(\mu, \phi; \mu', \phi') \sin \theta' d\theta' d\phi' \quad (52)$$

where  $j_{\lambda}(s)$  may be defined from equation (12), if the element of mass  $dm$  is in local thermodynamic equilibrium.

The absorption and scattering coefficients are assumed to depend on position  $s$  only. When the direction of propagation  $\vec{s}$  is specified such that there is no dependence of intensity on  $\mu'$  and  $\phi'$ , equation (51) becomes the following inhomogeneous linear first-order differential equation in the one variable,  $s$

$$\frac{dI_{\lambda}(s)}{ds} = -\beta(s) I_{\lambda}(s) + j_{e,\lambda}(s) \quad (53)$$

This equation may be readily solved if both sides are multiplied by the integrating factor  $\exp[\int \beta_{\lambda}(s) ds]$ . Hence the equation takes the form

$$\frac{d}{ds} \left\{ I_{\lambda}(s) \exp\left[\int \beta_{\lambda}(s) ds\right] \right\} = j_{e,\lambda}(s) \exp\left[\int \beta_{\lambda}(s) ds\right] \quad (54)$$

Integration of this equation and division by  $\exp[\int \beta_\lambda(s) ds]$  results in the following solution:

$$I_\lambda(s) = C \exp[-\int \beta_\lambda(s) ds] + \exp[-\int \beta_\lambda(s) ds] \int j_{e,\lambda}(s') \exp[\int \beta_\lambda(s) ds] ds' \quad (55)$$

where  $s'$  is a point along the vector  $\vec{s}$  between  $s = 0$  and  $s = s$ , and the optical thickness  $\tau_\lambda(s)$  is

$$\tau_\lambda(s) = \int_0^s \beta_\lambda(s) ds = \int_0^s (\kappa_\lambda + \sigma_\lambda) ds . \quad (56)$$

The constant  $C$  can be determined from appropriate boundary conditions. Equation (55) is still not a true solution of equation (53) unless the effective emission coefficient  $j_{e,\lambda}$  is a known function of the intensity  $I_\lambda(s)$ . Then equation (55) would be converted into an integral equation for intensity, for which an approximate solution could be obtained by numerical integration.

2. Purely Absorbing Medium. For a purely absorbing medium with very small particles (of the order of the size of molecules), the scattering coefficient  $\sigma_\lambda$  is approximately zero, and the index of refraction  $n_\lambda$  of the medium is approximately unity; hence,  $\beta_\lambda \approx \kappa_\lambda$  and  $j_{e,\lambda} \approx j_\lambda$ . Therefore, equation (53) reduces to

$$\frac{dI_\lambda(s)}{ds} = -\kappa_\lambda B_\lambda [T(s)] + j_\lambda(s) . \quad (57)$$

This equation is sometimes written in the form

$$\frac{1}{\kappa_\lambda} \frac{dI_\lambda(s)}{ds} = -B_\lambda [T(s)] + J_\lambda(s) , \quad (58)$$

where the function  $J_\lambda(s)$  is Chandrasekhar's "source function" defined as

$$J_\lambda(s) = \frac{j_\lambda(s)}{\kappa_\lambda(s)} . \quad (59)$$

The solution to equation (57) or (58), obtained by using an integrating factor similarly to the solution of equation (53), is

$$I_\lambda(s) = C \exp[-\int \kappa_\lambda(s) ds] \\ + \exp[-\int \kappa_\lambda(s) ds] \int j_\lambda(s') \exp[\int \kappa_\lambda(s) ds] ds' . \quad (60)$$

Using the boundary condition,  $I_\lambda(s) = I_\lambda(0)$  at  $s = 0$ , equation (60) becomes

$$I_\lambda(s) = I_\lambda(0) e^{-\tau_\lambda(s,0)} + \int_0^s j_\lambda(s') e^{-\tau_\lambda(s,s')} ds' , \quad (61)$$

where the optical thickness  $\tau_\lambda(s, s')$  is defined as

$$\tau_\lambda(s, s') = \int_{s'}^s \kappa_\lambda(s) ds . \quad (62)$$

It might be mentioned at this point that another quantity, the emissivity at the surface of a medium,  $\epsilon_\lambda(\mu)$ , may be expressed as

$$\epsilon_\lambda(\mu) = \frac{I_\lambda(0, \mu)}{B_\lambda(T)} , \quad (63)$$

where  $\mu = \cos\theta$ . The emissivity is an important factor in the calculation of heating rates from rocket exhausts. In general, the principle of conservation of energy holds such that the following relation is true:

$$1 = \alpha_{\lambda}(\mu) + \rho_{\lambda}(\mu) + t_{\lambda}(\mu) , \quad (64)$$

where  $\alpha_{\lambda}(\mu)$ ,  $\rho_{\lambda}(\mu)$ , and  $t_{\lambda}(\mu)$  are respectively the absorptivity, reflectivity and transmissivity of a particular medium. If Kirchoff's law holds,

$$\alpha_{\lambda}(\mu) = \epsilon_{\lambda}(\mu) . \quad (65)$$

In the present case [equation (57)], if no scattering is present,  $\rho_{\lambda}(\mu)=0$ , and the following expression may be written for the emissivity

$$\epsilon_{\lambda}(\mu) = 1 - t_{\lambda}(\mu) = 1 - e^{-\tau_{\lambda}/\mu} . \quad (66)$$

Hence, equation (63) may be written as

$$I_{\lambda}(0, \mu) = (1 - e^{-\tau_{\lambda}/\mu}) B_{\lambda}(T) , \quad (67)$$

where this value of  $I_{\lambda}(0)$  would be inserted into equation (61) to obtain the intensity of radiation entering the medium.

3. Purely Scattering Medium. One other simplified solution of equation (53) may be obtained if the absorption coefficient  $\kappa_{\lambda}(s)$  is set equal to zero. This may be the case for a purely (isotropically) scattering medium in which  $\beta_{\lambda}(s) = \sigma_{\lambda}(s)$ ,  $\kappa_{\lambda}(s) = j_{\lambda}(s) = 0$ , and the phase function  $p(\mu, \phi; \mu', \phi') = 1$ . Hence, equation (53) takes the form

$$\frac{dI_{\lambda}(s)}{ds} = -\sigma_{\lambda}(s) I_{\lambda}(s) + \frac{\sigma_{\lambda}(s)}{4\pi} \int_0^s \int_0^{\pi} \int_0^{2\pi} I_{\lambda}(s') ds' \sin\theta' d\theta' d\phi' . \quad (68)$$

The solution of this equation is

$$\begin{aligned}
I_{\lambda}(s) &= C \exp[-\int \sigma_{\lambda}(s) ds] \\
&+ \frac{1}{4\pi} \exp[-\int \sigma_{\lambda}(s) ds] \int \sigma_{\lambda}(s') I_{\lambda}(s') \exp[\int \sigma_{\lambda}(s) ds] ds' .
\end{aligned} \tag{69}$$

Applying the boundary conditions  $I_{\lambda}(s) = I_{\lambda}(0)$  at  $s = 0$ , equation (69) becomes

$$\begin{aligned}
I_{\lambda}(s) &= I_{\lambda}(0) e^{-\tau_{\lambda}(s,0)} \\
&+ \frac{1}{4\pi} \int_0^s \int_0^{\pi} \int_0^{2\pi} \sigma_{\lambda}(s') I_{\lambda}(s') e^{-\tau_{\lambda}(s,s')} ds' \sin\theta' d\theta' d\phi' ,
\end{aligned} \tag{70}$$

where the optical thickness  $\tau_{\lambda}(s, s')$  is defined as

$$\tau_{\lambda}(s, s') = \int_{s'}^s \sigma_{\lambda}(s) ds . \tag{71}$$

4. Plane-Parallel Case. One final solution of the equation may be described briefly. This is the plane-parallel case which has certain applications in determining the thermal radiation from a rocket exhaust (by dividing the exhaust into various homogeneous isothermal layers).

In this case the element of length  $ds$  will be represented by  $dz/\mu$ , where  $\mu = \cos \theta$ . The equation of transfer, equation (51), may now be written in the form

$$\begin{aligned}
\mu \frac{dI_{\lambda}(z, \mu, \phi)}{dz} &= -(\kappa_{\lambda} + \sigma_{\lambda}) I_{\lambda}(z, \mu, \phi) + j_{\lambda}(z) \\
&+ \frac{\sigma_{\lambda}(z)}{4\pi} \int_0^{\pi} \int_0^{2\pi} I_{\lambda}(z, \mu', \phi') p(\mu, \phi; \mu', \phi') \sin\theta' d\theta' d\phi'
\end{aligned} \tag{72}$$

If the scattering is isotropic, the integral on the right becomes

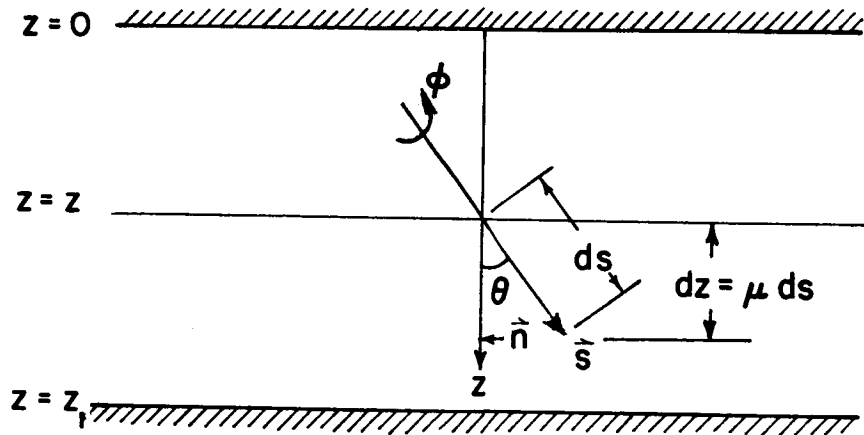
$$\int_0^\pi \int_0^{2\pi} I_\lambda(z, \mu', \phi') \sin \theta' d\theta' d\phi' = 2\pi \int_{-1}^1 I_\lambda(z, \mu' \phi') d\mu' . \quad (73)$$

If two parallel planes or layers,  $z = 0$  and  $z = z_1$ , can be drawn close enough together, as in Figure 3, in a rocket exhaust such that the composition between the two layers is homogeneous and at some averaged temperature, the intensities on the boundaries may be specified as

$$I_\lambda(z, \mu, \phi) = I_\lambda(0, \mu, \phi) \text{ at } z = 0, \mu < 0$$

and (74)

$$I_\lambda(z, \mu, \phi) = I_\lambda(z, \mu, \phi) \text{ at } z = z_1, \mu > 0 .$$



$$\mu = \cos \theta$$

FIGURE 3. SKETCH OF COORDINATE SYSTEM FOR PLANE-PARALLEL CASE

Hence, equation (72) may be written as

$$\frac{dI_\lambda(z, \mu, \phi)}{dz} = -\frac{\beta_\lambda(z)}{\mu} I_\lambda(z, \mu) + \frac{j_{e,\lambda}(z)}{\mu} , \quad (75)$$

where equation (52) has been used. By using the integrating factor

$\exp \left[ \int \frac{\beta_{\lambda}(z) dz}{\mu} \right]$ , the solution of equation (75) may be obtained as

$$I_{\lambda}(z, \mu, \phi) = C \exp \left[ - \int \frac{\beta_{\lambda}(z) dz}{\mu} \right] + \exp \left[ - \int \frac{\beta_{\lambda}(z) dz}{\mu} \right] \int j_{e, \lambda}(z') \exp \left[ \int \frac{\beta_{\lambda}(z) dz}{\mu} \right] \frac{dz'}{\mu} \quad (76)$$

Applying the boundary conditions of equation (74), the solution is

$$I_{\lambda}(z, \mu, \phi) = \begin{cases} I_{\lambda}(z_1, \mu, \phi) \exp \left[ - \int_z^{z_1} \frac{\beta_{\lambda}(z) dz}{\mu} \right] + \int_z^{z_1} j_{e, \lambda}(z') \exp \left[ \int_z^{z'} \frac{\beta_{\lambda}(z) dz}{\mu} \right] \frac{dz'}{\mu} & \text{for } 0 \leq \mu \leq 1 \\ I_{\lambda}(0, \mu, \phi) \exp \left[ - \int_0^{z_1} \frac{\beta_{\lambda}(z) dz}{\mu} \right] + \int_0^{z_1} j_{e, \lambda}(z') \exp \left[ \int_z^{z'} \frac{\beta_{\lambda}(z) dz}{\mu} \right] \frac{dz'}{\mu} & \text{for } 1 \leq \mu \leq 0. \end{cases} \quad (77)$$

$$(78)$$

There are many other ways (including numerical approximations) in which the equation of transfer may be solved. However, it is not the purpose of this report to go into all the detailed solutions to the equation of transfer by various authors. Rather, it is to study the theories of absorption and scattering and attempt to predict emissivities of the rocket exhausts so that thermal radiation from the exhausts may be calculated.

## GASEOUS RADIATION

This section presents gaseous radiation, including band models and absorption coefficients, from liquid propellant rocket exhausts. The principal gaseous molecular emitters in exhausts of hydrocarbon-fueled engines such as

the H-1 and F-1 are CO<sub>2</sub>, CO, and H<sub>2</sub>O, while only H<sub>2</sub>O emits appreciably in the exhausts of hydrogen-fueled engines such as the J-2 and RL-10. Gaseous HCl is also an emitter in solid propellant motor exhausts in which NH<sub>4</sub>ClO<sub>4</sub> is used as the oxidizer in the propellant. Gaseous radiation from molecules is a result of electronic energy transitions in the visible and the ultraviolet wavelength region, vibration-rotation energy transitions in the near infrared region, and pure rotational energy transitions in the far infrared region. This type of radiation is emitted in the form of band spectra as opposed to radiation from hotter solid particles such as carbon or Al<sub>2</sub>O<sub>3</sub>, which is emitted over a continuous spectra.

The general subject of gaseous radiation has been discussed by hundreds of authors in the last 50 or so years, and no attempt will be made to give a comprehensive treatment of it here. Instead, a generalized review of its important aspects as applied to rocket exhausts (such as determination of spectral absorption coefficients) will be given. Excellent references which review problems in this area include Yossa [50], Huffaker [4 and 51], Ferriso et al. [52], Thompson [53], Simmons [54], and Ritland et al. [55]. In this section the radiation from an accelerating charge will first be mentioned; the shape and broadening of spectral lines will then be discussed; the concept of band models will then be introduced; and finally solutions to the equation of transfer as they apply to radiation from liquid propellant engine exhausts will be treated.

## Radiation from an Accelerated Charge

In this section the radiation from a charged particle which is accelerated in an external field will be discussed. An expression for the spectral intensity will be determined consequently as a function of frequency and electronic charge. This expression, known as the Lorentz line shape, will be further discussed in the next section on shape and broadening of spectral lines. The analysis in this section is based upon classical electrodynamical theory, of which excellent treatments are by Jackson [56], Panofsky and Phillips [57], Heitler [58], Reitz and Milford [59], Marion [60], and Sommerfeld [61].

The equation of motion for a charged particle which is being accelerated in the  $\vec{x}$  direction by a driving or external force may be written as

$$m\vec{x} = \vec{F}_{\text{EXTERNAL}} + \vec{F}_{\text{SELF}} + \vec{F}_{\text{ELASTIC}} \quad (79)$$

The elastic or restoring force on the charge is

$$\vec{F}_{\text{ELASTIC}} = - G \vec{x}, \quad (80)$$

where  $G$  is the force constant. The self-force on the charge (the force which the field produced by the charge exerts on the charge itself) is

$$\vec{F}_{\text{SELF}} = \frac{2}{3} \frac{e^2}{c^3} \ddot{\vec{x}}, \quad (81)$$

where  $e$  is the electronic charge on the particle. The external or Lorentzian force is

$$\vec{F}_{\text{EXTERNAL}} = e \vec{E} + \frac{e}{c} (\vec{u} \times \vec{B}), \quad (82)$$

where  $\vec{u}$  is the velocity of the charged particle,  $\vec{E}$  is the electric field vector, and  $\vec{B}$  is the magnetic field vector.

The speed of light  $c$  has been introduced into the second term on the right-hand side of equation (82) corresponding to the Gaussian system of units, to show that this term may be neglected when  $u \ll c$ .

If the charged particle is moving with simple harmonic motion, the quantity  $\ddot{\vec{x}}$  in the self-force term [equation (81)] may be approximated by differentiating the expression

$$\ddot{\vec{x}} = - \frac{G}{m} \vec{x} = - \omega_0^2 \vec{x} \quad (83)$$

as

$$\ddot{\vec{x}} = - \omega_0^2 \dot{\vec{x}}, \quad (84)$$

where  $\omega_0$  is the natural frequency of vibration (equal to  $2\pi \nu_0$ ).

The external force will thus be written in terms of a harmonic function

$$\vec{F}_{\text{EXT}} = e \vec{E}_0 e^{-i\omega t} . \quad (85)$$

By making the above substitutions, the equation of motion for the charged particle now becomes

$$\vec{x} + \gamma \dot{\vec{x}} + \omega_0^2 \vec{x} = \frac{e \vec{E}_0}{m} e^{-i\omega t} , \quad (86)$$

where

$$\gamma = \frac{2}{3} \frac{e^2}{c^3} \frac{\omega^2}{m} , \quad (87)$$

and the second term on the left-hand side of equation (86) is thus a dissipative or radiation damping term.

The solution of equation (86) may be written as

$$\vec{x} = \vec{E}_0 \frac{e}{m} \left( \frac{1}{\omega_0^2 - \omega^2 - i\omega\gamma} \right) e^{-i\omega t} . \quad (88)$$

The acceleration of the charge is thus

$$\ddot{\vec{x}} = \vec{E}_0 \frac{e}{m} \left( \frac{-\omega^2}{\omega_0^2 - \omega^2 - i\omega\gamma} \right) e^{-i\omega t} . \quad (89)$$

The acceleration of the charge can be related to the electric field by the following equation

$$\vec{E} = \frac{e}{c^2 r^3} [ \vec{r} \times (\vec{r} \times \ddot{\vec{x}}) ] , \quad (90)$$

where  $\vec{r}$  is the distance from the radiation field to the accelerating charge.

Through the use of vector calculus, it can be shown that the term in brackets in equation (90) reduces to  $\vec{x} \cdot \ddot{\vec{x}}$  such that the above equation becomes

$$\vec{E} = \frac{e}{c^2} \frac{\ddot{\vec{x}}}{r} \quad (91)$$

With the insertion of equation (89) for  $\ddot{\vec{x}}$ , equation (91) becomes

$$\vec{E} = \frac{e^2}{c^2 r m} \frac{(-\omega^2)}{(\omega_0^2 - \omega^2 - i\omega\gamma)} \vec{E}_0 e^{-i\omega t} \quad (92)$$

The above case of an electronic charge which vibrates harmonically because of an external electromagnetic field, i. e., equation (86), is important in the classical theories of absorption, scattering, and dispersion of radiation, and consequently is discussed in more detail in the next section. In the case below, the intensity of radiation corresponding to a bound electronic charge following a transient disturbing impulse, but not experiencing a forced vibration, is derived. This case corresponds to the classical theory of spectral emission. In this manner, the equation of motion, equation (86), may be written as

$$\ddot{x} + \gamma\dot{x} + \omega_0^2 x = 0, \quad (93)$$

where the vector notation has been dropped for convenience.

The solution to this equation yields a harmonic oscillation with amplitude  $x_0$ , decaying in time as  $e^{-(\gamma/2)t}$  in the following form:

$$x = x_0 e^{-(\gamma/2)t} e^{-i\omega_0 t} \quad (94)$$

The acceleration of the charge is thus

$$\ddot{x} = x_0 \left(-\frac{\gamma}{2} + i\omega_0\right)^2 e^{-(\gamma/2)t} e^{-i\omega_0 t} \quad (95)$$

Hence, the radiation field is

$$E = \frac{e}{c^2 r} \ddot{x} = \frac{e}{c^2 r} \left[ x_0 \left(-\frac{\gamma}{2} + i\omega_0\right)^2 e^{-(\gamma/2)t} e^{-i\omega_0 t} \right], \quad (96)$$

which is a function of the natural frequency  $\omega_0$ .

The above equation may be written in the same form as equation (94), as

$$E = E_0 e^{-(\gamma/2)t} e^{-i\omega_0 t} . \quad (97)$$

Since the oscillating charge has been radiation damped, the emitted radiation intensity will not be monochromatic, but will be broadened and composed of an infinite number of harmonic waves. The line width of this intensity distribution may be obtained by expanding the electric field, equation (97), in a Fourier series as

$$E = \int_{-\infty}^{+\infty} E_{\omega} e^{-i\omega t} d\omega , \quad (98)$$

where

$$E_{\omega} = \frac{E_0}{2\pi} \int_0^{\infty} e^{-i\omega_0 t} e^{-(\gamma/2)t} e^{i\omega t} dt . \quad (99)$$

Integration of the above equation yields the relation

$$E_{\omega} = \frac{E_0}{2\pi} \frac{1}{i(\omega - \omega_0) - \gamma/2} . \quad (100)$$

The radiation intensity distribution,  $I_{\omega}$ , may now be written as

$$I_{\omega} \approx |E_{\omega}|^2 = I_0 \frac{\gamma}{2\pi} \frac{1}{(\omega - \omega_0)^2 + \gamma^2/4} . \quad (101)$$

The exact relationship between the electric field and the radiant intensity is expressed by means of the Poynting vector, as discussed in the next section, subtitle "Rayleigh Scattering Theory."

Equation (101) may be normalized such that

$$I_0 = \int_{-\infty}^{+\infty} I_{\omega} d\omega . \quad (102)$$

The parameter  $\gamma$  in equation (101) represents the frequency width at half intensity (sometimes called "natural" half-width) and is written as in equation (87), as

$$\gamma = \Delta\omega_h = \frac{2}{3} \frac{e^2}{c^3} \frac{\omega_o^2}{m} . \quad (103)$$

Equation (101) is known as the Lorentz line shape, further discussions of which are given in the next two sections on shape and broadening of spectral lines and band models and absorption coefficients.

## Shape and Broadening of Spectral Lines

Before a description of the several types of broadening of spectral lines is given, it is necessary to summarize and discuss briefly the monochromatic energy transitions between discrete energy levels of a molecule. The total energy,  $E$ , of a molecule may be given according to Baker et al. [71] as

$$E = E_T + E_E + E_R + E_V + E_{ES} + E_{NS} + E_{IE} , \quad (104)$$

where  $E_T$  represents the translational energy;  $E_E$  is the sum of the orbital energies of the electrons;  $E_R$  is the sum of the rotational energies;  $E_V$  is the sum of the vibrational energies;  $E_{ES}$  is the sum of the electron-spin energies;  $E_{NS}$  is the sum of the nuclear-spin energies; and  $E_{IE}$  is the sum of the interaction energies among these modes.

Since translational energies in equation (104) occur in a continuum, any value is possible. However, all of the other energies are quantized and must be specified by quantum numbers. For a polyelectronic atom, these quantum numbers are usually designated as the principal quantum number,  $n$ , (measures extent of electron "cloud"), azimuthal quantum number,  $l$ , (specifies electron angular momentum), magnetic quantum number,  $m_l$ , (gives the component of angular momentum in a given direction), and spin quantum number,  $m_s$ , (gives the component of spin,  $s$ , in a given direction). For a molecule, at least two other quantum numbers ( $J$ , the rotational quantum number, and  $v$ , the vibrational quantum number) must be considered.

To understand adequately the fine structure of the infrared molecular spectrum, it is necessary to consider three types of molecular models. The first of these is the anharmonic oscillator which is characterized by a parabolic potential curve. The second is the nonrigid rotator which represents a rotating system composed of two mass points connected by a massless spring. The third model is the vibrating rotator (or rotating oscillator) in which it is assumed that both rotation and vibration can take place simultaneously. Since the third model represents a combination of the other two, only the energy level of this vibrating rotator is given. This is

$$\begin{aligned} \frac{E}{hc}(\nu, J) = & \omega_e \left(v + \frac{1}{2}\right) - \omega_e x_e \left(v + \frac{1}{2}\right)^2 + \omega_e y_e \left(v + \frac{1}{2}\right)^3 + \dots \\ & + B_e J(J+1) - \alpha_e \left(v + \frac{1}{2}\right) J(J+1) - D_e J^2(J+1)^2 - \beta_e \left(v + \frac{1}{2}\right) J^2(J+1)^2 + \dots \end{aligned} \quad (105)$$

The terms on the right-hand side of the first line represent the energy caused by the anharmonic oscillators; the  $B_e$  and  $D_e$  terms on the second line represent the energy associated with the nonrigid rotations; and the  $\alpha_e$  and  $\beta_e$  terms represent coupling energy associated with the vibrating rotations. The quantities  $x_e$ ,  $y_e$ ,  $B_e$ ,  $D_e$ ,  $\alpha_e$ , and  $\beta_e$  are constants defined by Herzberg [62].

The analysis of energy quantization as applied to atoms and molecules, of course, belongs in the realm of atomic and molecular spectroscopy, the details of which will not be given here. Excellent references in this area are the three books by Herzberg [62, 63, 64], and the books by Penner [65], Griem [66], Bauman [67], Barrow [68], Bond et al. [69], and Harrison et al. [70].

As the temperature of a molecule rises, the translational energy is first increased; then the rotational states, the vibrational states, and finally the electronic states become excited. The quantized energy changes correspond to the theory of Bohr as stated by equation (7) (repeated for convenience) as

$$E_n - E_m = h\nu_{nm} \quad (7)$$

Since the rotational energy change,  $E_n - E_m$ , is comparatively small (of the order of hundredths of an electron volt), the frequency  $\nu_{nm}$  is small; hence this type of energy transition occurs only in the far infrared. Vibrational

energy changes (and associated frequencies) are slightly larger (of the order of tenths of an electron volt); therefore, this type of transition occurs at a slightly shorter wavelength (near infrared). Electronic energy changes (and frequencies) are the highest; hence, this wavelength is the shortest, and these changes occur in the visible and ultraviolet region. These three types of energy level transitions may be seen in Figure 4, which shows a typical energy level diagram for upper and lower excited electronic states in a diatomic molecule.

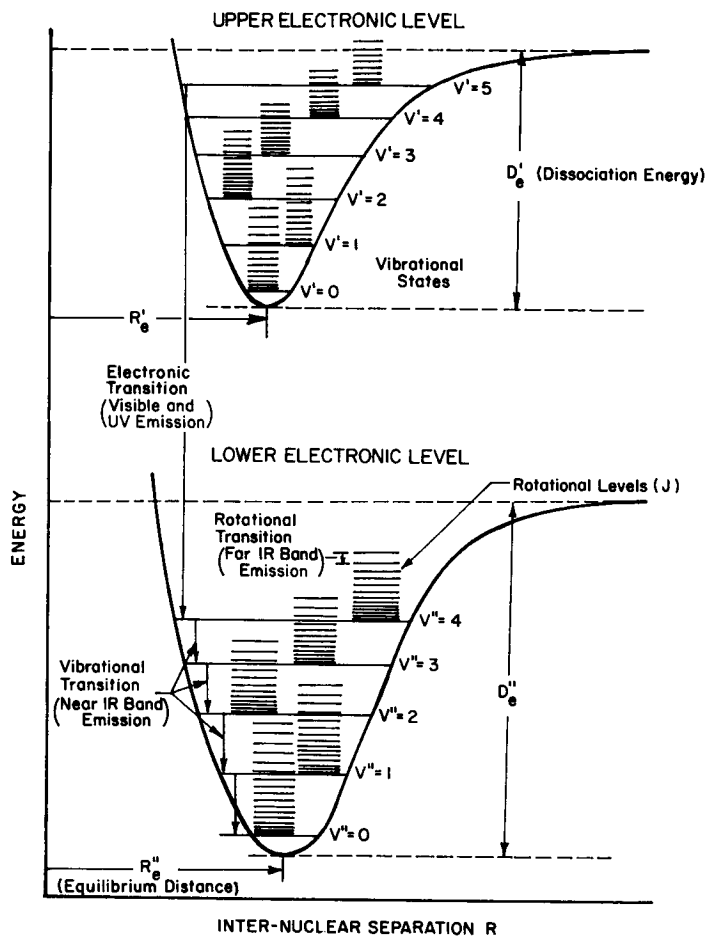


FIGURE 4. ENERGY LEVEL TRANSITIONS FOR A DIATOMIC MOLECULE

For atoms in a monatomic gas (uncombined atoms), the vibrational and rotational energy states are absent, and the spectrum is merely a sharp, discontinuous series of individual lines. For molecules in a more dense gas (such as a rocket exhaust), the spectrum is made up of a nearly infinite number of very closely spaced lines (or bands). This band emission of polyatomic gases

is concentrated mostly in the infrared part of the spectrum, representing vibrational-rotational and purely rotational transitions. The radiative intensity from rocket exhausts in the infrared is consequently much higher than the intensity observed in the visible and ultraviolet regions.

Since it is known that gaseous emission and absorption do not take place at a single frequency but occur in a broadened portion of the spectrum, it is necessary to establish the factors which bring about this broadening phenomenon and to discuss briefly some of the types of broadening. In general, there are three major types of broadening of spectral lines: (1) natural-line broadening (the finite lifetime of initial and final states caused by spontaneous emission), (2) Doppler broadening (random Doppler shift as a result of the thermal motion of the molecules), and (3) pressure broadening (perturbations or displacement of energy levels during collisions of the molecules with adjacent molecules). Each of the above processes is discussed below based upon the references of Marganeau [72,73], Marganeau and Watson [74], Marganeau and Lewis [75], Ch'en and Takeo [76], Breene [77,78], Aller [79], Thompson [80], Mitchell and Zemansky [81], Seshadri and Jones [82], Garbuny [43], and Benedict et al. [83].

1. Natural-Line Broadening. A spectral line emitted by an atom is not infinitely sharp because of the phenomenon of radiation damping. (See section entitled "Gaseous Radiation," subsection "Radiation from an Accelerated Charge.") By this damping process, an oscillating, and hence radiating, electronic charge is continuously losing radiant energy, and its amplitude of oscillation decreases as the charge continues to oscillate about its natural frequency,  $\omega_0$ . However, the damped oscillation is not monochromatic, as shown by the Lorentz profile of intensity, equation (101) (repeated here for convenience) as

$$I_{\omega} = I_0 \frac{\gamma}{2\pi} \frac{1}{(\omega - \omega_0)^2 + \gamma^2/4} \quad (101)$$

The quantity,  $\gamma$ , which equals  $\Delta\omega_h$ , the natural half-width, is also equal to the reciprocal of the time constant,  $\tau$ . This equality comes from Heisenberg's uncertainty principle in quantum theory

$$\Delta E \Delta t = \hbar \Delta\omega \tau = \frac{\hbar}{2\pi} \Delta\omega \tau = \frac{\hbar}{2\pi} \quad (106)$$

as applied to the transition from an excited (upper) level  $E_n$  to the ground state  $E_1$ . In this manner there is an uncertainty of energy  $\Delta E$  (and hence of frequency  $\Delta\omega$ ) associated with a finite lifetime  $\tau$  of the upper level. The lifetime  $\tau$  is very large for the ground state of an atom and very small ( $\sim 10^{-8}$  sec) for an excited state. The energy level corresponding to the ground state  $E_1$  will be infinitely sharp, but the excited states will have a natural width. The actual lifetime in the excited state will not be any longer than the natural lifetime, and according to equation (106), the half-width of the observed spectral line cannot be any less than its natural width  $\Delta\omega$ .

It must also be mentioned that, if a transition occurs from a higher level with a lifetime  $\tau_3$  to a lower level not in a ground state, but one with a lifetime  $\tau_2$ , the resulting uncertainties must add up to

$$\Delta E = \Delta E_3 + \Delta E_2 \quad . \quad (107)$$

In this case  $E_1$  would represent the ground state. Thus, the resulting half-width is

$$\Delta\omega_{32} = \gamma_{32} = \frac{1}{\tau_3} + \frac{1}{\tau_2} = A_{32} + A_{31} + A_{21} \quad , \quad (108)$$

where the  $A_{nm}$  are the Einstein transition probabilities originally discussed in the section entitled "Equation of Radiation Transfer." The natural width  $\nu_{32}$  is thus affected by the lifetime of the upper state as well as that of the lower state.

2. Doppler Broadening. Doppler broadening is a major cause of broadening in rocket exhaust gases (especially at very low pressures) and is associated with the thermal motion of the atoms in the gas. When an oscillating charge at frequency  $\nu_0$  moves with velocity  $v_x$  in a direction  $x$  to the observer, the emitted wavetrains arrive at a higher frequency  $\nu$ . This frequency, by virtue of Doppler's principle, is

$$\nu = \nu_0 \left( 1 - \frac{v_x}{c} \right) \quad . \quad (109)$$

From equilibrium statistical mechanics, the fractional number of molecules  $dn/n$  moving with linear velocities between  $v_x$  and  $v_x + dv_x$  may be written in a Maxwell-Boltzmann distribution as

$$\frac{dn}{n} = \left( \frac{m}{2\pi kT} \right)^{\frac{1}{2}} \left[ \exp \left( \frac{-mv_x^2}{2kT} \right) \right] dv_x, \quad (110)$$

where  $n$  is the total number of molecules per volume, and  $m$  equals the mass per molecule. The intensity distribution,  $I_\nu$ , within the spectral line is proportional to the number of molecules radiating at a frequency,  $\nu$ , and can be written as

$$I_\nu d\nu = I_0 \exp \left[ \frac{-mc^2}{2kT} \left( \frac{\nu - \nu_0}{\nu_0} \right)^2 \right] d\nu = I_0 \exp[-\psi(\nu - \nu_0)^2] d\nu, \quad (111)$$

where

$$I_0 = \left( \frac{mc^2}{2\pi kT\nu_0^2} \right)^{\frac{1}{2}}. \quad (112)$$

This Doppler broadening of line intensity thus follows a Gaussian distribution of frequencies of the form  $\exp[-\psi(\nu - \nu_0)^2]$ . The Doppler width is thus determined as the increment in frequency for which  $I = I_0/2$  and is given by

$$\Delta\nu_h = 2\nu_0 \left[ (2 \ln 2) \frac{kT}{mc^2} \right]^{\frac{1}{2}} \quad (113)$$

It might be mentioned that the Doppler shift principle has been used, together with a laser beam, to measure velocities of particles in wind tunnels. Discussions of this technique are reported by Robertson et al. [84], Foreman et al. [85], and James, Seifert and Babcock [86].

3. Pressure Broadening. Pressure broadening includes several types of broadening which involve interactions between randomly emitting atoms and molecules, the interactions in each type all increasing with increased pressure. The two main types of pressure broadening discussed in this section are collision broadening (including resonance broadening) and Stark broadening. Two general theories, the statistical theory and the impact (or interruption) theory, are associated with pressure broadening and are briefly discussed in this section.

a. Collision broadening. Collision broadening represents the shortening of an oscillator lifetime by a collision between some light emitting (excited) atom (or molecule) and another atom or "perturber." In considering these interactions between an excited atom and its neighboring atoms, a distinction between the type of neighboring atom (or molecule) must be made. The surrounding atoms may be either of the same kind as the excited atoms or may be of a different kind.

If the surrounding atoms are of the same kind, the possibility of resonance (energy of excitation of one being absorbed by the other) may exist. In this manner, when an excited atom passes by an unexcited atom of the same kind, a finite probability exists that the excitation energy will be transferred from the first to the second atom, without the intervention of radiation. This consequently results in a reduction of the excited atom's lifetime and a corresponding broadening of the line emitted.

By classical description of this resonance, each atom is usually replaced by an oscillator with a single natural frequency,  $\nu_0$ , and a coupling force is then introduced between two dipoles. This coupling force has the form

$$F_{ij} = \frac{\text{Const}}{r_{ij}^4} , \quad (114)$$

where  $r_{ij}$  is the distance between the  $i^{\text{th}}$  and  $j^{\text{th}}$  oscillator. Since, under the same interaction force  $F_{ij}$ , two unlike atoms result in an inverse 6<sup>th</sup> power dependence (instead of an inverse 4<sup>th</sup> power dependence for the like atoms) on the atomic separation, greater broadening will result from interactions with like atoms (or molecules). However, it is nearly always assumed that the number of foreign (different) atoms or molecules surrounding an excited atom is far greater than the number of like atoms surrounding the excited atom, so that resonance broadening can usually be neglected.

In the rest of this discussion on collision broadening, it will be assumed that the broadening is caused by unlike atoms (foreign gas) interacting with the excited atoms. The original analysis of this type of broadening was discussed by Lorentz [87]. He assumed that, while an atom is being forced to vibrate by the incident light wave, its vibrations are suddenly stopped as the atom collides with the other atoms and the energy becomes wholly kinetic. This type of process will reduce the total intensity of the line in addition to broadening its shape. The spectrum of the electrical oscillations is given by the same relation for radiation damping, except for the increased factor,  $\Gamma$ , as

$$I_{\omega} = I_0 \frac{\Gamma}{2\pi} \frac{1}{(\omega - \omega_0)^2 + \Gamma^2/4} \quad (115)$$

The parameter  $\Gamma$  is defined as

$$\Gamma = \gamma_{\text{TR}} + \gamma_{\text{COLL}} \quad (116)$$

where  $\gamma_{\text{TR}}$  is the spontaneous transition probability, and  $\gamma_{\text{COLL}}$  is a collision frequency given by kinetic theory as

$$\gamma_{\text{COLL}} = 6.8 \times 10^{10} d_1 d_2 \left( \frac{1}{M_1} + \frac{1}{M_2} \right)^{\frac{1}{2}} P(T)^{-\frac{1}{2}} \quad (117)$$

Here,  $d_1$  and  $d_2$  are the optical collision diameters of the molecules in  $\text{\AA}$ ;  $M_1$  and  $M_2$  are molecular weights in g/mole;  $P$  is the partial pressure in atm; and  $T$  is the absolute temperature in degrees K.

For similar intensities and line widths, the collision (Lorentz shape) intensity curve has higher values of  $I/I_{\text{max}}$  (plotted versus  $\nu$ ) in the wings than the Doppler (Gaussian shape) curve. Also, it is known that at high altitudes (low pressures) and at high temperatures, the Doppler half-width is considerably higher than the collision half-width. Ritland [55] presents a table which shows that, for  $\text{CO}_2$  in the  $4.3\text{-}\mu$  band at sea level and at  $273^\circ \text{K}$ , the ratio of Doppler half-width to collision half-width is only  $1/30$ , while at 200,000 feet and at  $2000^\circ \text{K}$ , this ratio increases to 360. For  $\text{H}_2\text{O}$  in the  $2.7\text{-}\mu$  band at sea level and at  $273^\circ \text{K}$ , the Doppler half-width - collision half-width ratio is only  $1/19$ , while at 200,000 feet and at  $2000^\circ \text{K}$  this ratio increases to 600. These ratios of Doppler half-width to Lorentz half-width are plotted in Figures 5 and 6 for  $\text{H}_2\text{O}$  and  $\text{CO}_2$ , respectively.

b. Stark broadening. Stark broadening is pressure broadening caused by the electric polarization of radiation by the electric fields of neighboring atoms. This type of broadening, which is very important in plasmas and ionized rocket exhausts, was originally investigated by Stark [86]. Stark determined experimentally that spectral lines are split in the presence of electric fields, and that excited atoms and their neighbors exert a distribution of electric perturbations on each other. He found that, since a uniform electric field with strength,  $E$ , would split a spectral line into its so-called Stark components, a

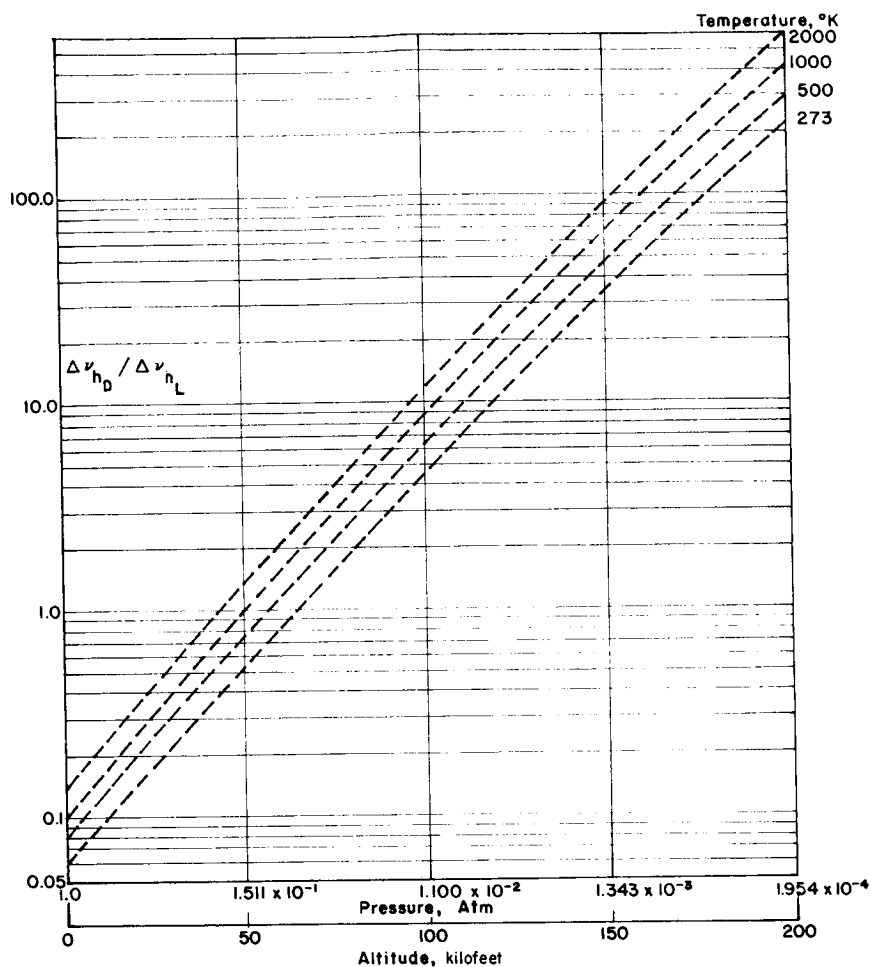


FIGURE 5. RATIO OF DOPPLER TO LORENTZ HALF-WIDTHS AS A FUNCTION OF ALTITUDE OR PRESSURE FOR  $H_2O$  IN  $2.7\text{-}\mu$  BAND AT VARIOUS TEMPERATURES

non-uniform field would produce a whole series of Stark components, and thus result in broadening of the line.

Holtzmark [87], on the basis of the Stark effect, developed a theory of line broadening which assumed that the radiating atoms are in the electric fields of ions, dipoles, or quadrupoles. On the basis of this theory, when a spectral line is under the influence of a given field, the line is perturbed in some predictable manner. That is, it may be split (linear Stark effect) or shifted (quadratic Stark effect).

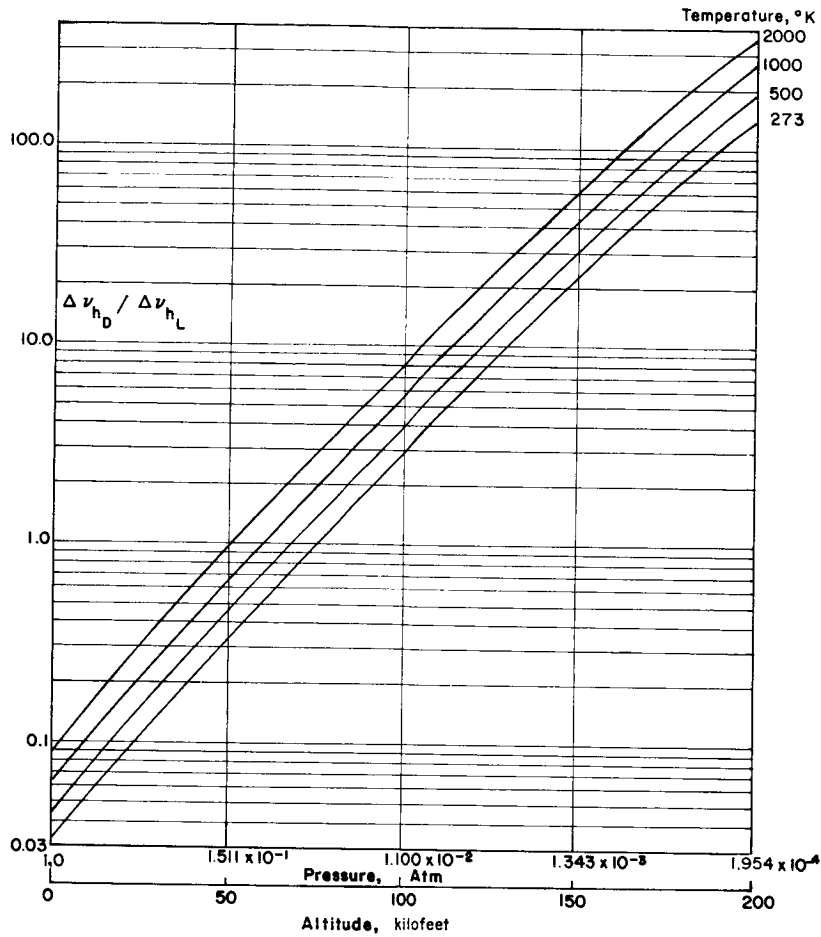


FIGURE 6. RATIO OF DOPPLER TO LORENTZ HALF-WIDTHS AS A FUNCTION OF ALTITUDE OR PRESSURE FOR  $\text{CO}_2$  IN  $4.3\text{-}\mu$  BAND AT VARIOUS TEMPERATURES

The linear Stark effect vanishes for all atoms except the hydrogen atom. For the hydrogen atom a line under the effect of an electric field,  $E$ , splits into two components with a frequency interval  $\Delta\nu_{\text{ST}}$  of

$$\Delta\nu_{\text{ST}} = \frac{3h}{8\pi^2 m_e} n_k E = aE, \quad (118)$$

where  $n_k$  is a quantum number and  $a$  is the split width per unit strength. When a large number of atoms which have an average field,  $E_D$ , from the surrounding dipoles is involved, the broadened line has a half-width of

$$\Delta\nu_h = \frac{\gamma}{2\pi} = aE_D, \quad (119)$$

The line shape is similar to that in Lorentz-type broadening:

$$I_\nu = \frac{\gamma I_0}{(\omega - \omega_0)^2 + \gamma^2/4} = \frac{2I_0}{\pi} \frac{aE}{4(\nu - \nu_0)^2 + (aE)^2} \quad (120)$$

The half-width is thus determined as

$$\Delta\nu_h = aE_D = 4.54 a n \mu, \quad (121)$$

where  $\mu$  is the dipole moment and  $n$  is the number concentration of the molecules.

For molecules having a quadrupole moment  $q$  in a field of strength,  $E_q$ , the Holtmark theory predicts the half-width to be

$$\Delta\nu_h = 0.67 a E_q = 5.52 q n^{4/3} a. \quad (122)$$

For ions of number density  $n_i$ , in a field of strength,  $E_i$ , the Holtmark theory gives for the half-width

$$\Delta\nu_h = 1.25 a E_i = 3.25 e n_i^{2/3} a. \quad (123)$$

The quadratic Stark effect appears in non-hydrogen-like spectra, and it involves a shift of the line (rather than a split) which is determined as

$$\delta\nu = \nu - \nu_0 = bE^2. \quad (124)$$

The quadratic Stark effect may be analyzed classically if it is assumed that the application of the electric field induces a polarization,  $P$ , proportional to the electrical field. In this case the polarization is

$$P = \beta E , \quad (125)$$

where  $\beta$  is the polarizability of the atom. The work performed in producing an increment of polarization  $dP$  is therefore

$$\Delta W = \int_0^E \beta E \, dP = \frac{1}{2} \beta E^2 , \quad (126)$$

which implies a quadratic dependence on the electric field,  $E$ .

c. Statistical theory. The statistical theory of broadening is used to analyze the broadening phenomenon associated with an emitting atom or molecule which is placed in the midst of an aggregation of broadeners under static conditions. This theory assumes that the atoms or molecules are stationary and account is taken of only the static distribution of energy levels during encounters. The broadening by coupling (Stark effect) results from the statistical distribution of distances which various neighboring atoms may assume with respect to the emitting atom during times presumed to be long in comparison with that of the emission process.

In analyzing the statistical theory, the Franck-Condon potential curves should be considered. These curves merely represent two electronic energy states of a radiating atom plotted versus distance  $r$  from another atom. Where the atoms are at large distances from each other, the two energy levels are undisturbed; however, when the atoms are moved closer together, a strong repelling force is exerted on each atom. In general, the energy difference  $\Delta E$  between the two states is not constant so that the emitted frequency depends on the instantaneous position,  $r$ , of the excited atom. If the atom (or molecule) radiates when the separation is  $r$ , the net change in energy,  $\Delta E$ , is

$$\Delta E = h\nu = E_2(r) - E_1(r) . \quad (127)$$

This energy differs from that ordinarily radiated since  $E_2 - E_1$  will change with  $r$  as a result of perturbations caused by other molecules, and the

position of the spectral line will be shifted. If a statistical theory is used which involves a van der Waals force interaction, the static frequency shift is

$$\Delta\nu = \frac{\Delta E}{h} = \frac{-\beta}{r^6}, \quad (128)$$

where  $\beta$  is a constant to be determined.

According to Breene [77], an expression may be written for the probability that the broadening atoms (or molecules) will be so distributed in space as to distort the natural frequency to a particular value. The intensity in the resulting spectral line will be proportional to the desired frequency and may be written as

$$I(\Delta\nu) = \gamma(\Delta\nu)^{-3/2} e^{-\pi\gamma/\Delta\nu}, \quad (129)$$

where

$$\gamma = \frac{2}{3} \pi\beta^{1/2} N. \quad (130)$$

Here  $N$  is the density of the perturbers and  $\beta$  is the van der Waals constant in equation (128).

The half-width may then be written as

$$\Delta\nu_h = 0.82 \pi \gamma^2. \quad (131)$$

The shift of the intensity maximum for van der Waals forces is then determined as

$$\Delta = \frac{2}{3} \pi \gamma^2. \quad (132)$$

d. Impact theory. The impact (or interruption) theory is used when the velocities of the perturbing atoms or molecules are so large that the times of interaction are small compared to the duration of the emission process. This theory leads to the equation for Lorentz or collision broadening. In this case it is assumed that an atom or molecule is absorbing or emitting at a sharp frequency  $\nu_0$  during the time between collisions. Then at the moment of collision the radiation process stops completely, and the energy of vibration is converted purely into kinetic energy.

A detuning of natural frequency  $\omega_0$  is thus experienced as the perturbing particle approaches the emitting atom with a uniform velocity,  $v$ . Resulting is a net phase shift  $\delta\omega$  which depends on the inverse power of the separation distance  $r$  as

$$\delta\omega = \frac{C}{r^n}, \quad (133)$$

where  $C$  is a constant. The total phase shift,  $\eta$ , is thus found by integrating over the duration of the encounter as

$$\eta = \int_{-\infty}^{+\infty} \delta\omega dt = C \int_{-\infty}^{+\infty} \frac{dt}{(\rho^2 + v^2 t^2)^{n/2}} = \frac{C}{v \rho} a_n, \quad (134)$$

where  $a_n$  is a function of gamma functions and  $\rho$  is a "closest approach" parameter.

The intensity distribution of a spectral line may be obtained as a function of the time between encounters,  $t$ , and mean time between encounters,  $t_0$ , according to Aller [79] as

$$I_\nu = A \int_0^\infty \frac{1}{t_0} \left[ \frac{\sin \pi (\nu - \nu_0) t}{\pi (\nu - \nu_0)} \right]^2 e^{-t/t_0} dt = \frac{A}{2\pi} \frac{1}{(\nu - \nu_0)^2 + \left(\frac{1}{2\pi t_0}\right)^2}, \quad (135)$$

where  $A$  is determined by the condition that

$$\int_{-\infty}^{+\infty} I(\nu) d\nu = I_0. \quad (136)$$

According to Wooly and Stibbs [21], the half-width may be obtained from impact theory as

$$\Delta\nu_h = \frac{\gamma_c}{4\pi} = \frac{1}{2\pi\tau} = \frac{1}{2} \rho_o^2 \bar{v} N, \quad (137)$$

where  $\gamma_c$  is the collision frequency defined by equation (116);  $N$  is the number of particles per  $\text{cm}^3$  responsible for the broadening; and  $\rho_o$  represents the distance of closest encounter. This distance is given by

$$\rho_o = \left( \frac{3\pi^2 C}{4 \bar{v}} \right)^{1/5}, \quad (138)$$

when  $C$  is a constant and  $\bar{v}$  is the mean relative speed of the radiating and perturbing particles given by kinetic theory as

$$\bar{v} = \left[ \frac{8kT}{\pi M_o} \left( \frac{1}{A_1} + \frac{1}{A_2} \right) \right]^{1/2}. \quad (139)$$

Also,  $M_o$  is the mass of a particle of unit atomic weight, and  $A_1$  and  $A_2$  are the atomic weights of the radiating and perturbing atoms.

This concludes the section on the shape and broadening of spectral lines. Much more information on these phenomena may be obtained by consulting the works of other authors [21, 43, and 73-89]. In the next section the various band models are discussed. These models are important in the calculation of absorption coefficients, which are, in turn, necessary for predicting radiation heating from rocket exhausts.

## Band Models

To predict accurately the gaseous radiation from a rocket exhaust, the spectral absorption coefficient,  $\kappa_\lambda$  (or  $\kappa_\nu$ ), as a function of wavelength (or frequency) for a particular temperature, pressure, and concentration must be known. A considerable number of experimental measurements have been made of absorptance and transmittance of rocket exhaust gases in the last several

years. However, it is not possible to obtain enough experimental data for all possible variations in temperature, pressure, concentration and frequency which might occur across a particular slant path in a rocket exhaust as viewed by a radiometer or spectrometer.

Because of this lack of experimental data, the concept of band models has been developed to predict the absorption in a particular band composed of a nearly infinite number of spectral lines. Through the use of band models (which are assumed to be mathematically correct), the absorption, and consequently the emission of a rocket exhaust may be determined as a function of path length  $\ell$  and pressure of the gas,  $P$ .

According to Jamieson et al. [90], the absorption of a gas represented by band models depends on the number of lines in the band, on the relative spacing of the lines with respect to each other, on the number of spectral lines with a given value of the intensity, on the half-width of the spectral lines, and on the line shape (particularly in the wings of the lines). Theoretically, the band model is considered to have an infinite number of absorption lines of uniform statistical properties. An interval of this particular theoretical type containing many lines is assumed to have properties similar to those of an actual interval of the band being analyzed. In the band model, each interval will be flanked by statistically similar intervals; however, in a real band this is not necessarily the case.

In this section, five particular band models (including the single-line model) are discussed: (1) single-line model (exact method for absorption by isolated lines), (2) Elsasser model (band composed of identical, uniformly spaced lines), (3) statistical model (band composed of spectral lines with arbitrary intensity distribution and with random spacing between lines), (4) random Elsasser model (band composed of several groups of lines, each of which forms an Elsasser band, but the groups are superposed with random spacing), and (5) quasi-random model (band composed of spectral lines whose intensities and variation of spacing from line to line are accurately simulated).

There have been numerous references on the general subject of band models in the last 25 years. The references most referred to in this section include the articles by Plass [91-96], Openheim and Ben-Aryeh [97-98], Kaplan [99,100], Simmons [101], Penzias and Maclay [102], Maclay and Brabov [103], Green and Wyatt [104], Wyatt, Stull, and Plass [105,106], Elsasser [107], Godson [108], Greif [109], Goody [25], and Yossa [50].

1. Single-Line Model. The simplest band model to be discussed is the single-line model of Lorentz shape in which the lines are so narrow that there is essentially no overlapping of lines. The overlapping or nonoverlapping refers to the extent to which absorption in some small spectral interval is caused by contributions from a number of lines as opposed to absorption by a particular well-isolated line. When the lines do overlap, each line absorbs a smaller percentage of the radiation than it does when it is isolated from the other lines.

A fundamental quantity to be used in band model theory is known as the spectral absorptance,  $A_\nu$ , equal to the spectral emissivity,  $\epsilon_\nu$ , when LTE is assumed, and defined as

$$A_\nu = 1 - e^{-\kappa_\nu \ell} = \epsilon_\nu, \quad (140)$$

where  $\ell$  is the path length through the absorbing gas. An analogous expression for  $A_\nu$  was originally introduced in the section entitled "Equation of Radiation Transfer" as  $\alpha_\lambda$ , the spectral absorptivity. In band model theory this is usually written in terms of frequency  $\nu$  and termed absorptance; therefore, the notation of equation (140) will be used throughout the rest of this section.

The spectral absorption coefficient,  $\kappa_\nu$ , may be written for a Lorentz line shape (the most common shape occurring in actual practice) as

$$\kappa_\nu = \frac{S}{\pi} \frac{\gamma}{(\nu - \nu_0)^2 + \gamma^2}, \quad (141)$$

where  $S$  is known as the line strength and is defined by

$$S = \int_0^\infty \kappa_\nu \, d\nu. \quad (142)$$

The half-width  $\gamma$  is defined in a manner similar to equation (116) as

$$\gamma = \gamma_a^0 P_a + \gamma_b^0 P_b, \quad (143)$$

where  $\gamma_a^0$  represents the half-width at unit pressure for self-broadening (collisions between the absorbing molecules), and  $P_a$  is the pressure of the absorbing gas. The quantity  $\gamma_b^0$  represents the half-width at unit pressure for foreign gas broadening (collision between absorbing molecules and other molecules in the exhaust gas which are not absorbing radiation at a frequency  $\nu$ ). The quantity  $P_b$  represents the pressure of the nonabsorbing line-broadening gas.

The line strength  $S$  is also related to the pressure of the absorbing gas, expressed as

$$S = S^0 P_a \quad , \quad (144)$$

where  $S^0$  is the strength at unit pressure.

The total or integrated absorptance,  $W$ , (also known as equivalent width) of a single line may be specified at a particular temperature by means of the line strength,  $S$ , the line half-width,  $\gamma$ , and the path length,  $\ell$ . This integrated absorptance (or equivalent width) may be written as

$$W = \int_0^{\infty} \tilde{A}_{\nu} d\nu = \int_0^{\infty} (1 - e^{-\kappa_{\nu} \ell}) d\nu \quad (145)$$

If equation (141) is inserted into equation (145) and the result integrated from zero to infinity, it can be shown, as it is by Ladenberg and Reiche [110], that

$$W = 2\pi\gamma f(x) \quad , \quad (146)$$

where

$$x = \frac{S\ell}{2\pi\gamma} \quad , \quad (147)$$

and  $f(x)$  may be expressed in terms of Bessel functions as

$$f(x) = x e^{-x} [J_0(ix) - iJ_1(ix)] . \quad (148)$$

Two useful asymptotic forms occur for equation (148). When the parameter  $x$  is very small (linear approximation),  $f(x) \rightarrow x$ , and the integrated absorptance can be written as

$$W = 2\pi\gamma x = S\ell = S^0 P_a \ell , \quad (149)$$

which represents a linear variation of  $W$  as a function of  $P_a$ .

Another important parameter,  $\beta$ , in band model theory is defined as

$$\beta = \frac{2\pi\gamma}{d} , \quad (150)$$

where  $d$  represents the average spacing between the spectral lines.

The integrated absorptance may thus be written as

$$W = \beta x d \quad \text{or} \quad \frac{W}{d} = \beta x . \quad (151)$$

For large values of  $x$  (square root approximation),  $f(x) \rightarrow (2x/\pi)^{\frac{1}{2}}$  and

$$W = 2\gamma(2\pi x)^{\frac{1}{2}} = 2(S\ell\gamma)^{\frac{1}{2}} . \quad (152)$$

The integrated absorptance may also be written in terms of  $\beta$  as

$$W = d(2\beta^2 x/\pi)^{\frac{1}{2}} , \quad (153)$$

and if it is assumed that  $\gamma = \gamma^0 P_a$  and  $S = S^0 P_a$ , equation (153) may be written as

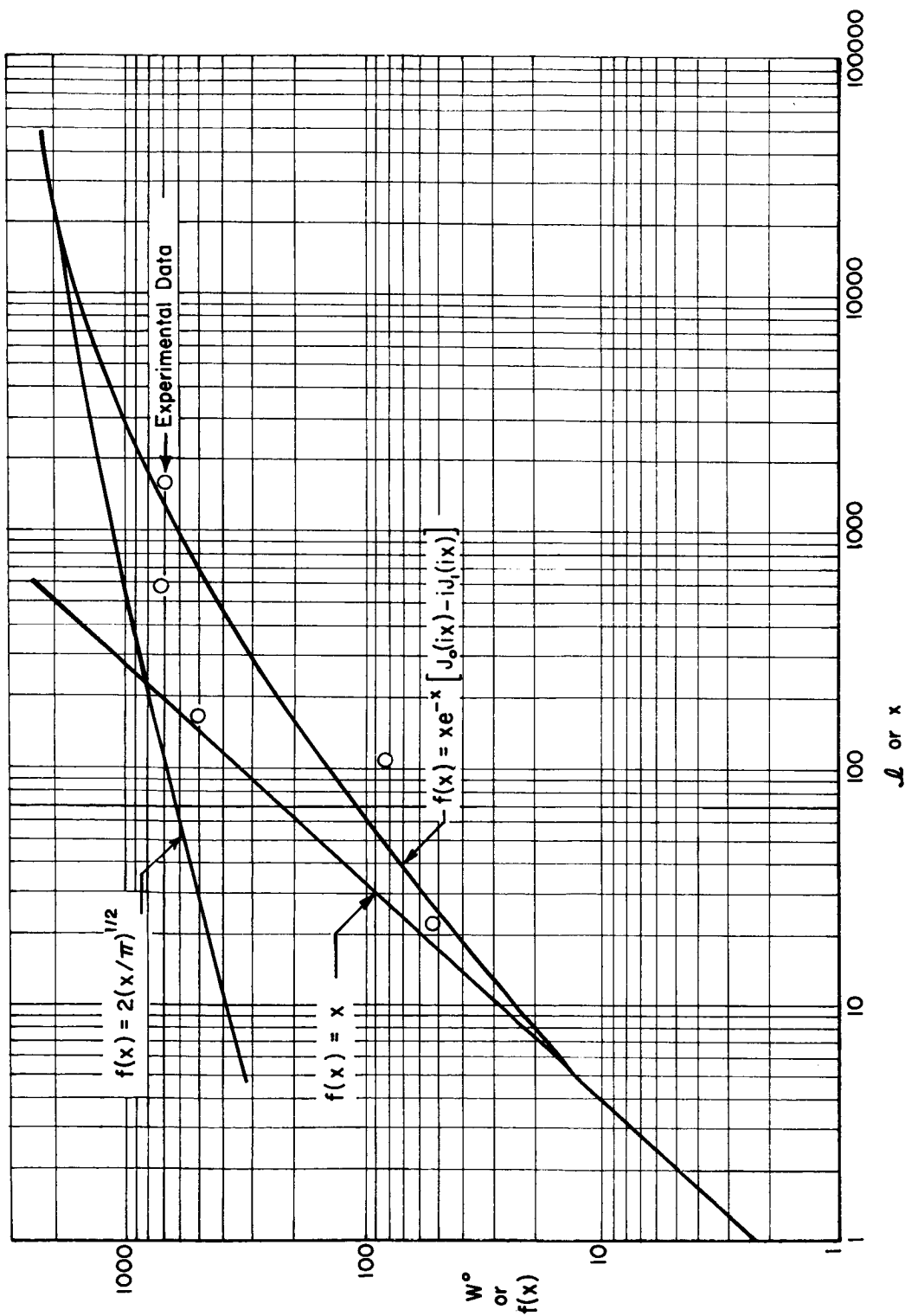


FIGURE 7. LADENBERG-REICHE FUNCTION, SHOWING STRAIGHT-LINE AND SQUARE ROOT APPROXIMATION

$$W = 2(\gamma^{\circ} S^{\circ} P_a^2 \ell)^{\frac{1}{2}} \quad \text{or} \quad W^{\circ} = 2(\gamma^{\circ} S^{\circ} \ell)^{\frac{1}{2}}, \quad (154)$$

which is known as the square root approximation for the integrated absorptance. This square root approximation, together with the linear approximation, is shown in Figure 7 in comparison with the Ladenberg and Reiche equation (148).

The quantities  $\gamma^{\circ}$  and  $S^{\circ}$  may be determined theoretically as by Howard et al. [111, 112] or experimentally as by Benedict et al. [83]. Since the above theoretical method can predict integrated absorptance readily, provided sufficient spectroscopic data are available, it is called the exact theoretical method. The above equations are valid for absorption by a band of spectral lines, provided the lines do not overlap. This assumption holds true when both the pressure and path length are small. At high altitudes (or low pressures), the Doppler contribution to the line shape can be important (as seen in Figures 5 and 6). Plass and Fivel [113] and Struve and Elvey [114] discuss this contribution and suggest various logarithmic expressions for the integrated absorptance (or equivalent width). In the next four sections on band models, various approximate methods of determining absorptance which may involve overlapping of the spectral lines are discussed.

2. Elsasser Model. The Elsasser band model, which was the earliest band model investigated [115], assumes an infinite array of spectral lines of equal intensity which are regularly spaced a distance  $d$  apart. This configuration is represented by the sketch in Figure 8.

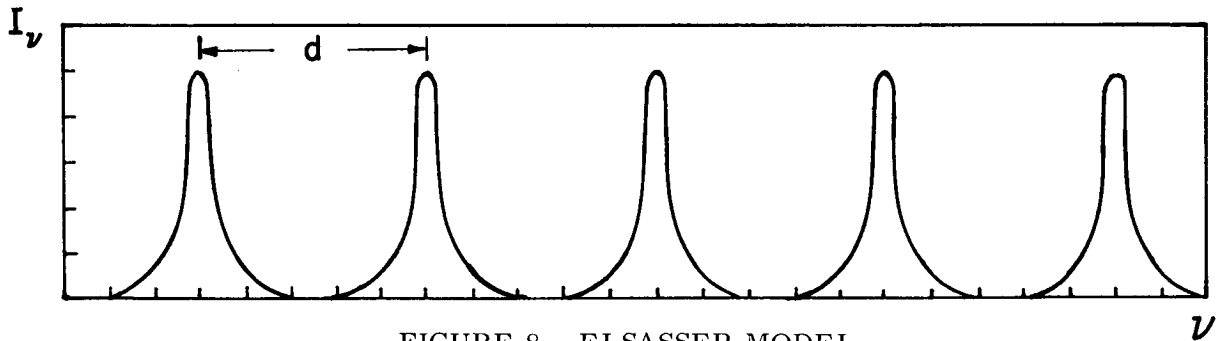


FIGURE 8. ELSASSER MODEL

Figure 8, compared with Figure 9, shows that there is greater absorption in this model in which the spectral lines are evenly spaced than when the line spacing is nearly random. Some portions of the  $\text{CO}_2$  spectrum may be

represented with a fair amount of accuracy with the Elsasser model; however, in the actual CO<sub>2</sub> spectrum there are always weaker lines between the strong, regular-spaced lines in the Elsasser model.

The Elsasser model uses the Lorentz line shape, equations (101) and (141), with a slight modification. The absorption coefficient,  $\kappa_\nu$ , is summed over all the spectral lines in the band, and thus represents the total contribution to  $\kappa_\nu$  from all the lines as

$$\kappa_\nu = \sum_{n=-\infty}^{n=+\infty} \frac{S}{\pi} \frac{\gamma}{(\nu - nd)^2 + \gamma^2} \quad (155)$$

It was shown by Elsasser (115) that this summation may be written in a simplified form as

$$\kappa_\nu = \frac{S}{d} \frac{\sinh \beta}{\cosh \beta - \cos \zeta} \quad (156)$$

where

$$\zeta = 2\pi\nu/d \quad (157)$$

With the insertion of equation (156) into the equation for the absorptance, equation (140), and using Elsasser's expression for average absorptance at the band center,

$$\bar{A}_\nu = \int_{-\infty}^{+\infty} A_\nu d\nu / \int_{-\infty}^{+\infty} d\nu \quad (158)$$

where

$$d\nu = (d/2\pi) d\zeta \quad (159)$$

the average absorptance may be written as

$$\bar{A}_\nu = 1 - \frac{1}{2\pi} \int_{-\pi}^{+\pi} \exp \left[ -\frac{S\ell}{d} \frac{\sinh \beta}{\cosh \beta - \cos \zeta} \right] d\zeta \quad (160)$$

Two approximations of equation (160) exist: the so-called "strong-line" approximation and the "weak-line" approximation. The strong-line approximation is valid when the spectral lines are far apart compared to their half-width ( $d \gg \gamma$ , or  $\beta \rightarrow 0$ ). In this case the absorption is practically complete near the centers of the strongest lines in the band. The expression for the absorptance thus becomes

$$\bar{A}_\nu = \text{erf}(z) = 2/(\pi)^{\frac{1}{2}} \int_0^z e^{-z^2} dz, \quad (161)$$

where

$$z = \left( \frac{1}{2} \beta^2 x \right)^{\frac{1}{2}} = \left( \frac{\pi \gamma S \ell}{d^2} \right)^{\frac{1}{2}}. \quad (162)$$

The weak-line approximation is valid when the spectral lines are close together ( $d \rightarrow 0$ , or  $\beta \rightarrow \infty$ ). In this case the absorption is small at all frequencies in the band even including those near the center of the strong absorption lines. The expression for the absorptance then becomes

$$\bar{A}_\nu = 1 - \frac{1}{2\pi} \int_{-\pi}^{+\pi} e^{-\ell S/d} d\zeta = 1 - e^{-\beta x} = \bar{\epsilon}_\nu. \quad (163)$$

This expression is analogous to equation (140) and is known as the Beer-Lambert equation.

3. Statistical Model. The statistical or random band model, originally developed by Mayer [116] and Goody [117], assumes a band in which there is no correlation between line intensities and frequencies, and in which there is a random spacing of lines. The intensity of the spectral lines may vary in any manner as long as it can be represented by a particular distribution function. Also, as a result of different quantum transitions, series of spectral lines may

overlap in several bands. It is known that the absorption of H<sub>2</sub>O may be represented by the statistical band model over a moderate range of pressures and path lengths. Figure 9 shows a sketch of the statistical band model showing regions of overlapping lines.

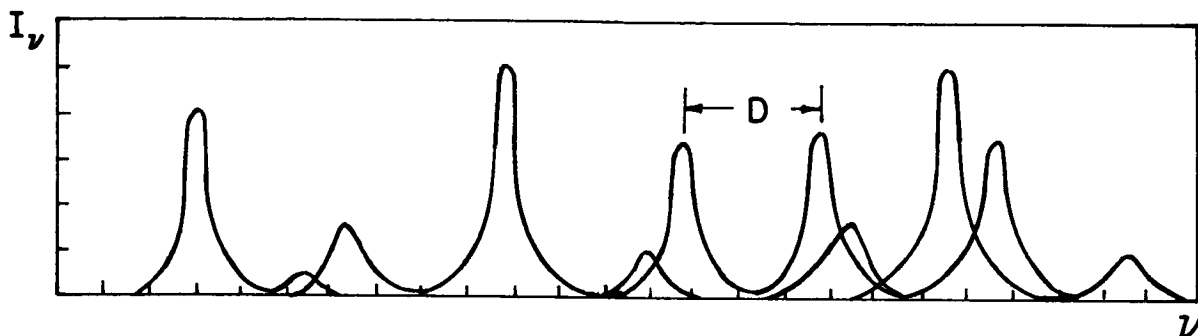


FIGURE 9. STATISTICAL MODEL

The basis of the statistical band model is the determination of the most probable average transmittance at the center of a frequency interval as a result of the absorption by  $n$  lines of intensity  $S_i$  ( $i = 1, 2, 3, \dots, n$ ). In this theory various probability distributions are introduced in the following manner. If  $N(\nu)$  is the probability that a spectral line lies between  $\nu$  and  $\nu + d\nu$ , and  $N(\nu_1, \nu_2) d\nu_1, d\nu_2$  is the probability that one line lies between  $\nu_1$  and  $\nu_1 + d\nu_1$  and that a second line lies between  $\nu_2$  and  $\nu_2 + d\nu_2$ , then the probability of finding  $n$  lines in some frequency interval  $D$  is unity, or

$$\int_D N(\nu_1, \nu_2, \dots, \nu_n) d\nu_1, d\nu_2, \dots, d\nu_n = 1. \quad (164)$$

Also, on the same basis, the probability that a given spectral line has an intensity between  $S_i$  and  $S_i + dS_i$  is  $P(S_i)$ . This probability function may usually be expressed in terms of the Dirac delta function,  $\delta(S - \bar{S})$ , or an exponential function,  $(1/\bar{S}) \exp(-S/\bar{S})$ , where  $\bar{S}$  is some mean line intensity, described by Malkmus [118]. Normalizing this probability results in the relation

$$\int_0^\infty P(S_i) d(S_i) = 1. \quad (165)$$

The weighted average of the transmittance,  $\bar{\tau}_\nu$ , over the frequency interval,  $D$ , may now be written in terms of the above probability functions as

$$\bar{t}_\nu = \frac{\int_{-\frac{1}{2}D}^{\frac{1}{2}D} \dots \int_{-\frac{1}{2}D}^{\frac{1}{2}D} N(\nu_1, \nu_2, \dots, \nu_n) d\nu_1 d\nu_2 \dots d\nu_n \int_0^\infty \dots \int_0^\infty \prod_{i=1}^n P(S_i) \exp[-S_i(\nu_i)\ell] dS_i}{\int_{-\frac{1}{2}D}^{\frac{1}{2}D} \dots \int_{-\frac{1}{2}D}^{\frac{1}{2}D} N(\nu_1, \nu_2, \dots, \nu_n) d\nu_1 d\nu_2 \dots d\nu_n \int_0^\infty \dots \int_0^\infty \prod_{i=1}^n P(S_i) dS_i} \quad (166)$$

The random distribution hypothesis is now introduced to simplify the above equation. This hypothesis assumes that it is equally probable that each spectral line has its center at a given frequency  $\nu$  in the frequency interval  $D$  of  $n$  lines, regardless of the position of the other lines. In this manner the expression  $N(\nu_1, \nu_2, \dots, \nu_n)$  equals a constant; i. e., it is independent of frequency, and may be written as

$$N(\nu_1, \nu_2, \dots, \nu_n) = D^{-n} \quad (167)$$

Since the integral over each line is equal to the integral over any other line, equation (166) reduces to

$$\bar{t}_\nu = D^{-n} \left[ \int_{-\frac{1}{2}D}^{\frac{1}{2}D} d\nu \int_0^\infty P(S) \exp(S\ell) dS \right]^n \quad (168)$$

Since the average absorptance,  $\bar{A}_\nu$ , in the case of a nonscattering gas (reflectance equals zero) is equal to  $1 - \bar{t}_\nu$ , the following expression for  $\bar{A}_\nu$ , following the mathematical procedure of Plass [91], may be written as

$$\bar{A}_\nu = 1 - \left[ 1 - D^{-1} \int_0^\infty \bar{W}_{S.L.}(S) P(S) dS \right]^n \quad (169)$$

If the average value of the equivalent width of a single line is given as

$$\bar{W}_{S.L.} = \int_0^\infty W_{S.L.}(S) P(S) dS, \quad (170)$$

the expression for the average absorptance finally reduces to

$$\bar{A}_\nu = 1 - \exp[-(\bar{W}_{S.L.}/d)] . \quad (171)$$

Since  $\bar{W}_{S.L.}$  is the same as  $W$  in equation (146), a strong-line approximation results in which  $f(x) \rightarrow (2x/\pi)^{\frac{1}{2}}$ , and the average absorptance may be written as

$$\bar{A}_\nu = 1 - \exp \left[ -(2\beta^2 x/\pi)^{\frac{1}{2}} \right] . \quad (172)$$

A weak-line approximation results when  $f(x) \rightarrow x$  as

$$\bar{A}_\nu = 1 - e^{-\beta x} , \quad (173)$$

which has the same form as the weak-line approximation in the Elsasser band model, equation (163).

The regions of validity for the statistical model, as well as the Elsasser model, for various band absorption approximations such as strong-line, weak-line, and non-overlapping line approximations are given by Plass [94, 95].

4. Random Elsasser Model. The random Elsasser model, in general, provides a more accurate representation of spectral bands than either the Elsasser or statistical model. The random Elsasser band model assumes that the absorption may be characterized by the random superposition of Elsasser bands, each of which may have a different line intensity and spacing between the lines. Through the use of this model, the absorption of HCl has been predicted quite accurately by Stull and Plass [119] and Malkmus et al. [120].

Figure 10 shows a sketch of a random Elsasser model. Four different Elsasser bands, each with a different intensity and line spacing, are superimposed on the figure. In this manner, as many of the weak spectral lines may be used as desired to make a satisfactory prediction of absorption for the particular pressures and path length considered in the rocket exhaust.

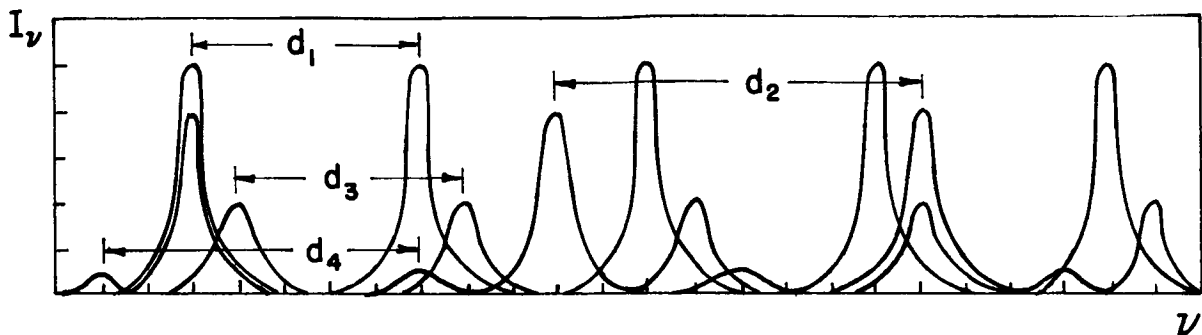


FIGURE 10. RANDOM ELSASSER MODEL

For this model it is assumed that  $d_i$  represents the spectral line spacing of the  $i^{\text{th}}$  Elsasser band and  $n$  is the number of superimposed Elsasser bands. The average spacing  $\delta$  between the spectral lines is thus

$$\delta = \left( \sum_{i=1}^n \frac{1}{d_i} \right)^{-1} . \quad (173)$$

An equivalent width for the  $i^{\text{th}}$  Elsasser band may be written as

$$W_{E,i}(x_i, \beta_{di}) = d_i \left[ 1 - \bar{t}_{E,i}(x_i, \beta_{di}) \right] = d_i \left[ \bar{A}_{E,i}(x_i, \beta_{di}) \right] , \quad (174)$$

where  $\beta$  is the parameter defined by equation (150),  $x$  is defined by equation (147), and  $\bar{t}_{E,i}$  and  $\bar{A}_{E,i}$  are the average transmittance and absorptance, respectively, of the  $i^{\text{th}}$  Elsasser band. By a procedure similar to that in the preceding section, the average absorptance from a random superposition of  $n$  Elsasser bands can be written as

$$\bar{A}_\nu = 1 - \prod_{i=1}^n \int_0^\infty \left[ 1 - d_i^{-1} W_{E,i}(x_i, \beta_i) \right] P_E(S_i) dS_i , \quad (175)$$

where  $P_E(S_i) dS_i$  represents the probability of the  $i^{\text{th}}$  Elsasser band having an intensity in the range  $dS_i$ .

An average equivalent width  $\overline{W}_{E,i}$  may be defined in the same manner as equation (170). The average absorptance from a random superposition of  $n$  Elsasser bands, each of which may have a different intensity, half-width, and line spacing, can be written as

$$\overline{A}_\nu = 1 - \prod_{i=1}^n \left( 1 - \frac{W_{E,i}}{d_i} \right) \quad (176)$$

If the line spacings and half-widths are all assumed equal ( $d = n \delta$ ), the average absorptance may be written as

$$\overline{A}_\nu = 1 - \left[ 1 - \left( \frac{\overline{W}_{E,i}}{n \delta} \right) \right]^n \quad (177)$$

In terms of the quantities  $\beta$  and  $x$  (or of  $S$  and  $P$ ), the strong-line approximation for the Elsasser model is

$$\overline{A}_\nu = 1 - \prod_{i=1}^n \left\{ 1 - \operatorname{erf} \left[ \left( \frac{1}{2} \beta_i^2 x_i \right)^{\frac{1}{2}} \right] \right\} \quad (178)$$

and the weak-line approximation is

$$\overline{A}_\nu = 1 - e^{-\beta_i x_i} \quad (179)$$

5. Quasi-Random Model. The quasi-random band model is possibly the most accurate model of the five mentioned in this report. In an actual band the spectral lines are not as regularly arranged in frequency or intensity as in the Elsasser or random Elsasser models, nor are they arranged in as random a manner as in the statistical model. The quasi-random model is thus better able to simulate the actual intensity distribution (including many weak lines) and the relative spacing of all the spectral lines. Furthermore, this model is able to take into account the effect of the absorptances of the adjacent frequency intervals on the particular frequency interval being analyzed. However, because of certain complexities in its usage, this model has not yet been programmed for rocket exhaust radiation calculations.

Using the quasi-random model, the absorptance is first calculated over frequency intervals  $\delta$  which are smaller than the particular interval size of interest. These intervals are assumed so small that the spectral lines lying in any one of them may be considered to lie at random positions, without any appreciable errors being introduced. This confines the stronger lines to a narrow interval around their actual position and prevents overlapping. Theoretically, if the interval spacing were decreased to zero, this band model would locate each line exactly, with no approximations needed at all. However, a large enough spacing is, of course, taken to simplify calculations. Also, the lines in each frequency interval  $\delta$  are divided into intensity subgroups according to the respective magnitudes of their line strengths,  $S_i$ .

The average absorptance at the frequency  $\nu$  resulting from  $n$  lines in the intervals  $\delta_k$  with line centers at the frequencies  $\nu_i$  ( $i = 1, 2, \dots, n_k$ ) may be calculated similarly to the statistical model as

$$\bar{A}_{k\nu} = 1 - \bar{t}_{k\nu} = 1 - \frac{1}{\delta^{n_k}} \prod_{i=1}^{n_k} \int_{\delta_k} e^{-S_i \ell} d\nu_i . \quad (180)$$

According to Wyatt et al. [105], it has been determined that only the first five intensity decades for each frequency contributes appreciably to the absorptance (or transmittance). Hence, equation (180) may be written as

$$\bar{A}_{k\nu} = 1 - \prod_{i=1}^5 \left[ \frac{1}{\delta} \int_{\delta_k} e^{-\bar{S}_i \ell} d\nu_i \right]^{n_i} , \quad (181)$$

where  $\bar{S}_i$  is the average value of the line intensity, and the total number of lines  $n_k$  in the frequency interval can be written as

$$n_k = \sum_{i=1}^5 n_i . \quad (182)$$

To calculate the absorptance at a frequency  $\nu$  which is influenced by the wings whose centers are outside of the interval which contains the frequency  $\nu$ , the following equation is used:

$$\bar{A}_{\nu} = 1 - \prod_{j=1}^{\infty} t_{j\nu} , \quad (183)$$

where  $\bar{t}_{j\nu}$  is the transmittance at  $\nu$  as a result of  $n_j$  lines in the frequency interval  $\delta_j$ . It may be restated that equation (181) represents the total absorptance at  $\nu$  for both direct and wing contributions.

According to Jamieson et al. [90], the strong-line approximation for the absorptance using the quasi-random model can be written as

$$\bar{A}_\nu = 1 - \prod_{i=1}^n \left\{ e^{-\xi_i^2} - \frac{1}{\pi^{1/2}} \xi_i [1 - \text{erf}(\xi_i)] \right\}, \quad (184)$$

where

$$\xi_i^2 = 8 \gamma_i^2 x_i / \delta_k^2. \quad (185)$$

Equation (184) represents only the absorptance from the spectral lines whose centers lie within the small interval  $\delta_k$ . The concentration from the wings of the lines in adjacent intervals must be added by using equation (183).

Several other band models and approximations have appeared in the literature. One of the approximations, the Curtis-Godson approximation, is discussed in the next section, as well as certain apparent emissivity relations. Also, various programs for predicting gaseous radiant heating to the base of Saturn space vehicles caused by the exhaust of H-1, F-1, and J-2 engines are described. Some of these programs are based on the above applications of band models.

## Methods of Predicting Gaseous Radiation from Rocket Exhausts

In this section various methods of predicting the radiation heating to the base of large rocket vehicles (of the Saturn class) are described. Three general methods are discussed, each of which was either generated under NASA/Marshall Space Flight Center (MSFC) contract or was an MSFC in-house effort.

The first method, an MSFC in-house effort described by Heatherly et al. [121] and [122], used the total emissivity method of Hottel [123]. The second method was a University of California method which involved apparent emissivity and mean path length relations and was developed under contract to MSFC's

P&VE Laboratory. This method is summarized by Tien and Abu-Romia [124-126] and by Giedt et al. [127]. The third general method was originally programmed for rocket exhaust applications at Rocketdyne under P&VE contract and is described by deSoto [128-130]. This method, which uses spectral absorption coefficient data, was modified to include the Curtis-Godson approximation by Warner-Swasey Company and General Dynamics/Convair and further documented by Brown Engineering Company--all under MSFC Aero-Astrodynamic Laboratory contract. A detailed review of the third method is given by Huffaker [4, 51].

1. Total Emissivity Method. The total emissivity method of Hottel was used to predict the radiation heating from the five J-2 engines of the Saturn V, S-II stage to the S-II stage thrust structure and heat shield as reported by Heatherly and Dash [121]. The complete gas dynamic and radiation computer program using this method for the intersection regions of hydrogen-oxygen plumes for a multi-engine space vehicle is given by Heatherly et al. [122].

By the total emissivity method, the radiation heating from a non-isothermal, isobaric gas can be written as

$$q/A = \frac{1}{\pi} \int_{\omega} \int_X \sigma_B T(d\epsilon/dX) \cos\theta \, d\omega \, dX, \quad (186)$$

where the parameter  $X$  is the optical beam length which is defined as

$$X = P_w \ell . \quad (187)$$

$P_w$  is the partial pressure of the water vapor in the exhaust ( $H_2O$  assumed to be the only emitter in the  $LH_2$ -lox system), and  $\ell$  is the path length through the gas. The quantity  $\sigma_B T^4$  is the Planck blackbody function,  $B_\lambda(T)$ .

A solid angle shape factor,  $F$ , may be defined as

$$F = \frac{1}{\pi} \int_{\omega} \cos\theta \, d\omega , \quad (188)$$

where  $\theta$  is the angle which the line of sight to the rocket exhaust makes with the normal to the area where the radiation heating is to be determined.

Equation (186) may now be written, with the insertion of equation (188), as

$$q/A = F \sigma_B \int_{P_w \ell} T^4 \frac{d\epsilon}{d(P_w \ell)} d(P_w \ell) \quad (189)$$

In this program, total emissivity,  $\epsilon$ , versus optical beam length,  $P_w \ell$ , for various values of temperature,  $T$ , was obtained by curve fitting with polynomials, the curves as presented by Hottel [123]. This total emissivity program, while simple in scope, is limited to systems of one molecular emitter (i. e.,  $H_2O$  in  $LH_2$ -lox systems). The program does have its advantages in that integration over all wavelengths (use of total emissivity rather than spectral emissivity) is avoided.

2. Apparent Emissivity and Mean Path Length Method. The apparent emissivity method of predicting gaseous radiation is based upon the following equation from Eckert and Drake [131] for apparent spectral emissivity,  $\epsilon_\lambda$ , of a semi-infinite cylindrical gaseous body.

$$\epsilon_\lambda = \frac{1}{\pi} \int_{\beta} \int_{\phi} (1 - e^{-\kappa_\lambda s}) \sin \beta \cos \beta \, d\beta \, d\phi \quad (190)$$

In this equation,  $\beta$  represents the polar angle and  $\phi$  the azimuthal angle as seen in Figure 11. The quantity  $s$  is the path length (analogous to  $\ell$  in equation (187)). Equation (190) may be nondimensionalized by using the following parameters:

$$H = \frac{h}{r_e}, \quad R = \frac{r}{r_e}, \quad K_\lambda = \kappa_\lambda r_e, \quad \text{and} \quad S = \frac{s}{r_e} \quad (191)$$

where  $r_e$  is the radius of the rocket nozzle exit,  $h$  is the height of the nozzle exit as measured from the base plane,  $r$  is the radial distance in the base plane, and  $\kappa_\lambda$  is the spectral absorption coefficient.



$$F = \frac{1}{\pi} \int_{\beta} \int_{\phi} \sin \beta \cos \beta \, d\beta \, d\phi \quad \text{and} \quad \epsilon_{\lambda c} = \frac{1}{\pi} \int_{\beta} \int_{\phi} e^{-K_{\lambda} S} \sin \beta \cos \beta \, d\beta \, d\phi. \quad (194)$$

The quantity  $F$  is the configuration factor or the blackbody apparent emissivity (analogous to equation (188)), and  $\epsilon_{\lambda c}$  is the contribution to the emissivity caused by the finite absorption coefficient of the gaseous body. Equations (192) and (193) may be further modified by making the substitution:  $\tan \beta = \sec \phi \tan \beta'$  (see Figure 11). In this manner the quantities  $F$  and  $\epsilon_{\lambda c}$  become

$$F = \frac{1}{\pi} \int_{\beta'} \int_{\phi} \frac{\cos^2 \phi \tan \beta' \sec^2 \beta'}{(\cos^2 \phi + \tan^2 \beta')^2} \, d\beta' \, d\phi \quad \text{and} \quad (195)$$

$$\epsilon_{\lambda c} = \frac{1}{\pi} \int_{\beta'} \int_{\phi} e^{-K_{\lambda} S} \frac{\cos^2 \phi \tan \beta' \sec^2 \beta'}{(\cos^2 \phi + \tan^2 \beta')^2} \, d\beta' \, d\phi .$$

Using these relations, curves for the apparent spectral emissivity as a function of  $R$  for various values of  $H$  and  $K_{\lambda}$  have been given by Tien and Abu-Romia [132] and [133] for both semi-infinite cylindrical and conical bodies. Figure 12 shows the curves for  $H = 1$  as taken from these references. It may be seen that the apparent spectral emissivity for a conical body of 10-deg cone angle is much higher than that for a cylindrical body for the same value of  $R$ .

The above expressions apply only for a gray-gas assumption. In this manner the total nondimensionalized absorption coefficient,  $K$ , equals the spectral nondimensionalized absorption coefficient,  $K_{\lambda}$ , and the total emissivity,  $\epsilon$ , equals the spectral emissivity,  $\epsilon_{\lambda}$ . However, by making use of the mean path length,  $L$ , (defined as the path length averaged over all path lengths viewed at different angles from a certain location in the base plane), an expression for total emissivity may be obtained without making the gray-gas assumption. This dimensionless mean path length is a function of  $H$  and  $R$  and may be defined in the expression

$$\epsilon_{\lambda} \equiv F(1 - e^{-K_{\lambda} L}) . \quad (196)$$

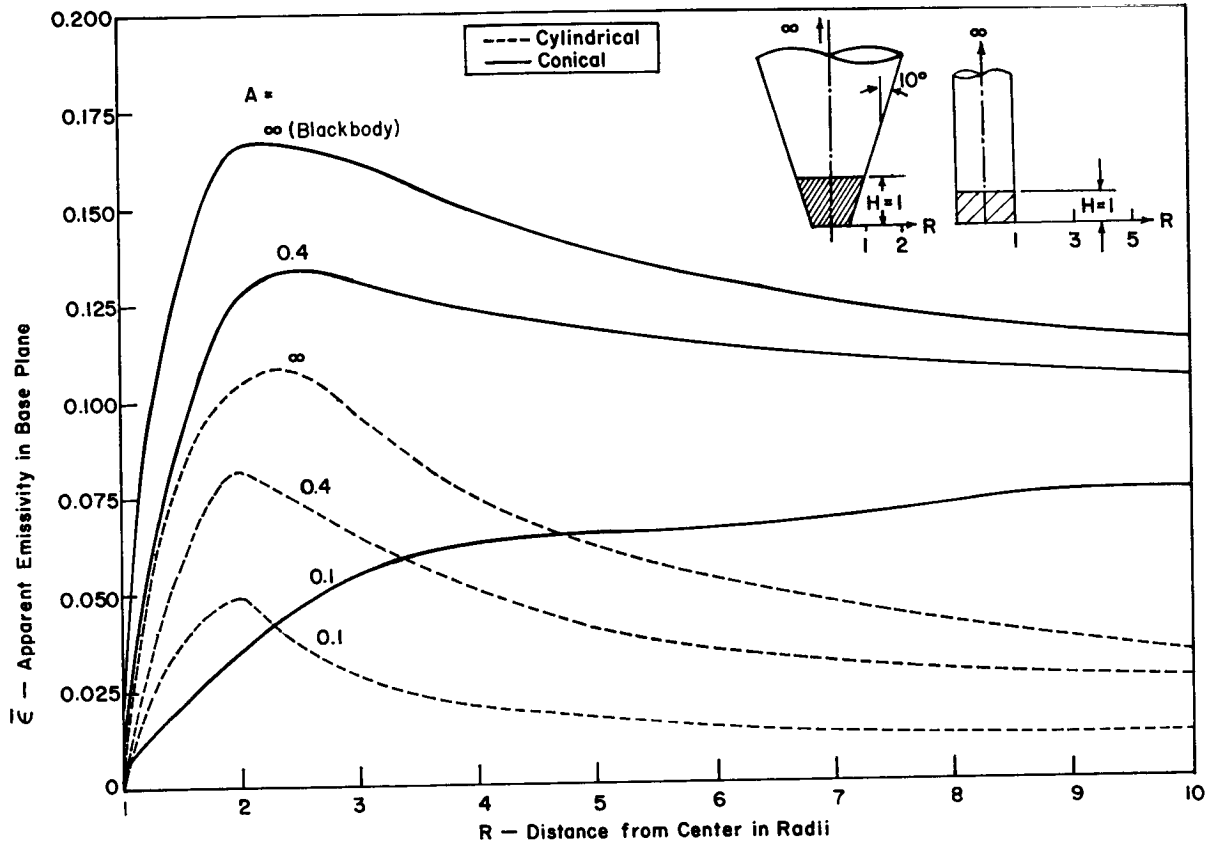


FIGURE 12. APPARENT EMISSIVITIES IN THE BASE PLANE OF A CYLINDRICAL AND A CONICAL GRAY-GAS BODY FOR  $H = 1$

The total emissivity may now be written, with the insertion of equation (196), as

$$\epsilon(H, R) = \frac{\int_0^{\infty} \epsilon_{\lambda} B_{\lambda} d\lambda}{\int_0^{\infty} B_{\lambda} d\lambda} = \frac{\pi C_1 F}{\sigma_B T^4} \int_0^{\infty} \frac{[1 - \exp(-K_{\lambda} L)] d\lambda}{\lambda^5 [\exp(C_2/\lambda T) - 1]} \quad (197)$$

where

$$C_1 = c^2 h \quad \text{and} \quad C_2 = \frac{ch}{k} \quad (198)$$

In these equations,  $h$  is Planck's constant and  $k$  is Boltzmann's constant.

If the infrared spectrum is known (experimentally or theoretically) in a narrow band width, equation (197) may be approximated by the relation

$$\epsilon(H, R) = F \sum_i [1 - \exp(-K_\lambda L)] (D_{2i} - D_{1i}) \quad , \quad (199)$$

where the quantities  $D_{ni}(\lambda_{ni}, T)$  are known as the relative cumulative spectral radiance, tabulated by Pivovsky [134], and are defined as

$$D_{ni}(\lambda_{ni}, T) \equiv \frac{1}{\sigma_B T^4} \int_0^{\lambda_{ni}} \frac{\pi C_1 d\lambda}{\lambda^5 [\exp(C_2/\lambda T) - 1]} \quad . \quad (200)$$

For a cylindrical semi-infinite body with shielding ( $H \neq 0$ ), Giedt et al. [127] and Tien and Abu-Romia [133] suggest the following semi-empirical equation for  $L(H, R)$ :

$$L(H, R) = \frac{4 \sin \beta'_0}{\tan^{-1}(\sin \beta'_0 \tan \phi_0)} \left[ E_2 R \left( \frac{\pi}{2}, \frac{1}{R} \right) - \left( \frac{R^2 - 1}{R} \right) E_1 \left( \frac{\pi}{2}, \frac{1}{R} \right) + \frac{\pi \cos^2 \beta'_0}{16 R^3} \right] \quad , \quad (201)$$

where  $E_1$  and  $E_2$  are the elliptic integrals of the first and second kind, respectively.

Other expressions for the mean path length based on the experimental data of Howard, Burch, and Williams [135] have been given by Tien and Wang [136]. For conditions in which a power law type of correlation of integrated absorptance can be used, such as

$$W = \int_\nu A_\nu d\nu = C w^a P_e^b \quad , \quad (0.5 \leq a \leq 1, 0 \leq b \leq 0.5) \quad , \quad (202)$$

where  $w$  is the absorber concentration and  $P_e$  is an equivalent pressure defined by Burch, Singleton, and Williams [137], the mean path length may be represented as

$$L = \frac{1}{\pi} \int_{\omega} r^a \cos \phi \, d\omega , \quad (203)$$

where  $r$  is the distance between the differential area on the confining surface and the differential gas volume.

For large values of  $w$  in which the following logarithmic form of integrated absorptance may be used:

$$W = \int_{\nu} A_{\nu} \, d\nu = E + F \ln (w P_e^m) , \quad m \leq 1 , \quad (204)$$

where  $E$  and  $F$  are constants defined by Howard et al. [135], the mean path length may be expressed as

$$L = \exp \left[ \frac{1}{\pi} \int_{\omega} (\ln r) \cos \phi \, d\omega \right] . \quad (205)$$

Tien and Wang [136] and Rolfe [138] present ratios of mean path length of a non-transparent gas to that of a transparent gas for spherical enclosures, for an enclosure composed of two infinite parallel planes, for an infinite circular cylindrical enclosure, and for radiation to the center of the base of a finite circular cylinder.

In summary, the general method of apparent emissivity and mean path length, while yielding more accurate values of radiative heating than the total emissivity method of Hottel, is felt to be inferior to the method described below in which band models and/or spectral absorption coefficients are used.

3. Spectral Absorption Coefficient Methods. The following three methods (two of which use band models) of predicting radiation heating from liquid propellant rocket exhausts are based upon the use of spectral absorption coefficients. These methods will be termed (a) "weak-line or exact absorption

coefficient method," (b) "statistical band model method with Curtis-Godson approximation," and (c) "generalized method with modified Curtis-Godson approximation."

a. Weak-line or exact absorption coefficient method. The weak-line or exact absorption coefficient method does not make use of band models, since for this method the absorption is assumed not to depend on the spectral arrangement of lines in the band. This method sometimes provides more conservative values of radiation heating than methods (b) or (c) described below. However, one objection to the method is that to obtain a sufficiently accurate numerical calculation in certain regions, the wave number ( $1/\lambda$ ) interval must be made extremely small ( $\sim 0.01 \text{ cm}^{-1}$ ).

The basic equation to be solved with the weak-line method is equation (57), given in the section entitled "Equation of Radiation Transfer." The integrated form of this equation is equation (61) with  $I_\lambda(0)$ , the incident intensity upon the plume assumed equal to zero. Equation (61) can thus be written in the form

$$I_\nu(s) = \int_0^s j_\nu(s) \exp \left[ -\int_0^s \kappa_\nu(s') ds' \right] ds, \quad (206)$$

where the  $s$  and  $s'$  notation has been reversed from that used in equation (61) and the subscript  $\nu$  has been used instead of  $\lambda$ .

Assuming that Kirchoff's Law holds, the emission coefficient  $j_\nu$  can be written as in equation (12) with the refractive index of the medium  $n_\nu$  assumed equal to unity. The mass absorption coefficient  $\kappa_{m,\nu}$  will be used instead of  $\kappa_\nu$ . Equation (206) now becomes

$$I_\nu(s) = \int_0^{s_m} \rho \kappa_{m,\nu} B_\nu(T) \exp \left[ -\int_0^s \rho \kappa_{m,\nu} ds' \right] ds, \quad (207)$$

where  $s_m$  is the upper limit of the variable  $s$  in the plume along all lines of sight beyond which there is zero contribution to the radiation.

The radiative heat transfer per unit area may now be obtained by integrating equation (207) over all frequencies  $\nu$  and solid angles  $d\omega = \sin\theta d\theta d\phi$  as

$$q/A = \int_{\nu} \int_{s} \int_{\phi} \int_{\theta} \rho \kappa_{m,\nu} B_{\nu}(T) \exp \left[ - \int_0^s \rho \kappa_{m,\nu} ds' \right] \sin \theta \cos \theta d\theta d\phi ds d\nu. \quad (208)$$

The absorption coefficients in equation (208) may be obtained experimentally or from band model calculations such as tabulated by Ferriso et al. [52]. Dash [139] describes calculations of radiative heating from the Saturn S-IVB stage J-2 engine to the S-IVB thrust structure using equation (208). The numerical solution of equation (208) was discussed by deSoto [128-130], but this program was limited to a single rocket plume with axisymmetric geometry. However, Tarbell and Alligood [140] and Alligood [141], using local partial pressures and spectral coefficients evaluated at standard conditions in equation (208), described a numerical solution to equation (208) which could be used for any number of rocket plumes.

The numerical integration of equation (208), as discussed by Tarbell and Alligood [140], is performed in the following manner. The integral of the absorption coefficient is first treated as

$$A(s_j, \nu, \theta, \phi) = \sum_{i=1}^n \rho \kappa_{m,\nu} \Delta s_i; \quad (209)$$

the integral over the line of sight is next evaluated as

$$B(\nu, \theta, \phi) = \sum_{i=1}^n \exp[-A(s_i, \nu, \theta, \phi)] \rho \kappa_{m,\nu} B_{\nu}(T) \Delta s_i; \quad (210)$$

the integral over frequency  $\nu$  is next obtained as

$$C(\theta, \phi) = \sum_{i=1}^n B(\nu, \theta, \phi) \Delta \nu_i; \quad (211)$$

the integral over  $\phi$  is next evaluated as

$$D(\phi) = \sum_{i=1}^n C(\theta, \phi) \sin \theta \cos \theta \Delta \theta_i; \quad (212)$$

and the final integral over  $\theta$  is obtained as

$$q/A = E = \sum_{i=1}^n D(\phi) \Delta\phi_i . \quad (213)$$

b. Statistical band model method with Curtis-Godson approximation. The statistical band model method with the Curtis-Godson approximation has been described in detail by Krakow et al. [142] and by Huffaker [4, 51]. This method is felt to be superior to the weak-line or exact absorption coefficient method described above in that it does not depend upon such a small wave number (or frequency) interval for integration. Also, it has its advantages in that the band model data such as line strength,  $S$ , line spacing,  $d$ , and line half-width,  $\gamma$ , can be obtained from homogeneous samples of gas and then applied to an inhomogeneous gas such as a rocket exhaust.

The equation for spectral intensity used in this method is actually the same as deSoto's equation (206), but has been modified as described by Krakow et al. [142], Krakow [143] and Tourin and Krakow [144] in the following finite-sum approximation:

$$I(\nu_j, \Delta\nu_j) = \sum_{i=1}^n B(\nu_j, T_i) [\bar{t}_{i-1}(\nu_j, \Delta\nu_j) - \bar{t}_i(\nu_j, \Delta\nu_j)] , \quad (214)$$

where  $\bar{t} = \exp(-\rho\kappa_m, \nu s)$  is the transmittance of the section of sample in zone  $i$ . The quantity  $\nu$  now represents the wave number (1/cm) instead of the frequency as originally defined.

The heat flux equation, (208), now becomes

$$q/A = \int_{\omega} \sum_{j=1}^m I(\nu_j, \Delta\nu_j) \Delta\nu_j \cos\theta \, d\omega . \quad (215)$$

In this method of predicting radiation heating, the statistical band model (See this section, subsection entitled "Band Models," part 3.) with equal line strengths and equal line widths was used. Equation (171) was then used for the average integrated absorptance. This equation now takes the form

$$\bar{A}_\nu = 1 - \exp \left[ -(\bar{W}_{S.L.}/d) \right] = 1 - \bar{t}_\nu = 1 - \exp \left[ -\frac{2\pi\gamma}{d} f(x) \right] , \quad (216)$$

where  $\bar{t}_\nu$  denotes the average transmittance in the wave number interval  $\Delta\nu$ , and  $f(x)$  is the Ladenberg-Reiche function in equation (148).

If  $\bar{t}_\nu$  in equation (216) represents the transmittance of an inhomogeneous gas, such as a rocket exhaust, then it is possible that some hypothetical homogeneous sample, such as obtained in a laboratory burner, would have the same  $\bar{t}_\nu$  if it had certain values of  $\gamma/d$  and  $x$ . The Curtis-Godson approximation [142] as given in equations (217) and (218) is thus used to obtain the band model parameters of the hypothetical homogeneous gas sample:

$$\frac{S}{d} \ell = \sum_i \frac{S_i}{d} \ell_i = \sum_i x_i \frac{-\ln \bar{t}_i}{f(x_i)} \quad (217)$$

and

$$\frac{S}{d} \ell \frac{\gamma}{d} = \sum_i \frac{S_i}{d} \ell_i \frac{\gamma_i}{d} = \frac{1}{2\pi} \sum_i x_i \left[ \frac{-\ln \bar{t}_i}{f(x_i)} \right]^2 . \quad (218)$$

By dividing equation (218) by equation (217) the following value of  $(\bar{\gamma}/d)_i$ , which is the value of  $\gamma/d$  for the hypothetical homogeneous gas sample, is obtained:

$$\left( \frac{\bar{\gamma}}{d} \right)_i = \frac{\sum_{h=1}^i P_h^a (S^0/d)_h \ell_h \left[ (\gamma_a^0/d)_h P_h^a + (\gamma_b^0/d)_h P_h^b \right]}{\sum_{h=1}^i (S^0/d)_h P_h^a \ell_h} . \quad (219)$$

By dividing equation (217) by  $2\pi\gamma/d$ , the following value of  $\bar{x}_i$ , which is the value of  $x$  for the hypothetical homogeneous gas sample, is obtained:

$$\bar{x}_i = \frac{\left[ \sum_{h=1}^i (S^0/d)_h P_h^a \ell_h \right]^2}{2\pi \sum_{h=1}^i (S^0/d)_h P_h^a \ell_h \left[ (\gamma_a^0/d)_h P_h^a + (\gamma_b^0/d)_h P_h^b \right]} . \quad (220)$$

In the above two equations the subscript a stands for absorbing gas and the subscript b stands for broadening gas (such as N<sub>2</sub>). The quantities P<sub>h</sub><sup>a</sup> and ℓ<sub>h</sub> are the pressure of the absorbing gas and the path length of zone h, respectively. Ferriso et al. [52] give details in the determination of the band model parameters S<sup>0</sup>/d and γ<sup>0</sup>/d for H<sub>2</sub>O, CO<sub>2</sub>, and CO.

The transmittance in equation (214) may now be obtained as follows:

$$-\ln \bar{t}_i(\nu_j, \Delta\nu_j) = 2\pi(\bar{\gamma}/d)_i f(\bar{x}_i), \quad (221)$$

where  $(\bar{\gamma}/d)_i$  and  $\bar{x}_i$  are evaluated from equations (219) and (220).

Two other expressions for W/d may be used instead of the one in equation (216), which involves Bessel functions. One of these expressions is the exponential probability distribution described by Ferriso et al. [52]:

$$\frac{W}{d} = \frac{S^0 \ell}{d} \left( 1 + \frac{S^0 \ell}{\pi \gamma^0 P} \right)^{\frac{1}{2}}, \quad (222)$$

which has a more gradual transition region between the two asymptotic regions (weak- and strong-line regions) as a result of intensity distribution among the spectral lines.

The other expression for W/d is the effective absorption coefficient expression of Ferriso, Ludwig, and Abeyta [145]:

$$\frac{W}{d} = \kappa_{\text{eff}}(\nu) P_a \ell \left[ 1 + \frac{\kappa_{\text{eff}}(\nu) P_a \ell}{4(\bar{\gamma}/d)} \right], \quad (223)$$

where

$$\kappa_{\text{eff}} = \frac{S^0}{d} = \frac{2\pi}{P_a \ell} \frac{\gamma}{d}. \quad (224)$$

Plass [91] shows that equation (223) and the W/d expression in equation (216) agree to within 10 percent.

c. Generalized method with modified Curtis-Godson approximation. The generalized method uses an integrated form of the Curtis-Godson equations, (217) and (218), to obtain radiation from inhomogeneous gases in which the Beer-Lambert equations, equations (140) and (163), are not applicable. This method, which has been proven to be accurate for strong concentration and temperature gradients, also takes into account the Doppler broadening effects which are important at low pressures ( $\sim 0.1$  atm). Ferriso et al. [52] and Huffaker [4,51] describe this method in detail, and Alligood [146] and Conway, Yossa, and Alligood [147] describe a computer program involving this method.

The equation for heat transfer rate per unit area in the generalized program, which is similar to equation (208) except for the transmittance factor,  $t_\nu$ , is

$$q/A = \int_{\nu} \int_{\phi} \int_{\theta} \int_s B_{\nu}(T) \frac{dt_{\nu}}{ds} ds \sin\theta \cos\theta d\theta d\phi d\nu. \quad (225)$$

The transmittance  $t_\nu$  is equal to  $\prod_i t_{\nu}(i)$ , a product over the various radiating species in the rocket exhaust. The quantity  $t_{\nu}(i)$  may be calculated by two methods. The first method, described by Alligood [146], based on the investigation of Ferriso et al. [52], considers only the larger of collision and Doppler broadening (but not both as does the second method). For the first case, the transmittance may be written in terms of the statistical band models as

$$t_{\nu}(i) = \exp \left\{ - \left[ \begin{array}{c} D_c(i) \\ D_D(i) \end{array} \right] \right\} = \exp \left\{ - \left[ \begin{array}{c} (W/d)_c(i) \\ (W/d)_D(i) \end{array} \right] \right\}, \quad (226)$$

where the notation in braces implies the larger of  $D_c(i)$  and  $D_D(i)$  and the subscripts c and D stand for collision and Doppler broadening, respectively.

The quantity  $D_c(i)$  may be written similarly to equation (223) as

$$D_c(i) = F(i) \left\{ 1 + \frac{1}{4} \frac{[F(i)]^2}{A_c(i)} \right\}^{-\frac{1}{2}}, \quad (227)$$

and the quantity  $D_D(i)$  may be written as

$$D_D(i) = \frac{1.7A_D(i)}{F(i)} \left\{ \ln \left[ 1 + \left( \frac{0.589[F(i)]^2}{A_D(i)} \right)^2 \right]^{\frac{1}{2}} \right\} . \quad (228)$$

The quantity  $F(i)$  is defined as

$$F(i) = \int_0^s \rho(i) \kappa_{m,\nu} ds = \int_0^s \frac{S(i)}{d(i)} ds , \quad (229)$$

where  $S(i)$  is the line intensity originally defined in equation (142).

The parameters  $A_c(i)$  and  $A_D(i)$  represent the modified Curtis-Godson approximation and are equal to

$$A_c(i) = \int_0^s \frac{\gamma_c(i)}{d(i)} \frac{dF(i)}{ds} ds \quad (230)$$

and

$$A_D(i) = \int_0^s \frac{\gamma_D(i)}{d(i)} \frac{dF(i)}{ds} ds , \quad (231)$$

where

$$\frac{dF(i)}{ds} = \rho(i) \kappa_{\nu}(i) . \quad (232)$$

The fine structure parameters (Doppler half-width,  $\gamma_D$ , collision half-width  $\gamma_c$ , and line density,  $1/d$ ) are given by Alligood [146] for  $H_2O$  (all bands),  $CO_2$  (4.3  $\mu$  and 2.7  $\mu$  bands), and  $CO$  (5  $\mu$  bands). The tables of  $\kappa_{\nu}$  as a function of wave number and temperature (300° K, 600° K, 1200° K, 1500° K, 1800° K, 2400° K, and 3000° K) are found in Ferriso et al. [52]. A more accurate listing of absorption coefficients and fine structure parameters for  $H_2O$  has been tabulated by Ludwig et al. [148] for temperatures between

1200° K and 3000° K and for path lengths of 2, 5 and 10 feet. Herget, Muirhead and Golden [149] present revised tables of band model parameters for H<sub>2</sub>O for temperatures between 300° K and 1400° K and for pressures from 0.1 to 2.0 atm.

The other method of evaluating the transmission  $t_\nu$  is given by Ferriso et al. [52] which combines both the Doppler and collision broadening in the expression

$$t_\nu(i) = F(i) (1 - y^{-\frac{1}{2}})^{\frac{1}{2}}, \quad (233)$$

where

$$y = \left\{ 1 - \left[ D_c(i)/F(i) \right]^2 \right\}^{-2} + \left\{ 1 - \left[ D_D(i)/F(i) \right]^2 \right\}^{-2} - 1. \quad (234)$$

It is felt that the generalized method (including the modified Curtis-Godson approximation) of predicting radiation heat transfer from rocket exhausts is the best of all of the methods described in this section. Huffaker [51] states that the difference between the measured inhomogeneous gas transmittance and that calculated by the modified Curtis-Godson approximation is within experimental error and not greater than 2 percent.

Using the generalized method with the modified Curtis-Godson approximation, calculations of spectral intensity have been made for the J-2 engine exhaust, as described by Huffaker [51]. Figure 13, taken from Huffaker, shows a comparison between calculations and measured values of spectral intensity from a J-2 engine exhaust during a sea level static firing. Figure 14 shows theoretical radiation calculations compared with experimental data obtained from the exhaust of a 1/45-scale F-1 engine fired at Cornell Aeronautical Laboratory which used O<sub>2</sub> and C<sub>2</sub>H<sub>4</sub> as propellants. The radiation calculations for this engine show better agreement with the data than for the J-2 engine (Fig. 13); however, it is known that the spectrometer used for the J-2 test was not calibrated properly after the firing. Additional calculations will be made by Thermal Environment Branch to compare with spectral intensity measurements taken during altitude firings (in which there is no atmospheric absorption) of the J-2 engine. These measurements will be performed in the AEDC J-4 test cell at Tullahoma, Tennessee, in the spring of 1967.

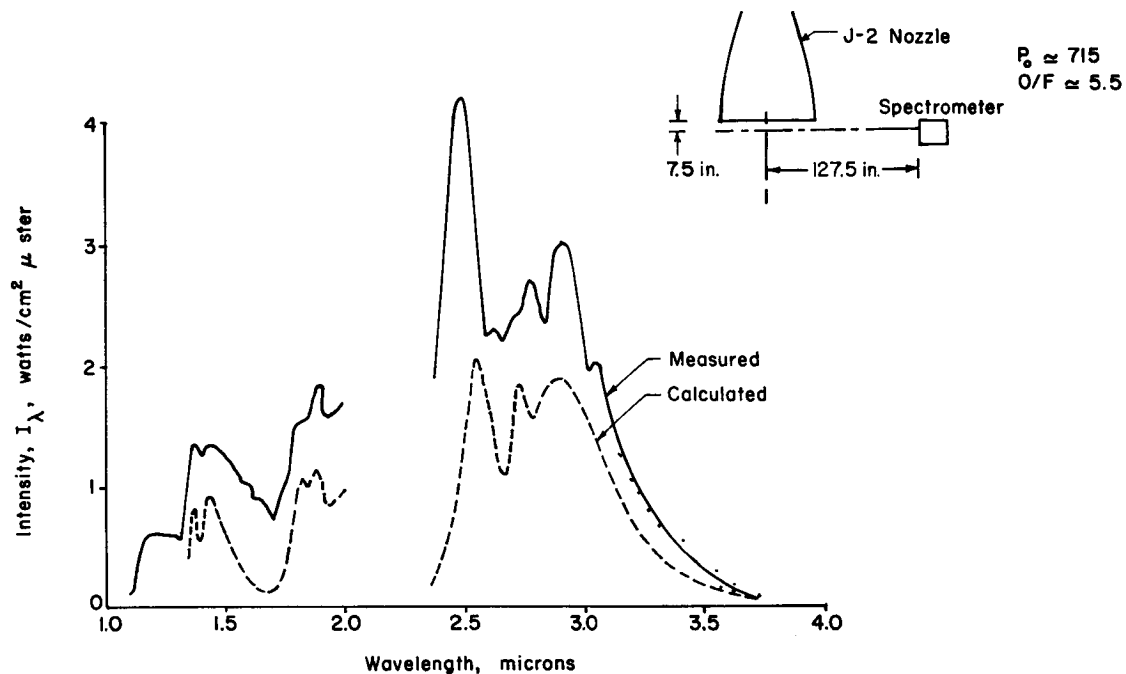


FIGURE 13. COMPARISON OF MEASURED AND CALCULATED INTENSITY FOR J-2 ENGINE FIRED AT SEA LEVEL

This concludes the section on gaseous radiation. It is felt that the basic points of the theory such as radiation from accelerated charges, shape and broadening of spectral lines, band models, and methods of predicting gaseous radiation from rocket exhausts have been covered sufficiently. For additional detail on gaseous radiation the more than 90 references mentioned in this section should be consulted. For details on the rocket exhaust plume programs which must be generated before the radiation heating can be predicted, it is suggested that references such as Farmer, Prozan, Ratliff, and McGimsey [1], Prozan [150], and Ratliff [151] be consulted.

## RADIATION FROM CARBON PARTICLES

Thermal radiation from carbon particles is the dominant means of radiant heating from exhausts of hydrocarbon-fueled rocket engines such as the H-1 and F-1, which power the first stages of the Saturn I and Saturn V vehicles,

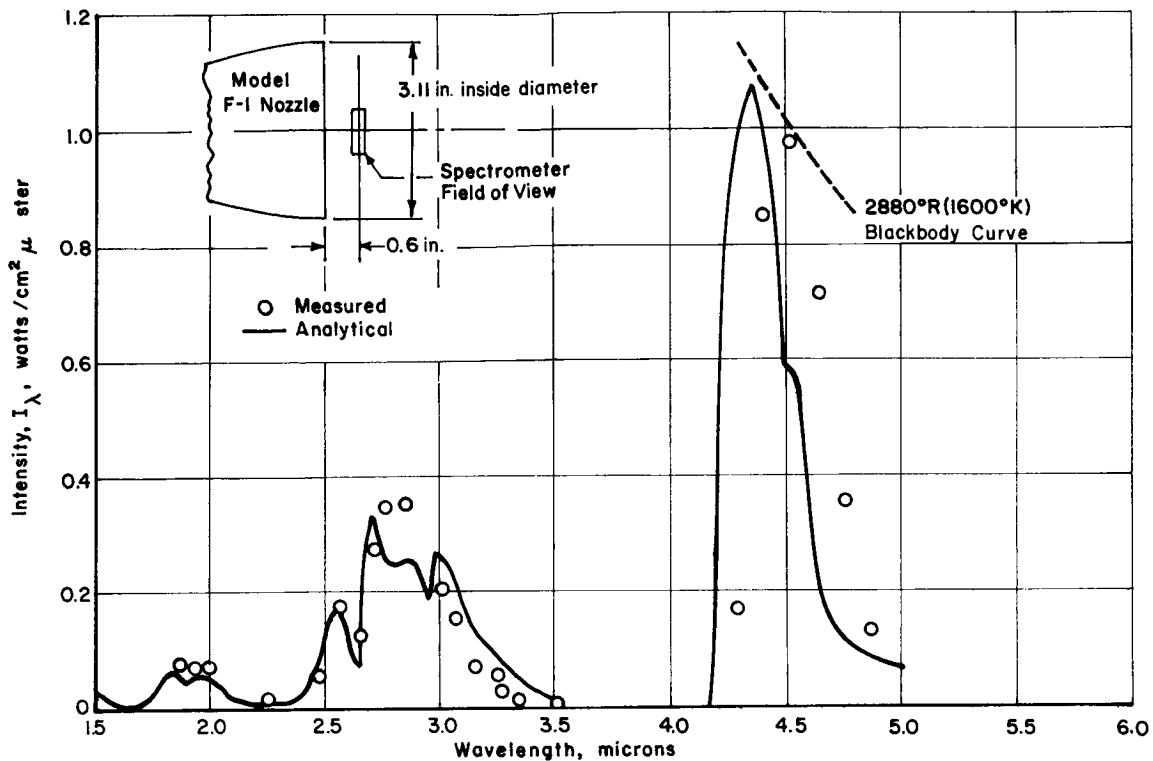


FIGURE 14. COMPARISON OF MEASURED AND CALCULATED INTENSITY NEAR THE EXIT OF A 1/45-SCALE F-1 ENGINE FIRED AT CAL AT 120,000 FEET

respectively. These engines burn RP-1 (kerosene) as the fuel as opposed to other hydrocarbon-fueled engines which burn ethyl alcohol (ethanol) or aeroxine-50, and consequently produce little or no carbon in their exhausts.

The carbon emission spectrum from H-1 and F-1 engines is practically continuous (follows a graybody or blackbody distribution, depending on optical depth) near the exit plane in the 1- $\mu$  to 4- $\mu$  wavelength region. This is in contrast to the emission spectrums of the H<sub>2</sub>O, CO<sub>2</sub> and CO gaseous molecules which are frequency dependent (emit in certain bands only) in the infrared wavelength region (as shown in the previous section). At distances far downstream of the exit (at altitudes less than about 100,000 feet) when afterburning is still present, the carbon spectrum is no longer continuous. Also, if a spectrometer which views the plume is mounted a considerable distance from the exit, atmospheric absorption bands can absorb the carbon continuum as seen by

the spectrometer in the 1.4- $\mu$ , 1.9- $\mu$ , 2.7- $\mu$  and 6.3- $\mu$  H<sub>2</sub>O bands and 2.7- $\mu$  and 4.3- $\mu$  CO<sub>2</sub> bands. This carbon continuum spectrum can be seen in such reports as Simmons [152], de Bell, Simmons, and Levin [153], Levin, Wagner, and Thomson [154], an Aerojet-General report [155], Wagner [156], and in Figure 15 of this report. Figure 16, presented for comparison with Figure 15, shows the spectrum of an exhaust from an N<sub>2</sub>O<sub>4</sub>/UDMH propellant engine. The lack of carbon continuum for the exhaust of this non-kerosene liquid-fueled engine is easily seen. In Levin, Wagner, and Thompson [154] evidences of chemiluminescence can be seen by noting the peaks of C<sub>2</sub>, CN, and CH emission above the carbon continuum.

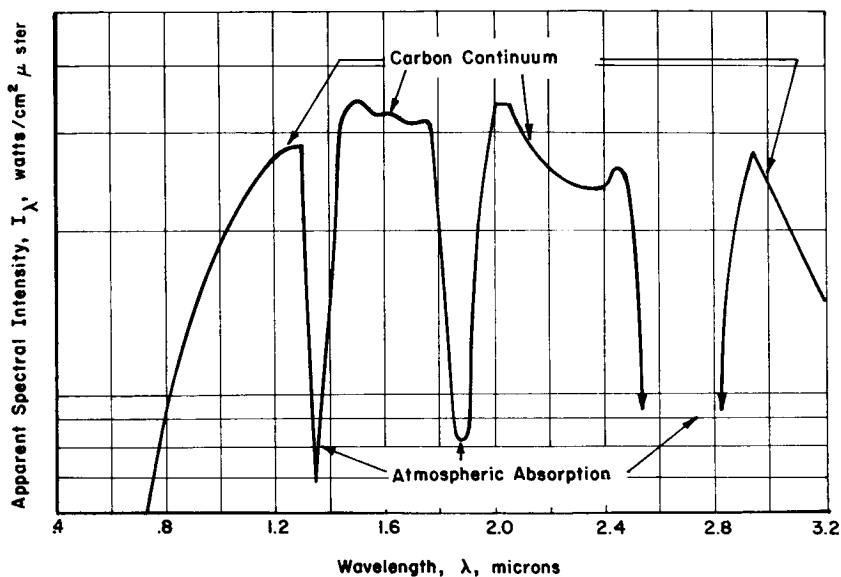


FIGURE 15. SPECTRUM OF LOX/RP-1 PLUME SHOWING CARBON CONTINUUM

Accurate predictions of radiant heating from carbon particles is difficult for a number of reasons. In the gas generator, carbon is a nonequilibrium product of combustion because of the rather low temperatures ( $\sim 900^\circ$  K) involved; hence, its concentration in this region must be calculated with finite reaction-rate chemical kinetics. It is possible, however, that carbon is in equilibrium in the combustion chamber, nozzle, and near-field of the exhaust because of the higher temperatures in these regions. The concentration of carbon in these regions should be calculated by present equilibrium thermochemical programs; however, this has not yet been accomplished satisfactorily because of the uncertainties in the O/F distribution in these regions. A plot of carbon concentration versus O/F ratio for various temperatures shows that, for a small

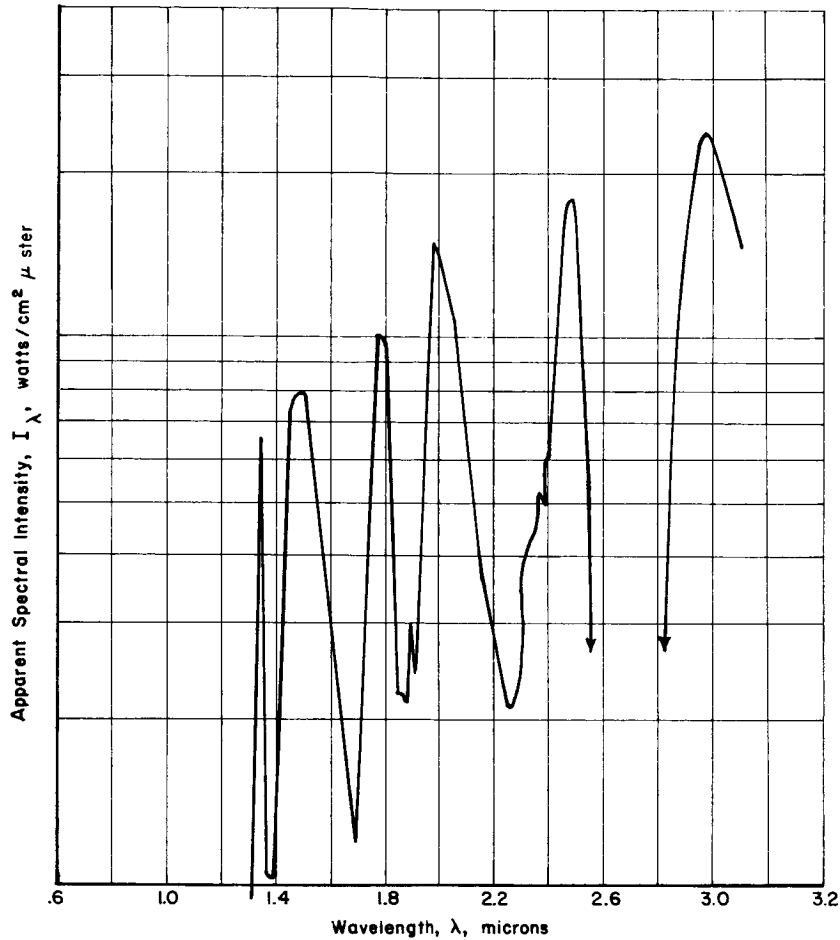


FIGURE 16. SPECTRUM OF  $N_2O_4$ /UDMH PLUME SHOWING LACK OF CARBON CONTINUUM

increment in O/F ratio (for a given temperature), a very large increment in carbon concentration will result. To treat radiation from carbon particles adequately, therefore, the mechanism of carbon formation must be fully understood, the size distribution of carbon particles must be known, the optical properties of carbon (dispersion theory, scattering phenomena, etc.) must be analyzed, and the emissivity of carbon particles must be calculated (or measured).

Scattering of radiation by carbon particles is frequently assumed negligible, although this phenomenon may not be legitimately neglected if the size of the

particles is large and the wavelength under consideration is small. Scattering by carbon particles may thus be calculated by Rayleigh scattering theory in which  $\alpha \ll 1$ , where  $\alpha = 2\pi r_p/\lambda$  ( $r_p$  is the radius of the particle), and by Mie scattering theory in which  $\alpha \sim 1$ . Since carbon particles usually fall in the realm of Rayleigh scattering, this theory is discussed in this section; the Mie theory is discussed in the following section since it applies mainly to larger ( $\text{Al}_2\text{O}_3$ ) particles. This section discusses in succession the formation of carbon particles in luminous flames, the determination of carbon particle sizes, the dispersion equation for carbon, the Rayleigh scattering theory, and methods of predicting absorption coefficients and emissivities for carbon particles.

## Formation of Carbon Particles in Luminous Flames

In recent years there has been a tremendous amount of literature written regarding the mechanism of carbon formation in luminous flames (including rocket and turbojet combustion chambers and exhausts). Some of the more detailed reviews pertaining to carbon formation include the books by Gaydon [157], Gaydon and Wolfhard [158] and Palmer and Cullis [159], and the articles by Parker and Wolfhard [160], Porter [161] and [162], Thomas [163], Street and Thomas [164], Daniels [165], Singer and Grumer [166], Tesner [167], and van der Held [168]. Other less detailed articles regarding carbon formation which also contain much experimental data were written by Gaydon and Fairbairn [169], Arthur and Napier [170], Scully and Davies [171], Fenimore, Jones, and Moore [172], Ferguson [173], Lee, Thring, and Beer [174], and Stehling, Frazee, and Anderson [175]. Some of the many books and articles which discuss combustion in luminous flames and combustion chambers (some of which also contain descriptions of carbon formation) were written by Godsave [176], Khitrin [177], Wicke [178], Yagi and Kunii [179], Behrens [180], Paushkin [181], Minkoff and Tipper [182], Fristrom [183], Penner [184], McCafferty and Hibbard [185], Penner and Datner [186], Wise and Agoston [187], Spalding [188], Williams [189], Fristrom and Westenberg [190], and Bahn [191].

In a rocket combustion chamber such as that of the H-1 or F-1 engine, the fuel (RP-1) and the oxidizer (liquid oxygen) are pumped into the chamber by a turbopump, which is driven by a gas turbine. The gas turbine is, in turn, driven by the exhaust of a gas generator. Inside the combustion chamber, combustion takes place at a relatively high O/F ratio ( $\sim 2.5$ ) and at a high temperature ( $\sim 3000^\circ\text{K}$ ). However, in the gas generator, combustion takes place at a low O/F ratio ( $\sim 0.4$ ) and at a low temperature ( $\sim 900^\circ\text{K}$ ). Before

the RP-1 fuel is injected into the combustion chamber, however, it is routed around the chamber and nozzle to cool these components regeneratively. Carbon may thus be formed in the relatively high O/F ratio, high temperature region of the combustion chamber or in the relatively low O/F ratio and temperature regions of the gas generator and the walls of the combustion chamber and nozzle. It is expected that more carbon will be formed in the latter regions because of the excess fuel and lower temperature experienced in these regions.

Paushkin [181] states that the formation of carbon in combustion chambers depends upon a number of factors such as degree of atomization and temperature of the fuel and oxidizer, design of the combustion chamber (including its chamber pressure), and surface tension, viscosity, and composition of fuel (aromatic hydrocarbon content). Since RP-1 fuel (kerosene) contains a large amount of aromatic (cyclic) components (~20 percent) compared to aliphatic (straight-chained) components, it is usually assumed that the majority of the carbon formed comes from this aromatic portion of the fuel.

In a given combustion chamber, Penner and Datner [186] state that the amount of carbon deposited, for a wide variety of hydrocarbon fuels, can be correlated by an empirical equation of the form

$$C = \frac{1}{K_3} \ln (K_1 R - K_2) + \frac{T_b}{K_4} - K_5, \quad (235)$$

where  $C$  is the rate of carbon deposition,  $R$  is the carbon-to-hydrogen ratio,  $T_b$  is the boiling temperature of the fuel, and  $K_1$  to  $K_5$  are empirically determined constants such as found in the article by Starkman, Cattaneo, and McAllister [192]. The rate of combustion of a cloud of carbon particles in luminous flames, according to Lee, Thring, and Beer [174] may be determined from the following equation based upon experimental data:

$$\frac{\rho_c d_o}{6 m_o^{1/3} m^{2/3}} \frac{dm}{dt} = 1.085 \times 10^4 \frac{P_{O_2}}{T^{1/2}} \exp\left(-\frac{39,300}{RT}\right), \quad (236)$$

where  $\rho_c$  is the density of carbon particles (soot),  $d_o$  is the initial diameter of the particles,  $m_o$  is the initial mass flow,  $m$  is the mass flow after time,  $t$ ,  $P_{O_2}$  is the partial pressure of oxygen,  $T$  is the particle (or flame) temperature, and  $R$  is the gas constant. According to Howard and Essenhigh [193],

the complete sequence of events for carbon particle combustion takes place in four steps: heating, ignition, pyrolysis, and heterogeneous combustion. Gas-phase combustion will occur simultaneously with heterogeneous combustion on the surface of the particle if the surface flux of volatile pyrolysis is small; however, if the surface flux is large, the reaction zone will be forced away from the solid surface, thereby screening the carbon particle from oxygen attack.

Flames occurring in combustion chambers of liquid-fueled rocket engines are neither diffusive nor completely premixed; hence, the general theories of carbon formation in both diffusion and premixed flames must be considered. According to Gaydon and Wolfhard [158], in a pure diffusion flame, the combustion processes are assumed to take a fairly long time for their completion; however, there is little or no contact between the oxidizer and fuel. For purely premixed flames, the oxidizer and fuel are in direct contact, but the combustion processes are limited by the very short time of passage through the reaction zone. Carbon formation theories differ, depending on what type of flame (diffusion or premixed) occurs, but also these theories differ from author to author, so that there is no one general theory available which will adequately describe carbon formation. In the remainder of this section some of these various carbon particle (and ion) formation theories are briefly analyzed.

1. The C<sub>2</sub>, Atomic Carbon, and C<sub>3</sub> Condensation Theories. The C<sub>2</sub> condensation theory was originally developed by Smith [194], and has been discussed by Gaydon and Wolfhard [158] and Parker and Wolfhard [160]. Smith, after performing a spectroscopic study of ethylene burning in air, surmised that carbon was produced by a polymerization of C<sub>2</sub> molecules. He also discussed the experiments of Klemenc, Wechsberg, and Wagner [195], who investigated the decomposition of carbon suboxide, C<sub>3</sub>O<sub>2</sub>, and found C<sub>2</sub> bands in absorption. After passing through a reddish stage in color, the C<sub>2</sub> rapidly polymerized to normal solid carbon. Gaydon and Wolfhard [158] and Parker and Wolfhard [160], however, believed that this C<sub>2</sub> condensation theory is not valid in practice because of the low times of reaction and concentration usually involved. Gaydon [156] states that semi-quantitative estimates of the amount of C<sub>2</sub> in flames, studies of flash photolysis, and the relative positions of C<sub>2</sub> and carbon in flames also tend to make this theory unbelievable.

Gaydon and Wolfhard [158] state that it is possible that free carbon atoms may be condensed directly from flames since, in equilibrium with graphite, the concentration of C atoms is several orders of magnitude greater than that of C<sub>2</sub>. Cabannes [196] believes that solid carbon in flames could be formed by the condensation of carbon vapor whose main constituent is assumed to be C<sub>3</sub>.

2. The Hydrocarbon Polymerization-Condensation Theory. This theory involves the general pyrolysis (or decomposition) of pure hydrocarbons as discussed by Gaydon and Wolfhard [158], Porter [161,162], Palmer and Cullis [159], Thomas [163], Street and Thomas [164], Gordon [197], and many others. According to Gaydon and Wolfhard [158], during the pyrolysis of hydrocarbons, a number of processes are found to occur, such as hydrogenation, dehydrogenation, cracking to simple hydrocarbons, polymerization, and sometimes condensation to aromatics. The particular type of pyrolysis depends upon the temperature and the presence of catalysis. The basis of all the hydrocarbon polymerization theories is that polymerization of the fuel occurs first, aided sometimes by oxidation, followed by dehydrogenation (in which oxidation may be a factor), finally resulting in carbon being the end product. Street and Thomas [164] present an elaborate diagram which shows probable interrelationships among the possible routes to the formation of carbon involving polymerization.

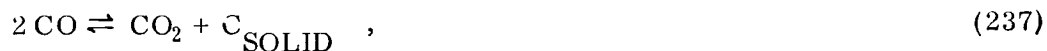
Thomas [163] gives a description of "soot" formation from hydrocarbon fuels using the polymerization-condensation theory, and states that "soot" is not carbon, but has a polybenzenoid hydrocarbon structure. Rummel and Veh [198] were the first to suggest that aromatics and polycyclic hydrocarbons preceded the formation of carbon (or soot). A current investigation at Rocketdyne [199], performed under Thermal Environment Branch contract, is under way to attempt to determine the chemical formulation of the soot molecule.

3. The Acetylene Theory. Porter [161,162] and Anderson [200] state that, while low temperature ( $< 1000^{\circ}\text{C}$ ) pyrolysis of hydrocarbons tends to produce higher polymers, at high temperatures ( $> 1000^{\circ}\text{C}$ ) decomposition of hydrocarbons predominates over polymerization. Because of these high temperatures, Porter [161] concludes that, when the time for half reactions is of the order of one second or less, the pyrolysis of hydrocarbons does not result in polymerization, but in decomposition to smaller molecules. Porter [161] further concludes that the thermal decomposition of hydrocarbons results in dehydrogenation and cracking to smaller molecules, and the last stable hydrocarbon to be observed before carbon formation is acetylene. It is known that acetylene, which is a very endothermic substance, is then very easily decomposed to carbon and hydrogen. Discussions of experimental investigations of carbon formation from acetylene have been reported by Stehling, Frazee, and Anderson [175] and by Westbrook, Hellwig, and Anderson [201].

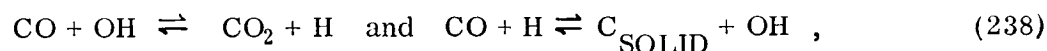
4. The Surface Decomposition Theory. This theory, which was discussed by Tesner [167], involves the formation of carbon through decomposition of hydrocarbons on the particle surface. Tesner studied the formation of

carbon black in an externally heated reaction tube and concluded that the process took place in two stages: (1) nuclei formation and (2) particle growth. He found that when a hydrocarbon is thermally decomposed in a flow system, the spontaneous formation of nuclei of carbon black particles in the main part of the gas is accompanied by the simultaneous surface formation of a solid carbon layer on the reaction chamber walls.

5. The Boudouard Reaction Theory. It has been proposed by Behrens [180] and van der Held [168] that the Boudouard reaction, which is the reaction predicted in an equilibrium chemistry analysis,



may contribute to carbon formation in premixed flames. This reaction, which, in the presence of hydrogen, proceeds through the stages



is usually so slow, however, that in typical reaction times in combustion chambers ( $\sim 5 \times 10^{-3}$  sec), the Boudouard reaction would be far from complete. Foster [202] states that carbon (soot) is not likely to appear in equilibrium in the products of fuel-rich premixed combustion because the decomposition of hydrocarbons to carbon proceeds more rapidly than oxidation reactions of hydrocarbon or soot with  $\text{CO}_2$  or  $\text{H}_2\text{O}$ . These latter reactions would cause the system to be in equilibrium if it were allowed to proceed for a sufficient length of time.

Carpenter, Foreman, and Goldstein [14] state that to determine the amount of free carbon with considerable accuracy, it would be necessary to consider the dissociation of each constituent in the exhaust gas and to match the dissociation of each constituent subject to the constraint that the total number of atoms remain constant in the resulting mixture. Such calculations are given by Gaydon and Wolfhard [158], Huff, Gordon, and Morrell [203], Penner [204], and Dodge [205] who states that carbon deposition for the Boudouard reaction is possible only if  $n_{\text{CO}}^2/n_{\text{CO}_2}$  is equal to or greater than  $K_p/P$ , where  $K_p$  is the equilibrium constant for the process,  $P$  is the total pressure of the mixture, and  $n_{\text{CO}}$  and  $n_{\text{CO}_2}$  are the number of moles of CO and  $\text{CO}_2$ , respectively.

6. "Vapor Pocket" Theory. Boynton [206] relates a possible theory for carbon formation in rocket combustion chambers using the "vapor pocket" theory. He believes that the individual drops of fuel and oxidizer in the chamber evaporate soon after injection to form small vapor "pockets" whose size depends upon the characteristics of the particular injector. These vapor pockets would thus interact with each other, burn at the edges, and then break up, coalesce, and circulate very rapidly. The reaction zone would transfer heat by conduction into the fuel vapor pocket interior, breaking the vapor into fragments which react to form carbon particles. The carbon would be more apt to form from the larger vapor pockets in which the fuel vapor volume-burning surface ratio is larger, and would also be more apt to form (Boynton and Neu [201]) when less efficient injectors are used. This theory is compatible with the combustion inefficiency calculations of Farmer et al. [1].

7. New Carbon Formation Theories. Several new theories on carbon particle formation were discussed at the Eleventh Symposium (International) on Combustion held at Berkley, California, August 14-20, 1966. Homann and Wagner [208] discussed experiments of acetylene and benzene premixed flames and stated that for acetylene flames, the polycyclic aromatic hydrocarbons form some distance behind the oxidation zone and are similar to those evaporating from soot samples when heated in a mass spectrometer under reduced pressure. Their concentration profiles in acetylene flames showed that they were by products instead of intermediates for carbon. For benzene flames, however, it was found that these polycyclic aromates appeared during fuel oxidation such that their concentration was much larger in the region where solid carbon formed. Echigo, Nishiwaki, and Hirata [209] discussed spectroscopic analyses of ten hydrocarbon flames and proposed a new theory that the combustion process results in dehydrogenation and polymerization reactions in the fluid phase. They found the resulting, unsaturated hydrocarbons ("pre-soot substances") emitted band spectra rather than a continuum and that eventually soot particles were agglomerated after dehydrogenation and polymeration were complete.

Also in the Eleventh Symposium, Tesner, Snegyreva, and Soorovikin [210] discussed formation of carbon by thermal decomposition and incomplete hydrocarbon combustion, describing a two-step process: the generation of carbon nuclei and the growth of the carbon particles. They measured rates of carbon particle formation during thermal decomposition of acetylene in laminar diffusion flames and decomposition of aromatic hydrocarbons when mixed with a turbulent flow of hot combustion products. They found that, because of chain branching, soot particle formation occurred with a tremendous

speed, but because of quadratic terminations, was rapidly suppressed; hence the curve of rate of particle formation acquired a sharp peak. Cullis, Read, and Trimm [211] discussed another theory at this symposium and stated that it is unlikely that carbon formation always involves the intermediate production of acetylene. They conducted experiments on the pyrolysis of acetylene and vinylacetylene (a polyunsaturated compound) at 500° C and 700° C and found, in contrast to a wide variety of acetylenic products formed during acetylene pyrolysis, vinylacetylene was converted directly to solid carbon products.

8. Carbon Ionization Theories. Certain investigators such as Singer and Grumer [166], Carpenter, Foreman, and Goldstein [14], Einbinder [212], Shuler and Weber [213], Smith [214], and Sugden and Thrush [215] have shown that carbon particles can be responsible for ions observed in flames and rocket exhausts. Singer and Grumer [166] believe that the ionization in hydrocarbon-fueled flames must be caused by accumulating species which are either carbon nuclei or carbon precursors of low ionization potential. This ionization potential (or work function) for carbon particles has a low value (between 4.35 eV for solid carbon and 13.3 eV for gaseous carbon) compared to the reaction intermediates and products of flames (H<sub>2</sub>O, CO, CO<sub>2</sub>, OH, O, and H) which have ionization potentials of between 12 and 16 eV.

Shuler and Weber [213] studied the ionization of carbon particles in acetylene-oxygen flames burning in air and proposed that the free electron concentration be given by the Saha [216] or equilibrium thermionic emission equation

$$N_e = K = \frac{2 (2\pi m_e k T)^{3/2}}{h^3} e^{-\phi/kT}, \quad (239)$$

where  $\phi$  is the carbon particle work function,  $m_e$  is the mass of the electron,  $T$  is the temperature in degrees K, and  $k$  and  $h$  are the Boltzmann and Planck constants, respectively. Sugden and Thrush [215] also studied carbon particle ionization in acetylene flames and proposed the following modified equation:

$$N_e = \frac{2 (2\pi m_e k T)^{3/2}}{h^3} \exp[-(\phi + N_e e^2/r_p N_p)/kT], \quad (240)$$

where  $r_p$  and  $N_p$  are the radius and concentration, respectively, of the carbon particles and  $e$  is the electronic charge. Einbinder [212] presents a further

modification to equation (239) by writing the ratio of the electron concentration to the carbon particle concentration as

$$N_e/N_p = (r_p k T/e^2) \ln (K/N_e) + \frac{1}{2}, \quad \text{for } (N_e/N_p \geq 3), \quad (241)$$

where  $K$  is determined from equation (239).

Pergament [217] and Pergament and Calcote [218], Kurzias [219] and other workers at AeroChem have investigated chemi-ionization effects in rocket combustion chambers and exhausts when solid carbon is present. They state that the electrons and chemi-ions such as  $\text{CHO}^+$  and  $\text{H}_3\text{O}^+$  may be formed if carbon gas is in equilibrium with hydrogen atoms in the process



the  $\text{CH}$  combines with free oxygen to produce  $\text{CHO}^+$  ions and electrons in the process



The  $\text{CHO}^+$  ions are then combined with water to produce hydronium ions,  $\text{H}_3\text{O}^+$ , in the process



The Thermal Environment Branch at MSFC is sponsoring an experimental program at altitude at Cornell Aeronautical Laboratory involving the use of resonant cavity probes to determine electron concentrations in an ethylene-oxygen plume (scale model of the F-1 engine). Later, it is planned to make the same type measurements in the plumes of model solid propellant ullage and retro motors of the Saturn vehicle. The theoretical programs at AeroChem and at Boeing [220, 221] will be used to check the experimental data.

In summary, the problem of determining a suitable theory for formation of carbon particles and ions in flames and rocket exhausts is very difficult. The Thermal Environment Branch, with assistance from one of its contractors, plans to initiate a program soon to determine carbon particle formation and concentration associated with H-1 and F-1 engine exhausts. This program would involve basically the study of the mixing processes of RP-1 and liquid oxygen, the study of the chemical composition of RP-1 and its pyrolysis products, and the chemical reactions leading to soot formation. Another program sponsored by this branch which is being performed at General Applied Science Laboratories by Edelman [222] involves the analytical investigation of plume afterburning associated with H-1 and F-1 engines. In this analysis the diffusion equations are combined with the finite-rate chemical kinetic equations to handle the mixing and combustion along the plume boundary. The radiation to the vehicle base from carbon particles present in the mixing layer is then analyzed in the program. A preliminary report has been completed on this subject [223].

## Carbon Particle Size Determination

Accurate knowledge of carbon particle sizes in flames and rocket exhausts is an important factor in determining the scattering and emission processes and consequently the thermal radiation from these flames and exhausts. Measurements of the size of carbon particles in luminous flames and rocket exhausts vary, depending upon the various methods used to obtain the particular samples. In general, however, most investigators have found that the radius,  $r_p$ , of carbon particles lies between 50 Å to 1000 Å. Wolfhard and Parker [224] have obtained electron micrographs for carbon particles in hydrocarbon flames showing this 50 Å to 1000 Å range for particle radius. Parker and Wolfhard [160] found that in non-smoky acetylene flames all particles were of about the same size ( $r_p \sim 50$  Å); however, in a smoky flame large particles of approximately 250 Å were also found. Lee, Thring, and Beer [174], using a gaseous hydrocarbon mixture of 70 percent  $C_3H_8$ , 10 percent  $C_2H_4$ , and 20 percent  $C_3H_6$  found an initial average particle radius of 200 Å, but found that the size of the particle decreased as the particle underwent combustion. Scully and Davis [171] experimenting with various aromatic hydrocarbons, found that the average particle radii ranged from 100 Å to 400 Å.

Erickson, Williams, and Hottel [225] performed light-scattering measurements on soot in a benzene-air flame and also obtained electron micrographs of samples on a probe showing an average soot particle radius of 125 Å. Measurements of particle radius obtained by light-scattering measurements were

considerably higher ( $r_p \sim 700 \text{ \AA}$ ) than the electron micrographs; however, it was determined that the soot in the flame was partially agglomerated such that the experimental data were strongly affected. Kunugi and Jinno [226] also used light-scattering techniques to obtain sizes and concentrations of soot particles in diffusion flames. These investigators calculated particle size by comparing the measured ratio of the two light-scattering intensities for perpendicular and parallel polarizations, with the intensities calculated by Mie scattering theory, and obtained a value of  $r_p$  of between  $600 \text{ \AA}$  and  $1000 \text{ \AA}$ . These values were 3 to 5 times higher than those obtained for soot particles collected on a solid surface inserted into a flame; however, these authors state that the light-scattering method used tended to measure only the larger particles which scatter the light more effectively than the smaller ones. Singer and Grumer [166] obtained particle samples on stainless steel screens in rich, flat flames of propane-air and ethylene-air. These investigators also obtained evidence of agglomeration in the shape of long filaments with opaque granules at the tips or bends of the filaments. Particle radii as large as  $2500 \text{ \AA}$  were observed on the filaments. Millikan [227, 228] attempted to circumvent the agglomeration problem by sucking the particle-containing gas through a small orifice into a quartz tube, expanding it to a low pressure and catching the particles upon a cold target. The carbon particles obtained in this manner were about  $50 \text{ \AA}$  in radii 6 mm from the burner exit and grew to about  $200 \text{ \AA}$  in radii at 12 mm above the burner exit.

Tesner [167] also obtained carbon particle size distributions in various hydrocarbon flames and found virtually no particles at all below a radius of  $50 \text{ \AA}$ , and an average particle radius of about  $200 \text{ \AA}$ . He also found carbon concentrations ranging from  $2 \times 10^{10}$  to  $2 \times 10^{12}$  particles per  $\text{cm}^3$ . Johnson and Anderson [229] recently investigated carbon particles formed by pyrolysis at  $500^\circ \text{ C}$  to  $1000^\circ \text{ C}$  for a large number of hydrocarbon fuels. They found that the various types of solid carbon particles formed varied from small, isolated specks of material, about  $50 \text{ \AA}$  in radius up to large dense particles about  $2500 \text{ \AA}$  in radius, which were approximately spherical in shape and which were hooked together into networks of chain-like structures. It was found that, by varying the pyrolysis temperature, contact time, and hydrocarbon concentration, there appeared to be a gradual transition between one type of particle to another with no sharp dividing line between particular types at any stage.

Boynton [206] obtained carbon particle samples on flat plates from the exhaust of small rocket engines ( $P_c = 500 \text{ psia}$ , nozzle exit diameter = 1.5 inches,  $A_e/A_t = 8$ ) using RP-1 as the fuel and liquid oxygen as the oxidizer. The flat plates were mounted on a water-cooled pendulum which was moved

rapidly through the plume. The pendulum was swung through the plume at various distances downstream of the exit, with the amount of deposited carbon determined by weighing the disks on an analytical balance. It was found that the amount of carbon on the flat plates decreased with increasing distance downstream and that the average radius of the particle was approximately  $175 \text{ \AA}$ , the size distribution being Gaussian.

In a recent investigation performed at Rocketdyne [199] under a Thermal Environment Branch contract, carbon particle sizes were determined from full-scale F-1 engine exhausts. The particles were pumped through a water-cooled probe shown in Figure 17 which was immersed 1.12 inches and 4.12 inches into the plume for two engine firings. It was shown that the average particle radius ranged from  $100 \text{ \AA}$  to  $300 \text{ \AA}$ , a range which agreed well with previous samplings taken from model F-1 engine exhausts.

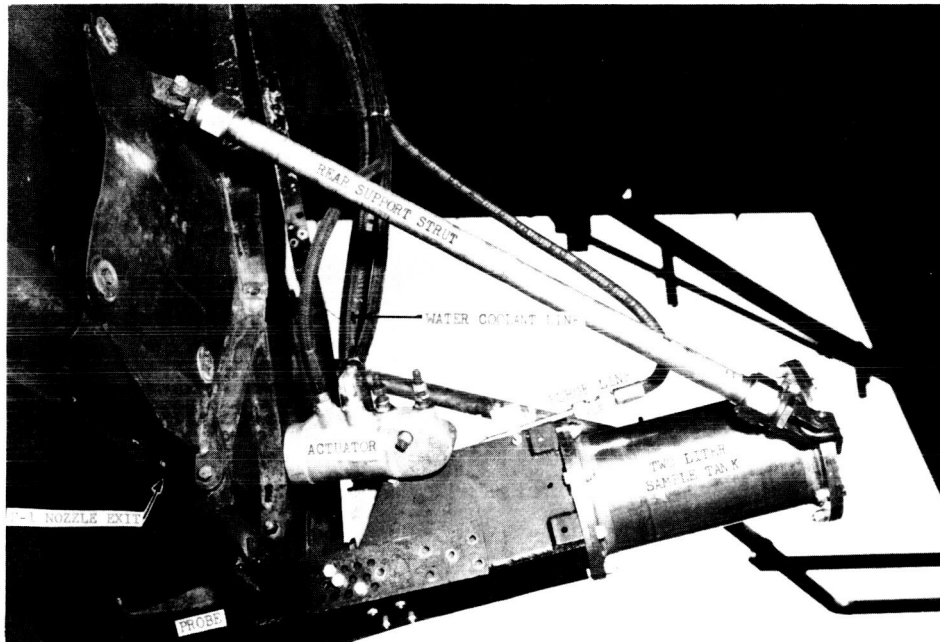


FIGURE 17. ROCKETDYNE F-1 HOT GAS SAMPLER SHOWING 4.12-INCH PROBE IMMERSION

Ferriso et al. [230] and Boynton et al. [231] also report on measurements of carbon particle size in rocket exhausts. They, as did Boynton [206], collected the particles on small water-cooled plates which were rapidly passed

through the plume at four inches downstream of the nozzle exit. The samples of carbon particles were taken at various oxidizer-fuel ratios for three engines of area ratio,  $A_e/A_t$ , of 5.25, 3.0 and 1.5 (See this section, subtitle "Methods of Predicting Carbon Absorption Coefficients and Emissivities," part 4.). However, it was found that at oxidizer-fuel ratios smaller than 1.6 the carbon deposits were too heavy and the particles agglomerated considerably during the collecting process such that it was impossible to distinguish individual particles. Using stereographic photomicrographs with shadow casting, it was found that at O/F ratios greater than 1.6 the mean value for  $r_p$  was approximately  $200 \text{ \AA}$ , a value which is representative of all the mean particle radii mentioned in this section.

## Dispersion Equation for Carbon

In this section the dispersion equation for carbon is discussed and the relations for conductivity,  $\sigma$ , polarization,  $P$ , dielectric constant,  $\epsilon$ , and index of refraction  $n = n_1 - in_2$  are determined. The Rayleigh theory of scattering by carbon particles is dependent upon this dispersion theory, as will be seen in the next section.

The classical theories of dispersion in gases, liquids and solids, and metals (conducting materials) are described by Stratton [232], Slater and Frank [233, 234], Born and Wolfe [235], Panofsky and Phillips [57], Sommerfeld [236], Böttcher [237], Fleagle and Businger [238], and Wood [239]. A dispersive medium is defined as one in which the index of refraction of the medium varies with frequency of propagation. Another definition sometimes used is that a dispersive medium is one in which the phase velocity  $v$  of a superposition of harmonic wave trains of infinite length and duration varies with the frequency of propagation. In a nonconducting (dielectric), nonmagnetic medium, a wave is propagated with a phase velocity  $v = c/n$ , where  $c$  is the velocity of light in empty space and  $n$  is the index of refraction equal to  $(\epsilon\mu)^{1/2} \approx \epsilon^{1/2}$ , since the permeability  $\mu$  is usually assumed close to unity (except for ferro-magnetic materials).

For gases, the dispersion theory was actually discussed in the previous section, subtitle "Radiating from an Accelerated Charge," to predict the radiation (absorption) by a classic dipole. In this manner, an electron of charge  $e$  was acted on by a force  $eE$  of an external electric field  $E = E_0 e^{-i\omega t}$  and received a linear restoring (elastic) force,  $-Gx = -m\omega_0^2 x$ , proportional to the

displacement  $x$  of the electron, and also a damping or dissipative force,  $-m\gamma\dot{x}$ , proportional to the velocity of the electron. This equation, (86), will now be rewritten in the form

$$m\ddot{x} + m\omega_0\dot{x} + m\gamma x = eE \quad , \quad (245)$$

which has the solution

$$x = E \frac{e}{m} \left( \frac{1}{\omega_0^2 - \omega^2 - i\omega\gamma} \right) \quad . \quad (246)$$

It may be noted that in the remainder of this section (and the following section) the quantities,  $E$ ,  $J$ ,  $P$ ,  $D$ ,  $x$ ,  $\dot{x}$ , and  $\ddot{x}$  are all vector quantities.

The polarization,  $P$ , will now be defined as

$$P = e \sum_k N_k x_k = E \sum_k \frac{N_k e^2/m}{\omega_0^2 - \omega^2 - i\omega\gamma_k} \quad , \quad (247)$$

where  $N_k$  is the number of electrons per unit volume characterized by the constants  $\omega_k$  and  $\gamma_k$ .

The dielectric constant  $\epsilon$  will now be written as

$$\epsilon = 1 + N \frac{\beta}{\epsilon_0} \quad , \quad (248)$$

where  $\beta$  is the polarizability and is equal to the dipole moment  $ex$  divided by the electric field  $E$ .

Hence, equation (248) may be written as

$$\epsilon = 1 + \sum_k \frac{N_k e^2/m\epsilon_0}{\omega_{0k}^2 - \omega^2 - i\omega\gamma_k} = (n_1 - in_2)^2 \quad . \quad (249)$$

For an absorbing gas the dielectric constant is a complex quantity and may be written in terms of its real and imaginary components,  $n_1$  and  $n_2$ . Furthermore, the second term in equation (249) is usually small in gases with respect to unity so that the square root of equation (249) can be written as

$$\epsilon^{\frac{1}{2}} = n_1 - in_2 = 1 + \frac{1}{2} \sum_k \frac{N_k e^2/m\epsilon_0}{\omega_{o_k}^2 - \omega^2 - i\omega\gamma_k} , \quad (250)$$

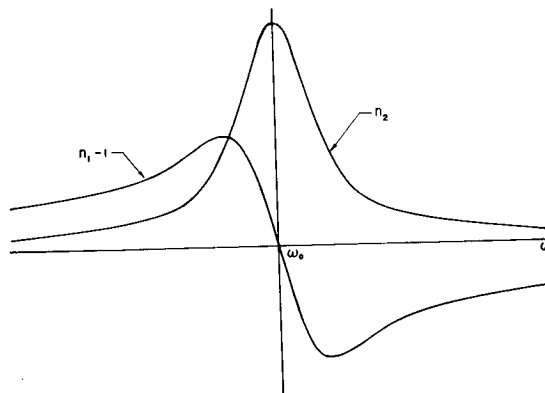
in which the real part  $n_1$  and imaginary part  $n_2$  are, respectively,

$$n_1 = 1 + \frac{1}{2} \sum_k \frac{(N_k e^2/m\epsilon_0) (\omega_{o_k}^2 - \omega^2)}{(\omega_{o_k}^2 - \omega^2)^2 + \omega^2 \gamma_k^2} , \quad (251)$$

and

$$n_2 = 1 + \frac{1}{2} \sum_k \frac{(N_k e^2/m\epsilon_0) \omega \gamma_k}{(\omega_{o_k}^2 - \omega^2)^2 + \omega^2 \gamma_k^2} . \quad (252)$$

As the frequency increases, the index of refraction  $n$  experiences the phenomenon of "anomalous dispersion" in the vicinity of each of the resonant frequencies,  $\omega_{o_k}$ . This phenomenon can be seen in Figure 18 as at  $\omega_o$  the quantity  $n_1 - 1$  changes sign while the quantity  $n_2$  (and hence the absorption) is a maximum.



Showing Real ( $n_1$ ) and Imaginary ( $n_2$ ) Parts of Index of Refraction  $n = n_1 - in_2$  in Neighborhood of Resonant Frequency,  $\omega_o$ .

FIGURE 18. ANOMALOUS DISPERSION

For solids and liquids it cannot be assumed that the force acting on an electron is merely equal to the electric vector of the electromagnetic wave in free space. Instead, the added force on the electron caused by the polarization of the body must be considered. According to Slater and Frank [234], a small sphere with its center at the position of the electron in question may be considered to have been cut out of the medium. Charges are then induced on the surface of the sphere producing a force at the center of the sphere which now has a total electric field at the center of the sphere of

$$E' = E + \frac{P}{3\epsilon_0} \quad (253)$$

This contribution to the field because of polarization of the body is also known as the Lorentz field. The polarization,  $P$ , as given in equation (247) now becomes

$$P = \left( E + \frac{P}{3\epsilon_0} \right) \sum_k \frac{N_k e^2/m}{\omega_{0k}^2 - \omega^2 - i\omega\gamma_k} \quad (254)$$

and an expression for the dielectric constant may be written as

$$\frac{\epsilon - 1}{\epsilon + 2} = \frac{(n_1 + in_2)^2 - 1}{(n_1 + in_2)^2 + 2} = \frac{1}{3} \sum_k \frac{N_k e^2/m\epsilon_0}{\omega_{0k}^2 - \omega^2 - i\omega\gamma_k} \quad (255)$$

For conducting materials such as metallic or carbon particles, a slightly different approach to the dispersion theory is developed. It is assumed that not all of the electrons are bound to the atoms (i. e., bound electrons,  $N_k$ ), but some are free to move about within the material (i. e., conduction electrons). Both the bound and conduction electrons of the material are forced to oscillate by the incident, periodic electromagnetic wave. The total number of electrons per unit volume,  $N$ , may be thus written as

$$N = \sum_k N_k + N_c = \frac{Zd}{m_a} \quad (256)$$

where  $Z$  is the atomic number,  $m_a$ , the mass in grams of one atom of the conducting material, and  $d$  is the density of the conducting material.

It is usually assumed that the fixed, positive ions of the conductor comprise a region of constant electrostatic potential. Within this region a cloud of free or conduction electrons wanders about and thus carries the current in the direction of an applied electric field,  $E$ . The motion of free electrons is opposed by collisions at the lattice points which are occupied by the heavy ions. The momentum transfer from the drifting electrons to the lattice points results in thermal vibrations of the ions and a damping of the electron motion. The resulting equation of motion is thus similar to equation (245) except that there is no restoring force; hence,  $\omega_0$  is zero. This equation takes the form

$$m\ddot{x} + m\gamma_c \dot{x} = eE \quad , \quad (257)$$

whose steady-state solution may be written as

$$x = \frac{1}{\gamma_c - i\omega} \frac{ieE}{m} \quad . \quad (258)$$

Since  $N_c$  represents the number of conduction or free electrons per unit volume, the current density  $J$  may be written in the form

$$J = N_c e \dot{x} = \frac{N_c e^2/m}{\gamma_c - i\omega} E \quad . \quad (259)$$

However, since the static conductivity  $\sigma'$  may be defined as  $J = \sigma'E$ , a complex conductivity  $\sigma$  may thus be defined as

$$\sigma = \frac{N_c e^2/m}{\gamma_c - i\omega} = \frac{i(e^2/m) N_c}{\omega + i\gamma_c} \quad . \quad (260)$$

The dielectric constant may now be written as

$$\epsilon = \frac{D}{E} = \epsilon_0 + \frac{P}{E} \quad , \quad (261)$$

where  $E$  is now  $E = E' - P/3\epsilon_0$ .

Hence, the dielectric constant may be written as

$$\epsilon = \epsilon_0 + \frac{\frac{e^2}{m} \sum_k \frac{N_k}{(\omega_{0k}^2 - \omega^2 - i\omega\gamma_k)}}{1 - \frac{e^2}{3\epsilon_0 m} \sum_k \frac{N_k}{(\omega_{0k}^2 - \omega^2 - i\omega\gamma_k)}} \quad (262)$$

But the Lorentz field may be assumed negligible in the visible and infrared compared with  $E$ ; then  $E' = E$ , and equation (262) becomes

$$\epsilon = \epsilon_0 + (e^2/m) \sum_k \frac{N_k}{(\omega_{0k}^2 - \omega^2 - i\omega\gamma_k)} \quad (263)$$

The complex propagation constants of a particular conducting sphere (carbon particle) and the surrounding medium ( $k_1$  and  $k_2$ , respectively) can be written in the form

$$k_1 k_2 = k^2 = \mu\epsilon\omega^2 + i\sigma\mu\omega \quad (264)$$

where  $\mu$  is the magnetic permeability of the medium and  $n$  equals  $k_1/k_2$ , according to Stull and Plass [240]. If equations (260), (263), and (264) are solved simultaneously, the following equations for the real and imaginary parts of the index of refraction result:

$$n_1^2 - n_2^2 = 1 + \frac{e^2}{m\epsilon_0} \sum_k \frac{N_k (\omega_{0k}^2 - \omega^2)}{(\omega_{0k}^2 - \omega^2)^2 + \omega^2 \gamma_k^2} + \frac{e^2}{m\epsilon_0} \frac{N_c}{\omega^2 + \gamma_c^2} \quad (265)$$

and

$$2 n_1 n_2 = \frac{e^2}{m\epsilon_0} \sum_k \frac{N_k \omega \gamma_k}{(\omega_{0k}^2 - \omega^2)^2 + \omega^2 \gamma_k^2} + \frac{e^2}{m\epsilon_0} \frac{N_c}{\omega^2 + \gamma_c^2} \quad (266)$$

Stull and Plass [240] obtained values for the constants in equations (265) and (266) from Halpern and Hall [241], who investigated fast-charged particles in carbon, and from Senftleben and Benedict [242], who measured  $n_1$  and  $n_2$  for amorphous carbon at 2250° K in the visible part of the spectrum and the reflection coefficient  $\rho_\lambda$  (or reflectivity) in the infrared. This reflection coefficient is defined by Fresnel's equation as

$$\rho_\lambda = \frac{(n_1 - 1)^2 + n_2^2}{(n_1 + 1)^2 + n_2^2} \quad (267)$$

Stull and Plass [240] then solved equations (256), (265), (266), and (267) for the four unknowns  $\gamma_C$ ,  $\gamma_4$ ,  $N_C$  and  $N_4$  and obtained for a temperature of 2250° K the dispersion equations for amorphous carbon to be

$$\begin{aligned} n_1^2 - n_2^2 = 1 + \frac{6.448 \times 10^{32}}{4.062 \times 10^{35} - \omega^2} + \frac{3.224 \times 10^{32}}{9.549 \times 10^{33} - \omega^2} + \frac{3.224 \times 10^{32}}{5.217 \times 10^{33} - \omega^2} \\ + \frac{6.348 \times 10^{32} (1.966 \times 10^{32} - \omega^2)}{(1.956 \times 10^{32} - \omega^2)^2 + 1.369 \times 10^{33} \omega^2} - \frac{3.05 \times 10^{31}}{2.323 \times 10^{31} + \omega^2} \end{aligned} \quad (268)$$

and

$$\begin{aligned} 2 n_1 n_2 = \frac{6.347 \times 10^{32} \times 3.70 \times 10^{16} \omega}{(1.956 \times 10^{32} - \omega^2) + 1.369 \times 10^{33} \omega^2} \\ + \frac{3.05 \times 10^{31} \times 4.82 \times 10^{15}}{(2.323 \times 10^{31} + \omega^2) \omega} \end{aligned} \quad (269)$$

These two equations have been used by several investigators to obtain emissivities of carbon, as will be discussed later in this section.

## Rayleigh Scattering Method

This section describes the general theory of scattering by small particles such as carbon particles (in which  $\alpha \ll 1$ ) known as Rayleigh scattering. This type of scattering involves the radiation from an oscillating dipole as described

in the previous section. Among the many references which discuss Rayleigh scattering are Oster [243], Cadle [244], Green and Lane [245], van de Hulst [246], Sinclair [247], Sinclair and La Mer [248], Dallavalle [249], Orr and Dallavalle [250], Sommerfeld [236], Humphries [251], Tverskoi [252], and Bullrich [253].

According to the basic theory of Rayleigh [254-256], the oscillating electric field of the radiation incident upon a transparent optically isotropic particle in which  $\alpha$  equals  $(2\pi r_p/\lambda) \ll 1$  induces an electric moment in the particle. The statement that the particle is optically isotropic implies that the polarizability and index of refraction are independent of direction in the particle. Since the particle acts like a linear electric oscillator, it does not radiate light along other directions, however, and the scattered light is plane-polarized if seen at  $90^\circ$  to the incident ray, whether the incident ray is polarized or unpolarized. This polarization of radiation scattered by a particle cloud (such as the exhaust of a hydrocarbon-fueled rocket engine) is seen in Figure 19.

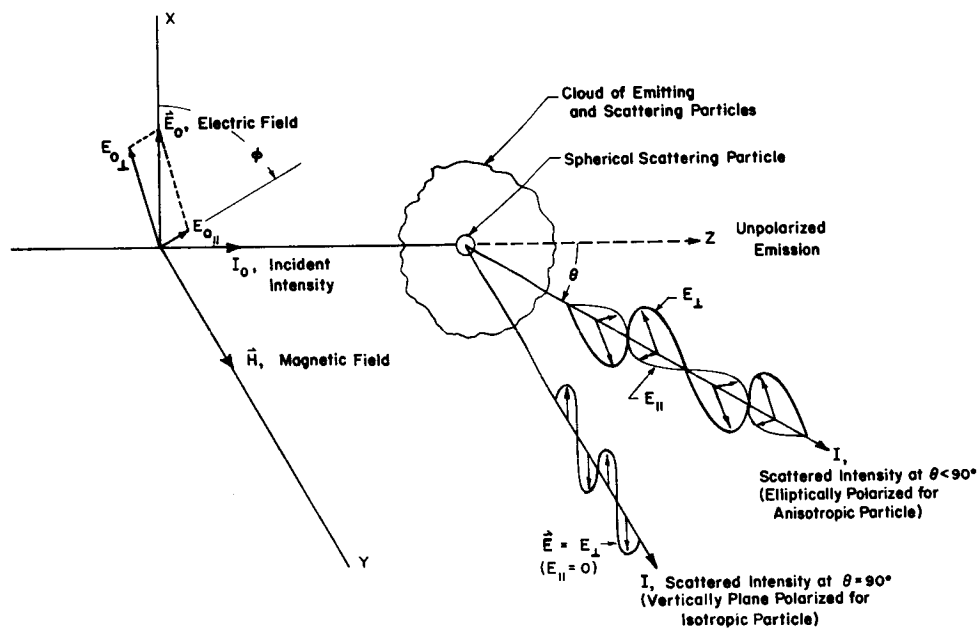


FIGURE 19. POLARIZATION OF RADIATION SCATTERED BY A PARTICLE CLOUD

If the particles were anisotropic, the direction of the incident radiation's electric field  $E$  might not coincide with the direction of the induced dipole moment  $p$ . In this case the radiation scattered at right angles would not be completely plane-polarized with vertical vibrations (as for an isotropic particle),

but would have a weak horizontal component. This isotropic versus anisotropic scattering phenomenon is also shown in Figure 19.

When the incident radiation is plane-polarized on an isotropic particle, the intensity scattered at an angle  $\psi$  can be written according to Sinclair [247] as

$$I_{\psi} = I_o \left( \frac{9\pi^2}{R^2} \left| \frac{n^2 - 1}{n^2 + 2} \right|^2 \frac{V^2}{\lambda^4} \right) \sin^2 \psi , \quad (270)$$

where  $R$  is the distance from the sphere (carbon particle) to the point of observation,  $\psi$  is the angle between the propagation direction of the scattered radiation and the electric vector in the direction of incident radiation, and  $V$  is the volume of the sphere equal to  $4/3 \pi r_p^3$ . The scattered radiation is thus plane-polarized and has its electric vector lying in the plane formed by the electric vector in the direction of incident radiation and the direction of propagation of the scattered radiation.

When the incident ray is unpolarized, the intensity of radiation scattered in the direction  $\theta$ , according to Sinclair [247], is

$$I_{\theta} = I_o \left( \frac{9\pi^2}{2R^2} \left| \frac{n^2 - 1}{n^2 + 1} \right|^2 \frac{V^2}{\lambda^4} \right) (1 + \cos^2 \theta) = i_1 + i_2 , \quad (271)$$

where  $\theta$  is the angle between the direction of propagation of the incident and scattered radiation. This equation shows that the radiation scattered by the particle consists of two incoherent, plane-polarized components whose planes of polarization are mutually perpendicular. The component  $i_1$  (the quantity in parentheses multiplied by unity) has its vibrations (electric vector) at right angles to the plane of observation. The component  $i_2$  (the quantity in parentheses multiplied by  $\cos^2 \theta$ ) has its vibrations parallel to the plane of observation.

Figure 20 shows the angular distribution of intensity and polarization of the radiation scattered from a small isotropic scattering particle if the incident radiation is unpolarized. The solid line represents the total intensity according to equation (271), and the dotted lines the intensities of the polarized components. Curve 2, which represents the  $\cos^2 \theta$  term in equation (271), is the component which is horizontally polarized, and curve 1, which represents the unity term in

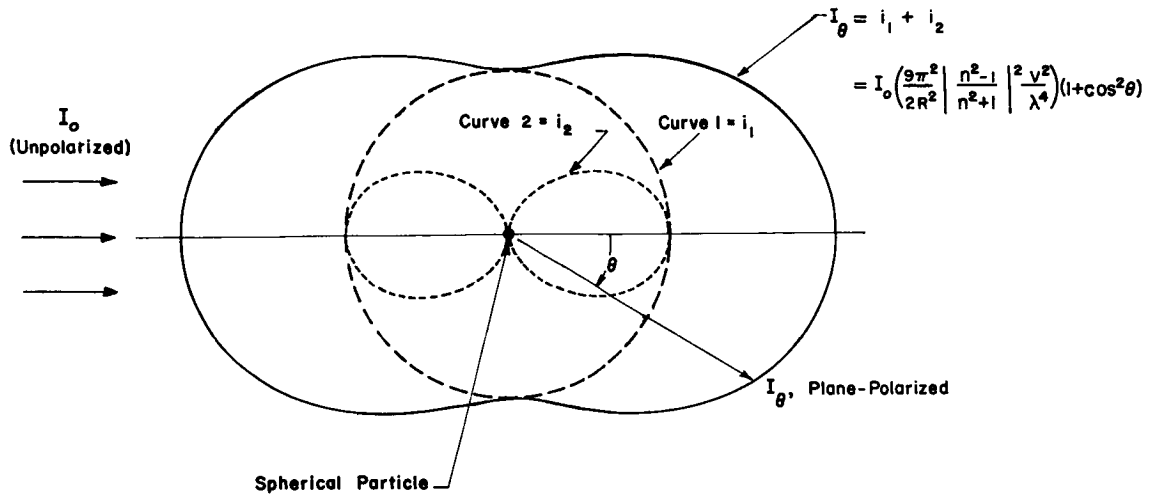


FIGURE 20. RAYLEIGH SCATTERING DIAGRAM SHOWING SCATTERED INTENSITY,  $I_{\theta}$ , AS A FUNCTION OF  $\theta$  FOR UNPOLARIZED INCIDENT RADIATION OF INTENSITY,  $I_0$

equation (271) is the term which is vertically polarized. From this figure it is thus seen that light scattered at  $90^\circ$  is vertically plane-polarized.

To obtain the scattering cross-section  $\sigma_s$ , which is necessary in predicting emissivities of carbon particles, the methods of Stratton [232], Sommerfeld [236], Born [257], Slater and Frank [234], or van de Hulst [246] should be consulted. The electric field of a scattered wave may be written according to van de Hulst in terms of the distance  $R$  from a dipole ( $R$  assumed much greater than  $\lambda$ ) as

$$E_{\theta} = \frac{k^2 p \sin \gamma}{R} e^{-ikR} \quad , \quad (272)$$

where  $\gamma$  is the angle the scattered ray makes with the induced dipole moment  $p = \beta E_0$  (where  $\beta$  is the polarizability which is equal to  $\epsilon x/E$ ) and  $k$  is the wave number which is equal to  $2\pi/\lambda$ . The intensities of the incident and scattered radiation,  $I_0$  and  $I_{\theta}$ , respectively, may be taken from the time average of the Poynting vector,  $\vec{S}^*$ , of the plane wave

$$\vec{S}^* = \frac{1}{2} \text{Re} (E_{\theta} \vec{H}_{\phi}) \quad , \quad (273)$$

where  $H_\phi$  is the average magnetic field corresponding to the current element in the dipole. These intensities, using Gaussian units, reduce to

$$I_o = \frac{c}{8\pi} |E_o|^2 \quad \text{and} \quad I = \frac{c}{8\pi} |E|^2 \quad (274)$$

If the scattered intensity  $I$  is integrated over a sphere, the total energy scattered in all directions, according to van de Hulst, is

$$W = \frac{1}{3} k^4 c |p|^2 . \quad (275)$$

The scattering cross-section  $\sigma_s$  may now be defined according to Slater and Frank [234] as the area on which enough energy falls from the plane wave to equal the scattered intensity. Hence, by dividing equation (275) by  $I_o$ , the scattering cross-section is obtained as

$$\sigma_s = \frac{8\pi}{3} k^4 |\beta|^2 = \frac{128\pi^5}{3\lambda^4} |\beta|^2 . \quad (276)$$

For spherical particles small with respect to the wavelength ( $\alpha \ll 1$ ), the polarizability  $\beta$  may be written according to the Lorentz-Lorenz equation as

$$\beta = \frac{3}{4\pi} \left| \frac{n^2 - 1}{n^2 + 2} \right| V = \left| \frac{n^2 - 1}{n^2 + 2} \right| r_p^3 = \frac{ex}{E} , \quad (277)$$

where  $x$  is given by equation (246).

Hence, the scattering cross-section may be written as

$$\sigma_s = \frac{128\pi^5}{3\lambda^4} r_p^6 \left| \frac{n^2 - 1}{n^2 + 2} \right|^2 , \quad (278)$$

showing an inverse wavelength to the fourth power dependence.

The fractional decrease of the incident radiation scattered in all directions may now be written in the following form:

$$I = I_0 e^{-\tau\lambda} = I_0 e^{-N_p \sigma_s \ell} = I_0 \exp \left[ -\frac{128}{3} \frac{\pi^5}{\lambda^4} r_p^6 \left| \frac{n^2 - 1}{n^2 + 2} \right| N_p \ell \right], \quad (279)$$

where  $N_p$  is the concentration of scattering particles per unit volume and  $\ell$  is the path length through the medium.

Another method for obtaining the scattering cross-section for Rayleigh scattering is sometimes used [79, 105]. In this manner a solution to the macroscopic wave equation,

$$\frac{\partial^2 E}{\partial x^2} = \frac{1}{v^2} \frac{\partial^2 E}{\partial t^2}, \quad (280)$$

where the phase velocity  $v$  equals  $c/n$ , may be found as

$$E = E_0 \exp \left[ i2\pi\nu \left( t - \frac{x}{v} \right) \right] = E_0 \exp \left[ -2\pi\nu n_2 x/c \right] \exp \left[ i2\pi\nu \left( t - n_1 x/c \right) \right]. \quad (281)$$

Since the intensity varies as the square of  $E$ , the intensity becomes

$$I = I_0 \exp \left[ -4\pi\nu n_2 x/c \right] = I_0 \exp(-N_p \sigma_s x), \quad (282)$$

where  $x$  is the same quantity as  $\ell$  in equation (279).

With the introduction of equation (252) for  $n_2$  (put in terms of frequency  $\nu$ ) and the insertion of equation (87) for  $\gamma$ , it is shown by these authors that for  $(\nu - \nu_0) \gg \gamma$  the scattering cross-section becomes

$$\sigma_s = \frac{8\pi e^4}{3m^2 c^4} \frac{1}{\left[ \left( \frac{\nu_0}{\nu} \right)^2 - 1 \right]^2}. \quad (283)$$

When  $\nu_0 \gg \nu$  the cross-section becomes

$$\sigma_s = \frac{8\pi e^4}{3m^2 c^4} \frac{\nu^4}{\nu_0^4} = \frac{8\pi e^4 \lambda_0^4}{3m^2 c^4} \frac{1}{\lambda^4} \quad (284)$$

This is the Rayleigh scattering equation which implies that the scattering varies as the inverse of the wavelength to the fourth power (see equation (278)). It might be mentioned that for  $\nu_0 \ll \nu$  the scattering cross-section reduces to

$$\sigma_s = \frac{8\pi e^4}{3m^2 c^4} \quad , \quad (285)$$

which is the Thompson scattering cross-section for free electrons, and shows no dependence upon wavelength.

Equations (283) and (284) are actually the same form as equation (276) if it is remembered that the polarizability in equation (276) can be written as  $ex/E$  and equation (246) is used for  $x$ . In the next section these expressions for scattering cross-section are used to predict emissivities from carbon particles.

## Methods of Predicting Carbon Absorption Coefficients and Emissivities

This section discusses several methods which have been used to predict absorption coefficients and emissivities of carbon particles in luminous flames, in certain types of carbon suspensions, and in exhausts of hydrocarbon-fueled rocket engines. The first general method to be discussed involves the theory of Rayleigh scattering discussed in the last section; the next method involves calculations made using Mie theory (which is discussed more thoroughly in the next section for  $Al_2O_3$  particles); the third method is concerned with the inverse wavelength method; and the final method involves various experimental measurements.

1. Rayleigh Theory Method. Using the Rayleigh theory of predicting scattering and absorption cross-sections, Main and Bauer [258] have calculated absorption coefficients for particulate carbon in carbon-air mixtures. These

calculations were performed for particle radii of 50 Å to 1600 Å and for wavelengths of 2000 Å, 4000 Å, and 8000 Å.

Using the Rayleigh (or Mie) theories, the absorption coefficient for a particle cloud may be written in the form of the total or extinction cross-section  $\sigma_t$  as

$$\kappa_\lambda = \sigma_t N_p, \quad (286)$$

where  $\sigma_t$  equals  $\sigma_s + \sigma_a$  and  $\sigma_a$  is the absorption cross-section. The cross-sections  $\sigma_s$ ,  $\sigma_a$ , and  $\sigma_t$  are related to the efficiency factors  $Q_s$ ,  $Q_a$ , and  $Q_t$ , respectively, in the following manner:

$$\frac{\sigma_s}{\pi r_p^2} = Q_s, \quad \frac{\sigma_a}{\pi r_p^2} = Q_a, \quad \text{and} \quad \frac{\sigma_t}{\pi r_p^2} = Q_t. \quad (287)$$

By using equation (276) for the scattering cross-section, the following relation for the scattering efficiency factor is obtained:

$$Q_s = \frac{8}{3} \alpha^4 \left| \frac{n^2 - 1}{n^2 + 2} \right|^2, \quad (288)$$

where  $\alpha = kr_p = (2\pi/\lambda) r_p$ . The absorption efficiency factor,  $Q_a$ , derived in the next section, may be written as

$$Q_a = -4\alpha \operatorname{Im} \left( \frac{n^2 - 1}{n^2 + 2} \right). \quad (289)$$

The concentration,  $N_p$ , of carbon particles of mean radius  $r_p$ , which makes up a dispersion of mass density  $\rho$  can be written according to Main and Bauer [258] as

$$N_p = \rho / \left[ \left( \frac{4}{3} \right) \pi r_p^3 \delta \right], \quad (290)$$

where  $\delta$  is the density of solid graphite. The absorption coefficient may thus be written in the form

$$\kappa_{\lambda} = \sigma_t N_p = \frac{3}{4} \left( \frac{\rho}{\delta} \right) \frac{Q_t}{r_p} = \frac{3}{4 r_p} \left( \frac{\rho}{\delta} \right) \left[ \frac{8}{3} \alpha^4 \left| \frac{n^2 - 1}{n^2 + 2} \right|^2 - 4\alpha \operatorname{Im} \left( \frac{n^2 - 1}{n^2 + 2} \right) \right] . \quad (291)$$

However, for particle radii of  $200 \text{ \AA}$  or smaller (close to the median size of carbon particles in flames or rocket exhausts as discussed in the second part of this section) and for wavelengths greater than about  $2 \mu$ , Main and Bauer found that the scattering cross-sections were several orders of magnitude smaller than the absorption cross-sections. Hence, the absorption coefficient  $\kappa_{\lambda}$  reduces to

$$\kappa_{\lambda} = \sigma_a N_p = \frac{3}{4} \left( \frac{\rho}{\delta} \right) \left[ -4 \operatorname{Im} \left( \frac{n^2 - 1}{n^2 + 2} \right) \right] . \quad (292)$$

This relation for absorption coefficient thus depends only upon the index of refraction  $n$  (and hence the wavelength of radiation,  $\lambda$ ) and is thus independent of radii of the particles. Using values of  $n_1$  and  $n_2$  of graphite at  $2250^{\circ} \text{ K}$  based upon the calculations of Stull and Plass [240] and the measurements of Senftleben and Benedict [242], Main and Bauer [258] calculated values of  $\kappa_{\lambda}$  for a carbon-air suspension in which the amount of carbon was varied from 0 to 100 percent by weight. These calculations were made for temperatures of  $3000^{\circ} \text{ K}$  to  $10,000^{\circ} \text{ K}$  and for pressures of 0.0316 atm and 1 atm.

2. Mie Theory Method. The detailed derivations of the equations involved in the Mie scattering theory are discussed in the section entitled "Radiation from  $\text{Al}_2\text{O}_3$  Particles," where it is shown that the Rayleigh theory is merely a limiting case of the Mie theory. Although the Mie theory has usually been used for larger particles of 1 to  $5 \mu$  in radius and in which the parameter  $\alpha$  is approximately 1, various investigators such as Stull and Plass [240], Krascella [259], Beheshti [260], Foster [261], Erickson, Williams, and Hottel [225], Howarth, Foster, and Thring [262], and Yagi [263] and Ruedy [264] (in two very early analyses) have used Mie theory for carbon particles in which  $\alpha$  is generally assumed to be less than unity.

In Stull and Plass's [240] investigation, carbon particle emissivities were obtained for a range of particle radii from  $0.005 \mu$  to  $0.1 \mu$  and a wavelength range of  $0.4 \mu$  to  $20 \mu$ . Krascella [259] considered particle radii ranging from  $0.05 \mu$  to  $1.0 \mu$  and a wavelength range of  $0.25 \mu$  to  $4.0 \mu$ . Beheshti [260] investigated particle radii from  $0.005 \mu$  to  $1.0 \mu$  and wavelengths varying from  $0.2 \mu$  to  $40 \mu$ . Foster [261] treated particle radii from  $0.05 \mu$  to  $0.4 \mu$  and a wavelength range of  $0.5 \mu$  to  $6.0 \mu$ .

Erickson, Williams, and Hottel [225] made both theoretical calculations and experimental measurements to determine intensity of radiation scattered from a premixed laminar benzene-air flame. In the experimental investigation, relative intensities for both the parallel and perpendicular components were measured at a number of angular positions in the range of scattering angle  $\theta = 30$  to  $150$  deg. For the theoretical investigation using Mie theory, values of intensity were calculated for refractive indices  $n = 1.71 - 0.76i$  and  $n = 1.40 - 1.00i$  for values of  $\alpha$  of  $0.8$  to  $1.30$  and for wavelengths of  $4358 \text{ \AA}$  and  $5461 \text{ \AA}$ .

Howarth, Foster, and Thring [262] evaluated the extinction coefficient  $Q_t$  for carbon particles less than  $600 \text{ \AA}$  in diameter in the  $1\text{-}\mu$  to  $4\text{-}\mu$  wavelength range and over a temperature range of  $1000^\circ \text{ K}$  to  $2000^\circ \text{ K}$ . These authors calculated the damping constants  $\gamma_1, \gamma_2, \gamma_3$ , and  $\gamma_c$  appearing in equations (265) and (266) as a function of temperature and found that in the  $1\text{-}\mu$  to  $4\text{-}\mu$  wavelength range and  $1000^\circ \text{ K}$  -  $2000^\circ \text{ K}$  temperature range the value of  $Q_t$  varied from  $0$  to  $30$  percent. It was found that the mean value of extinction coefficients measured over a non-isothermal optical path varied less than  $10$  percent.

In all of the above investigations mentioned, the carbon particles were assumed to be spherical and embedded in an infinite, homogeneous, non-conducting medium. The general equations for the Mie total and scattering cross-sections are given by Mie [265], Stratton [232], van de Hulst [246], Born and Wolfe [235], and are derived in the section entitled "Radiation from  $\text{Al}_2\text{O}_3$  Particles," of this report as

$$\sigma_t = \frac{2\pi r^2}{\alpha^2} \text{Re} \sum_{m=1}^{\infty} (2m+1) (a_m + b_m) \quad (293)$$

and

$$\sigma_s = \frac{2\pi r^2}{\alpha^2} \sum_{m=1}^{\infty} (2m+1) (|a_m|^2 + |b_m|^2), \quad (294)$$

where the  $a_m$  and  $b_m$  are the Mie coefficients which may be expressed in terms of spherical Bessel and Hankel functions,  $J_m$  and  $H_m^{(1)}$ , respectively.

The equations for  $a_m$  and  $b_m$  may be simplified if the carbon sphere and the external medium are assumed to have the same magnetic permeability ( $\mu_1 = \mu_2$ ), if the recursion relation is used for  $J_m$  and its derivatives, and if the Neumann function  $Y_m = i (J_m - H_m^{(1)})$  is used. The discussion of the above method to obtain Mie coefficients, together with another method, the logarithmic derivative method, is given in the following section.

The eight groups of investigators mentioned [225, 240, and 259-264] found, as Main and Bauer [258], using the Rayleigh theory, that the absorption cross-sections  $\sigma_a$  (and hence  $Q_a$ ) were much larger than the scattering cross-sections  $\sigma_s$  (and hence  $Q_s$ ) for low values of  $\alpha$ . Figure 21 (taken from Foster [261]) shows this phenomenon at a wavelength of  $1.8 \mu$ . It will be shown in the following section that with further increase in  $\alpha$  the total or extinction efficiency factor will oscillate about the value 2.0.

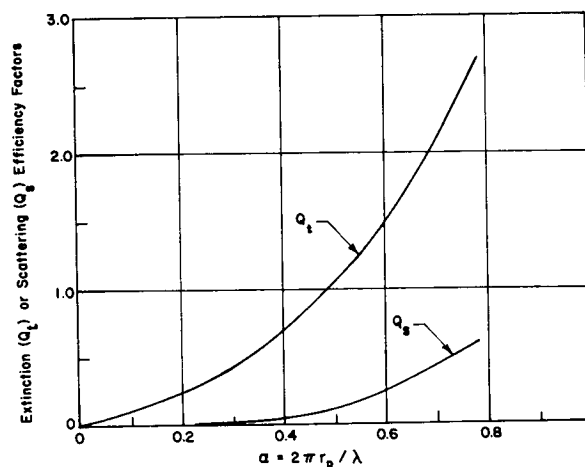


FIGURE 21. EXTINCTION AND SCATTERING EFFICIENCY FACTORS FOR CARBON PARTICLES AS A FUNCTION OF  $\alpha$  FOR  $\lambda = 1.8 \mu$

After the scattering and absorption cross-sections have been obtained, the emissivity of a cloud of particles may be obtained as

$$\epsilon = 1 - e^{-N_p(\sigma_s + \sigma_a)\ell} = 1 - e^{-N_p \sigma_t \ell} \quad (295)$$

Both Stull and Plass [240] and Beheshti [260] present curves of emissivity for carbon particle clouds as a function of wavelength for various values of  $L = N_p \ell$  and particle radii. Stull and Plass also present curves of intensity (discussed in the following subsection) and emissivity for two distributions of particle sizes. One of these was a symmetrical distribution of particle radii about  $200 \text{ \AA}$  and was calculated as

$$N(r_p) dr_p = (N_p/159.52) \exp \left\{ - \left[ (r_p - 200)/90 \right]^2 \right\} dr_p, \quad (296)$$

where  $r_p$  was in angstroms. Another distribution, which was asymmetrical, was calculated as

$$N(r_p) dr_p = 4.75 \times 10^5 N_p r_p^{-3} e^{-640/r_p} dr_p \quad (297)$$

for  $50 \text{ \AA} < r_p < 1000 \text{ \AA}$  and was assumed to be zero outside of this range.

Figure 22, taken from Stull and Plass [240], shows emissivity as a function of wavelength using Mie theory and equation (297) as the particle distribution. It is apparent from this figure that scattering is important only for the small wavelengths ( $\lambda < 2 \mu$ ). For  $L = 10^{13}$  particles/cm<sup>2</sup>, it can be seen that emissivity is that of a blackbody over practically all of the infrared wavelength region. Thompson [266], who made radiation measurements in the exhaust of an F-1 turbine, showed that, for a value of  $L$  of  $2.72 \times 10^{13}$  (corresponding to a path length of  $4 \frac{3}{4}$  in.), using equation (297), an  $800^\circ \text{ K}$  blackbody curve resulted for the emissivity. Figure 23 (taken from Beheshti [260]) shows emissivity as a function of wavelength for various particle radii and values of  $L$ . These values of  $r_p$  and  $L$  are felt to be representative of exhausts of RP-1 fueled rocket engines.

3. Inverse Wavelength Method. In addition to the Rayleigh and Mie theories of predicting emissivities of carbon particles, numerous investigators have used approximate relations based on an inverse wavelength dependence which is derived from experimental data. Some of these investigators include Becker [267], Rossler and Behrens [268], Pepperhoff [269], Naeser and Pepperhoff [270], Pepperhoff and Bahr [271], Plyler and Humphreys [272], Rossler [273], Heidman and Priem [274], Yagi and Lino [275], Hottel and Broughton [276], Millikan [227,228], Schack [277], and Siddall and McGrath [278].

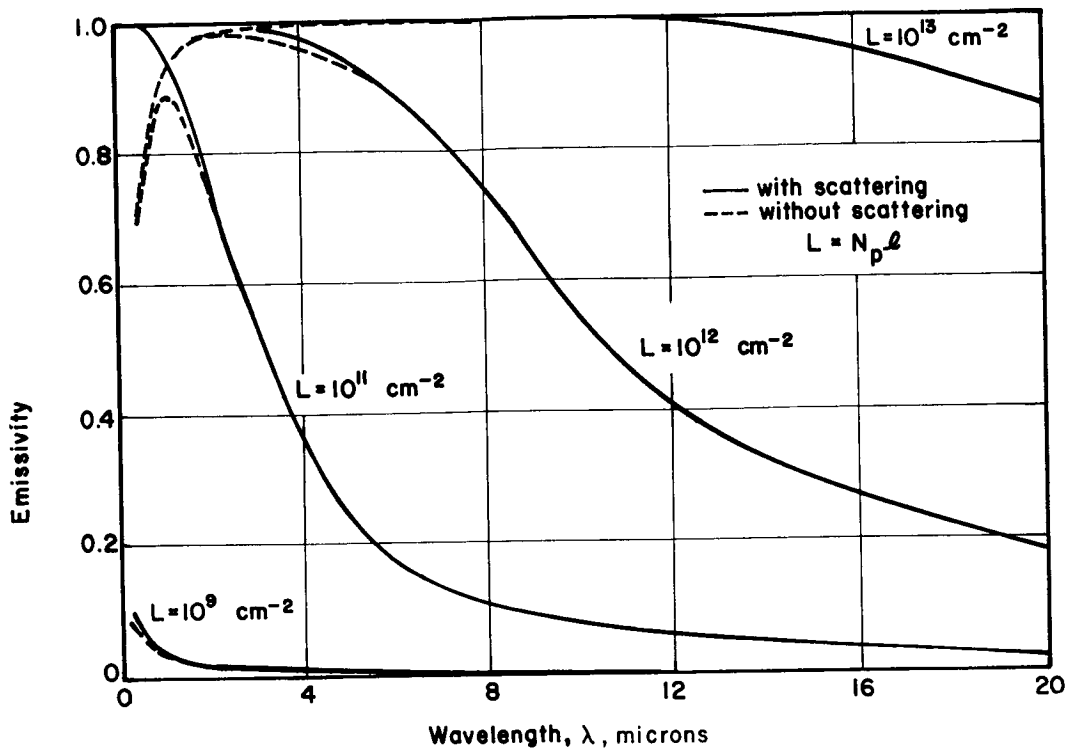


FIGURE 22. CARBON PARTICLE EMISSIVITY AS A FUNCTION OF WAVELENGTH FOR THE PARTICLE SIZE DISTRIBUTION OF EQUATION (297)

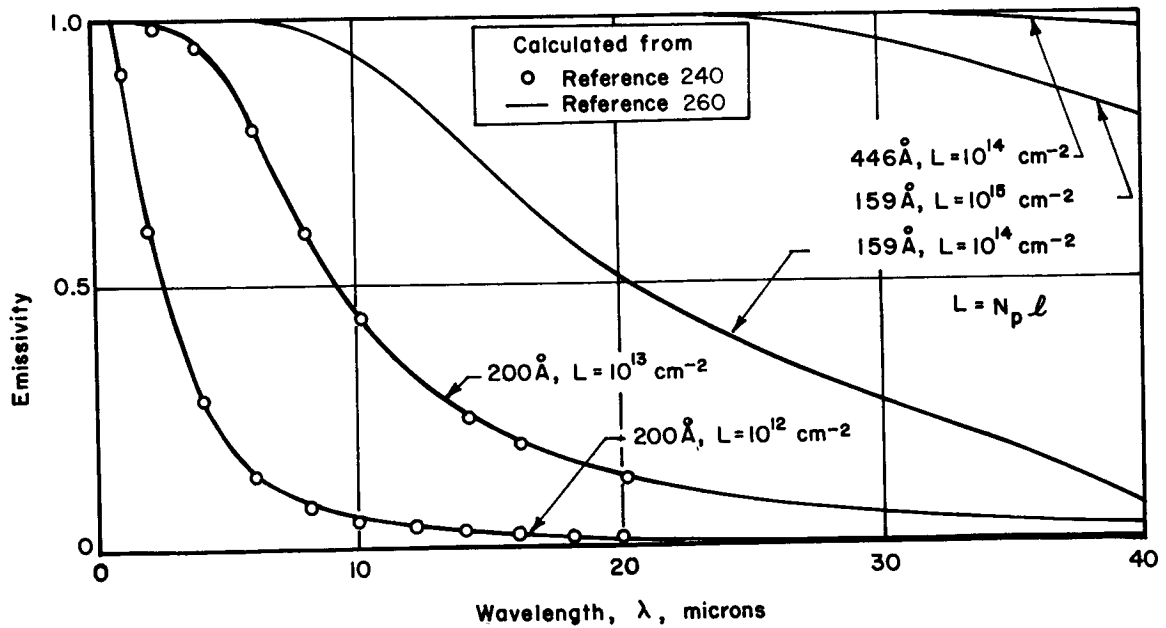


FIGURE 23. CARBON PARTICLE EMISSIVITY AS A FUNCTION OF WAVELENGTH FOR PARTICLES OF VARIOUS RADII

These empirical expressions for mass absorption coefficient  $\kappa_{m,\lambda}$  and spectral emissivity  $\epsilon_\lambda$  have usually been expressed in the following form:

$$\kappa_{m,\lambda} = C\lambda^{-A} \quad \text{and} \quad \epsilon_\lambda = 1 - \exp(\kappa_{m,\lambda}\rho\ell) = 1 - \exp(C\lambda^{-A}\rho\ell). \quad (298)$$

In these equations  $C$  is a constant independent of wavelength, but  $A$  is not necessarily independent of wavelength. The total emissivity is usually found from equation (298) by integrating over all wavelengths as

$$\epsilon = \frac{\int_0^\infty [1 - \exp(C\lambda^{-A}\rho\ell)] B_\lambda d\lambda}{\int_0^\infty B_\lambda d\lambda}, \quad (299)$$

where  $B_\lambda$  is the Planck blackbody intensity function defined in equation (19).

Hottel and Broughton [276], who analyzed various experimental data of soot deposited on glass, concluded that the exponent  $A$  could be represented by a value of 0.95 in the infrared down to  $0.8 \mu$ . In the visible part of the spectrum they recommended an average exponent of 1.39 for various amyl acetate, acetylene, and city-gas soots. Pepperhoff [269] and Rossler [273] state that values of  $A$  higher than unity may be attributed to the effect of particle size. Millikan [228], however, states that for the particle diameter range 600 to 800 Å the exponent  $A$  is independent of particle size, state of aggregation, or temperature. He comments that the exponent  $A$  is determined mainly by the hydrogen content of the sample, since he found that  $A$  increased from 0.9 to 1.9 as the hydrogen content varied from 0.8 to 4.1 percent by weight.

Siddall and McGrath [278] summarize results of various experimental investigations involving determination of the exponent  $A$ . They state that, in the visible part of the spectrum,  $A$  can be assumed independent of wavelength, but in the infrared, it should be written in the form  $A = a - b \ln \lambda$ . They also comment that the parameter  $A$  is independent of soot layer thickness but is dependent upon the fuel from which the soot is formed.

Sato and Matsumoto [279] calculate (and measure) radiation from a carbon particle cloud using equation (298) for spectral emissivity as

$$\epsilon_{\lambda p} = 1 - \exp(-C \rho \ell / \lambda^A) = 1 - \exp[-(C_2 / T \lambda^A) (C \ell \rho T / C_2)] = 1 - e^{-\xi \chi} \quad (300)$$

where  $C_2$  is given in equation (198) as  $ch/k$ .

The total emissivity from a carbon particle cloud is then found as

$$\epsilon_p = 1 - \frac{15}{\pi^4} \psi'''(\chi + 1) \quad , \quad (301)$$

where the quantity  $\psi'''(\chi + 1)$  is defined in terms of the gamma function  $\Gamma(\chi + 1)$  as

$$\int_0^{\infty} \frac{\xi^3}{e^{\xi} - 1} e^{-\chi \xi} d\xi = \frac{d^4}{d\chi^4} \ln \Gamma(\chi + 1) = \psi'''(\chi + 1) \quad . \quad (302)$$

The exponent  $A$  was considered to be unity, and the mass absorption coefficient  $\kappa_{m,\lambda}$  was taken from Schack [277] to be

$$\kappa_{m,\lambda} = C \lambda^{-A} = 5.7 \times 10^5 / \lambda \quad , \quad (303)$$

where  $\lambda$  is measured in microns and  $\kappa_{\lambda}$  is in  $m^{-1}$ . The expression for total emissivity,  $\epsilon_p$ , [equation (301)] was then used to predict radiation from a cloud of carbon particles, as will be discussed in the following section.

Siddall and McGrath [278] and Thring et al. [280] discuss another expression for mass absorption coefficient  $\kappa_{m,\lambda} = C \lambda^{-A}$  which is based upon the Mie theory calculations of Hawksley [281] to obtain the total or extinction efficiency factor  $Q_t$ . In this manner the absorption coefficient  $\kappa_{\lambda}$  may be expressed as

$$\kappa_{\lambda} = \rho \kappa_{m,\lambda} = Q_t N_p A , \quad (304)$$

where  $A$  is the projected area of a particle (equal to  $\pi d_p^2/4$ ), and the total or extinction efficiency factor may be written as

$$Q_t = \frac{24 \pi d_p}{\lambda} \frac{n_1^2 n_2}{[(n_1^2 + n_1^2 n_2^2)^2 + 4(n_1^2 - n_1^2 n_2^2 + 1)]} = \frac{24 \pi d_p}{\lambda} F(\lambda) \quad (305)$$

where the index of refraction  $n$  is now written as  $n = n_1(1 - in_2)$ .

The absorption coefficient may now be written as

$$\kappa_{\lambda} = \frac{36 \pi V' F(\lambda)}{\lambda} , \quad (306)$$

where  $V'$  is the average volume of particles per unit volume of the cloud and may be defined as

$$V' = N_p \pi d_p^3 / 6 \quad (307)$$

where  $N_p$  is the average number of particles per unit volume.

Ferriso et al. [230] used equation (306) in the following form

$$\kappa_{\lambda} = 36 \pi \rho F(\lambda) / \rho_0 \lambda , \quad (308)$$

where  $\rho$  is the carbon particle mass density ( $\text{g/cm}^3$  of cloud) and  $\rho_0$  is the density of carbon in bulk form, to plot the parameter  $\kappa_{\lambda} \lambda / \rho$  for values of temperature from 150 to 3000° K and values of wavelength from 1 to 10  $\mu$ . This curve is reproduced as Figure 24 of this report.

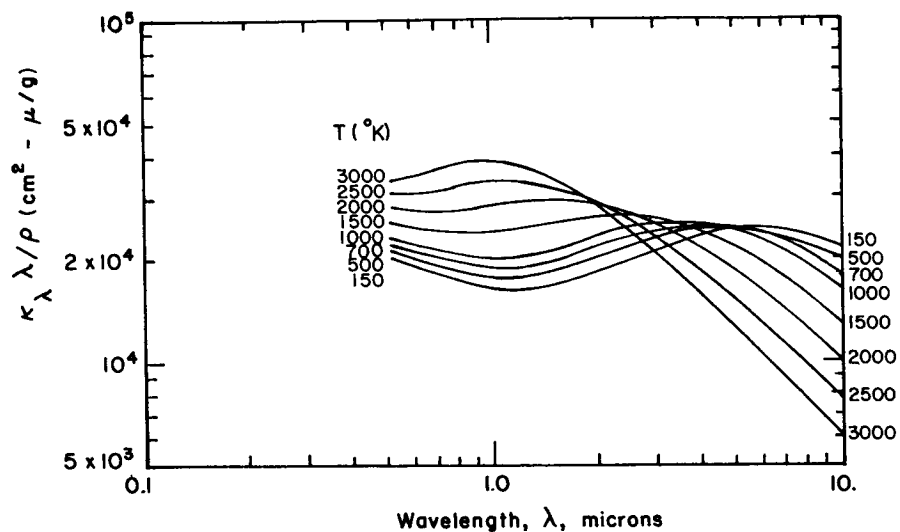


FIGURE 24. LINEAR ABSORPTION COEFFICIENT FOR CLOUDS OF VERY SMALL CARBON PARTICLES

To evaluate the parameters  $n_1$  and  $n_1 n_2$  (originally given in equation (268) and (269)), Ferriso et al. [230] made the following approximations for wavelengths greater than about  $1 \mu$ .

$$n_1^2 - n_1^2 n_2^2 \approx 4.36 - 1.31 \frac{\delta}{\beta^2} \quad (309)$$

and

$$n_1^2 n_2 \approx \frac{0.58}{\delta} + \frac{1.675 \lambda}{\beta} \quad (310)$$

where

$$\beta = \sigma(2250^\circ \text{ K}) / \sigma(T)$$

$$\delta = N_c(2250^\circ \text{ K}) / N_c(T) \quad (311)$$

$$\sigma(T) = e^2 N_c / m \epsilon_0 \mu \gamma_c$$

where  $\lambda$  is the wavelength in microns,  $\sigma$  is the dc conductivity [equation (260)] evaluated according to Stull and Plass [240] based upon measurements of Senftleben and Benedict [242], and  $N_c$  is the number of conduction electrons per  $\text{cm}^3$ .

4. Experimental Methods. Various experimental methods of obtaining absorption coefficients, emissivities, reflectivities or transmissivities of carbon samples or carbon particle clouds are discussed in this section. This discussion is in addition to the brief one in the last section in which experimental data were mentioned in connection with the inverse wavelength calculation of absorption coefficients and absorptivities [equations (298) and (299)]. In the last 50 years or so, there have been numerous experimental programs performed to determine the emissivity of carbon or graphite samples placed in furnaces or other devices, carbon particles placed in various suspensions such as  $\text{H}_2\text{O}$ , He, or  $\text{N}_2$ , and of carbon particles in luminous flames. Only in the last few years, however, has there been an attempt to determine experimentally carbon emissivities and absorption coefficients from rocket exhaust gases.

Plunkett and Kingery [282], Rutgers [283], and MacPherson [284] review the literature for emissive and reflective properties of carbon or graphite samples (polished or unpolished) placed in such devices as carbon tube furnaces and heated by electrical current or electrical resistance heaters. These investigators state that spectral emissivity generally decreases with increasing wavelength above  $1 \mu$ ; however, in the visible region the spectral emissivity closely approaches that of a graybody (i. e.,  $\epsilon_\lambda$  is essentially constant for all visible wavelengths). These authors also comment that there appears to be no temperature dependence on the spectral emissivity, while the total or integrated emissivity appears to have a positive temperature dependence.

Lanzo [285] and Lanzo and Ragsdale [286] discuss transmissivity measurements made on four carbon powders of particle diameters  $0.08 \mu$ ,  $0.15 \mu$ ,  $0.45 \mu$ , and  $1.40 \mu$  suspended in water for the wavelength range  $0.2 \mu$  to  $1.0 \mu$ . Spectral transmissivity measurements were obtained with a spectrophotometer, and total transmissivity measurements were obtained with a xenon-arc source and a radiation detector. It was found that transmissivity (and hence emissivity) was essentially independent of wavelength in the visible range, thus agreeing with Plunkett and Kingery [282], Rutgers [283], and MacPherson [284].

Marteney [287] measured extinction (absorption plus scattering) of carbon particles of size  $r_p = 0.0045 \mu$  suspended in He and  $\text{N}_2$  carrier gases in the wavelength range  $0.255 \mu - 0.545 \mu$ . Extinction coefficients were again

found to be essentially constant with wavelength in the visible range. It was found that the application of de-agglomeration aerodynamic shear forces in a nozzle through which the carrier gas-particle mixture was passed caused an increase by a factor of nearly six in the extinction coefficient for the carbon particles.

Numerous investigators such as Millikan [227, 228], Plyler and Humphries [272], Silverman [288], Tourin [289], and Sato and Matsumoto [279] have made experimental measurements of emissivity in luminous flames. In the last several years there has been a considerable amount of literature involving the experimental determination of emissivities, spectral radiance, and temperatures in luminous rocket exhausts. Some of the unclassified references in this area include Rossler [273], Simmons and de Bell [290-292], Herget et al. [293], Boynton et al. [231], Ferriso et al. [230], and Hendershot and McCaa [294, 295]. Some of the classified references in this area (pertaining mainly to H 1 and F-1 engines) include Thompson [296], Simmons [152, 297], de Bell and Speiser [298], de Bell and Simmons [299], Herget, Schumacher, and Enloe [300], Wagner [156], Levin, Wagner, and Thompson [154], and Tourin [301].

The measurement of emissivity for both flames and rocket exhaust gases depends upon the principles of monochromatic gas pyrometry as discussed by Silverman [288], Hecht [302], Hill [303], Hornbeck [304], Brenden [305], Branstetter [306], Tourin [307, 308], Brewer and McGregor [309], Harrison [310], and de Bell et al. [153]. In this manner the intensity  $I_{F\lambda}$ , as seen by the radiometer or spectrometer viewing the flame or rocket exhaust may be written in the Planckian form as

$$I_{F\lambda} = \epsilon_{F\lambda} \frac{2C_1}{\lambda} \frac{1}{[\exp(C_2/\lambda T_F) - 1]} = \epsilon_{F\lambda} B_{\lambda} \quad , \quad (312)$$

and the intensity  $I_{G\lambda}$  of the continuous source (graybody) also seen by the radiometer or spectrometer is

$$I_{G\lambda} = \epsilon_{G\lambda} \frac{2C_1}{\lambda^5} \frac{1}{[\exp(C_2/\lambda T_G) - 1]} = \epsilon_{G\lambda} B_{\lambda} \quad . \quad (313)$$

However, when a monochromatic beam of radiation of known intensity  $I_{G\lambda}$  passes through a gas, part of it is absorbed by the gas such that only a fraction,  $I_{T\lambda}$ , is transmitted through the gas and received by the detector. The fraction lost is thus the spectral absorptivity of the flame,  $\alpha_{F\lambda}$ , which, by Kirchoff's law, must equal the spectral emissivity,  $\epsilon_{F\lambda}$ . These quantities are expressed as

$$\alpha_{F\lambda} = \frac{I_{G\lambda} - I_{T\lambda}}{I_{G\lambda}} = 1 - \frac{I_{T\lambda}}{I_{G\lambda}} = \epsilon_{F\lambda} \quad (314)$$

This spectral emissivity may thus be measured as a function of wavelength for a known value of  $\epsilon_{G\lambda}$  for the graybody source. In determining the flame temperature,  $T_F$ , as seen by the detector, equation (312) is divided by equation (313), and the following equation results:

$$T_F = \frac{C_2}{\lambda \ln \left\{ 1 + \left( \frac{I_{G\lambda}}{\epsilon_{G\lambda} I_{T\lambda}} \right) \left( 1 - \frac{I_{T\lambda}}{I_{G\lambda}} \right) [\exp(C_2/\lambda T_G) - 1] \right\}} \quad (315)$$

Ferriso et al. [230] and Boynton et al. [231] used this equation to determine the gas temperatures of a small RP-1/gaseous oxygen engine exhaust at 4.4  $\mu$ , the CO<sub>2</sub> and CO vibration-rotation bands, and at 2.2  $\mu$  (region of no molecular emission) to obtain the carbon temperature.

Simmons and de Bell [290,291] discuss the use of two path pyrometry to determine simultaneously the spectral emissivity and temperature of a luminous rocket exhaust. The main advantage to this method is that a comparison source behind the rocket exhaust is not needed. Instead, a corner-cube reflector (glass prism) is placed behind the exhaust in effect to double the apparent depth of the plume. The radiant intensity thus obtained when a reflector is placed behind the plume can be written as

$$I_{F\lambda} = \left[ 1 + \rho_{\lambda} (1 - \alpha_{F\lambda}) \right] \epsilon_{F\lambda} B_{\lambda} \quad (316)$$

where  $\rho_\lambda$  is the reflectivity corresponding to the wavelength of the reflector. Assuming thermal equilibrium,  $\epsilon_{F\lambda} B_\lambda = I_{F\lambda}'$ , and the absorptivity  $\alpha_{F\lambda}$  equals the emissivity, which is then written as

$$\epsilon_{F\lambda} = 1 - \left( \frac{1}{\rho_\lambda} \right) \left( \frac{I_{F\lambda}'}{I_{F\lambda}} - 1 \right). \quad (317)$$

Assuming that the Wien law for blackbody radiation is sufficiently accurate, the temperature at the nozzle exit may be calculated as

$$T_{F_e}^{-1} = T_{BR}^{-1} + \frac{\lambda}{C_2} \ln \left[ 1 - \left( \frac{1}{\rho_\lambda} \right) \left( \frac{I_{F\lambda}'}{I_{F\lambda}} - 1 \right) \right], \quad (318)$$

where  $T_{BR}$  is the single-path brightness temperature at the nozzle exit and  $I_{F\lambda}'/I_{F\lambda}$  is thus the ratio of the double-path spectral intensity to the single-path spectral intensity.

Most of the spectral and total emissivity data from the exhausts of the 1,500,000-lb thrust F-1 engine and the 200,000-lb thrust H-1 engine are classified. However, most engineers who have calculated radiative heating to the base of the Saturn vehicles are inclined to use a value close to unity for the emissivity in the infrared wavelength region. Simmons [297] developed an empirical relation (which is classified) for spectral emissivity in the visible spectrum for an RP-1/lox rocket exhaust. This empirical relation was a function of wavelength, mixture ratio, chamber pressure, and thrust chamber size.

Perhaps the most extensive experimental analysis of emissivity from carbon particles has been determined by Ferriso et al. [230] and Boynton et al. [231] at General Dynamics/Convair under NASA/MSFC contract. In this investigation, the dependence of the carbon spectral absorption coefficient on wavelength in the 0.7- $\mu$  to 5- $\mu$  range and on temperature from 1045° K to 2600° K was determined. Three small contoured-nozzle rocket motors of nozzle area ratio 5.25, 3.0, and 1.5 were used in the investigation. The motors used the Foelsch [311] nozzle to produce a constant temperature near the exit. By varying the chamber pressure and, hence, O/F ratio, various

values of constant temperature were obtained for each motor. These temperatures were 1045° K, 1290° K, 1415° K, and 1680° K for the 5.25 area ratio motor; 1230° K, 1470° K, and 1760° K for the 3.0 area ratio motor; and 1700° K, 1900° K, 2370° K, and 2600° K for the 1.5 area ratio motor.

All of the above temperatures were calculated from a relation such as equation (315). The emissivity of the entire plume,  $\epsilon_\lambda$ , was obtained from experimental measurements as shown in equation (314). This emissivity can be expressed in terms of carbon, H<sub>2</sub>O, and CO<sub>2</sub> absorption coefficients as

$$\epsilon_\lambda = 1 - \exp \left\{ - \left[ (\kappa_{m,\lambda} \rho) c^\ell + (\bar{\kappa}_{m,\lambda} u)_{\text{H}_2\text{O}} + (\bar{\kappa}_{m,\lambda} u)_{\text{CO}_2} \right] \right\} , \quad (319)$$

where  $u$  represents the quantity  $\rho \ell$  taken at standard temperature and pressure. The contribution to the emissivity of CO and other molecular emitters is neglected.

The equation for the quantity  $(\bar{\kappa}_{m,\lambda} u)_{\text{H}_2\text{O}}$  using the statistical band model, was given by Ferriso et al. [230] (see equation (227)) as

$$(\bar{\kappa}_{m,\lambda} u)_{\text{H}_2\text{O}} = u \kappa_{m,\lambda} \left( 1 + u \kappa_{m,\lambda} / 4\bar{a} \right)^{-\frac{1}{2}} , \quad (320)$$

where  $\bar{a}$  represents a fine structure term represented by

$$\bar{a} = \frac{\gamma^0}{d} \left( \frac{300}{T} \right)^{\frac{1}{2}} P_T \left\{ C_{\text{H}_2\text{O}} \left[ \left( \frac{300}{T} \right)^{\frac{1}{2}} + \sigma \right] (1 - C_{\text{H}_2\text{O}}) \sigma_x \right\} . \quad (321)$$

In this equation,  $\sigma$  is the ratio of half-widths due to self-broadening,  $\sigma_x$  is the ratio of foreign gas half-width to H<sub>2</sub>O half-width, and  $C_{\text{H}_2\text{O}}$  is the concentration of water vapor. For CO<sub>2</sub>, the average absorption coefficient can be determined by the Beer-Lambert equation. In this case,  $\bar{\kappa}_\lambda$  equals  $S/d$ , where  $S/d$  was given as a function of temperature and wavelength by Malkmus [312].

Figure 25, taken from Ferriso et al. [230], shows the quantity  $(\bar{\kappa}_{m,\lambda} \rho)_c$  for the 5.25 area ratio motor. The calculated curves are based upon bulk carbon properties as determined by equations (308-311). Good agreement with experimental data was obtained up to 1700° K, after which the experimental data were practically independent of wavelength. At temperatures below 1200° K and at wavelengths less than 0.8  $\mu$ , the observed emitted intensity was greater than the blackbody intensity. However, it was felt that the effects of scattering or a non-equilibrium distribution of non-emitting states in the rocket exhaust could have contributed to this phenomenon.

## Radiant Heating Calculations for Luminous Flames and Rocket Exhausts

This section discusses various methods of predicting radiant heating based upon the emissivity relations of the preceding section. The general methods are applicable to both luminous flames or rocket exhausts in which carbon is the principal emitter. The problem of thermal equilibrium between carbon particles and the gas is also described. The base radiant thermal environment used as design criteria for the Saturn I, S-I stage, and Saturn IB (now Uprated Saturn I), S-IB stage caused by H-1 rocket exhausts and for the Saturn V, S-IC stage caused by F-1 rocket exhausts is also discussed.

Stull and Plass [240] present an equation for the radiant intensity from a distribution of carbon particles which absorb, scatter, and emit radiation isotropically and which are at a constant temperature equal to that of the gas. Integration of this equation over wavelength  $d\lambda$  and solid angle  $d\omega$  would thus yield the radiant heating rate per area. This equation, which includes higher-order scattering terms, is

$$\begin{aligned}
 I_{\lambda}(\theta_o, \phi_o) &= B_{\lambda}(T) N_p \sigma_a \int_0^{z_{\max}} \exp(-N_p \sigma_t z \sec \theta_o) \\
 &\left\{ 1 + \left( \frac{N_p \sigma_s}{4\pi} \right) \int_{V'} \frac{1}{R'^2} \exp(-N_p \sigma_t R') \right. \\
 &\left. \left\{ 1 + \left( \frac{N_p \sigma_s}{4\pi} \right) \int_{V''} \frac{1}{R''^2} \exp(-N_p \sigma_t R'') \{1 + \dots\} dV'' \right\} dV' \right\} dz, \quad (322)
 \end{aligned}$$

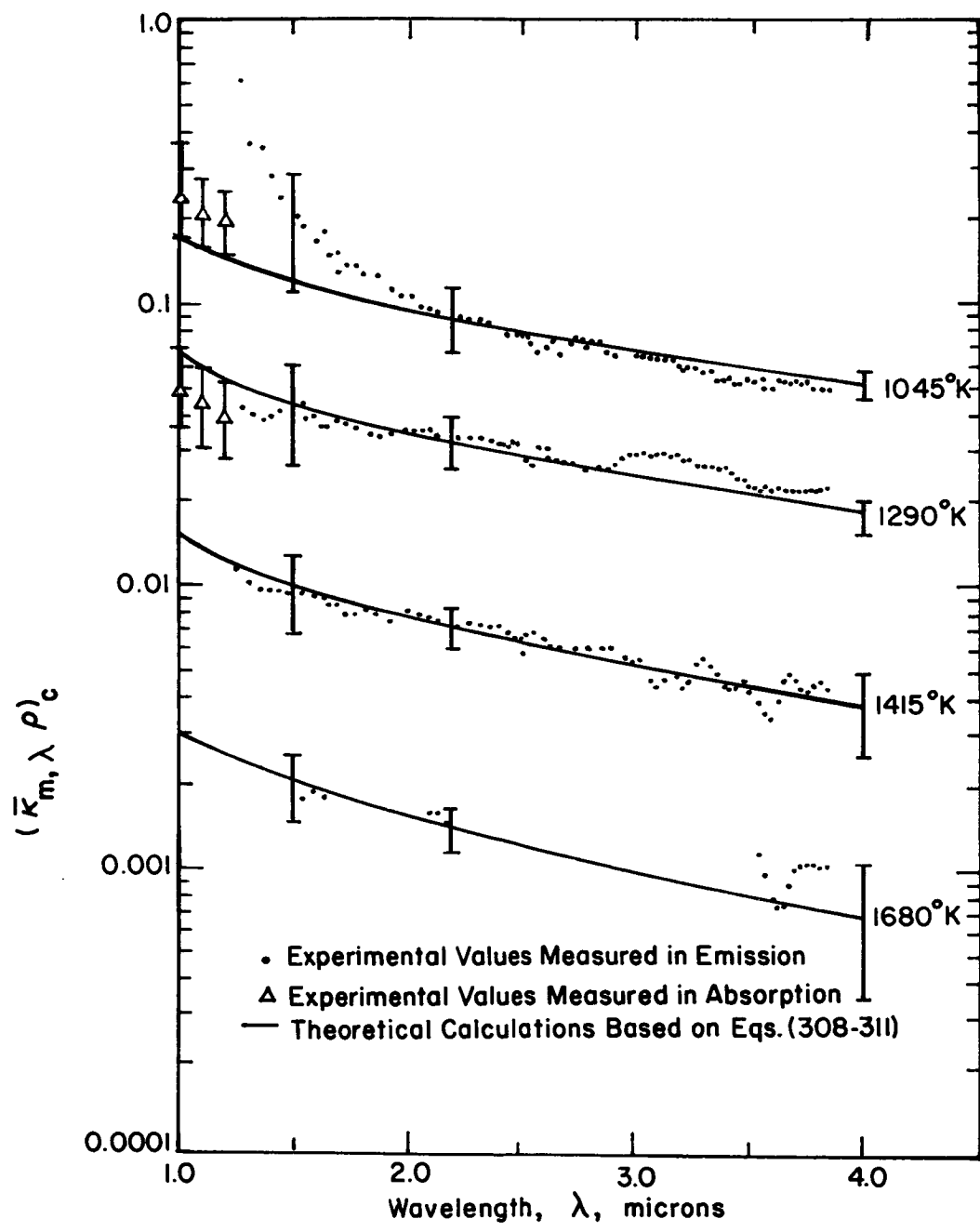


FIGURE 25. VALUES OF  $(\bar{\kappa}_{m,\lambda} \rho)_c$  FOR CARBON PARTICLES DETERMINED FROM MEASUREMENTS ON THE GD/C 5.25:1 AREA RATIO MOTOR

where  $\theta_0$  and  $\phi_0$  are the polar and azimuthal angles, respectively, from the element of area being heated to the emitting carbon particles in the volume element  $dV$ , and  $R$  is the path length from the element of area to the volume  $dV$ . The element of volume  $dV$  is  $R^2 d\omega dR$ , where  $R = z \sec \theta_0$  and  $d\omega$  is the element of solid angle. The  $dV'$  terms involve the amount of radiation emitted in the volume  $dV'$  scattered within a volume  $dV$  which is separated from the volume  $dV'$  by the path length  $R'$ . In this case the element of volume  $dV$  is  $dR' dA$ , where  $A = R'^2 d\omega$ . Also in this equation, the quantity  $\sigma_a N_p$  is equivalent to the quantity  $\kappa_\lambda = \rho \kappa_{m,\lambda}$  in equation (207), and  $\sigma_s N_p$  is the scattering coefficient  $\sigma_\lambda = \rho \sigma_{m,\lambda}$  defined in equation (29).

For the case in which scattering by the carbon particles may be neglected (i. e., for  $r_p < 300 \text{ \AA}$  and  $\lambda > 2 \mu$ ), the emitted intensity may be written by taking only the first term in equation (322) ( $\sigma_s = 0$  in the other terms) as

$$I_\lambda(\theta_0) = B_\lambda(T) \frac{\sigma_a}{\sigma_t} \cos \theta_0 \left\{ 1 - \exp[-\sigma_t L(\theta_0, \phi_0)] \right\}, \quad (323)$$

where

$$L(\theta_0, \phi_0) = N_p z_{\max} \sec \theta_0. \quad (324)$$

The quantity  $z_{\max}$  represents the total path length projected in the direction  $z$ , where  $z$  is measured in a direction at right angles to the front surface of the flame or rocket exhaust.

Stull and Plass [240] calculated spectral intensities for carbon particles with radii equal to  $200 \text{ \AA}$ , and for the two distributions, equations (296) and (297). They found that the maximum intensity for these carbon particles occurred at smaller wavelengths than the corresponding maximum of the blackbody intensity curve. The intensity was found to increase as the number of particles increased until the limiting blackbody intensity was reached. For particle radii of  $200 \text{ \AA}$ , about the average size reported by most investigators (See this section, subsection entitled "Carbon Size Particle Determination."), the intensity was practically negligible when there were less than  $10^{11}$  particles/cm<sup>2</sup>, and closely approached that of a blackbody when there were more than  $10^{14}$  particles/cm<sup>2</sup>. This characteristic can also be seen in the emissivity curve (Figure 19) for the particle distribution of equation (297).

Sato and Matsumoto [279] present another radiant heating equation which is based upon the inverse wavelength dependence of the carbon coefficient. This equation holds for luminous particles imbedded in a gas; however, the effects of scattering are neglected. It is assumed that the nonluminous gases, such as H<sub>2</sub>O and CO<sub>2</sub>, are uniformly distributed in the flame. Furthermore, it is assumed that the gas temperature equals the temperature of the carbon particles. The expression for the spectral emissivity may thus be written as

$$\epsilon_{\lambda} = 1 - \exp \left\{ -[(\kappa_{m,\lambda} \rho)_c + (\kappa_{m,\lambda} \rho)_g] \ell \right\}, \quad (325)$$

where the subscript c stands for carbon and the subscript g stands for non-luminous gas.

The radiant intensity may be written as in equation (63) for no scattering as

$$I_{\lambda} = \epsilon_{\lambda} B_{\lambda}(T) = \frac{C_1 \lambda^{-5}}{\exp(C_2/\lambda T) - 1} \left( 1 - \exp \left\{ -[(\kappa_{m,\lambda} \rho)_c + (\kappa_{m,\lambda} \rho)_g] \ell \right\} \right). \quad (326)$$

By integrating over wavelength  $d\lambda$  and solid angle  $d\omega$ , the expression for radiant heating rate per unit area becomes

$$q/A = \int_{\lambda} \int_{\omega} \frac{C_1 \lambda^{-5}}{\exp(C_2/\lambda T) - 1} \left( 1 - \exp \left\{ -[(\kappa_{m,\lambda} \rho)_c + (\kappa_{m,\lambda} \rho)_g] \ell \right\} \right) d\omega d\lambda. \quad (327)$$

By using the variables  $\xi = C_2/\lambda^A T$  and  $\chi = c \ell \rho T/C_2$  as defined in equation (300) and using the symbol  $\bar{\eta}$  for  $(\kappa_{\lambda} \rho_{\lambda})_g \ell$ , equation (327) becomes

$$q/A = \frac{C_1}{C_2^4} \int_{\omega} T^4 \left[ 1 - \frac{15}{\pi^4} \int_0^{\infty} \frac{\xi^3}{e^{\xi} - 1} e^{-(\chi \xi + \bar{\eta})} d\xi \right] d\omega. \quad (328)$$

By making the substitution of equation (302) and using the approximation  $e^{-\bar{\eta}} \approx 1 - \epsilon_g$ , equation (328) now becomes

$$q/A = \frac{C_1}{C_2^4} \int_{\omega} T^4 \left[ 1 - \frac{15}{\pi^4} (1 - \epsilon_g) \psi''' (\chi + 1) \right] d\omega . \quad (329)$$

Tuttle [313] presents another method of calculating radiant heating from carbon particles in a luminous gas. This particular calculation was for the exit plane of an H-1 engine on the Atlas vehicle. A form of equation (207) was used to obtain the spectral radiance,  $I_{\lambda}$ , as

$$I_{\lambda} = \int_0^s (\rho \kappa_{m,\lambda})_c B_{\lambda}(T) \exp \left[ - \int_0^s (\rho \kappa_{m,\lambda})_c ds' \right] = \int_0^{\tau_{\lambda}} B_{\lambda}(T) e^{-\tau'_{\lambda}} d\tau'_{\lambda} . \quad (330)$$

The dimensionless optical depth may thus be written as

$$\tau_{\lambda} = \int_0^{s_m} (\rho \kappa_{m,\lambda})_c ds = \int_0^{s_m} (N_p \sigma_a)_c ds . \quad (331)$$

For the temperature range considered in this analysis, Tuttle states that  $\kappa_{m,\lambda}$  is independent of temperature, and hence is not a function of path length in the gas. Therefore, the optical depth may be written as

$$\tau_{\lambda} = (\rho_m \kappa_{m,\lambda})_c \int_0^{s_m} \frac{\rho_c(s)}{\rho_{m_c}} ds , \quad (332)$$

where  $\rho_{m_c}$  is the mean particle density or the average number of carbon particles/cm<sup>3</sup>.

If the carbon is assumed to be amorphous with a specific gravity of 1.8, a radius of 500 Å, and a ratio of the mass of carbon to the total mass flow of 0.005, the mean particle density may be calculated to be 5.0 x 10<sup>8</sup> particles/cm<sup>3</sup>. Tuttle presents a temperature distribution curve based upon Simmons' [297] data as

$$B_{\lambda}(\tau'_{\lambda}) = a_{\lambda} + b_{\lambda} e^{-c_{\lambda}\tau'_{\lambda}} \quad \text{for } 0 \leq \tau'_{\lambda} \leq \tau_{c_{\lambda}} \quad (333)$$

and

$$B_{\lambda}(\tau'_{\lambda}) = a_{\lambda} + b_{\lambda} e^{-c_{\lambda}(2\tau_{c_{\lambda}} - \tau'_{\lambda})} \quad \text{for } \tau_{c_{\lambda}} \leq \tau'_{\lambda} \leq 2\tau_{c_{\lambda}}, \quad (334)$$

where  $a_{\lambda}$ ,  $b_{\lambda}$ , and  $c_{\lambda}$  are constants tabulated by Tuttle [313] and  $\tau_{c_{\lambda}}$  represents the optical depth at the center of the plume. Inserting these values of  $B_{\lambda}(\tau_{\lambda})$  into equation (330) results in the following equation:

$$I_{\lambda} = a_{\lambda}(1 - e^{-2\tau_{c_{\lambda}}}) + \frac{b_{\lambda}}{c_{\lambda}^2 - 1} \left[ (c_{\lambda} - 1) - 2c_{\lambda} e^{-(c_{\lambda} + 1)\tau_{c_{\lambda}}} + (c_{\lambda} + 1) e^{-2\tau_{c_{\lambda}}} \right] \quad (335)$$

This equation was compared with the spectral data of deBell and Speiser [298] in the 0.5- $\mu$  to 3- $\mu$  wavelength range. Very good agreement with the experimental data was obtained except at low wavelengths where scattering effects should be included and in the 1.4- $\mu$ , 1.9- $\mu$ , and 2.7- $\mu$  bands in which atmospheric absorption was present. Tuttle [313] also included expressions for upper and lower limits of radiation from the cone of the H-1 engine. The upper limit took into account the contribution of the H<sub>2</sub>O emission, and the lower limit neglected this emission.

Several new investigations of radiation from luminous flames and rocket exhausts have appeared in the literature recently. Thring, Beer, and Foster [314] discussed calculations of carbon emissivities based on Mie theory and also measurements of soot concentration from hydrocarbon-air turbulent diffusion flames. These authors found that in certain cases the measured emissivity was 2 to 3 times larger than the calculated value; however, they believed this to be because the refractive index of soot containing hydrogen was possibly very different from that of pure carbon. Wolfhard and Hinck [315]

discussed the excitation (non-equilibrium radiation) of OH molecules and alkali metals in luminous flames and rocket exhausts. Zirkind [316] presented a general review of radiation processes in rocket exhausts, discussing band models, scattering processes, and spectral profiles.

In all of the radiation analyses mentioned in this section, it has been assumed that the carbon particles were in thermal equilibrium with the gas (i. e.,  $T_p = T_g$ ). Simmons and Spadaro [317, 318] have investigated this thermal equilibrium assumption by determining the amount of thermal lag of carbon particles in rocket nozzle flow. These authors set up a heat balance equation for a single carbon particle consisting of (1) the rate of heat transfer by collision with the gas molecules, (2) the rate of radiant heat transfer to the external surroundings, and (3) the rate of change of the heat content of the particle.

Based upon the kinetic theory of gases and the thermal accommodation coefficient,  $\alpha$ , as discussed by Wiedmann and Trumpler [319], the heat transfer in time  $dt$  between the carbon particle and the gas,  $dQ_1$  may be written according to Dillon and Line [320] as

$$dQ_1 = \alpha (4\pi r_p^2) C_v \left[ \frac{(MW)}{2\pi R} \right]^{\frac{1}{2}} \frac{P}{(T_g)^{\frac{1}{2}}} (T_p - T_g) dt , \quad (336)$$

where  $(4\pi r_p^2)$  is the surface area of the spherical carbon particle;  $C_v$ , MW, R, P, and  $T_g$  are the specific heat at constant volume, molecular weight, gas constant, pressure, and temperature, respectively, of the gas; and  $T_p$  is the temperature of the carbon particle.

The radiant heating emitted per time from a single carbon particle may be expressed in the form

$$dQ_2 = (4\pi r_p^2) \sigma_B \epsilon_p (1 - \alpha_g) T_p^4 dt , \quad (337)$$

where  $\sigma_B$  is the Stefan-Boltzmann constant,  $\epsilon_p$  the total hemispherical emissivity of the particle, and  $\alpha_g$  is the average total absorptivity of the gas stream which is defined in terms of the Beer-Lambert equation as

$$\alpha_g = 1 - e^{-\kappa \lambda \ell} = 1 - e^{-(\pi d_p^2/4) N_p \ell} \quad (338)$$

In this equation the quantity  $\ell$  represents the average path length (radius of the stream), and  $N_p$  is the concentration of the particles in the gas.

The heat content of the particle may be written as

$$dQ_3 = \left(\frac{4}{3} \pi r_p^3\right) \rho_p C \frac{dT_p}{dt} dt, \quad (339)$$

where  $\rho_p$  and  $C$  are the density and specific heat, respectively, of the particle.

Combining these heat inputs ( $dQ_1$ ,  $dQ_2$ , and  $dQ_3$ ) the following equation is obtained:

$$\alpha C_v \left[ \frac{(MW)}{2\pi R} \right]^{\frac{1}{2}} \frac{P}{(T_g)^{\frac{1}{2}}} (T_p - T_g) + \sigma_B \epsilon_p e^{-(\pi d_p^2/4) N_p \ell} T_p^4 + \frac{\pi r_p}{3} P \rho_p C dT_p = 0 \quad (340)$$

Simmons and Spadero [317] solved this equation numerically for  $T_p$  as a function of axial distance  $x$  down the nozzle for three different rocket nozzles. This was done for accommodation coefficients,  $\alpha$ , of 0.5, 0.75, and 1.0, particle diameters  $10^{-3}$ ,  $10^{-4}$ ,  $10^{-5}$  cm, and for total gas emissivity of zero and unity. Figure 26, taken from Simmons and Spadero, shows that the higher the accommodation coefficient, the closer the particle temperature was to the gas temperature, and that for carbon particles of 500 Å or less in radius the particle and gas temperatures were practically the same.

A recent investigation at Rocketdyne [199] using the Abel inversion/zone radiometry technique as discussed by Herget et al. [293] has shown that it is possible for the temperature of the carbon particles in the region between the plume core and the afterburning mantle to be actually several hundred degrees Kelvin cooler than the gas temperature. When the carbon particles pass into the afterburning region, however, the temperature was found to be

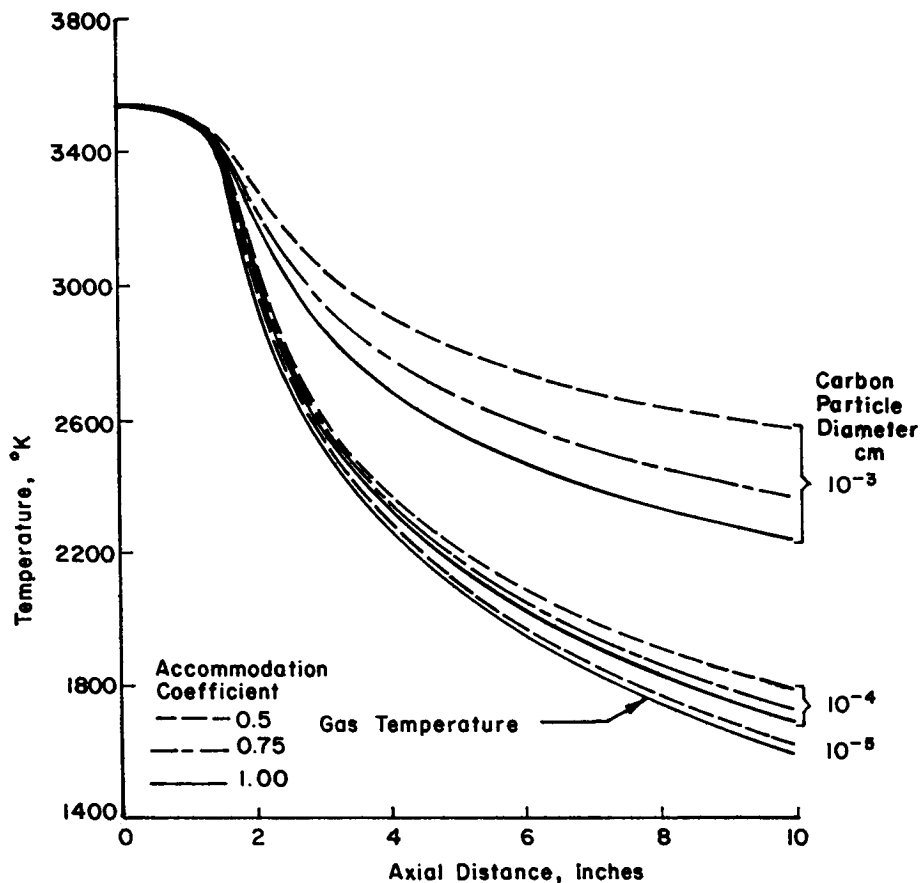


FIGURE 26. VARIATION IN CARBON PARTICLE TEMPERATURES ALONG THE AXIS OF THE ROCKETDYNE 2:1:8 AREA RATIO NOZZLE

equal to or slightly greater than the gas temperature. From the same investigation it was speculated that carbon particles may be formed just downstream of the first normal shock (in a fuel-rich region) in the plume, where the particles are again hotter than the gas.

In the last several years there have been numerous NASA/MSFC, Chrysler, and Boeing reports published that describe the thermal environment to the base of the S-I, S-IB, and S-IC stages, respectively. Because of the uncertainties in obtaining accurate spectral absorption coefficients for carbon particles, the emissivities of the H-1 and F-1 plumes have usually been assumed to be those of a blackbody (i. e., equal to unity), and scattering effects have usually been neglected. Plume shapes and properties have been calculated by the methods described by Farmer et al. [1], Prozan [150], and Ratliff [151].

The results of scale model data (from both short- and long-duration tests) and of all the in-flight radiation measurements on the unmanned Saturn flights have been extrapolated to the case of the manned and unmanned Saturn IB and V flights. It has been shown that radiation to the base of these vehicles is a maximum at sea level and drops off considerably at altitude because of the expansion of the plumes.

For the Saturn I vehicle, a summary of the base thermal environment caused by heating from the H-1 rocket engine exhausts has been presented by Payne and Jones [9], Jones [321], and by Hartley and Fricken [322]. The Saturn IB base thermal environment caused by heating from the H-1 engine exhausts is discussed by Francis [323], Fricken [324], Hartley [325-327], Fricken [328], and by Hartley and Fricken [322]. Most of these analyses assumed that the carbon density was five percent of the gas density (a value representing an upper limit as obtained from Rocketdyne data). Geraghty [329] presented a computer program for obtaining the form factors for the S-I and S-IB plumes. Figure 27, taken from Hartley and Fricken [322], shows the design criteria for incident radiation, total heating, recovery temperature, and wall temperature for the S-IB flame shield, the hottest part of the base of this stage for all vehicles up to vehicle AS-202. All vehicles after AS-202 had the inboard engine turbine exhaust dumped in this region, thus cooling the flame shield considerably. The general configuration of the base region of the Saturn IB vehicle S-IB stage is shown in Figure 28.

Mullen [330] and McEntire et al. [331] presented an analysis of the Saturn V S-IC stage base heating environment based upon plume temperature models obtained from radiant heating measurements taken during F-1 engine static firings. Hughes and Reid [332] presented a discussion of the radiation data obtained from these F-1 full scale static (sea level) firings. Jacobs [333] and Wasko [334] discussed the heating data (convection as well as radiation) obtained from S-IC scale model altitude tests with external flow using the Cornell short-duration shock tube technique. Patrick [335] discussed the radiation and total heating data obtained from exhausts of 1/20th scale F-1 engine firings at MSFC's Test Lab. Figure 29, taken from Mullen [330] shows the theoretical axial distribution of the sea level radiation heating on the base of the S-IC for various radial positions. Figure 30 shows the overall configuration of the base region of the S-IC stage.

The Thermal Environment Branch is continuing to improve its base heating analyses of radiant heating from H-1 and F-1 rocket engine exhausts. Radiation heating rates are currently being calculated for the launch umbilical

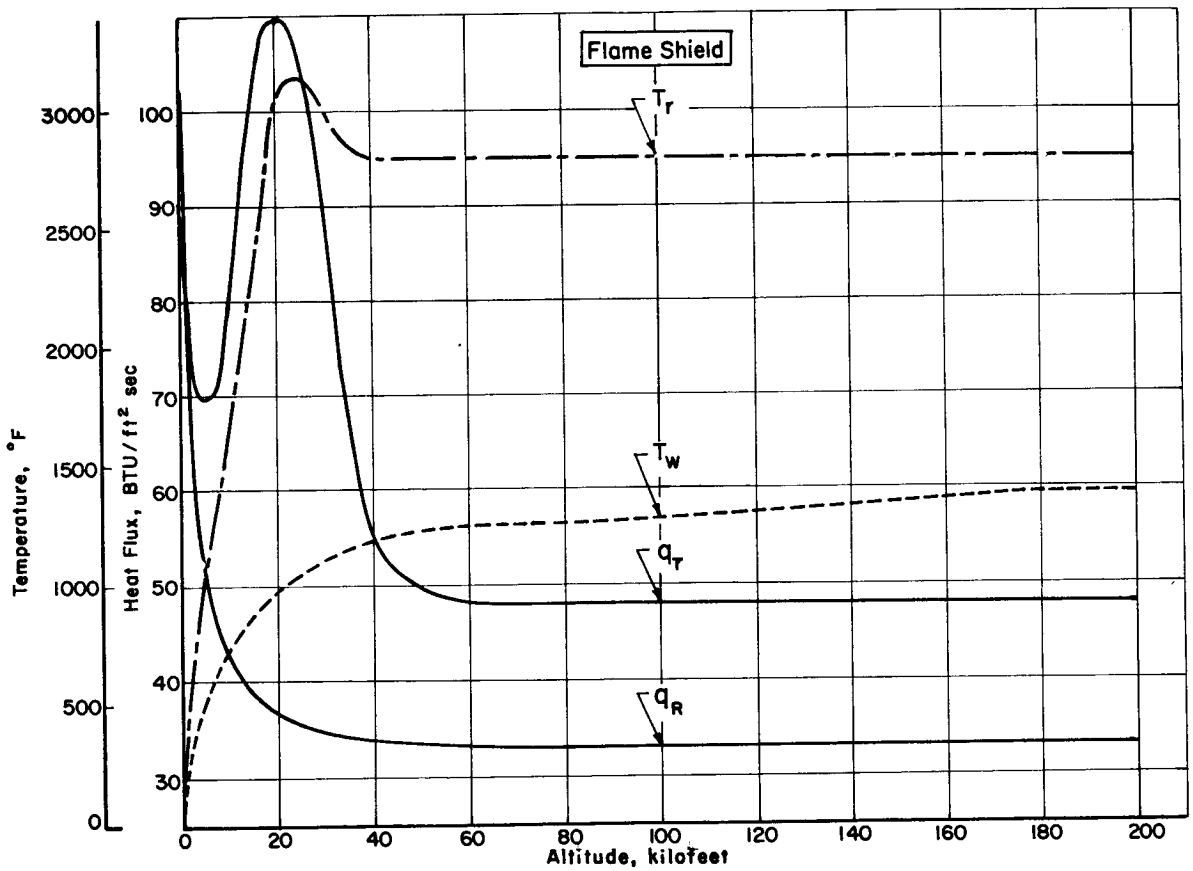
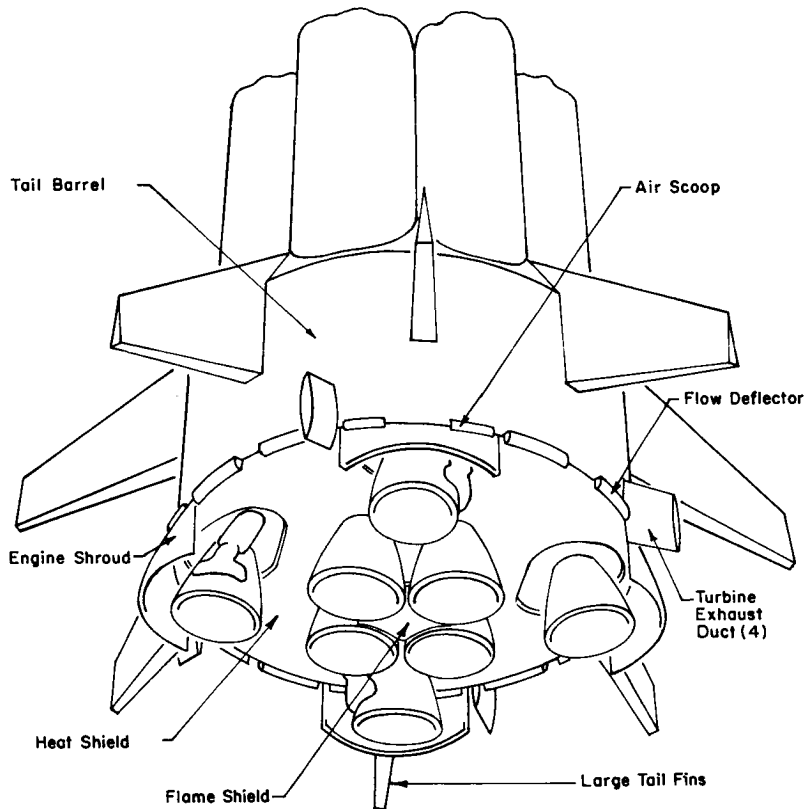


FIGURE 27. FLAME SHIELD DESIGN LEVELS FOR INCIDENT RADIATION,  $q_R$ , TOTAL HEAT FLUX,  $q_T$ , RECOVERY TEMPERATURE,  $T_R$ , AND WALL TEMPERATURE,  $T_W$ , ON S-1B FLAME SHIELD



NOT TO SCALE

FIGURE 28. SCHEMATIC OF THE S-IB BASE REGION

tower and various components near the launch deflector at Pad 39 at Cape Kennedy which will be exposed to heating during lift-off of the first Saturn V vehicle. Radiometer and radiation calorimeter measurements were made in November 1966 near the flame bucket for one of the static firings of the S-IC stage at the MSFC Test Laboratory. Figure 31 shows the 200- to 300-foot luminous plumes of the S-IC stage during an MSFC static firing. Finally, more accurate predictions of radiant heating from carbon particles are currently being obtained with the incorporation of the General Dynamics/Convair [230, 231] carbon absorption coefficient program. This program is currently being used at Chrysler in an attempt to match the onboard spectrometer data obtained in the base region of the S-IB stage for the AS-203 flight. The description of the radiation computer program which describes the use of the combined carbon,  $H_2O$ ,  $CO_2$ , and  $CO$  absorption coefficients for a single, axisymmetric plume has been written recently by Dash\*.

\* M. J. Dash, NASA/MSFC Memorandum to be published, 1967.

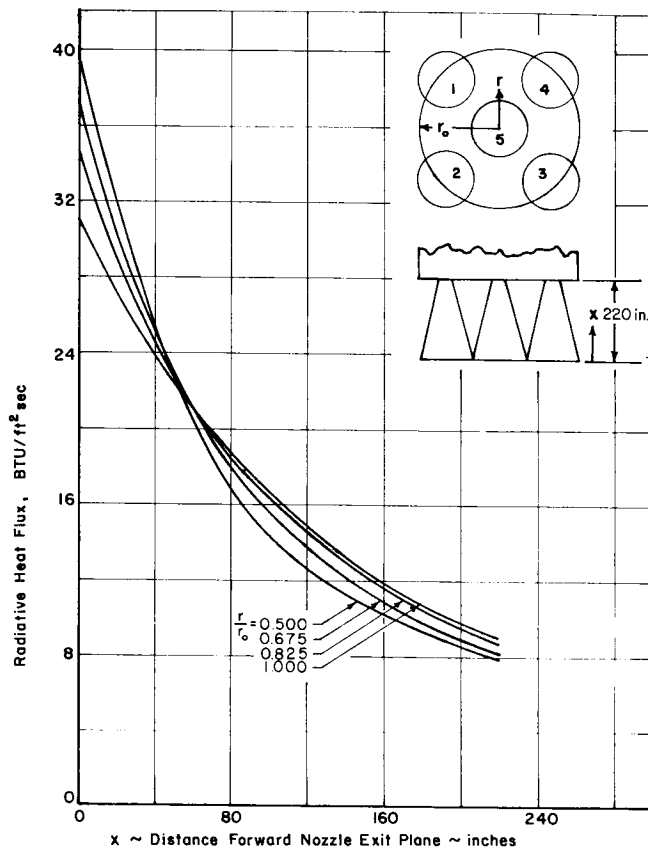


FIGURE 29. S-IC RADIATIVE BASE HEATING FROM F-1 ENGINES AT SEA LEVEL

This concludes the section on radiant heating from carbon particles. The general theory of carbon particle radiation, including formation, size, scattering, and emissive properties of carbon particles and discussions of radiation calculations have been presented. Although there is considerable room for improvement in the general theory, it is felt that the present state of the art has enabled MSFC and its associated contractors to predict satisfactorily radiation thermal environments caused by carbon emission from the Saturn I, S-IB, and S-IC stage engine exhausts.

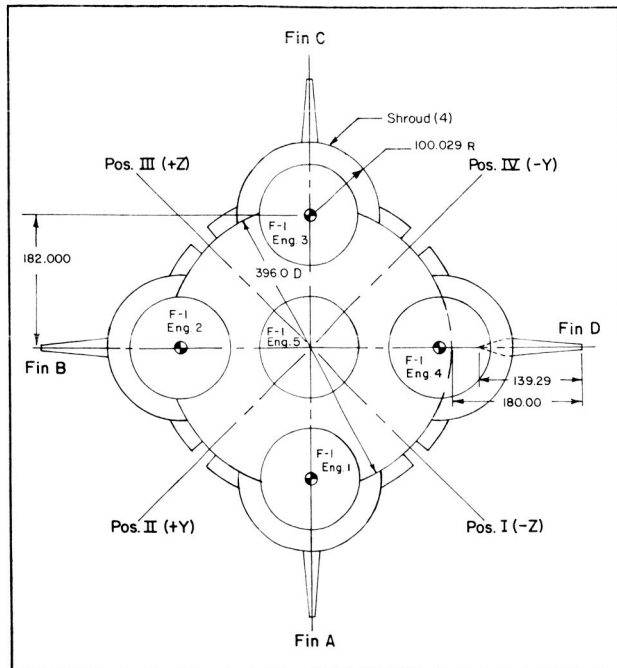


FIGURE 30. SCHEMATIC OF THE S-IC BASE REGION

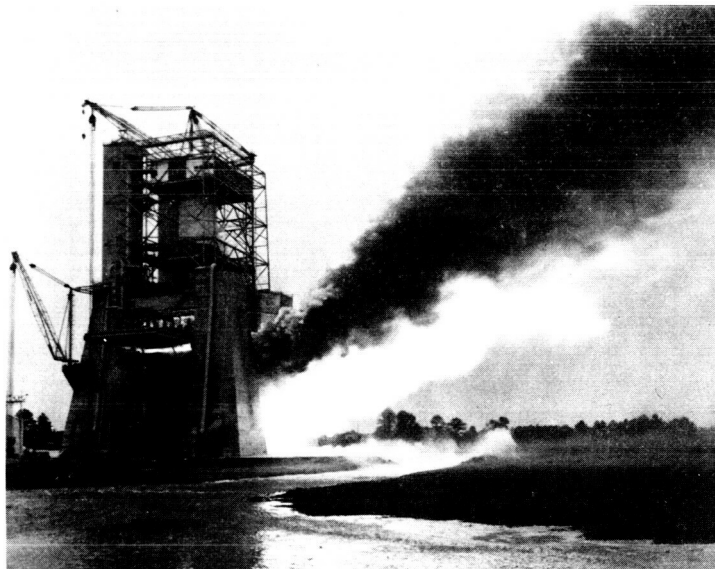


FIGURE 31. S-IC STATIC FIRING

## RADIATION FROM $\text{Al}_2\text{O}_3$ PARTICLES

Thermal radiation from the exhausts of aluminized solid propellant rocket motors is characterized by graybody (continuum) emission from the  $\text{Al}_2\text{O}_3$  particles and by  $\text{Al}_2\text{O}_3$  particle temperatures which are larger than the gaseous temperatures at the same point in the plume. The metallic particles in the propellant, which may be magnesium, beryllium, or iron, as well as aluminum, are added to the propellant to increase its specific impulse and consequently its performance. However, the corresponding thermal radiation from the metallic oxides in the exhaust may be several times higher than the corresponding gaseous radiation emitted in the various molecular bands. Excessive radiative heating from exhausts of solid propellant motors may thus damage portions of the base region if the motor(s) are used as the main source of propulsion, or may damage certain adjacent components and structures if the motor is used as an ullage or retro motor for stage separation purposes (such as for the Saturn vehicles). The problem of microwave attenuation through the exhaust of a solid propellant motor is also more critical than through the exhaust of a liquid propellant engine of comparable size and performance. However, this problem is not treated in this report.

In this section the radiative properties of  $\text{Al}_2\text{O}_3$  particles are surveyed and analyzed in detail. It may be mentioned that  $\text{MgO}$  (magnesia),  $\text{BeO}$  (beryllia), and  $\text{Fe}_2\text{O}_3$  (ferric oxide) also act as emitters in exhausts of certain types of solid propellant engines. However,  $\text{Al}_2\text{O}_3$  (alumina) is found in the exhausts of the majority of metallized propellants in existence at the present time, and since the radiative properties of  $\text{Al}_2\text{O}_3$  are more fully understood than those of the other oxides, this section is devoted almost exclusively to radiation from  $\text{Al}_2\text{O}_3$  particles.

It has been shown by many investigators such as Talbert et al. [336], Dimmock and Courtney [337], Wagner, Cramer, and Borough [338], Briscoe, Bullara, and Bressler [339], Sutton [340], Schindler and Penzias [341], Miller [342], Baker and Allport [343], Carlson [344], Carlson and Du Puis [345], Launstein et al. [346], two Aerojet-General reports [155, 347], Miller and Sternchak [348], Lai and Purgalis [35], a Bamirac report [349], and Condron [350] that the spectrum of the exhausts of solid-fueled engines follows a graybody continuum from about  $1 \mu$  to around  $3 \mu$ . It is known that the exhausts of double-base propellants of the nitroglycerine-nitrocellulose type, such as the Minuteman third stage, are similar to the carbon spectrums as discussed in the previous section. The double-base propellants generally

produce more carbon in the exhaust than do the composite solid propellants which are composed of a fuel, binder, and a finely ground oxidizer such as  $\text{NH}_4\text{ClO}_4$ .

The composite propellants such as those in the Minuteman first and second stages, Polaris, UTC-120 in. solids, and Saturn ullage and retro motors produce a continuous spectrum (on which gaseous band emission is superimposed) with a lower emissivity but with a higher particle temperature than do the double-base propellants. The composite propellants also produce an emission band of low intensity for the HCl molecule around  $3.5 \mu$ . It is believed that the continuum in composite propellant exhausts is caused mainly by  $\text{Al}_2\text{O}_3$  emission, although it is possible that carbon could also be emitting in the  $1 - 3\text{-}\mu$  region. Upon analysis of some of the references mentioned in the above paragraph, it was found by Carlson et al. [351] that when the  $\text{Al}_2\text{O}_3$  mass fraction was approximately doubled, the ratio of continuum to gas emission was approximately doubled, even though the carbon mass fraction was the same. This implies that the  $\text{Al}_2\text{O}_3$  was the major contributor to the continuum rather than the carbon. Also, spectrometer measurements at Aeronutronic [344] of the plume of an  $\text{H}_2\text{-O}_2\text{-Al}_2\text{O}_3$  water slurry motor confirm the presence of an  $\text{Al}_2\text{O}_3$  continuum for  $1\text{-}3 \mu$ .

This  $\text{Al}_2\text{O}_3$  continuum emission in the  $1.9\text{-}\mu$  to  $2.6\text{-}\mu$  region (where there are no molecular emitters) may be seen in Figure 32, which shows the spectrum of the exhausts of scale models of the S-II ullage and S-IC retro motors fired at Cornell at 100,000 feet. This continuum would have existed down to  $1 \mu$  or shorter, but the filter on the spectrometer cut off around  $1.7 \mu$ . The higher temperature of the  $\text{Al}_2\text{O}_3$  particles (higher than that of the carbon for the same gas temperature) produces a very luminous core of particles, the larger particles of the order of  $3$  to  $5 \mu$  tending to hug the plume axis and the smaller particles of the order of  $1 \mu$  or less tending to flare out beyond the gas plume. Some of these luminous solid propellant plumes are shown in Figures 33, 34, and 35, which are respectively, the plume of the Minuteman first stage motor fired at sea level, the plume of the S-II ullage rocket fired at 121,000 feet in the AEDC J-4 test cell, and the plume ( $\text{Fe}_2\text{O}_3$  instead of  $\text{Al}_2\text{O}_3$ ) of a scale model of the S-IB retrorocket fired at 200,000 feet in an altitude cell at Cornell.

It is possible that another type of radiation from solid propellant motors, the so-called "searchlight" radiation, may occur. This type of radiation involves liquid particles radiating at very high temperatures in the combustion chamber through the nozzle into the particle plume where the radiation is then scattered

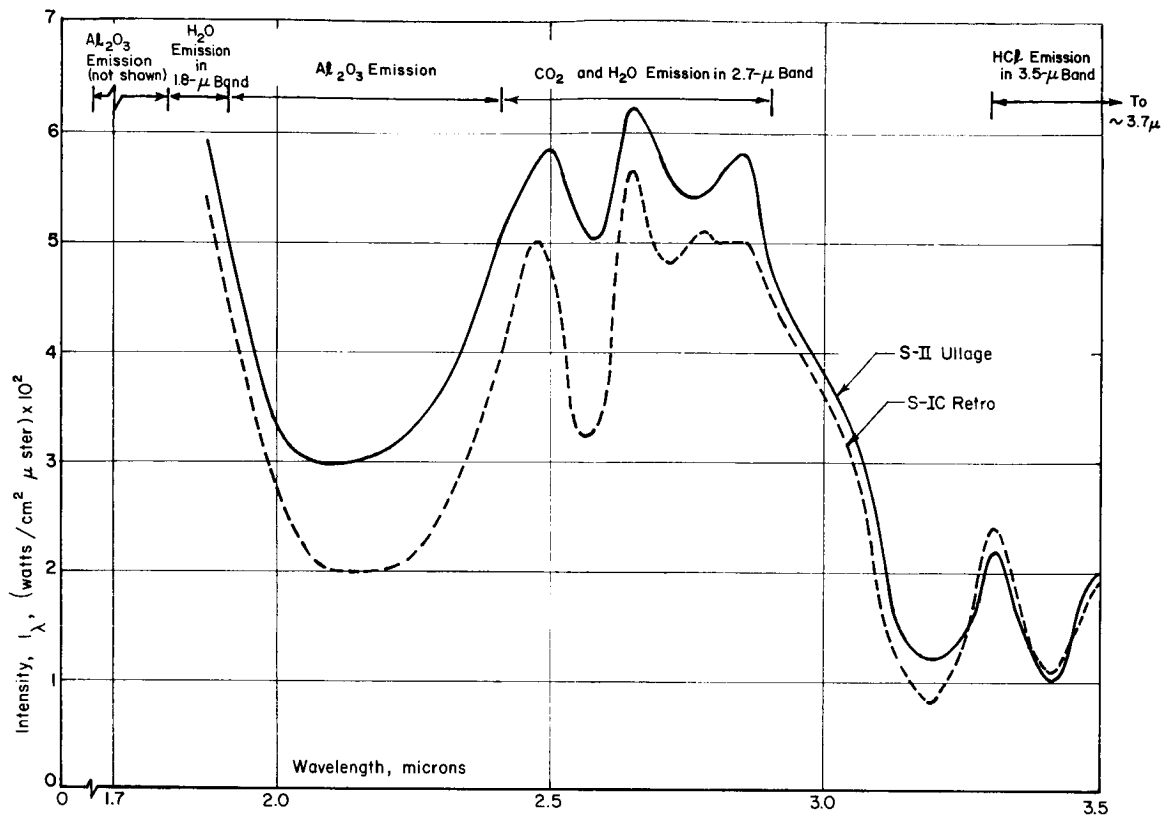


FIGURE 32. RADIATIVE INTENSITY FROM EXHAUSTS OF S-II ULLAGE AND S-IC RETRO MOTORS FIRED AT CAL

out of the plume. The radiation takes place in the visible or ultraviolet region ( $\lambda < 0.8 \mu$ ) because of the high temperatures, resulting in a blackbody curve which has its maximum in the visible or ultraviolet. The maximum radiation emitted would thus be equal to  $\sigma_B T_c^4 A_t$ , where  $T_c$  is the combustion chamber temperature and  $A_t$  is the throat area. This searchlight effect has been shown by Carlson et al. [352] to be an important factor with small nozzles or light aluminum loadings. Recent investigations at Rocketdyne [199] have indicated that this searchlight effect can also occur in hydrocarbon-fueled engines in the ultraviolet and visible regions.

Calculations of thermal radiation from particle plumes (such as  $Al_2O_3$  plumes) are difficult because the particles can scatter radiation considerably as well as emit radiation. The Mie theory of scattering for these large  $Al_2O_3$  particles, in which the parameter  $\alpha = 2\pi r_p/\lambda$  is of the order of unity, must

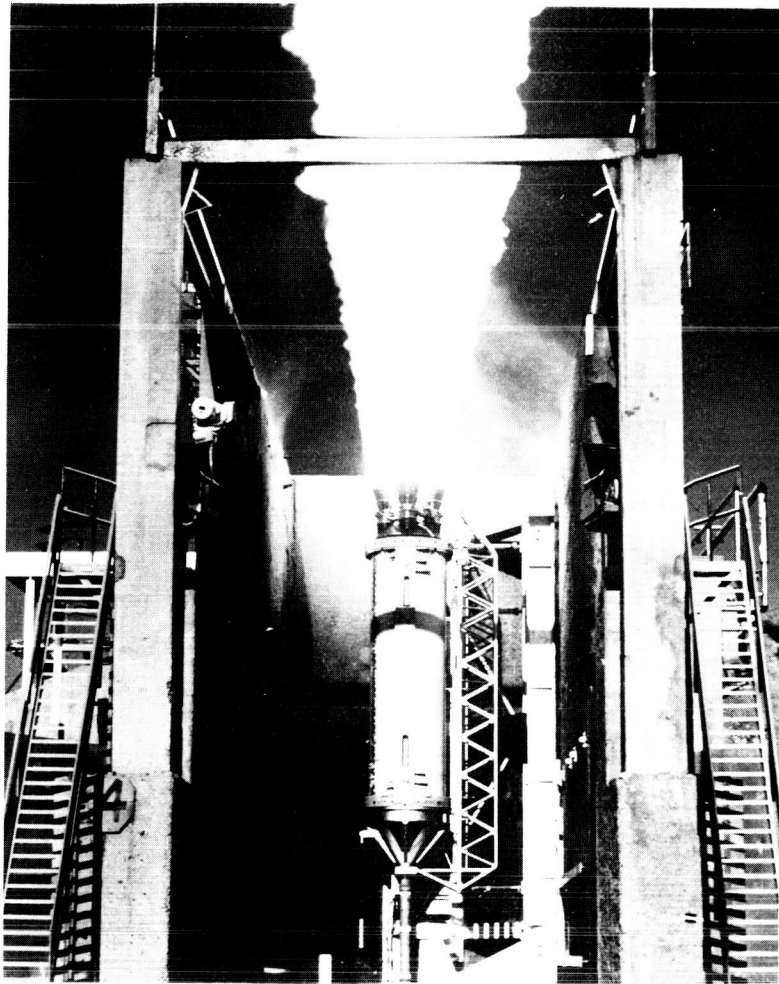


FIGURE 33. FIRST STAGE MINUTEMAN PLUME AT SEA LEVEL

be used to obtain scattering and absorption cross-sections,  $\sigma_s$  and  $\sigma_a$ , respectively (or efficiency factors  $Q_s$  and  $Q_a$ , respectively) from which the optical thickness,  $\tau$ , of the particle plume may be obtained. The cross-sections depend on the scattering angle,  $\theta$ , on the complex index of refraction of  $\text{Al}_2\text{O}_3$ ,  $n = n_1 - in_2$  (which depends on temperature of the particles and wavelength of radiation), and on the  $\text{Al}_2\text{O}_3$  particle size distribution. The emissivity of the particle cloud is then obtained from the ratio of absorption to extinction efficiency factors,  $Q_a/Q_t$ , and the optical thickness, which is a function of particle concentration,  $N_p$ , and path length,  $\ell$ , as well as of the extinction

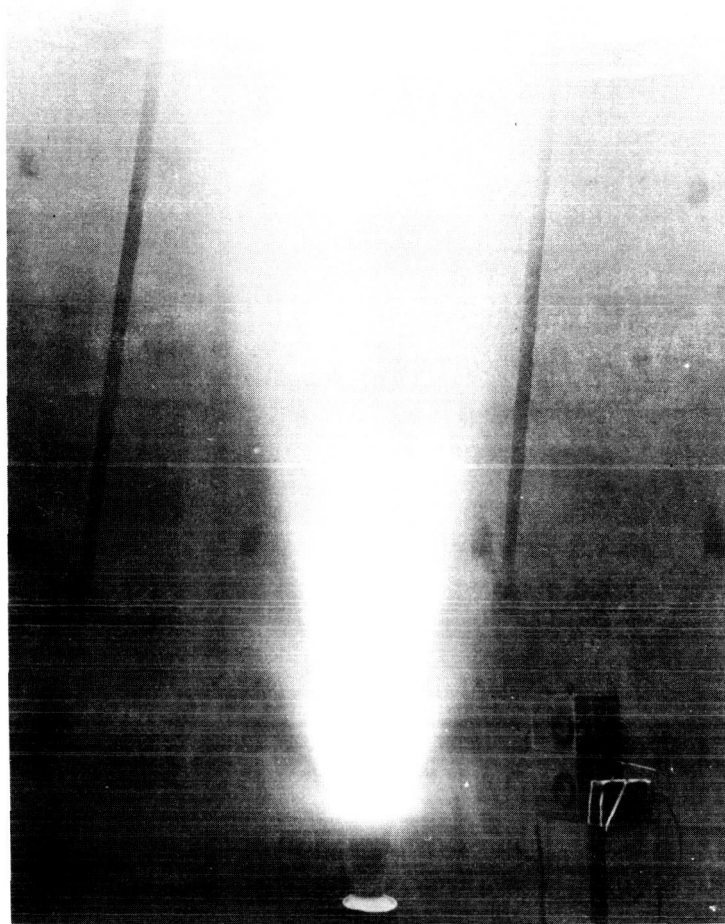


FIGURE 34. S-II ULLAGE ROCKET PLUME AT ~ 121,000 FEET  
IN AEDC J-4 TEST CELL

cross-section or efficiency factor. A two-phase plume program is used to compute the particle concentration,  $N_p$ , for use in the optical thickness expression and also the particle temperature,  $T_p$ . In this manner, the radiation from an  $Al_2O_3$  particle cloud may be determined with a reasonable degree of accuracy, depending upon various assumptions made, such as particle size and distribution.

This section discusses the Mie theory of scattering, the determination (both experimentally and theoretically) of  $Al_2O_3$  particle sizes and distributions and the determination of  $Al_2O_3$  particle cloud emissivities (including effects of

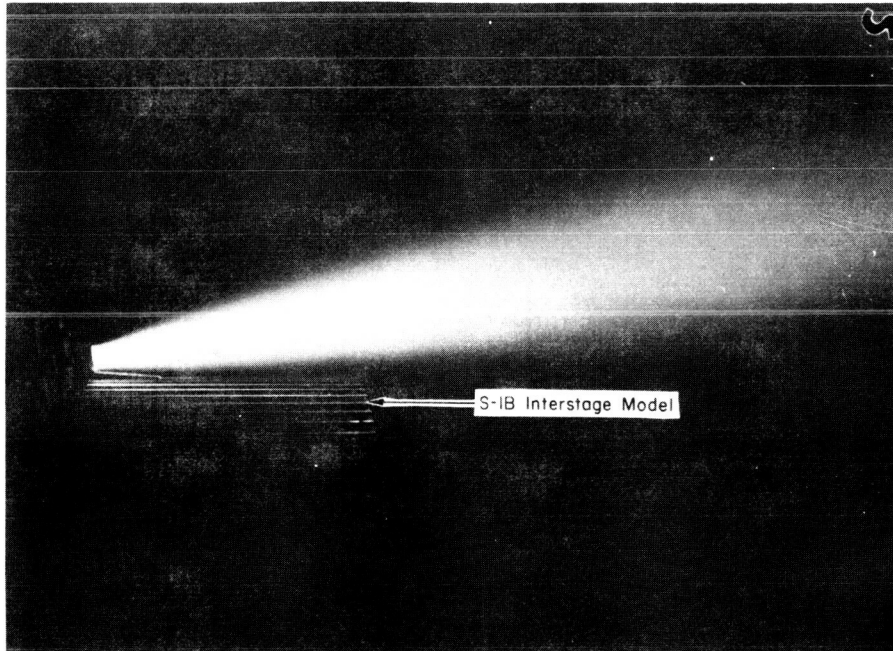


FIGURE 35. S-IB RETROROCKET PLUME AT  $\sim 200,000$  FEET  
IN CAL ALTITUDE CHAMBER

anisotropic and multiple scattering). The determination of  $\text{Al}_2\text{O}_3$  particle temperatures (two-phase flow phenomena) is then briefly treated, and finally various procedures for calculating radiation from aluminized rocket exhausts are analyzed.

## Mie Theory of Scattering

The Mie theory of scattering of plane, monochromatic electromagnetic waves by spherical homogeneous conducting particles (in this case  $\text{Al}_2\text{O}_3$  particles) in which  $\alpha \sim 1$  is described in this section. The end result of this theory is that expressions for extinction (or total) and scattering cross-sections  $\sigma_t$  and  $\sigma_s$ , respectively (or efficiency factors  $Q_t$  and  $Q_s$ ), are obtained as a function of  $\alpha$ . These quantities are then used in the emissivity expressions as discussed in the third part of this section. This section shows that one of the limiting cases of the Mie theory in which  $\alpha \ll 1$  results in the Rayleigh theory

of scattering as discussed in the following part. The other limit in which  $\alpha \gg 1$  belongs to the realm of geometrical optics and will not be analyzed here.

The Mie theory has been used by hundreds of authors since Mie [265] first developed it in 1908. Perhaps the most extensive lists of references on the general subject of Mie theory and light-scattering calculations and experiments are given in the bibliography compiled by Boudreau and Stone [353] (494 references), and in the reports and articles by Oster [243] (227 references), Hawksley [281] (227 references), Love and Wheasler [354] (167 references), and Pendorff [355] (117 references). The general derivations of the equations, starting from the Maxwell equations, are perhaps developed best by Stratton [232], Van de Hulst [246], Born and Wolfe [235], Havard [356], Svaton and Winer [357], Wyatt [358], Panofsky and Phillips [57], Goody [25], Morse and Feshbach [359], La Mer [360], Bromwich [361], Nawrocki and Papa [362], and Newton [363]. In this section the principal parts of the derivations as discussed by the above authors are given to determine the extinction and scattering cross-sections for use in emissivity predictions. This section covers the following areas: (1) determination of Mie coefficients,  $a_m$  and  $b_m$ ; (2) determination of extinction and scattering cross-sections,  $\sigma_t$  and  $\sigma_s$ , and efficiency factors,  $Q_t$  and  $Q_s$ ; (3) limiting case of Rayleigh scattering; and (4) discussion of the Mie theory calculations.

1. Determination of Mie Coefficients,  $a_m$  and  $b_m$ . In analyzing the problem of scattering of plane waves by homogeneous spherical particles, it is usually assumed that the incident radiation is linearly polarized and that the particles are randomly distributed and separated from each other by distances that are large compared to the wavelength of incident radiation. The Mie coefficients,  $a_m$  and  $b_m$ , (and consequently the cross-sections and efficiency factors) may then be obtained by solving Maxwell's equations and applying appropriate boundary conditions. Maxwell's equations in Gaussian units are

$$\nabla \times \vec{H} = \frac{4\pi}{c} \vec{J} + \frac{1}{c} \frac{\partial \vec{D}}{\partial t} \quad (341)$$

and

$$\nabla \times \vec{E} = -\frac{1}{c} \frac{\partial \vec{H}}{\partial t} \quad (342)$$

A third equation, the equation of conservation of charge, will be given as

$$\nabla \cdot \vec{J} + \frac{d\rho_e}{dt} = 0 \quad , \quad (343)$$

where  $\rho_e$  is the charge density and  $\vec{J}$  is the current density. If the time dependence of the steady-state fields may be described by the factor  $e^{i\omega t}$ , equations (341) and (342) reduce to the form

$$\nabla \times \vec{H} = i k n^2 \vec{E} \quad (344)$$

and

$$\nabla \times \vec{E} = - i k \vec{H} \quad , \quad (345)$$

where the quantity  $kn$  is the propagation constant in a medium of complex refractive index  $n$  (the quantity  $k$  represents the propagation constant in a vacuum). The quantities  $k$  and  $n$  may be defined as

$$k = \frac{\omega}{c} = \frac{2\pi}{\lambda} \quad \text{and} \quad n^2 = \epsilon - \frac{4\pi i\sigma}{\omega} \quad . \quad (346)$$

This notation differs slightly from that used by Stull and Plass [240] in equation (264).

For a homogeneous medium, it can be shown that the electric and magnetic field vectors,  $\vec{E}$  and  $\vec{H}$ , respectively, satisfy the vector wave equation.

$$\nabla^2 \vec{A} + k^2 n \vec{A} = 0 \quad , \quad (347)$$

where the vector  $\vec{A}$  may be either  $\vec{E}$  or  $\vec{H}$ . This equation may be solved (Havard [356]) by solving the following scalar wave equation:

$$\nabla^2 \psi + k^2 n \psi = 0 \quad . \quad (348)$$

If  $\psi$  is the solution of equation (348), then the vectors  $\vec{M}_\psi$  and  $\vec{N}_\psi$ , defined by van de Hulst [246] as

$$\vec{M}_\psi = \nabla \times (\vec{r}\psi) \quad \text{and} \quad nk \vec{N}_\psi = \nabla \times \vec{M}_\psi \quad , \quad (349)$$

will satisfy the vector wave equation (347). These vector quantities are related by the equation

$$nk \vec{M}_\psi = \nabla \times \vec{N}_\psi \quad . \quad (350)$$

According to van de Hulst, if  $u$  and  $v$  are two solutions of the scalar wave equation (348), and if  $\vec{M}_u$ ,  $\vec{N}_u$ ,  $\vec{M}_v$ , and  $\vec{N}_v$  are the derived vector fields, the equations (344) and (345) may be satisfied by the equations

$$\vec{H} = n(-\vec{M}_u + i\vec{N}_v) \quad (351)$$

and

$$\vec{E} = \vec{M}_v + i\vec{N}_u \quad . \quad (352)$$

By constructing three vector solutions  $\vec{L}_\psi = \nabla \psi$ ,  $\vec{M}_\psi$ , and  $\vec{N}_\psi$  for equation (347), it may be shown by Stratton [232] that the full components of  $\vec{M}_\psi$  and  $\vec{N}_\psi$  in polar coordinates may be written as

$$M_r = 0, \quad nk N_r = \frac{\partial^2 (r\psi)}{\partial r^2} + n^2 k^2 r\psi \quad (353)$$

$$M_\theta = \frac{1}{r \sin \theta} \frac{\partial (r\psi)}{\partial \phi}, \quad nk N_\theta = \frac{1}{r} \frac{\partial^2 (r\psi)}{\partial r \partial \theta} \quad (354)$$

and

$$M_{\phi} = -\frac{1}{r} \frac{\partial(r\psi)}{\partial\theta}, \quad nkN_{\phi} = \frac{1}{r \sin\theta} \frac{\partial^2(r\psi)}{\partial r \partial\theta} \quad (355)$$

Stratton and van de Hulst show that the magnetic and electric fields,  $\vec{H}$  and  $\vec{E}$  respectively, may be completely described by choosing solutions  $u$  and  $v$  to the scalar wave equation (348), for the incident wave outside the spherical particle, the scattered wave outside the spherical particle, and the field inside the spherical particle. For the outside, incident wave, the solutions are

$$u = A \sum_{m=1}^{\infty} K_m J_m(kr), \quad v = B \sum_{m=1}^{\infty} K_m J_m(kr) \quad (356)$$

For the outside scattered wave, the solutions are

$$u = A \sum_{m=1}^{\infty} -a_m K_m H_m^{(2)}(kr), \quad v = B \sum_{m=1}^{\infty} -b_m K_m H_m^{(2)}(kr) \quad (357)$$

For the inside wave, the solutions are

$$u = A \sum_{m=1}^{\infty} nC_m K_m J_m(nkr), \quad v = B \sum_{m=1}^{\infty} nd_m K_m J_m(nkr) \quad (358)$$

In these equations the quantities  $A$ ,  $B$ , and  $K_m$  are

$$A = e^{i\omega t} \cos\phi, \quad B = e^{i\omega t} \sin\phi \quad (359)$$

and

$$K_m = (-i)^m \frac{2m+1}{m(m+1)} P'_m(\cos\theta) \quad (360)$$

The quantities  $P'_m$  are the associated Legendre polynomials with  $\ell = 1$ . The  $a_m$  and  $b_m$  are the Mie coefficients to be determined subsequently, and the  $c_m$  and  $d_m$  are related to the  $a_m$  and  $b_m$ . The quantities  $H_m^{(2)}$  are the Hankel functions related to the spherical Bessel functions  $J_m(z)$  and  $N_m(z)$  as given by Morse and Feshbach [359] as

$$H_m^{(2)}(z) = J_m(z) - iN_m(z) \quad (361)$$

By using the Riccati-Bessel functions,

$$\psi_m(z) = zJ_m(z), \quad \chi_m(z) = -zN_m(z), \quad \text{and} \quad \zeta_m(z) = zH_m^{(2)}(z), \quad (362)$$

and equation (361), the following relation may be written:

$$\zeta_m(z) = \psi_m(z) + i\chi_m(z) \quad (363)$$

The components of the electric field vector in equation (351),  $E_\theta$  and  $E_\phi$ , both contain the quantities  $v$  and  $\frac{1}{n} \frac{\partial}{\partial r}(ru)$ , which are different inside and outside the spherical particle. The components of the magnetic field vector in equation (351),  $H_\theta$  and  $H_\phi$ , both contain the quantities  $nu$  and  $\frac{\partial}{\partial r}(rv)$  which are also different inside and outside the spherical particle. All of these quantities must be equal on the boundary of the spherical particle. Van de Hulst [246] presents boundary conditions which equate the quantity in brackets on either side of the boundary of the spherical particle.

$$[nu]: \quad \psi_m(\alpha) - a_m \zeta_m(\alpha) = nc_m \psi_m(\beta) \quad (364)$$

$$\left[ \frac{1}{n} \frac{\partial(ru)}{\partial r} \right]: \quad \psi'_m(\alpha) - a_m \zeta'_m(\alpha) = c_m \psi'_m(\beta) \quad (365)$$

$$[v]: \quad \psi_m(\alpha) - b_m \zeta_m(\alpha) = d_m \psi_m(\beta) \quad (366)$$

$$\left[ \frac{\partial(\mathbf{rv})}{\partial \mathbf{r}} \right]: \quad \psi'_m(\alpha) - b_m \zeta'_m(\alpha) = n d_m \psi_m(\beta) \quad (367)$$

where the primes denote derivatives and  $\beta = n\alpha = n \frac{2\pi r}{\lambda}$ .

If  $c_m$  is eliminated from the first pair of equations and  $d_m$  from the second pair, the Mie coefficients  $a_m$  and  $b_m$ , the electric and magnetic wave coefficients, respectively, may be obtained as

$$a_m = \frac{\psi'_m(\beta) \psi_m(\alpha) - n \psi_m(\beta) \psi'_m(\alpha)}{\psi'_m(\beta) \zeta_m(\alpha) - n \psi_m(\beta) \zeta'_m(\alpha)} \quad (368)$$

and

$$b_m = \frac{n \psi'_m(\beta) \psi_m(\alpha) - \psi_m(\beta) \psi'_m(\alpha)}{n \psi'_m(\beta) \zeta_m(\alpha) - \psi_m(\beta) \zeta'_m(\alpha)}, \quad (369)$$

where equation (362) would then be used. The Mie coefficients are sometimes expressed in other ways, such as with Neumann functions,

$$Y_m(z) = i \left[ J_m(z) - H_m^{(1)}(z) \right], \quad (370)$$

as written by Stull and Plass [240] as

$$a_m = - \left[ 1 + i \frac{n Y_m(\alpha) J_{m+1}(\beta) - J_m(\beta) Y_{m+1}(\alpha)}{n J_m(\alpha) J_{m+1}(\beta) - J_m(\beta) J_{m+1}(\alpha)} \right]^{-1} \quad (371)$$

and

$$b_m = - \left[ 1 + i \frac{(m+1)(n^2-1) Y_m(\alpha) J_m(\beta) + \beta Y_m(\alpha) J_{m+1}(\beta) - n^2 \alpha J_m(\beta) Y_{m+1}(\alpha)}{(m+1)(n^2-1) J_m(\alpha) J_m(\beta) + n \alpha J_m(\alpha) J_{m+1}(\beta) - n^2 \alpha J_m(\beta) J_{m+1}(\alpha)} \right]^{-1} \quad (372)$$

or in terms of the logarithmic derivative functions as used by Infield [364], Aden [365], Krascella [259], Beheshti [260], Tibbodeaux and Beheshti [12], and Smith [366]. These logarithmic derivative functions simplify the calculations when the index of refraction is complex and when the Bessel and Hankel functions are small and complex. In this manner the two functions  $\eta_m(z)$  and  $\xi_m(z)$  may be defined as

$$\eta_m(z) = \frac{d}{dz} \ln \left[ z H_m^{(2)}(z) \right] = \frac{H_{m-1}^{(2)}(z)}{H_m^{(2)}(z)} - \frac{m}{z} \quad (373)$$

and

$$\xi_m(z) = \frac{d}{dz} \ln \left[ z J_m(z) \right] = \frac{J_{m-1}^{(2)}(z)}{J_m^{(2)}(z)} - \frac{m}{z} \quad (374)$$

Using these quantities, the Mie coefficients may be written as

$$a_m = - \frac{J_m(\alpha)}{H_m^{(2)}(\alpha)} \left[ \frac{\eta_m(\alpha) - n \eta_m(\beta)}{\xi_m(\alpha) - n \eta_m(\beta)} \right] \quad (375)$$

and

$$b_m = - \frac{J_m(\alpha)}{H_m^{(2)}(\alpha)} \left[ \frac{\eta_m(\beta) - n \eta_m(\alpha)}{\eta_m(\beta) - n \xi_m(\alpha)} \right] \quad (376)$$

2. Determination of Scattering and Extinction Cross-Sections,  $\sigma_s$  and  $\sigma_t$ , and Efficiency Factors,  $Q_s$  and  $Q_t$ . The scattering and extinction cross-sections may be obtained by either of two methods. The first method involves the use of the following scattering matrix as discussed by van de Hulst [246]:

$$\begin{pmatrix} E_{||} \\ E_{\perp} \end{pmatrix} = \begin{pmatrix} S_2 & S_3 \\ S_4 & S_1 \end{pmatrix} \frac{\exp(-ikr + ikz)}{ikr} \begin{pmatrix} E_{o||} \\ E_{o\perp} \end{pmatrix}, \quad (377)$$

where the parallel and perpendicular components of the electric field of the incident wave,  $E_{o_{||}}$  and  $E_{o_{\perp}}$ , respectively, are

$$E_{o_{||}} = \cos \phi \quad \text{and} \quad E_{o_{\perp}} = \sin \phi \quad , \quad (378)$$

and the parallel and perpendicular components of the scattered wave are

$$E_{||} = E_{\theta} \quad \text{and} \quad E_{\perp} = - E_{\phi} \quad . \quad (379)$$

In the matrix, equation (377), the quantity  $S_3 = S_4 = 0$  for spherical particles, and the quantities  $S_1$  and  $S_2$  depend only on  $\theta$ . Substituting the asymptotic form  $(i^{n+1}/kr) e^{-ikz}$  for  $H_m^{(2)}(kr)$  for large distances  $r$  from the particles in equation (357), for the scattered wave, the resulting field components may be written as

$$E_{||} = E_{\theta} = H_{\phi} = - \frac{i}{kr} \exp(-ikr + i\omega t) \cos \phi S_2(\theta) \quad , \quad (380)$$

and

$$E_{\perp} = - E_{\phi} = H_{\theta} = - \frac{i}{kr} \exp(-ikr + i\omega t) \sin \phi S_1(\theta) \quad , \quad (381)$$

where the functions  $S_1(\theta)$  and  $S_2(\theta)$  are, thus,

$$S_1(\theta) = \sum_{m=1}^{\infty} \frac{2m+1}{m(m+1)} \left[ a_m \pi_m(\cos \theta) + b_m \tau_m(\cos \theta) \right] \quad (382)$$

and

$$S_2(\theta) = \sum_{m=1}^{\infty} \frac{2m+1}{m(m+1)} \left[ b_m \pi_m(\cos \theta) + a_m \tau_m(\cos \theta) \right] \quad . \quad (383)$$

The quantities  $\pi_m(\cos \theta)$  and  $\tau_m(\cos \theta)$  are defined as

$$\pi_m(\cos \theta) = \frac{1}{\sin \theta} P_m^1(\cos \theta) = \frac{dP_m(\cos \theta)}{d \cos \theta} \quad (384)$$

and

$$\tau_m(\cos \theta) = \frac{d}{d\theta} P_m^1(\cos \theta) = \cos \theta \left[ \pi_m(\cos \theta) \right] - \sin \theta \frac{d\pi_m(\cos \theta)}{d \cos \theta} \quad (385)$$

The total or extinction cross-section  $\sigma_t$  is related to the total or extinction efficiency factor,  $Q_t$ , as  $\sigma_t = Q_t \pi r_p$ . The efficiency factor  $Q_t$  may be obtained from equations (382) and (383) by setting  $\theta = 0$  so that  $S_1(\theta) = S_2(\theta) = S(0)$  for  $\theta = 0$ . The total efficiency factor is then found, as described by van de Hulst [246], as

$$Q_t = \frac{4}{\alpha^2} \operatorname{Re}[S(0)] = \frac{2}{\alpha^2} \sum_{m=1}^{\infty} (2m+1) \operatorname{Re}(a_m + b_m) \quad , \quad (386)$$

where the expression  $\operatorname{Re}(a_m + b_m)$  denotes the real part of  $a_m + b_m$ .

The scattering efficiency factor,  $Q_s = \sigma_s / \pi r_p^2$ , may be written in terms of the intensity functions  $i_1$  and  $i_2$  which are defined as

$$i_1 = \left| S_1(\theta) \right|^2 \quad \text{and} \quad i_2 = \left| S_2(\theta) \right|^2 \quad . \quad (387)$$

The quantity  $i_1$  is proportional to the intensity whose electric oscillations are perpendicular to the plane of scattering (polarized light in the horizontal plane). The quantity  $i_2$  is proportional to the intensity whose electric oscillations are in the plane of scattering (polarized light in the vertical plane). The polarization,  $P$ , is then related to these intensity functions by the following equation:

$$P = \frac{i_1(\theta) - i_2(\theta)}{i_1(\theta) + i_2(\theta)} \quad (388)$$

According to Churchill et al. [42], the quantities  $i_1(\theta)$  and  $i_2(\theta)$  can be related to  $i(\theta, \phi)$ , which represents the power scattered by a spherical particle from a linearly polarized beam of unit intensity into a unit solid angle in the direction  $(\theta, \phi)$ . This quantity  $i(\theta, \phi)$  is written as

$$i(\theta, \phi) = \frac{\lambda^2}{4\pi^2} \left[ i_1(\theta) \cos^2 \phi + i_2(\theta) \sin^2 \phi \right] . \quad (389)$$

For a randomly polarized beam of unit intensity, the power scattered into a unit solid angle may be obtained by averaging  $i(\theta, \phi)$  over  $\phi$ , as

$$i(\theta) = \frac{\lambda^2}{8\pi^2} \left[ i_1(\theta) + i_2(\theta) \right] . \quad (390)$$

The scattering cross-section may now be defined according to Churchill et al. [42] as the total power scattered by a particle from a beam of unit intensity as

$$\sigma_s = 2\pi \int_0^\pi i(\theta) \sin \theta \, d\theta . \quad (391)$$

This definition is in agreement with that of van de Hulst [246], who states that if the total energy scattered in all directions is equal to the energy of the incident wave falling on the area  $\sigma_s$ , the scattering efficiency factor may be written in the integral form:

$$Q_s = \frac{\sigma_s}{\pi r_p^2} = \frac{1}{\alpha^2} \int_0^\pi [i_1(\theta) + i_2(\theta)] \sin \theta \, d\theta . \quad (392)$$

The conversion of equation (392) into the following one in terms of the Mie coefficients  $a_m$  and  $b_m$  is quite difficult and has been given by Debeye [367] as

$$Q_s = \frac{2}{\alpha^2} \sum_{m=1}^{\infty} (2m+1) \left\{ \left| a_m \right|^2 + \left| b_m \right|^2 \right\} . \quad (393)$$

The absorption efficiency factor  $Q_a$  or cross-section  $\sigma_a$  may thus be found as the difference, respectively, between  $Q_t$  and  $Q_s$  or  $\sigma_t$  and  $\sigma_s$ .

The second method of obtaining the total and scattering cross-sections or efficiency factors involves the use of the Poynting vector as discussed by Stratton [232], Svaton and Winer [357], Panovsky and Phillips [57], and Goody [25]. The energy absorbed from an incident electromagnetic wave by a spherical particle may be written as the divergence of the real part of the radial component of the complex Poynting vector  $\vec{S}^*$  as

$$\nabla \cdot \text{Re}(\vec{S}^*)_{\text{R}} = \frac{1}{2} \text{Re} \int_{\text{A}} \vec{S}^*_{\text{R}} \cdot d\vec{A} \quad (394)$$

The radial components  $\vec{S}^*_{\text{R}}$  may be written as

$$\begin{aligned} \vec{S}^*_{\text{R}} = \frac{1}{2} \left[ (\vec{E}_i + \vec{E}_s) \times (\vec{H}_i + \vec{H}_s) \right]_{\text{R}} &= \frac{1}{2} (E_{\theta_i} \vec{H}_{\phi_i} - E_{\phi_i} \vec{H}_{\theta_i}) \\ &+ \frac{1}{2} (E_{\theta_s} \vec{H}_{\phi_s} - E_{\phi_s} \vec{H}_{\theta_s}) + \frac{1}{2} (E_{\theta_i} \vec{H}_{\phi_s} + E_{\theta_s} \vec{H}_{\phi_i} - E_{\phi_i} \vec{H}_{\theta_s} - E_{\phi_s} \vec{H}_{\theta_i}), \end{aligned} \quad (395)$$

where the subscript i represents the incident wave and s represents the scattered wave.

If the external medium is assumed to be non-conducting, the first term in parenthesis on the right is equal to zero. The second term on the right measures the outward flow of the scattered energy from a concentric spherical surface of radius  $r$  which encloses the spherical particle of radius  $r_p$ . The third term on the right is thus equal to the sum of the absorbed and scattered energy which may be written as

$$\begin{aligned} W_t = W_a + W_s = & \\ & - \frac{1}{2} \text{Re} \int_0^{\pi} \int_0^{2\pi} (E_{\theta_i} \vec{H}_{\phi_s} + E_{\theta_s} \vec{H}_{\phi_i} - E_{\phi_i} \vec{H}_{\theta_s} - E_{\phi_s} \vec{H}_{\theta_i}) r^2 \sin \theta \, d\theta \, d\phi. \end{aligned} \quad (396)$$

The energies  $W_a$  and  $W_s$  may be evaluated by making use of asymptotic forms of Bessel functions  $J_m(z)$  and Hankel functions  $H_m^{(1)}(z)$  and with the use of certain orthogonal functions as discussed by Stratton [232]. The energy terms are thus

$$W_s = \pi \frac{E_o^2}{k_2^2} \left( \frac{\epsilon_2}{\mu_2} \right)^{\frac{1}{2}} \sum_{m=1}^{\infty} (2m+1) \left\{ \left| a_m \right|^2 + \left| b_m \right|^2 \right\} \quad (397)$$

and

$$W_t = \pi \frac{E_o^2}{k_2^2} \left( \frac{\epsilon_2}{\mu_2} \right)^{\frac{1}{2}} \operatorname{Re} \sum_{m=1}^{\infty} (2m+1) (a_m + b_m) \quad (398)$$

The scattering, absorption, and total (or extinction) cross-sections may be defined as the ratio of scattering, absorption, or total energy to the energy of the incident wave,  $W_i$  or

$$\sigma_s = \frac{W_s}{W_i}, \quad \sigma_a = \frac{W_a}{W_i}, \quad \sigma_t = \frac{W_t}{W_i} \quad (399)$$

Since the mean energy flow of the incident polarized electromagnetic wave per unit area (energy density) is

$$W_i = \vec{S}^* = \frac{1}{2} E_o^2 \left( \frac{\epsilon_2}{\mu_2} \right)^{\frac{1}{2}}, \quad (400)$$

the scattering and total cross-sections may be written as the ratio of scattered and total energy per second to the energy density of the incident wave, or

$$\sigma_s = \frac{2\pi}{k_2^2} \operatorname{Re} \sum_{m=1}^{\infty} (2m+1) \left\{ \left| a_m \right|^2 + \left| b_m \right|^2 \right\} \quad (401)$$

and

$$\sigma_t = \frac{2\pi}{k_2^2} \operatorname{Re} \sum_{m=1}^{\infty} (2m+1) (a_m + b_m) \quad (402)$$

These expressions reduce to equations (386) and (393) if the relations  $k_2 = \alpha/r_p = 2\pi/\lambda$ ,  $Q_s = \sigma_s/\pi r_p^2$  and  $Q_t = \sigma_t/\pi r_p^2$  are used.

3. Limiting Case of Rayleigh Scattering. It may be shown (Stratton [232], Born and Wolfe [235]) that a limiting case of the Mie theory of scattering occurs when the quantity  $\alpha \ll 1$  and the Rayleigh theory discussed previously may be used to compute the cross-sections and efficiency factors. In this manner the Mie coefficients  $a_m$  and  $b_m$  may be expanded in powers of  $\alpha$ . By neglecting all powers above the fifth, and assuming  $\mu_1 = \mu_2$ , the Mie coefficients become

$$a_1 \approx \frac{i}{45} (n^2 - 1) \alpha^5 \quad (403)$$

$$b_1 \approx -\frac{2i}{3} \left( \frac{n^2 - 1}{n^2 + 2} \alpha^3 - \frac{1}{10} \frac{n^4 - 1}{n^2 + 2} \alpha^5 \right) \quad (404)$$

and

$$b_2 \approx -\frac{i}{15} \frac{n^2 - 1}{2n^2 + 3} \alpha^5 \quad (405)$$

If  $\alpha$  is so small such that  $\alpha^5$  may be neglected compared to  $\alpha^3$ , only the first-order electric oscillation term needs to be considered, which is

$$b_1 = -\frac{2i}{3} \frac{n^2 - 1}{n^2 + 2} \alpha^3 \quad (406)$$

If this expression is used in equations (380) and (381), it may be shown, as in van de Hulst [246] or Stratton [232], that the resulting field of the fundamental mode is that of an electric dipole which has a dipole moment equal to

$$p = ex = \beta E = \left( \frac{n^2 - 1}{n^2 + 2} \right) r_p^3 \quad (407)$$

This expression was determined in the previous discussion of Rayleigh scattering. By using the above procedure, it may be shown (van de Hulst) that the first terms of the expansion for  $Q_t$  may be written as

$$Q_t = -\text{Im} \left[ 4\alpha \frac{n^2 - 1}{n^2 + 2} + \frac{4}{15} \alpha^3 \left( \frac{n^2 + 1}{n^2 + 2} \right)^2 \left( \frac{n^4 - 27n^2 + 38}{2n^2 + 3} \right) \right] + \alpha^4 \text{Re} \left[ \frac{8}{3} \left( \frac{n^2 - 1}{n^2 + 2} \right)^2 \right] + \dots \quad (408)$$

It will be recognized that the first imaginary term is the absorption efficiency factor as given by equation (289) and the first real term is the scattering efficiency factor as given by equation (288).

4. Discussion of the Mie Theory Calculation. Although the main purpose of this entire section is to discuss the use of the Mie theory for  $\text{Al}_2\text{O}_3$  particles immersed in a rocket exhaust gas, it appears necessary to cite the work of investigators whose main purpose was to make Mie theory calculations for other types of particles besides  $\text{Al}_2\text{O}_3$  (other than carbon, discussed in part 1 of "Methods of Predicting Carbon Absorption Coefficients and Emissivities" in the preceding section) for various values of index of refraction, particle radius, and wavelengths. Some of the work to be cited involved light-scattering experiments and calculations using Mie theory in attempts to obtain particle size distributions. These investigations were based on measurements of scattered intensity as a function of scattering angle  $\theta$  and the corresponding Mie theory calculations.

As can be understood from the many equations of the previous sections, the calculations of the cross-sections (or efficiency factors) using the Mie theory are exceedingly lengthy - especially if the index of refraction of the particles is complex (absorbing particles) and a size distribution of the particles is used rather than one particular size. Only in the last eight years or so when high-speed electronic computers became readily available, have the Mie theory calculations become feasible to perform. Throughout the last 10 to 15 years, however, there have been certain groups in the United States that have performed most of the Mie calculations and have published some rather lengthy tables for particles of various sizes, indices of refraction, and wavelengths. Although all the publications of even these seven major groups are too numerous to list completely, some of their most important publications are mentioned.

This list of groups includes (1) the group at the University of Michigan, Gumprecht and Sliepcevich [368-370], Boll, Leacock, Clark, and Churchill [371], Churchill, Chu, Leacock, and Chen [48], Churchill, Chu, Evans, Tien, and Page [42], Chu and Churchill [372], Boll, Gumprecht, and Sliepcevich [373], Boll and Sliepcevich [374], Chin, Sliepcevich, and Tribus [375, 376], Clark, Chu, and Churchill [377], Gumprecht, Sung, Chin, and Sliepcevich [378]; (2) the group at Rand Corporation, Deirmendjian [379-381], Deirmendjian and Clasen [382], and Deirmendjian, Clasen, and Viezee [383]; (3) the group at AVCO, Pendorff [384-392]; (4) the group at Wayne State University, Heller and Pangonis [393], Heller and Pugh [394], Heller and Tabibian [395], Heller, Nakagaki, and Wallach [396], Heller [397], Heller and Nakagaki [398], Nakagaki and Heller [399, 400], Pangonis and Heller [401], Stevenson, Heller, and Wallach [402], and Tabibian and Heller [403]; (5) the group at Clarkson College of Technology, Kerker [404] Kerker and Matejevic [405, 406], and Kerker and Hampton [407]; (6) the group at the University of Oklahoma, Love [29], Love and Wheasler [354], and Love and Beattie [408]; and (7) the group at Aeronutronic, Plass [409-411], Bauer [412], and Bauer and Carlson [413].

Of these seven groups perhaps the only one actively engaged in Mie theory calculations for  $\text{Al}_2\text{O}_3$  particles is Aeronutronic, although it is known that Svaton and Winer [357] at Douglas performed Mie theory calculations for  $\text{Al}_2\text{O}_3$  particles several years ago (as discussed in the last part of this section). However, the general results of the Mie theory calculations are the same whether the particles have the same index of refraction as alumina ( $\text{Al}_2\text{O}_3$ ) or some other index of refraction. That is, as the value of  $\alpha$  increases, the value of  $Q_t$  asymptotically approaches a value of 2.0 (total cross-section  $\sigma_t$  becomes twice as great as the geometric cross-section,  $\pi r_p^2$ ). This phenomenon may be seen from the results of Plass [409] for  $\text{Al}_2\text{O}_3$ , reproduced here in Figure 36, which also shows the Rayleigh limit. Also, for all values of index of refraction and values of  $\alpha$  in the Mie region, the intensity functions  $i_1(\theta)$  and  $i_2(\theta)$  are comparatively high in the forward scattering region ( $\theta \rightarrow 0$ ) and tend to decrease significantly with increasing  $\theta$  until they reach a minimum in the neighborhood of  $\theta = 100^\circ$  to  $110^\circ$ . The intensity functions then tend to rise gradually toward the back scattering region ( $\theta \rightarrow 180^\circ$ ), but still have a value at  $\theta = 180^\circ$  usually an order of magnitude lower than in the forward scattering region.

To predict cross-sections of alumina particles adequately using the Mie theory equations, the index of refraction of alumina (both the real part,  $n_1$ , and the complex part,  $n_2$ ) must be known as a function of both temperature and wavelength. Values of index of refraction at room temperature for alumina in

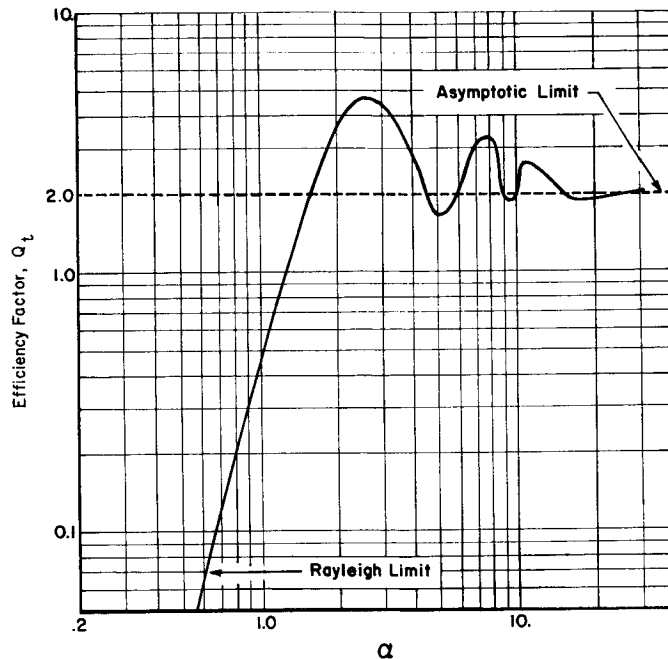


FIGURE 36. TOTAL EFFICIENCY FACTOR FOR ALUMINA AS A FUNCTION OF  $\alpha$  FOR  $\lambda = 2\mu$

the infrared wavelength region up to  $\lambda = 5.5 \mu$  are given by McCarthy, Wolfe, and Ballard [414], and Malitson [415,416]. Absorption coefficients and transmissivities (from which  $n$  may be determined) for alumina at both room temperatures and temperatures up to as high as  $1000^\circ \text{C}$  have been reported by Mergerian [417], McAlister [418], Monroe [419], Openheim and Even [420], and Lee and Kingery [421]. Gryvna and Burch [422,423] at Aeronutronic measured the absorption coefficient and index of refraction ( $n_1$  and  $n_2$ ) of single crystals of  $\text{Al}_2\text{O}_3$  (sapphire) which were heated in a furnace at temperatures up to  $1700^\circ \text{C}$  and over a wavelength range from  $0.546 \mu$  to  $6.0 \mu$ . Measurements of index of refraction and absorption coefficient of molten  $\text{Al}_2\text{O}_3$  (at a temperature of  $2020^\circ \text{C}$ ) were also obtained by Gryvna and Burch by immersing the alumina samples into a hydrogen-oxygen flame. Adams and Colucci [424] report measurements of the complex part of the index of refraction,  $n_2$ , which is equal to  $(\lambda/4\pi) \kappa_\lambda$ , of alumina at temperatures from about  $2100^\circ \text{C}$  to  $2600^\circ \text{C}$  based on their own and Carlson's [345] emissivity measurements in hydrogen-oxygen flames. The real part of the index of refraction,  $n_1$ , may be calculated from these emissivity measurements by combining equations (64-66), (267), and the above relation for  $n_2$ .

Plass [410] used the values of index of refraction as determined by Gryvnak and Burch [422,423] as a function of temperature and wavelength and found, by performing Mie theory calculations, that the absorption cross-section increased by a factor of about 40 as the temperature increased from 1200° C to 2020° C. These Mie theory calculations (using Gryvnak's and Burch's data) are believed to be the most valid for  $\text{Al}_2\text{O}_3$  at the present time and were used in the radiation calculations discussed in the last part of this section. In the next section, various experimental data and theoretical predictions for  $\text{Al}_2\text{O}_3$  particle sizes and distributions are given, as these data are also a very important input to the Mie theory for cross-section and, consequently, emissivity predictions.

## Determination of $\text{Al}_2\text{O}_3$ Particle Sizes and Distributions

The size of  $\text{Al}_2\text{O}_3$  particles found in exhausts of aluminized solid propellant motors depends on the combustion process of the aluminum in the propellant, the  $\text{Al}_2\text{O}_3$  condensation process (liquid particles changing to solid particles), and possibly on chamber pressure, chamber residence time, and throat size of the engine. Aluminum oxide particle sizes have usually been determined by one of three experimental methods: (1) firing small engines into tanks and collecting the residue on the walls, from which it is then scraped off and analyzed under a microscope or with a Micromerograph; (2) sampling the particle plume with probes, microscope slides, and other types of collecting devices and consequently analyzing the deposits; and (3) using optical (light-scattering) techniques. Carlson [5] gives an excellent review of sizes and distributions for both  $\text{Al}_2\text{O}_3$  and BeO particles obtained by these three general methods. In the present section Carlson's review is summarized and additional work performed in this area which was not mentioned by him is reviewed. Since the combustion of aluminum powder to  $\text{Al}_2\text{O}_3$  particles is an important process in particle size determination, it is briefly treated first in this section. The experimental determination of  $\text{Al}_2\text{O}_3$  particle sizes and distributions and the theoretical determination of  $\text{Al}_2\text{O}_3$  particle sizes and distributions are then discussed.

1. Combustion of Aluminum Powder to  $\text{Al}_2\text{O}_3$  Particles. The size and distribution of the  $\text{Al}_2\text{O}_3$  particles found in the exhaust depend upon the combustion process of the aluminum powder (which usually has a size range of 10 to 25  $\mu$ ) in the propellant. Many investigators have analyzed this phenomenon of metal (such as aluminum) combustion in solid propellant motors. However, there are some disagreements as to whether the metal burns by a surface or by a vapor phase combustion process. These two combustion processes are

distinguished, according to Glassman [425], by the fact that, if the boiling temperature of the  $\text{Al}_2\text{O}_3$  is higher than that of the aluminum powder, the combustion process takes place in the vapor phase; however, if the aluminum boiling temperature is greater than that of the  $\text{Al}_2\text{O}_3$ , a surface combustion process occurs. These two processes are strictly for steady-state combustion, because the ignition phenomena could be quite different.

Some of the many investigators who have analyzed surface and vapor phase combustion processes in solid propellant motors include Glassman [425, 426], Brzustowski and Glassman [427], Fassell et al. [428-430], Gordon [431-433], Wood [434, 435], Avery [436], Henderson and Bowen [437], Friedman and Maček [438], Markstein [439], Davis [440], and Kurtovich and Pinson [441, 442].\* In the particular case of aluminum, experimental data such as obtained by Wood [435], Watermeier, Aungust, and Pfaff [443], and McCarty [444] tend to favor the vapor phase combustion process involving the formation of  $\text{Al}_2\text{O}_3$  particles.

Fassell et al. [428] state that the aluminum combustion process takes place in four distinct phases: (1) pre-ignition, (2) ignition, (3) bubble expansion, and (4) quasi-steady-state combustion. According to Avery [436], the oxidizer (such as  $\text{NH}_4\text{ClO}_4$ ) and the binder are first vaporized, heated to combustion temperature, and then carry the aluminum particles with them into the flame front. The molten aluminum is heated, according to Wood [434], first to a dull red color, which then changes to a yellow-orange color. The actual combustion takes place by the establishment of an incandescent reaction zone around the particle. Davis [440] states that the diameter of the aluminum flame is greater than the diameter of the aluminum particle, thus indicating that the reaction zone is not situated on the particle surface, but is actually some distance from the particle - similar to the halo of a diffusion flame found around a burning liquid droplet. It is known that this zone expands during the ignition process and slowly contracts during the remainder of the combustion process. The ignition of large particles is delayed longer since the larger particles conduct more heat from the surface than the smaller particles.

As the aluminum particle is heated to ignition, a shell of oxide forms on the particle. Because of the intense radiant heating occurring at this time, the aluminum is quickly vaporized and, according to Avery [436], as the oxygen immediately surrounding the burning particle is rapidly depleted, the vaporized aluminum attempts to obtain oxygen away from its surface. Since this process

---

\*Also additional information was obtained from D. D. Kirtovich and G. T. Pinson in an unpublished Boeing report of January 1960, entitled "Radiation Characteristics of Rocket Engine Exhausts."

has proceeded so rapidly, the oxide shell is not able to increase in thickness and is consequently vaporized by the high radiant heating. This entire process takes place in the vapor phase, with suboxides such as  $AlO$ ,  $Al_2O_2$ , and  $Al_2O$  possibly also occurring, according to Gibbons and Siegel [445]. The liquid  $Al_2O_3$  is then formed during the expansion process in the nozzle when it is condensed from the vapor phase.

The surface combustion process occurs as described by Brown and McCarty [446] and Kurtovich and Pinson [441,442].\* In this process, the aluminum metal coalesces to large droplets on the propellant surface which are then expelled from the surface and have an oxide coating formed around them. After melting, the entire particle assumes a spherical shape because of surface tension and vapor pressure. Continued combustion vaporizes the aluminum inside the shell as the higher pressure inside the shell causes the aluminum to be forced out in a stream of liquid vapor. The  $Al_2O_3$  particles are thus formed by rapid oxidation of the molten aluminum jet coming out of the shell. It is possible, according to Kurtovich and Pinson, that the oxide shell, which is made rigid by the internal pressure caused by the boiling aluminum, will occasionally burst, sending shell fragments out into the exhaust plume. To understand this surface mechanism of combustion satisfactorily, it is necessary, according to Markstein [439], to analyze the absorption of oxygen on the surface of the molten oxide and the transport of oxygen or metal through the oxide layer. Also, it is necessary to consider the reactions which occur at the oxide-gas and at the oxide-aluminum interface as well as those within the oxide layer.

Because most of the  $Al_2O_3$  particles recovered from the exhausts of aluminized motors are small solid spheres of  $\alpha$ -alumina, rather than hollow oxide spheres, it is believed that the vapor phase combustion process of aluminum is the type of combustion process actually occurring in this type of motor. According to Avery [436], when hollow spheres are found in exhausts, such as mentioned by Kurtovich and Pinson, poor combustion occurred (such as at the end of a firing), the radiation heating in the chamber was lower, and the particles were formed by a surface mechanism process. Also, Brown and McCarty [446] and Avery [436] state that if the surface mechanism process were involved, rather than the vapor phase, the size of the  $Al_2O_3$  particles found would be greater than the size of the aluminum particles ( $10 \mu < d_p < 25 \mu$ ) placed in the propellant. This is not the case, as will be seen in the next section.

---

\*Also additional information was obtained from D. D. Kurtovich and G. T. Pinson in an unpublished Boeing report of January 1960, entitled "Radiation Characteristics of Rocket Engine Exhausts."

2. Experimental Determination of  $Al_2O_3$  Particle Sizes and Distributions. The sizes of  $Al_2O_3$  particles collected from rocket exhausts by the majority of investigators are found to have an average particle radius,  $r_p$ , of between 1 and 3  $\mu$ . Some investigators, such as Sehgal [447] and Allport et al. [448], by firing small rockets into tanks, found a definite size dependence on motor chamber pressure. Other investigators, such as Dobbins [449,450] and Dobbins and Jizmagian [451,452] using optical techniques, and Brown and McCarty [446] by passing microscope slides through the plume, did not find such a chamber pressure dependence.

Carlson [5] presents a figure, reproduced here as Figure 37, which shows this mean size (particle diameter) obtained by several investigators as a function of chamber pressure. In most of these experimental tests, the motors used were of a relatively small size having a throat diameter of one inch or less. However, as can be seen from Figure 37, Nack's, Delaney's, and Bartlett's data\* were for one rather large motor ( $d_t = 7.5$  in.) and one very large (120-in. solid) motor ( $d_t = 37.8$  in.), and the particle sizes found were several times higher than those of the smaller motors. Cheung's and Cohen's [453] set of data (for the longer residence time) falls right on Sehgal's curve; however, the short-residence time data shows a much smaller mean particle size. Allport's data, curve 3, which were collected from motors fired into a tank, agree closely with Sehgal's data at low values of chamber pressure and with Brown and McCarty's data at the higher values of chamber pressure. Dobbin's data obtained by light-scattering techniques using Mie theory (discussed in the next section) showed the lowest particle size of all ( $d_p$  about 0.4-0.6  $\mu$ ).

The Air Force Rocket Propulsion Laboratory at Edwards Air Force Base, California, has made considerable measurements recently (some of which are shown in Fig. 37) of particle size from exhausts of 120-, 156-, and 260 inch diameter solid-fueled motors. Smith [459] has found that the mean particle size can be represented best as a function of throat radius for a large range of motor sizes. Figure 38, reproduced from Smith, shows this curve of  $d_{43}$  as a function of  $r_t$  showing a correlation not seen previously (such as in Fig. 37). In Figure 38 the 260-inch motor had a throat radius of 35 inches; the 156-inch motors had throat radii of 30 and 17.5 inches; and the 120-inch motors had throat radii of 18.9 and 12 inches. The particle collection technique

---

\* This information is contained in two 1966 Aerospace Corporation unpublished reports: "Two Phase Flow Phenomena in Rocket Motors" by T. H. Nack and L. J. Delaney, and "Particle Size in Two Phase Nozzle Flow" by R. W. Bartlett and L. J. Delaney. Additional information was received through private communication with Mr. Delaney and the author.

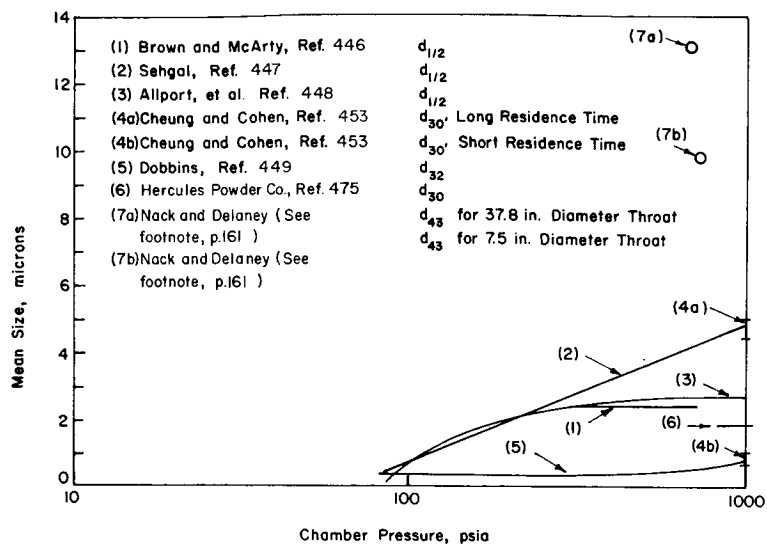


FIGURE 37.  $Al_2O_3$  PARTICLE SIZES DETERMINED FROM DIFFERENT STUDIES

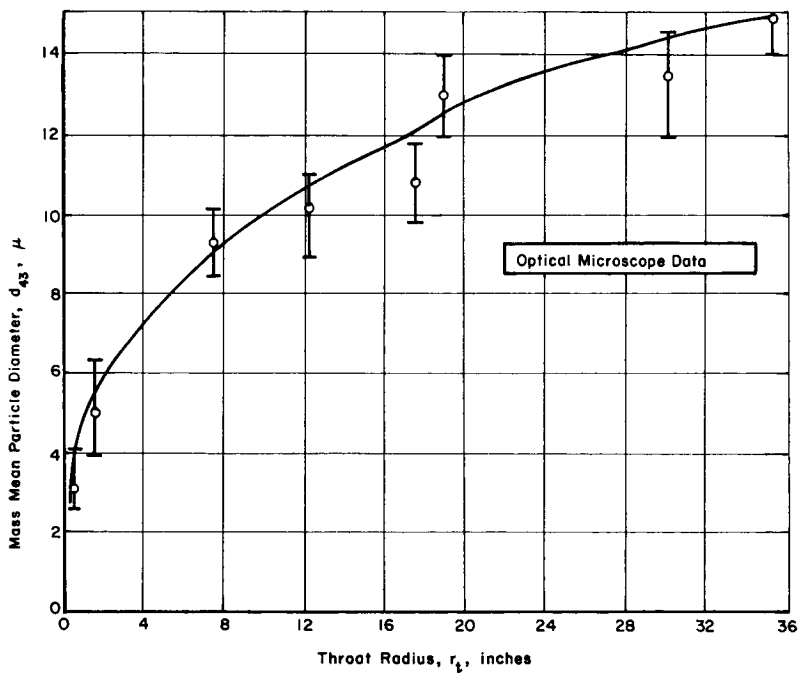


FIGURE 38.  $Al_2O_3$  PARTICLE SIZE VARIATION WITH THROAT RADIUS AS MEASURED BY AFRPL

for the vertically-fired 260- and 156-inch motors was rather unique in that an RB-57 airplane flew into the cloud of the exhaust about 15 to 20 seconds after the end of the firing and collected the particles in a wing-tip pod which had a 10-inch opening for the particles.

Since many of the investigators analyzing particle sizes use various definitions for an average or a mean size, it is necessary to list the various types of sizes (diameters) mentioned in the literature. Carlson [5] presents such a list as follows:

1. Mass median diameter,  $d_{1/2}$ :

$$d_{1/2} = \int_0^{d_{p1/2}} f(d_p) d_p^3 d(d_p) = \frac{1}{2} \int_0^{\infty} f(d_p) d_p^3 d(d_p) \quad (409)$$

2. Mass mean diameter,  $d_{43}$ :

$$d_{43} = \int_0^{\infty} f(d_p) d_p^4 d(d_p) / \int_0^{\infty} f(d_p) d_p^3 d(d_p) \quad (410)$$

3. Mass average diameter,  $d_{30}$ :

$$d_{30} = \left[ \frac{6}{\pi} \int_0^{\infty} f(d_p) d_p^3 d(d_p) / \int_0^{\infty} f(d_p) d(d_p) \right]^{\frac{1}{3}} \quad (411)$$

- and
4. Volume-to-surface diameter,  $d_{32}$ :

$$d_{32} = \int_0^{\infty} f(d_p) d_p^3 d(d_p) / \int_0^{\infty} f(d_p) d_p^2 d(d_p) \quad (412)$$

Some of these values of particle diameter are used in the theoretical determination of  $Al_2O_3$  sizes, as discussed in the next section.

Other investigators not mentioned by Carlson [5] have obtained  $Al_2O_3$  particle sizes similar to those shown in Figure 37. Preckel, Jacobs, and Gibson [455] at Allegany Ballistics Laboratory placed microscope slides in the exhaust, mounted at distances of 15 to 100 feet behind the motor exit.

The mean diameter of the particles collected on the slides in all cases was between 2 and 3  $\mu$ . Optical techniques were also used in which film density measurements were made with a Densicron on the photograph, and transmittances of visible light through the plume at a single wavelength for black-and-white photographs were obtained and at three wavelengths for color photographs. Using the Beer-Lambert equation (discussed in the next section), the optical depth was found to yield a mean particle diameter of about one micron.

Kurtovich and Pinson [441,442]<sup>\*\*</sup> at Boeing obtained  $\text{Al}_2\text{O}_3$  particle samples on glass slides from both 1/20<sup>th</sup> and full-scale Minuteman firings at a chamber pressure of about 760 psia. It was found that two types of particles existed on the slides - hollow micronic particles and solid, submicronic particles. The hollow micronic particles showed a distribution around  $d_p = 4 \mu$ , while the number of solid submicronic particles appeared to increase as the particle size decreased. Measurements at Rohm and Haas<sup>\*\*</sup> showed a mean  $\text{Al}_2\text{O}_3$  particle size of about 2 to 4  $\mu$ ; however, the results were believed to be inconclusive because of the amount of agglomeration and coalescence that resulted. Based upon theoretical specific impulse calculations using various propellants fired at Rhom and Haas, it is believed that the mean particle diameter should have been closer to one micron. Dimmock and Courtney [337] at Thiokol, who collected  $\text{Al}_2\text{O}_3$  particles in rocket exhausts in which the propellant had 8 percent aluminum and where the motor was fired at 750 psia, found the mean particle size to be between 0.1 and 1.0  $\mu$ . Povenelli and Rosenstein [456] obtained a mean particle diameter of about 1.6  $\mu$  in aluminized (9 percent) propellant strand burning tests. Burns [457] inserted a probe in the exhaust of an motor whose propellant had 19 percent aluminum and was fired at 630 psia. He obtained the very large mean diameter of 150  $\mu$ ; however, the particles collected were of a large porous nature, and it was believed that the probe-collecting device was biased in favor of the large particles, because many of the small particles followed the gas-stream lines and did not go into the probe.

---

\*Also additional information was obtained from D. D. Kurtovich and G. T. Pinson in an unpublished Boeing report of January 1960, entitled "Radiation Characteristics of Rocket Engine Exhausts."

\*\*W. A. Wood, private communication to the author, August 1966.

Measurements of  $\text{Al}_2\text{O}_3$  particle size and distribution were obtained at Aeronutronic [344, 345] from the exhaust of a small hydrogen-oxygen engine which was fired with a slurry of  $\text{Al}_2\text{O}_3$  particles dispersed in water. The  $\text{Al}_2\text{O}_3$  particles coming out of the exhaust were collected during the firings by means of a May-Welchman cascade particle analyzer and a shutter probe which was placed about 15 feet from the motor exit. It was found that the distribution of the collected  $\text{Al}_2\text{O}_3$  particles (which had a maximum diameter of about  $10 \mu$ ) agreed quite well with the  $\text{Al}_2\text{O}_3$  particle distribution (analyzed with a Micromerograph) put into the slurry before firing.

At the time of this writing an investigation is underway by Boeing\* performed in an altitude cell at MSFC Test Laboratory to determine  $\text{Al}_2\text{O}_3$  particle sizes in small ( $d_t = 3/4$  in.) solid propellant rocket exhausts. The chamber pressure is rather high (approximately 1500 psia); the expansion ratio of the motors is 8:1; and the amount of aluminum is 14 percent and 20 percent. A particle collector which is pressurized by argon gas to slow the particles down (described by McGregor [458]) is mounted at several axial distances varying from 27 to 43 inches from the exit and also at several radial distances from the axis. The particles impinge on the inside walls of the collector (after passing through an orifice) where they are flushed out with a solvent and analyzed with an optical microscope. It has been determined that the particles are nearly spherical, a result which agrees with most of the investigations mentioned above. To date (three firings) the average particle size (diameter) appears to be about  $5 \mu$ ; however, it is believed that the smallest particles are not being resolved by the optical microscope, so that Micromerograph techniques and possibly electron microscopes will be used in the future to obtain more accurate measurements.

3. Theoretical Determination of  $\text{Al}_2\text{O}_3$  Particle Sizes and Distributions. Various theoretical predictions based upon some of the experimental data mentioned above have been suggested for  $\text{Al}_2\text{O}_3$  sizes and distributions. Many of these have been used in calculations of radiant heating from aluminized rocket exhausts. Perhaps the simplest method used has been to assume that all of the particles are the same size, such as  $r_p = 2 \mu$  as used by Fontenot [459] and Bender and Mullin [460, 461]. A size distribution method based upon the analysis of Kliegel [462] was used by Morizumi and Carpenter [463], Gulrajani [464], Rochelle [465], and Hunt [466] for  $\text{Al}_2\text{O}_3$  particle radiation calculations. This was based on five sizes of particles,  $r_p = 0.79 \mu, 1.28 \mu, 1.76 \mu, 2.44 \mu,$  and  $3.95 \mu$ , each representing 20 percent of the total  $\text{Al}_2\text{O}_3$  particles in the exhaust. This size distribution was based upon Kliegel's [462] fitting the following logarithmic normal particle size distribution based upon Brown and McCarty's [446] data and some unpublished data obtained at TRW Systems:

---

\*M. Baker, private communication to the author, September 1966.

$$\dot{m}_p(d_p)/\dot{m}_p = \left[ (2\pi)^{\frac{1}{2}} d_p \ln \sigma_g \right]^{-1} \exp \left[ -\frac{(\ln d_p - \ln \bar{d}_p)^2}{2 \ln^2 \sigma_g} \right], \quad (413)$$

where  $\bar{d}_p = 3.5 \pm 1.0 \mu$ ,  $\sigma_g = 1.9 \pm 1.0 \mu$ ,  $\dot{m}_p$  is the particle mass flow, and  $\dot{m}_g$  is the gas mass flow.

Crowe and Willoughby [467] performed a theoretical investigation of  $\text{Al}_2\text{O}_3$  particle growth in a solid propellant rocket nozzle by particle collision and coalescence in the nozzle and shock waves of the exhaust plume. This was done in an attempt to explain certain UTC experimental data [448, 468] shown as curve 3 in Figure 37 which shows that particle size increases with chamber pressure up to a certain point, beyond which there is no increase in particle size. Besides chamber pressure effects on particle growth, Crowe and Willoughby [467] looked at effects of nozzle scale, aluminum content, and initial particle size effects on particle growth. The particular model which was used to predict the rate of particle collision per unit time is

$$\dot{N}_{1 \rightarrow 2} = \pi (r_{p_1} + r_{p_2})^2 N_{p_1} \left| v_{p_1} - v_{p_2} \right|, \quad (414)$$

where  $\dot{N}_{1 \rightarrow 2}$  is the number of particles of radius  $r_{p_1}$  which collide with particles of radius  $r_{p_2}$  per unit time,  $v_{p_1}$  and  $v_{p_2}$  are the particle velocities, and  $N_{p_1}$  is the number of particles of radius  $r_{p_1}$  per unit volume.

Nack and Delaney\* discuss a simplified aerodynamic model to predict average particle sizes as a function of propellant composition, nozzle size and contour, and motor operating conditions. They also discuss a mathematical model which describes the gas-particle flow through a nozzle, taking into account both agglomeration and break-up of particles. The four following first order partial differential equations are solved in their analysis: (1) total momentum, (2) particle motion, (3) particle heat transfer, and (4) particle agglomeration. Theoretical calculations for four motors ( $d_t = 2.5$  in., 7.5 in., 9.1 in., and 37.8 in.) show agreement within 10 percent of experimental data.

Fein [469] presented a theoretical model for predicting  $\text{Al}_2\text{O}_3$  particle size distribution in which he found the normalized distribution frequency  $f(V_p)$  to be

\* This information is derived from a 1960 Aerospace Corporation unpublished report by T. H. Nack and L. J. Delaney, entitled "Two Phase Flow Phenomena in Rocket Motors."

$$f(V_p) = \frac{2}{\bar{V}_{p_n}^{1/3} (6 V_p)^{2/3}} \exp \left[ -(6 V_p / \bar{V}_{p_n})^{1/3} \right], \quad (415)$$

where  $V_p$  is the volume of a single particle and  $\bar{V}_{p_n}$  is the number average particle volume. In this analysis Fein assumed the rate of growth of a particle  $dV_p/dt$  to be given by the relation

$$\frac{dV_p}{dt} = \frac{\gamma(C - C_e) A_p (MW)}{\rho}, \quad (416)$$

where  $\rho$ ,  $MW$ ,  $C$ , and  $C_e$  are, respectively, the density of the oxide particle in the condensed phase, molecular weight of the oxide particle, concentration of the oxide particle in the gas phase, and equilibrium concentration of the oxide particle in the gas phase at the chamber temperature and pressure of the oxide particle. Also,  $\gamma$  is the rate of growth constant, and  $A_p$  is the surface area of the particle, assuming that the particle is spherical in shape.

McGregor [458] assumed an  $Al_2O_3$  size distribution based upon the following normalized error function for the  $i^{th}$  particle (fraction of particles of the  $i^{th}$  size):

$$y_i = Ke^{-1/2(r_{p_i} - r_{p_m})^2}, \quad (417)$$

where the mean particle radius  $r_{p_m}$  is a linear function of the motor chamber pressure, as based on Sehgal's [447] chamber-pressure-dependent data as

$$r_{p_m} = 0.862(\ln P_c - 4.17), \quad (418)$$

where the chamber pressure  $P_c$  is in psia and  $r_{p_m}$  is measured in microns. The normalizing constant  $K$  is given by

$$K = \frac{1}{\sum_{i=1}^n \exp \left[ -1/2 (r_{p_i} - r_{p_m})^2 \right]} \quad (419)$$

Dobbins [449-452; 470-472] describes optical measurements using light scattering (Mie theory) calculations to obtain the particle size distribution (curve 5 in Fig. 37). The optical transmission of small rocket plumes was measured at two wavelengths, 0.365 and 1.01  $\mu$ , two spectral regions in which there was no H<sub>2</sub>O emission and absorption. For a polydispersion of spherical particles, the transmission expression may be written as the Beer-Lambert equation (9) as

$$\begin{aligned} I &= I_o e^{-\tau} = I_o \exp(-\sigma_t N_p \ell) \\ &= I_o \exp \left\{ - \left[ \int_0^{\infty} \bar{Q}_t(d_p) f(d_p) \frac{\pi d_p^2}{4} N_p \ell d(d_p) \right] \right\} \end{aligned} \quad (420)$$

where  $f(d_p)$  is a particle size distribution function defined such that

$$\int_{d_{p_1}}^{d_{p_2}} f(d_p) d(d_p) = P(d_{p_1} < d_p < d_{p_2}) \quad (421)$$

$P(d_{p_1} < d_p < d_{p_2})$  is the relative probability of occurrence of particles larger than  $d_{p_1}$  and smaller than  $d_{p_2}$ . A mean extinction efficiency factor,  $\bar{Q}_t$ , may be defined as

$$\bar{Q}_t = \frac{\int_0^{\infty} \bar{Q}_t(d_p) f(d_p) d_p^2 d(d_p)}{\int_0^{\infty} f(d_p) d_p^2 d(d_p)} \quad (422)$$

and, if the particle volume concentration  $c_v$  may be defined in terms of the particle number concentration  $N_p$  as

$$c_v = \frac{\pi}{6} N_p \int_0^{\infty} f(d_p) d_p^3 d(d_p) \quad , \quad (423)$$

and if the volume-to-surface mean diameter  $d_{32}$  is defined as in equation (412), the transmission law, equation (420), may be written as

$$\frac{I}{I_0} = \exp \left( - \frac{3}{2} \frac{\bar{Q}_t c_v \ell}{d_{32}} \right) \quad . \quad (424)$$

From this expression, using Mie theory and measuring the ratio  $I/I_0$  experimentally at the two wavelengths 0.365 and 1.01  $\mu$ , the volume-to-surface mean diameter  $d_{32}$  was calculated and plotted in Figure 37. It is known that other investigators such as those at United Technology Center\* have also made or are planning to make light-scattering measurements and Mie theory calculations to determine  $Al_2O_3$  particle sizes from rocket exhausts.

Holland and Draper [473] present the following  $Al_2O_3$  particle size distribution for a polydisperse cloud of particles:

$$f(d_p) d(d_p) = \frac{\rho}{M_0} \frac{s b^{4/s}}{\Gamma(4/s)} \exp \left[ -b(d_p/d_{p_0})^s \right] \frac{d(d_p)}{d_{p_0}} \quad , \quad (425)$$

where  $d_{p_0}$  is the median volume diameter of the particle,  $M_0$  is the mass of the median volume diameter particle,  $\rho$  is the mass of particles per unit volume, and  $s$  and  $b$  are parameters of the size distribution obtained from standard laboratory measurements of particle size. This size distribution function was used by Holland and Draper to investigate (theoretically and experimentally) the light-scattering effects of talc, carbon black, silicon dioxide, as well as  $Al_2O_3$ , for the LID effect as discussed by Adams and Holland [474].

---

\*W. Lai, private communication with the author, 1965.

This LID effect involves the interaction of plume radiation with particles brought over the solid propellant missile from the rocket exhaust by plume-induced flow separation.

Peterson et al. [475] fitted the following equation for size distribution,  $n(d_p)$  [number of particles whose diameter lies between  $d_p$  and  $d_p + d(d_p)$ ] based upon Brownian motion theory:

$$\frac{n(r_p)}{n_{\text{TOTAL}}} = 0.6 \times 10^{-2} d_p^2 e^{-0.3 d_p^2} \quad (426)$$

This equation, which is similar to Bauer and Carlson's equation discussed in the next paragraph, showed very good agreement with the experimental distribution (see curve 6 in Fig. 37 for mass average diameter).

Bauer and Carlson [413] present the following skew-symmetric equation for  $\text{Al}_2\text{O}_3$  particle size distribution (probability of finding a particle of radius  $r_p$  to  $r_p + dr_p$ ) in a rocket exhaust:

$$f(r_p) = \frac{a^{b+1}}{b!} r_p^b e^{-ar_p} \quad (427)$$

This type of expression was originally derived for size distribution in clouds of water droplets as reported by Bauer [412], Bartky [476], and Deirmendjian [380,381], but has been shown to fit  $\text{Al}_2\text{O}_3$  particle samples collected from rocket exhausts. Based on this distribution function, equation (427), the average particle area for a distribution of sizes may be written, according to Carlson et al. [477], as

$$\bar{A}_p = \frac{\pi \int_0^{\infty} f(r_p) r_p^2 dr_p}{\int_0^{\infty} f(r_p) dr_p} = \pi \frac{(b+1)(b+2)}{a^2} \quad (428)$$

and the average particle volume for a distribution of sizes may be written as

$$\bar{V}_p = \frac{\frac{4}{3} \pi \int_0^{\infty} f(r_p) r_p^2 dr_p}{\int_0^{\infty} f(r_p) dr_p} = \frac{4}{3} \pi \frac{(b+1)(b+2)(b+3)}{a^3}. \quad (429)$$

Bauer and Carlson [413] curve fitted equation (427) to the data of Brown and McCarty [446] and Sehgal [447], obtaining values of  $a$  and  $b$ , using Mie theory, and computed the corresponding scattering and absorption cross-sections for several  $\text{Al}_2\text{O}_3$  particle distributions. Carlson [477], using equation (427), calculated the size distribution function for the S-II ullage rocket using  $a = 1.895$  and  $b = 1.269$  as shown in Figure 39. In the analysis of particle radiation heating from Saturn ullage and retro motors (See subsection following, entitled "Radiation Calculations for Aluminized Solid Propellant Rocket Exhausts.") equation (427) was used to compute the absorption and scattering cross-sections and emissivities (discussed in the next section).

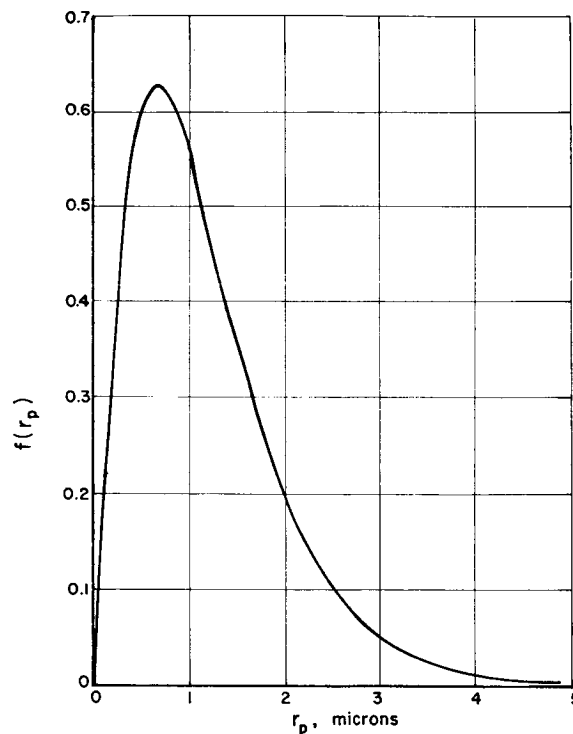


FIGURE 39. PARTICLE SIZE DISTRIBUTION FOR SATURN S-II ULLAGE ROCKET

## Determination of Al<sub>2</sub>O<sub>3</sub> Particle Cloud Emissivity

An accurate prediction of the emissivity of the Al<sub>2</sub>O<sub>3</sub> particle cloud in an aluminized rocket exhaust depends upon the absorption and scattering cross-sections, which depend on the index of refraction of the Al<sub>2</sub>O<sub>3</sub> particles as discussed in the section on Mie theory of scattering, and upon the particular size distribution of particles as discussed in the following section. However, this cloud emissivity is also a function of optical thickness,  $\tau$ , of the plume and the type of particle scattering involved (isotropic or anisotropic, single or multiple). In this section emissivity expressions for optically thick and thin particle clouds with various types of scattering are discussed. Three general methods for predicting Al<sub>2</sub>O<sub>3</sub> particle cloud emissivity are given: (1) inverse wavelength method, (2) neutron-scattering analogy method, and (3) one-dimensional beam approximation method. These methods are described in order of increasing complexity (and accuracy) and decreasing value of radiant heating predicted.

1. Inverse Wavelength Method. This method, which was developed by Fontenot [459] at Boeing as a simple approach to the radiation heating problem, provides a conservative estimate of particle cloud emissivity. A form of equation (298) was used to obtain the particle cloud spectral emissivity as

$$\epsilon_{p\lambda} = 1 - e^{-\kappa\lambda V\ell}, \quad (430)$$

where the absorption coefficient  $\kappa$  is obtained from Schack [277] as  $0.57/\lambda$  and  $V$  represents the volume fraction of Al<sub>2</sub>O<sub>3</sub> particles in the cloud. The total emissivity is obtained as by Sato and Matsumoto [279] from equation (301) with the exception that the quantity  $\chi$  in equation (301) may be expressed as

$$\chi = 0.57 V\ell T_{p_x}/C_2, \quad (431)$$

where  $T_{p_x}$  represents the particle temperature at a distance  $x$  from the nozzle exit. The quantity  $V$  may be expressed in terms of  $M$ , the mass of Al<sub>2</sub>O<sub>3</sub> particles per unit volume, as

$$V = \frac{M}{\rho_p} \left( \frac{r_e}{r_e + y} \right)^2, \quad (432)$$

where  $\rho_p$  represents the density of an  $\text{Al}_2\text{O}_3$  particle and  $y$  represents the quantity  $r - r_e$  where  $r$  is the radial distance from the axis and  $r_e$  is the nozzle exit radius. The quantity  $M$  can be approximated by the expression

$$M = \frac{W_p F}{g A_e I_{sp}^2}, \quad (433)$$

where  $W_p$  represents the weight fraction of particles in the plume,  $F$  is the thrust of the motor,  $I_{sp}$  is the specific impulse, and  $A_e$  is the nozzle exit area.

If equations (430), (301), and (431-433) are combined, the following expression for the total emissivity of an  $\text{Al}_2\text{O}_3$  particle cloud at a distance  $x$  from the nozzle exit may be written:

$$E_{p_x} = 1 - \frac{15\psi''''}{\pi^4} \left[ \frac{13.4 T_p}{\rho_p} \left( \frac{W_p F}{g A_e I_{sp}^2} \right) \frac{r_e^2}{(r_e + y)} + 1 \right]. \quad (434)$$

Although this prediction for particle cloud emissivity is much easier to make than that of the two methods discussed below, it is not believed to be as accurate because only one particle size ( $r_p = 2 \mu$ ) is assumed. Also, the effects of particle scattering are neglected, and it is believed that this inverse wavelength dependence for spectral emissivity is more valid for carbon particles (discussed in the previous section, "Radiation from Carbon Particles") than for  $\text{Al}_2\text{O}_3$  particles.

2. Neutron-Scattering Analogy Method. Morizumi and Carpenter [463] and Morizumi [478] present a method of predicting the apparent surface (hemispherical) emissivity from an  $\text{Al}_2\text{O}_3$  particle cloud whose particles are radiating isotropically, based upon a neutron-scattering analogy. Subsequently, Gulrajani [464] and Hunt [466] produced computer programs based on Morizumi's and Carpenter's [463] equations. The particular surface analyzed by these

investigators was the surface generated by the limiting particle trajectory of the smallest particle ( $r_p = 0.76 \mu$ ) considered. Five particle sizes were considered, corresponding to the size distribution assumed by Kliegel [462] discussed in the previous subsection. The cloud emissivity analysis was based upon the method of successive generations (multiple scattering) of neutrons as discussed by Stuart [479], Stuart and Woodruff [480] and Anthony [481]. In this manner, the neutron blackness,  $\beta(\tau)$ , which is defined as the probability that a neutron incident on a body will be absorbed within it, may be expressed as

$$\beta(\tau) = \left( \frac{\sigma_a}{\sigma_t} \right) \sum_{i=1}^{\infty} \left( \frac{\sigma_s}{\sigma_t} \right)^{j-1} \prod_{i=1}^j P_{i-1,k}(\tau) . \quad (436)$$

If photons in a particle cloud are substituted for the neutrons in the analysis given [479-481], the following expression may be written for the apparent emissivity of a slab or cylinder composed of  $Al_2O_3$  particles:

$$\epsilon_a = \epsilon_p \sum_{j=1}^{\infty} (1 - \epsilon_p)^{j-1} \prod_{i=1}^j P_{i-1,0}(\tau) , \quad (436)$$

where  $P_{i-1,0}$  represents the probability that the radiant heating originating isotropically from an  $Al_2O_3$  particle is reflected by another  $Al_2O_3$  particle within the slab or cylinder after having been reflected  $(i - 1)$  times. According to Morizumi and Carpenter [463], the quantities  $\sigma_a/\sigma_t$  and  $\sigma_s/\sigma_t$  are equivalent to the emissivity and reflectivity,  $\epsilon_p$  and  $1 - \epsilon_p$ , respectively, of an  $Al_2O_3$  particle (assuming the particle is opaque).

Equations for the first, second, and third collision probabilities,  $P_{0,k}$ ,  $P_{1,k}$ , and  $P_{2,k}$ , respectively, have been derived by Morizumi and Carpenter [463]. The first collision probability  $P_{0,k}$  which represents the probability that once-scattered photons escape through the surfaces  $z = 0$  and  $z = \ell$  is

$$P_{0,k} = (k + 1) \int_0^{\ell} N_p \sigma_t \tilde{E}_{k+1}(N_p \sigma_t z) dz , \quad (437)$$

where  $\tilde{E}_{k+1}$  is an integro-exponential function which may be written as

$$\tilde{E}_{k+1}(N_p \sigma_t z) = \int_0^1 \mu^{i-2} e^{-(N_p \sigma_t z)/\mu} d\mu, \quad (438)$$

where  $\mu = \cos \theta$  and  $k$  is a cosine distribution exponent equalling one for isotropic scattering. The second and third probability functions,  $P_{1,k}$  and  $P_{2,k}$ , respectively, are very complex functions of the optical thickness, which was summed over five particle sizes (mentioned in the previous subsection) as

$$\tau = \sum_{n=1}^5 \sigma_{t_n} \int_0^{\ell_n} N_{p_n}(x) dx, \quad (439)$$

where  $N_{p_n}$  is the particle concentration for the  $n^{\text{th}}$  size particle obtained from a two-phase plume program and  $\sigma_{t_n}$  is the total cross-section for the  $n^{\text{th}}$  size particle. Morizumi and Carpenter [463] used  $\sigma_{t_n} = Q_t \pi r_{p_n} = 2\pi r_{p_n}$ , using the asymptotic value of 2 (see Figure 36) for  $Q_t$  for large values of  $\alpha$ .

It may be mentioned that an approximation to the particle concentration,  $N_{p_n}$ , may be written without going to a two phase plume program. This approximation, which was suggested by French [482], is

$$N_{p_n} = \frac{\dot{m}_p}{(4/3) \pi^2 \rho_p v_g} \left( \frac{1}{r_{p_n}^3 K z^2 \theta_{L_n}^2} \right), \quad (440)$$

where  $\theta_{L_n}$  represents the limiting streamline of the  $n^{\text{th}}$  size particle (given as a function of  $r_p^2$  in French's work);  $v_g$  is the gas velocity;  $z$  is the axial distance downstream of the throat;  $K = v_p/v_g$  (where  $v_p$  is the particle velocity);  $\dot{m}_p$  is the particle mass flow; and  $\rho_p$  is the density of an aluminum particle. The quantity  $1 - K$  (velocity lag) was plotted in his work as a function of  $r_p(r_t)^{-1/2} z^{-1/4}$  where  $r_t$  is the throat radius.

To obtain the value of particle emissivity,  $\epsilon_{p_\lambda}$ , which Morizumi and Carpenter [463] designated as  $\sigma_{a_\lambda}/\sigma_{t_\lambda} = Q_{a_\lambda}/Q_{t_\lambda}$ , these investigators extrapolated data of bulk alumina emissivity measurements and plotted their own

emissivity data obtained from rocket exhausts. The apparent emissivity,  $\bar{\epsilon}_a$ , of the  $\text{Al}_2\text{O}_3$  particle plume was calculated from experimental measurements obtained during sub-scale Minuteman engines fired at AEDC, described by Byrd [483] as

$$\bar{\epsilon}_a = \frac{q}{\sigma_B \bar{T}^4} , \quad (441)$$

where  $q$ , the heat transfer rate (per area), was measured with radiometers (narrow-view angle); radiation calorimeters (wide-view angle), and spectrometers (narrow-view angle). The effective plume temperature,  $\bar{T}$ , was calculated as will be discussed in the section immediately following, and the optical thickness,  $\tau$ , was determined from equation (439). The particle emissivity  $\epsilon_p$  was then obtained from the cylinder curves presented by Morizumi and Carpenter [463] in which  $\bar{\epsilon}_a$  was plotted as a function of  $\tau$  for various values of  $\epsilon_p$ . It was found that a value of  $\epsilon_p$  of about 0.25 was valid for both the experimental Minuteman data and also the extrapolated bulk  $\text{Al}_2\text{O}_3$  emissivity data. Morizumi and Carpenter's apparent emissivity curves, which are presented here as Figure 40, can be represented fairly accurately according to French [464] by the following equation:

$$\bar{\epsilon}_a = \epsilon_p^{1/4} \left[ 1 - \exp(-C \epsilon_p^{3/4} \tau) \right] , \quad (442)$$

where  $C = 2/3$  for a cylinder and 2 for a slab.

It is mentioned by Carlson [477] that the ratio  $Q_a/Q_t$  should not be used for the  $\text{Al}_2\text{O}_3$  particle emissivity; instead, merely the absorption efficiency factor  $Q_a$  would be the true particle emissivity as stated by van de Hulst [246] on page 452 of his book. If the ratio  $Q_a/Q_t$  were used for a blackbody ( $\epsilon_p = 1$ ) in which the absorption cross-section,  $\sigma_a$ , would equal the geometric cross-section,  $\pi r_p^2$  ( $Q_a = 1$ ), the quantity  $Q_a/Q_t$  would be less than one since  $Q_s$  (and hence  $Q_t$ ) would be greater than one. Carlson [477] also believes that Morizumi and Carpenter's [463] experimental determination of  $\bar{\epsilon}_a$  is too high since it is based upon the Planck blackbody distribution. In the case of solid propellant exhausts, a number of sources (particles) will exist at different temperatures, and thus a Planckian distribution from such a multi-temperature source will not exist. Also, while the effects of one-dimensional multiple

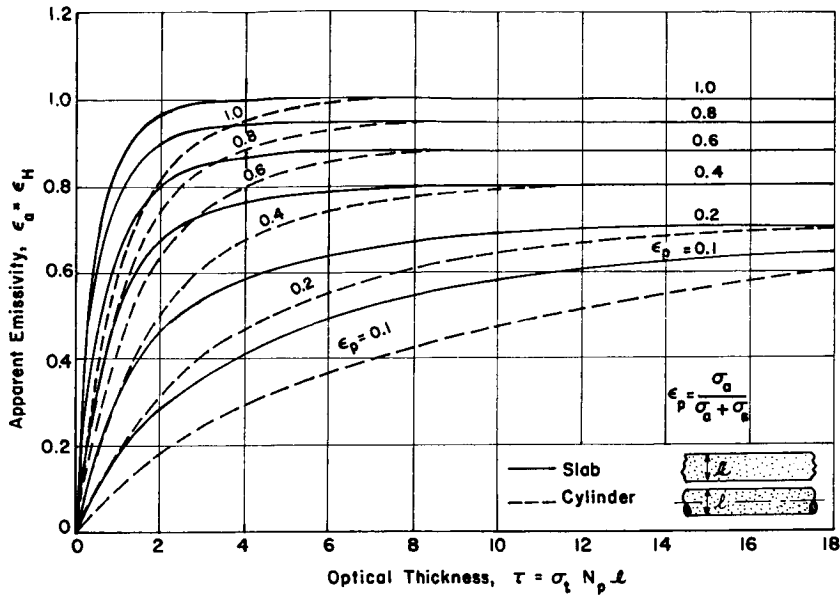


FIGURE 40. APPARENT EMISSIVITY FOR A CLOUD OF PARTICLES IN THE FORM OF A SLAB OR A CYLINDER

scattering are included in Morizumi's and Carpenter's analysis, the effects of anisotropic scattering (important at large values of  $\tau$ ) are not.

3. One-Dimensional Beam Approximation Method. This method is currently being used at Aeronutronic under MSFC contract to analyze particle radiation from the exhausts of Saturn ullage and retro motors and from exhausts of 120-inch strap-on motors for the Saturn improvement study. This analysis involves the study of optically thick plumes (where multiple and anisotropic scattering is important) as well as optically thin plumes in which the radiation from individual particles is summed over an incremental volume. It is generally felt that the plumes of the Saturn ullage and retro motors are optically intermediate (not thin to scattering, but thin to emission and absorption), and that the 120-inch plumes will possibly be optically thick, especially near the exit plane. Carlson [477] specifies the criteria for optical thickness by stating that, if

$$\ell^{(s)} / d_{PL} = \frac{1}{N_p \bar{A}_p d_{PL}} \ll 1, \quad (443)$$

the plume is optically thick for emission (anisotropic scattering centers). If the quantity

$$\ell^{(s)}/d_{PL} = \frac{1}{N_p \bar{A}_p d_{PL}} \gg 1, \quad (444)$$

then the plume is optically thin for scattering (isotropic scattering centers). In these equations the quantity  $\ell^{(s)}$  represents the scattering mean path,  $\bar{A}_p$  is the projected area of a mass-mean particle size, and  $d_p$  is the particle plume diameter.

In general, for an optically thin particle cloud, the cloud emissivity is independent of scattering angle  $\theta$ , the cloud emissivity for isotropic scattering is equal to the cloud emissivity for anisotropic scattering, and the hemispherical emissivity  $\epsilon_H$  is larger than the normal emissivity  $\epsilon_N$ . For an optically thick particle cloud, the cloud emissivity is a function of scattering angle  $\theta$ , the cloud emissivity for an anisotropic particle cloud is greater than that for an isotropic particle cloud, and the hemispherical emissivity  $\epsilon_H$  is less than the normal emissivity  $\epsilon_N$  (except for the one-dimensional case). The above facts may be seen in Figure 41 reproduced from Bartky and Bauer [34], which is discussed later in this section.

The particle emissivity  $\epsilon_p$ , which is equal to  $Q_a$ , for  $Al_2O_3$  particles was determined experimentally as reported by Carlson and du Puis [345], Carlson [344], and Burch and Gryvnak [422,423], all from Aeronutronic, and was found to be very much lower (especially in the solid phase) than the 0.25 value used by Morizumi and Carpenter [463]. The Aeronutronic investigators found that a large change in order of magnitude of  $\epsilon_p$  occurred when the  $Al_2O_3$  sample reached its melting point, as can be seen from Figure 42, which is reproduced from Carlson [344]. Additional measurements by Adams and Colucci [424] have agreed closely with this set of data above the melting point. Carlson [351] suggests several reasons why the  $Al_2O_3$  particle emissivity changes by such a large magnitude upon melting. These reasons include (1) the effect of a polycrystalline structure of the  $Al_2O_3$ , (2) chemical reactions occurring at the surface of the hot particles, (3) the "searchlight effect," and (4) the effects of impurities on the optical properties of the particles.

To determine the  $Al_2O_3$  particle cloud emissivity (hemispherical  $\epsilon_H$  or normal  $\epsilon_N$ ) by the one-dimensional beam approximation, the equation of

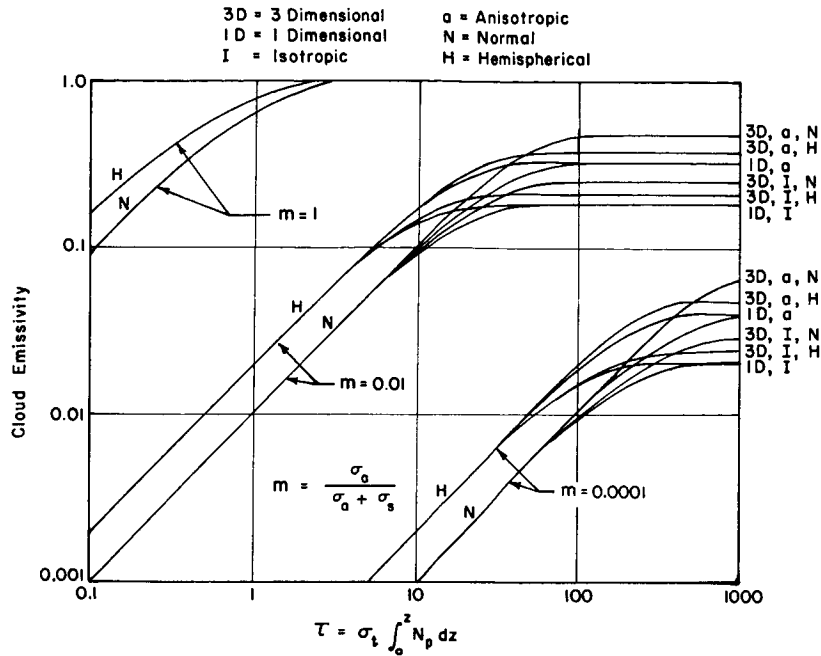


FIGURE 41. NORMAL AND HEMISPHERICAL EMISSIVITY OF PLANAR PARTICLE CLOUDS OF FINITE THICKNESS

transfer (72) for the plane-parallel case must be solved. Equation (72) may be written in the following form, which is consistent with Aeronutronic's notation, as

$$\begin{aligned}
 \mu \frac{dI_\lambda(z, \mu, \phi)}{dz} &= -N_p (\sigma_a + \sigma_s) I_\lambda(z, \mu, \phi) \\
 &+ N_p \frac{\sigma_s}{4\pi} \int_0^{2\pi} \int_{-1}^1 \gamma(\theta) I_\lambda(z, \mu', \phi') d\mu' d\phi' + N_p \sigma_a B_\lambda(T) \quad , \quad (445)
 \end{aligned}$$

if the following substitutions in equation (72) are made:

$$N_p \sigma_a = \kappa_\lambda, \quad N_p \sigma_s = \sigma_\lambda, \quad N_p \sigma_a B_\lambda(T) = j_\lambda, \quad \text{and} \quad \gamma(\theta) = p(\mu, \phi; \mu', \phi'). \quad (446)$$

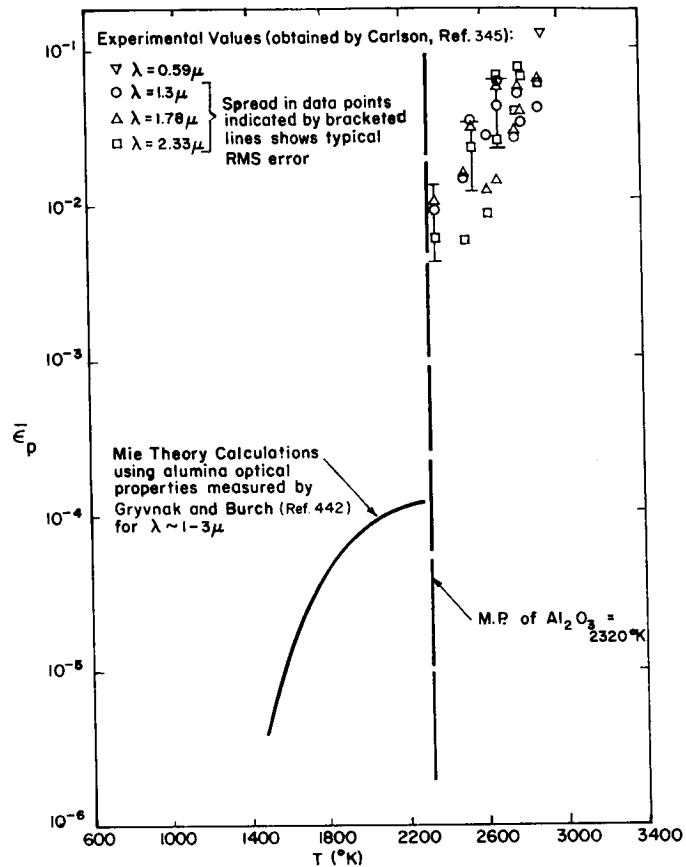


FIGURE 42. SPECTRAL EMISSIVITY OF ALUMINA PARTICLES

In equation (445) the first term on the right is the attenuation (scattering plus absorption) of the radiant beam of intensity  $I_\lambda$ , the second term represents the energy scattered in the direction  $\theta$ , and the third term is the energy emitted by the unit volume under consideration.

In equation (445) the expression  $\gamma(\theta)$  is the angular distribution function sometimes referred to as the differential scattering cross-section for which

$$\int_0^{2\pi} \int_0^\pi \gamma(\theta) \sin\theta \, d\theta \, d\phi = 4\pi \quad (447)$$

and which is defined as

$$\gamma(\theta) = \frac{1}{2} [i_1(\theta) + i_2(\theta)] \quad (448)$$

where  $i_1(\theta)$  and  $i_2(\theta)$  are the intensity functions defined in equation (387). For an isotropic particle cloud, it may be noted that  $\gamma(\theta) = 1$ .

To solve equation (445) for  $I_\lambda$  and consequently obtain the particle cloud emissivity, various approximations may be considered. For a purely absorbing medium ( $\sigma_a \gg \sigma_s$ ), discussed as one of the solutions to the equation of transfer in the first section, subtitle "Solutions to the Equation of Radiation Transfer," part 2, the emissivity as a function of  $\theta$  may be written as in equation (66). For  $\theta = 90^\circ$ ,  $\cos \theta = \mu = 1$ , and an expression may be written for the normal emissivity of the cloud (assumed homogeneous) as

$$\epsilon_N = 1 - e^{-\tau} = 1 - e^{-(\sigma_a N_p z)} \quad (449)$$

The expression for hemispherical emissivity may be found by integrating equation (66) over  $\theta$ , and may be written according to Bartky and Bauer [34] as

$$\epsilon_H = 1 - e^{-\tau} + \tau e^{-\tau} - \tau^2 E_1(\tau) = \epsilon_N + \tau e^{-\tau} - \tau^2 E_1(\tau) \quad (450)$$

where  $E_1(\tau)$  is the exponential integral defined as

$$E_1(\tau) = \int_{\tau}^{\infty} (e^{-x}/x) dx \quad (451)$$

The one-dimensional beam approximation solution (for anisotropic scattering) to equation (72) will now be discussed for the cloud emissivity expressions. The details of the solution will be given in the last part of this section, and the expressions for emissivity, reflectivity, and transmissivity ( $\epsilon$ ,  $\rho$ , and  $t$ , respectively) will be given in this section. A further approximation can be made for the one-dimensional beam method by assuming the intensity scattered in the forward direction ( $\theta = 0$ ) is equal to the intensity scattered in the backward direction ( $\theta = 180^\circ$ ), or

$$\alpha = \frac{1}{2} \int_0^{\pi/2} \gamma(\theta) \sin \theta \, d\theta = \frac{1}{2} = \beta = \frac{1}{2} \int_{\pi/2}^{\pi} \gamma(\theta) \sin \theta \, d\theta \quad (452)$$

where  $\alpha$  represents the fraction of radiation scattered forward and  $\beta = 1 - \alpha$  is the fraction of radiation scattered backward.

In this manner, the cloud emissivity may be written according to Bartky and Bauer [34] and Rossler [484] as

$$\epsilon(\tau) = \tau_{\infty} (1 - e^{-k\tau}) / (1 + \rho_{\infty} e^{-k\tau}) \quad , \quad (453)$$

where

$$\rho_{\infty} = \frac{1 - k}{1 + k} \quad , \quad \epsilon_{\infty} = 1 - \rho_{\infty} \quad (454)$$

and

$$k = (m)^{\frac{1}{2}} = \left( \frac{\sigma_a}{\sigma_a + \sigma_s} \right)^{\frac{1}{2}} \quad . \quad (455)$$

If  $2\tau$  is inserted for  $\tau$  in equation (453), the one-dimensional approximation for the hemispherical emissivity may be written.

For the general anisotropic scattering case, the assumption that  $\beta = \alpha = 0.5$  is not made, and the expressions become much more complex. For this general case Bartky and Bauer [34] present the following equations for  $\rho(\tau)$ ,  $t(\tau)$ , and  $\epsilon(\tau)$  based on the analyses of Mecke [485] and Havard [356]:

$$\rho(\tau) = (k'^2 - m^2) (e^{k'\tau} - e^{-k'\tau}) / D, \quad t(\tau) = 4 mk' / D \quad (456)$$

and

$$\epsilon(\tau) = 1 - \rho - t = 2m \left[ e^{k'\tau}(k' + m) + e^{-k'\tau}(k' - m) - 2k' \right] / D, \quad (457)$$

where

$$D = (k' + m)^2 e^{k'\tau} - (k' - m)^2 e^{-k'\tau} \quad (458)$$

and

$$k' = \left\{ m[2(1 - m)\beta + m] \right\}^{\frac{1}{2}}. \quad (459)$$

For an optically thick medium ( $\tau \rightarrow \infty$ ), the reflectivity reduces to that in equation (454), and the normal emissivity, for various limiting cases, can be written as

$$\epsilon_{\infty} = \frac{2m}{k' + m}, \quad \lim_{m \rightarrow 0} \epsilon_{\infty} = \left( \frac{2m}{\beta} \right)^{\frac{1}{2}}, \quad \text{and} \quad \lim_{\tau \rightarrow 0} \epsilon(\tau) = m\tau. \quad (460)$$

The hemispherical emissivity may be written by replacing  $\tau$  by  $2\tau$ .

For the three-dimensional exact (numerical) case, values of emissivity for isotropic scattering have been given by Bartky and Bauer [34], using values of the Chandrasekhar  $H(\mu)$  function, and for anisotropic scattering have been given by Romanova [486]. Bartky and Bauer plotted these three-dimensional isotropic (for  $\alpha = \beta = \frac{1}{2}$ ) and anisotropic emissivities mentioned above. Both hemispherical and normal emissivities were plotted as a function of the optical thickness for various values of the parameter  $m = \sigma_a/\sigma_t$ . Bartky and Bauer's set of curves is reproduced here as Figure 41. For an optically thin plume ( $\tau \rightarrow 0$ ), Bartky and Bauer presented the limiting case of cloud emissivity for both one- and three-dimensional cases for a semi-infinite medium. These limiting values are, for isotropic scattering,

$$\epsilon_{1D} = 2m^{\frac{1}{2}}, \quad \epsilon_{3D_H} = 2.31 m^{\frac{1}{2}}, \quad \text{and} \quad \epsilon_{3D_N} = 2.91 m^{\frac{1}{2}} \quad (461)$$

and, for anisotropic scattering, using Romanova's [486] data, as

$$\epsilon_{1D} = 3.93 \text{ m}^{\frac{1}{2}}, \quad \epsilon_{3D_H} = 4.8 \text{ m}^{\frac{1}{2}}, \quad \text{and} \quad \epsilon_{3D_N} = 6.6 \text{ m}^{\frac{1}{2}}. \quad (462)$$

It is suggested by Adams and Colucci [424] and Carlson [5] that a representative value of  $m$  for an aluminized rocket exhaust is of the order of 0.005. Based upon this value, Figure 41 shows that the exhaust of an aluminized rocket is not optically thick until  $\tau \approx 100$  and then its emissivity is only about 0.1 - 0.2. Carlson [5] states that BeO has a value of  $m$  of about 0.1; hence, its optically thick plume would have a cloud emissivity at least twice as great as that of an  $\text{Al}_2\text{O}_3$  plume. Figure 41 shows that, when the scattering cross-section  $\sigma_s$  approaches zero, the value of  $m$  approaches one (which is the case for carbon particles), and the optically thick cloud emissivity approaches unity (blackbody emission).

In the above analysis of one-dimensional anisotropic scattering for a particle plume, the effects of multiple scattering were included, but only in a one-dimensional sense. A two- or three-dimensional analysis of multiple scattering is very complex, even though it is felt by Bauer [412] and Goldstein [487] that single scattering is far greater than double scattering, except for very small scattering angles,  $\theta$ . Among the many investigators who have analyzed the effects of two- and three-dimensional multiple scattering (although not necessarily applied to rocket exhausts) are Chin and Churchill [488], Bellman et al. [489,490], Evans, Chu, and Churchill [491], Smart et al. [492], Ueno et al. [41], Twersky [493,494], Grosjean [495], Chu et al. [496], Sekera [497], Mullikin [498], Bauer [499], de Bary and Bullrich [500], Herman and Browning [501], Halpern, Luneberg, and Clark [502], and Richards [503].

In the next section the effective particle temperature, on which the absorption and scattering cross-sections (and consequently the cloud emissivity) are dependent, is derived, and finally, in the last part of this section, the various radiation programs are discussed, as they are based upon particle cloud emissivity and the effective temperature.

## Determination of $\text{Al}_2\text{O}_3$ Particle Cloud Effective Temperature

Since the particle cloud of an aluminized rocket exhaust is a non-isothermal cloud, especially near the exit plane, and has a definite thermal

lag between the gas and particles, it is necessary to determine some effective temperature at each increment in the plume through which the radiation can be analyzed. The particle temperature is a direct function of the radius of the particle, with the large particles experiencing a higher temperature than the smaller particles whose temperature approaches the gas temperature at the same point in the plume. The amount of coupling between the gas and particles is an important factor in determining particle temperatures. If the particle loadings,  $\phi = m_p/m_g$ , are large ( $\phi > 0.4$ ), the flow may be strongly coupled (gas dynamic flow field influenced by particle flow field and vice-versa), especially in the nozzle for small motors and at low altitudes. A case of weaker coupling arises when the particle flow field is influenced by the gas flow field, but not vice versa. A third case of completely uncoupled flow arises if both flow fields are independent of each other. This is the case in a highly under-expanded plume (of low  $\phi$ ) in which the mean free path becomes larger than the diameter of the particles and the particles lose more heat by radiation than by convection to the surrounding gas.

Hoglund [504] presents an excellent review of two-phase (gas-particle) nozzle flow-fields, surveying references through early 1962, and McGregor [458] reviews the effects of two-phase flows, presenting numerous references through the end of 1965. Carlson, Lewis, and Bartky [505] discuss the experimental and theoretical aspects of both near-field (including location of the first Mach disc) and far-field gas-particle flows. The early analyses of two-phase flow such as by Altman and Carter [506] and Gilbert, Davis, and Altman [507] were concerned with effects of the thermal and velocity lags on motor specific impulse. In general, these investigators assumed that the thermal lag was independent of velocity lag, and found that thermal lag had a smaller effect on specific impulse than did velocity lag. Kliegel [462] performed the first one-dimensional nozzle two-phase flow analysis that included both thermal and velocity lags along with the effects of particle lag on the gas properties. Kliegel and Nickerson [508, 509] performed the first two-dimensional (axisymmetric) coupled two-phase flow analysis in nozzles, and later in exhaust plumes. Since the early analyses of two-phase flow, numerous investigators have developed computer programs for both coupled and uncoupled solutions. Some of the many investigators in this area include Crowe et al. [510-512], Bailey et al. [513], Hoffman [514-516], Rannie [517], Simons [518], Hasson [519], Glauz [520], Morganthaler [521], Travis [522], Rudinger [523], Marble [524], Torobin and Gauvin [525], Lype [526], Soo [527, 528], Price et al. [529], Carlson [530, 531], and Carlson and Hoglund [532].

In most of the investigations, the basic equations for particle trajectories and particle temperatures involve the equation of motion for the particle as

$$\frac{d\vec{v}_p}{dt} = \frac{9}{2} K_D \frac{\mu_g}{\rho_p r_p^2} (\vec{v}_g - \vec{v}_p) , \quad (463)$$

and the energy equation for the particle as

$$-\frac{dT_p}{dt} = \frac{\pi r_p^2}{\rho_p C} \frac{\mu_g C_{pg} K_H}{Pr} (T_p - T_g) + \frac{\epsilon \sigma_B T_p^4}{\rho_p C} . \quad (464)$$

In these expressions,  $\mu_g$  is the gas viscosity,  $\vec{v}_p$ , the particle velocity,  $\vec{v}_g$ , the gas velocity,  $\rho_p$  the particle density, and  $C$  and  $C_{pg}$  the specific heats of the particle and gas, respectively. The parameters  $K_D$  and  $K_H$  are the values of the ratio of the actual drag coefficient and Nusselt number, respectively, to the Stokes values. These quantities,  $K_D$  and  $K_H$ , are inserted in the equations to account for Stokes law departures because of compressibility, inertial, or rarefaction effects. An empirical correlation of  $K_D$  is presented by Carlson [530] as

$$K_D = \frac{(1 + 0.15 \text{Re}^{0.687}) [1 + \exp(-0.427/M^{4.63} - 3.0/\text{Re}^{0.88})]}{1 + (M/\text{Re})(3.82 + 1.28 e^{-1.25 \text{Re}/M})} \quad (465)$$

and the quantity  $K_H$  may be expressed as

$$K_H = \frac{1}{2} \left[ \frac{2 + 0.459 \text{Re}^{0.55}}{1 + 3.42(M/\text{Re})(2 + 0.459 \text{Re}^{0.55})} \right] , \quad (466)$$

where  $M$  is the Mach number and  $\text{Re}$  is the Reynolds number.

Kliegel [462] obtained a simplified solution to equations (463) and (464), plus the overall momentum and overall energy equations given by Hoglund [504], by assuming a constant value for the ratio of gas to particle velocities and the ratio of gas to particle temperatures. Another simplified solution to equations (463) and (464), given by Carlson [477], may be obtained by assuming that there is no lag between the gas and particles, and the coupling effects may be accounted for by using an effective isentropic exponent  $\bar{\gamma}$  and an effective molecular weight  $\overline{MW}$  as

$$\bar{\gamma} = \gamma \left[ \frac{1 + \phi(C/C_{p_g})}{1 + \gamma\phi(C/C_{p_g})} \right] \quad \text{and} \quad \overline{MW} = \frac{MW}{1 - \phi} \quad (467)$$

Fontenot [459] made a simplified analysis for the particle temperature (assumed constant across the plume at a distance  $x$  from the nozzle exit) as a function of  $x$  by combining the Stefan-Boltzmann equation with the heat flux relation for the particle cloud, and obtained the following relation:

$$-\frac{dT_{p_x}}{dT_p^4} = \frac{2\pi r_x \sigma_B \epsilon_{p_x}}{\dot{m}_p C} \left[ 1 + \left( \frac{dr_x}{dx} \right)^2 \right]^{\frac{1}{2}} dx, \quad (468)$$

where  $\dot{m}_p$  is the particle mass flow. Solving equation (468) results in the relation

$$\frac{1}{T_{p_x}^3} = \frac{1}{T_{p_e}^3} + \frac{6\pi\sigma_B}{\dot{m}_p C} \int_0^x (r_e + y) \left[ 1 + \left( \frac{dy}{dx} \right)^2 \right]^{\frac{1}{2}} \epsilon_{p_x} dx, \quad (469)$$

where  $\epsilon_{p_x}$  is found from equation (434). The only unknown in equation (469) is thus  $T_{p_e}$  which may be obtained from a two-phase nozzle flow program.

French [482] presented a curve showing the particle temperature lag relation  $(T_{p_n} - T_g)/(T_c - T_g)$  as a function of  $r_p^{\frac{1}{2}}$  based upon data obtained by Kliegel [462] and Carlson [532]. This curve is based upon the assumption that the temperature lag approaches a constant value in the diverging part of the nozzle and remains constant in the rest of the nozzle and in the exhaust plume.

The two-phase nozzle (and plume) program which is used to predict particle temperature,  $T_{p_n}$ , and particle concentration,  $N_{p_n}$ , in Morizumi's and Carpenter's [463] radiation program is Kliegel's [462] method, which assumes five particle sizes (as discussed in the two preceding sections). After the particle temperature,  $T_{p_n}$ , for a particular size particle is determined from the two-phase plume, the average particle plume temperature along a given line of sight through the axis is obtained as

$$\bar{T} = \left[ \eta \frac{\int_{\ell_0}^{\ell_0 + \ell} \sum_{n=1}^5 N_{p_n} r_{p_n}^2 T_{p_n}^4 \frac{dx}{x^2}}{\int_{\ell_0}^{\ell_0 + \ell} \sum_{n=1}^5 N_{p_n} r_{p_n}^2 \frac{dx}{x^2}} \right]^{\frac{1}{4}}, \quad (470)$$

where the correction factor  $\eta$  is found by taking the temperature variation in a lateral plane of view and averaging it over the lines of sight contained in that plane weighted by the lateral variation of the shape factor.

Gulrajani [464] defines an effective particle temperature at any point in the plume as

$$T_{p_{\text{eff}}}^4 = \frac{\sum_{n=1}^5 N_{p_n} r_{p_n}^2 T_{p_n}^4}{\sum_{n=1}^5 N_{p_n} r_{p_n}^2} \quad (471)$$

and divides the plume into segments perpendicular to its axis. Equations (470) and (471) are used by Morizumi and Carpenter [463] and Gulrajani [464], respectively, in their radiation analyses, as discussed in the following section.

The effective plume temperature analysis in the Aeronutronic radiation program (one-dimensional beam approximation) includes a pseudo-two-dimensional routine for the subsonic flow field to the throat and is combined with the Lockheed/Huntsville method-of-characteristics program (at the throat). This program is, in turn, matched with the particle trajectory and thermal

history equations (463, 463, and 467) and particle size distribution equation (427). In this manner, the particle momentum and energy equations (463 and 464) are integrated using a modified Euler technique and a four-point interpolation scheme to determine the gas properties stored in an orthogonal mesh. The gas thermochemical data are obtained from the NASA/Lewis thermochemical programs, discussed by Svehla [533], Zeleznik and Gordon [534], and Gordon and Huff [535].

For an S-II ullage rocket, the particle temperatures computed by this program for 1- $\mu$ , 2- $\mu$ , and 5- $\mu$  radius particles are shown in Figure 43. The super-cooling curve is for the case of the heat of fusion never released and represents an upper limit to the particle temperature. The zero super-cooling curve represents the heat of fusion for liquid particles being released as soon

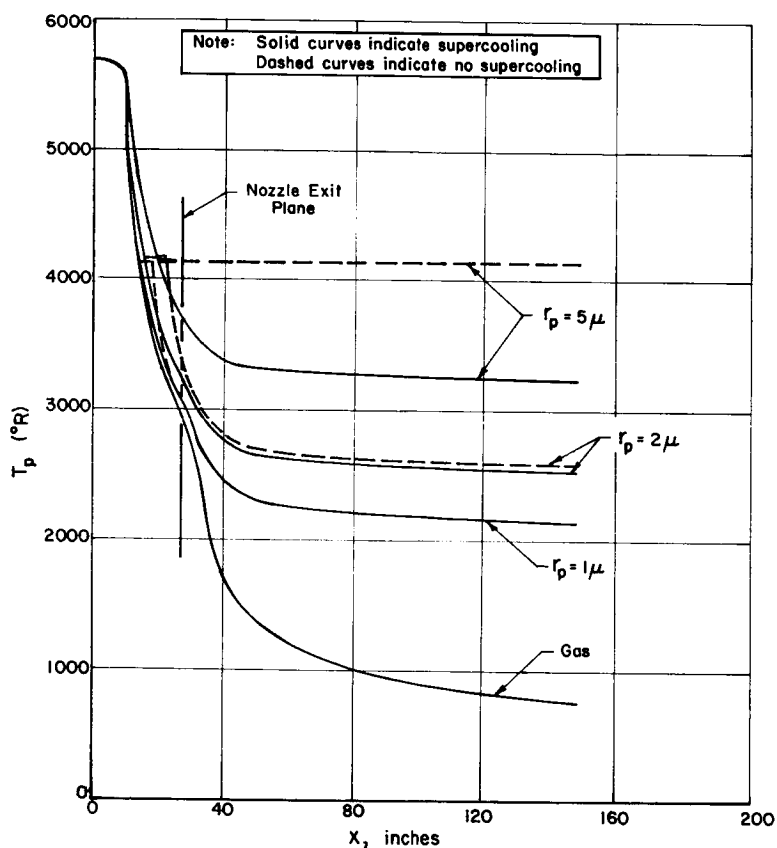


FIGURE 43. TEMPERATURE PROFILES FOR SATURN S-II ULLAGE ROCKET MOTOR AT 175,000 FEET

as possible and represents a lower limit for the particle temperature. Figure 44 shows the limiting particle streamlines (lines outside of which no particles

of a particular size exist) also computed by this Aeronutronic two-phase program for 1- $\mu$ , 2- $\mu$ , and 5- $\mu$  particles superimposed on Mach number contours at an altitude of 130,000 feet. This is the altitude at which the S-II ullage rocket was fired in the J-4 test cell at AEDC in which radiation measurements were obtained (as discussed in the following section).

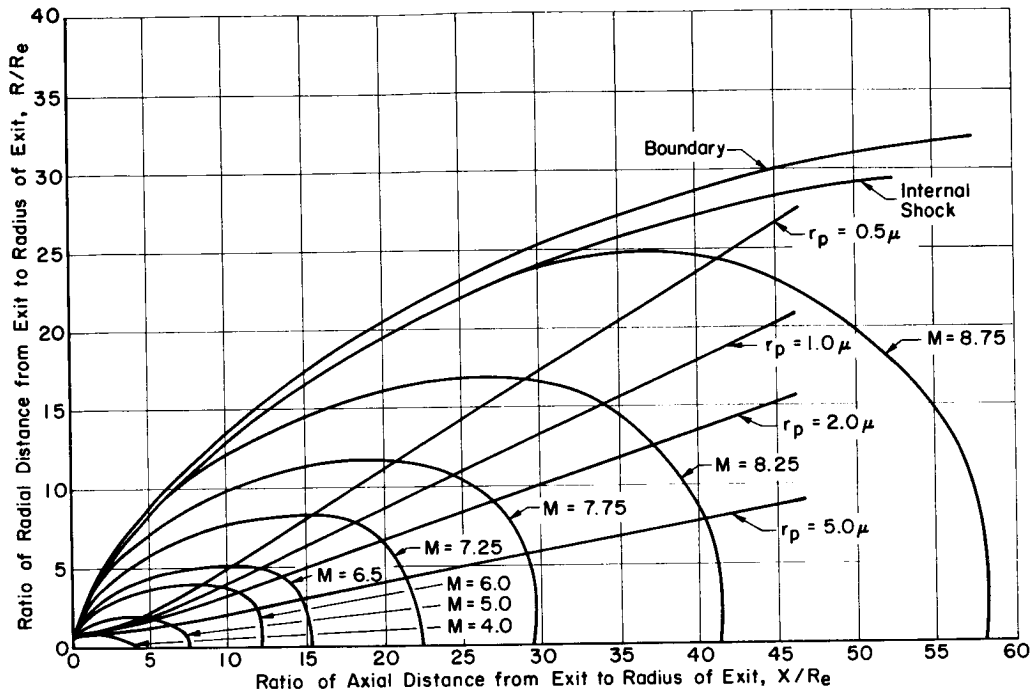


FIGURE 44. S-II ULLAGE ROCKET PLUME AT 130,000 FEET ALTITUDE SHOWING PARTICLE LIMITING STREAMLINES ( $Al_2O_3$ )

The effective temperature used for the radiation calculations in the Aeronutronic program is the temperature which is assumed in each isothermal, homogeneous slab viewed along the line of sight to the particular object on which the radiation is incident. In this manner, the average radiation emitted from a small increment of particle cloud is given by an average absorption cross-section,  $\langle\sigma_a\rangle$ , multiplied by the Planck blackbody function,  $B_\lambda(T_{eff})$  at the calculated effective temperature,  $T_{eff}$ , or

$$\langle\sigma_a\rangle B_\lambda(T_{eff}) = \int_0^\infty \frac{f(r_p) \sigma_a(r_p) B_\lambda[T(r_p)]}{N_p} dr_p, \quad (472)$$

where

$$\langle \sigma_a \rangle = \int_0^{\infty} \frac{f(r_p) \sigma_a(r_p)}{N_p} dr_p, \quad (473)$$

and

$$N_p = \frac{\phi \rho_g / \rho_s}{\frac{4}{3} \pi \int_0^{\infty} f(r_p) r_p^3 dr_p}. \quad (474)$$

In equation (474),  $f(r_p)$  is the size distribution obtained from equation (427),  $\rho_s$  is the alumina bulk density, and  $\rho_g$  is the gas density.

The next section discusses the incorporation of the effective temperature and particle cloud emissivity relations in the radiation calculations as determined by various methods which include the inverse wavelength, neutron scattering analogy, and one-dimensional beam approximation methods, as discussed in the preceding section.

## Radiation Calculations for Aluminized Solid Propellant Rocket Exhausts

Since the advent of large solid propellant missiles (and smaller ullage and retro motors), predictions of radiation heating from the motor exhausts to the surrounding base region (or to other nearby structures and components) have been very difficult to make. Before suitable radiation heating programs were available, reliance was made on crude blackbody or graybody predictions and on scale model and flight data. Some of the early analyses and measurements of radiant heating to the base of solid propellant missiles include, for the Minuteman first stage [536-549], Minuteman second stage [550-554], and Minuteman third stage [555-560], for the Polaris first and second stages [561-566], and for the 120-inch strap-ons to the Titan IIC [567-573].

An early analysis of radiant heating for  $Al_2O_3$  particles using the Mie theory with various mass fractions of  $Al_2O_3$  for particle sizes ranging from

$r_p = 0.5 \mu$  to  $10 \mu$  was performed by Svaton and Winer [357]. The radiant heating equation used was a modification of equation (208) as

$$q/A = \pi \int_{\nu} \int_{\omega} \int_{s} \sigma_t N_p B_{\nu}(T) \exp(-\int \sigma_t N_p ds) \cos \theta ds d\omega d\nu \quad (475)$$

where the quantity  $N_p$  represented the number of particles per unit volume and was given as

$$N_p = 0.2238 \frac{P(\text{MW}) W_p}{\rho_p T d_p} \quad (476)$$

where  $W_p$  is the percentage by weight of the  $\text{Al}_2\text{O}_3$  particles in the plume.

The pressure in Svaton and Winer's [357] analysis was varied from 1-20 atm for a theoretical isobaric plume of four inches in diameter. Radiant intensities (watts/cm<sup>2</sup>μ) were plotted as a function of wavelength for a temperature of 2000° K. The results are not believed to be representative of a practical case because the value of index of refraction of the  $\text{Al}_2\text{O}_3$  particles used was  $n = 1.315 - 0.0143 i$ , taken from Harris [574], a value not in agreement with the results of Carlson [344] and Gryvnak and Burch [422, 423]. Furthermore, Svaton and Winer's [357] analysis was made for an arbitrary temperature of 2000° K, with no suggestions as to the use of an effective temperature or particle size distribution throughout the plume.

Ohrenberger [575] presents another early analysis of particle radiation from an aluminized rocket exhaust plume. His final equation for the radiation from an isothermal cloud for particle size  $n$  to an element of area  $dA$  located at the vertex of the  $n^{\text{th}}$  cone of expansion is

$$q/A = \left(1 + \frac{\rho}{\epsilon} e^{-\tau}\right)^{-1} \sigma_{t_n} B_{\lambda}(T) \int_{\nu} N_{p_n} \left(\vec{n} \cdot \frac{\vec{R}}{R}\right) \exp\left(-\int_{R_c}^R N_{p_n} \sigma_{t_n} dR\right) \frac{dV}{R^2}, \quad (477)$$

where  $\rho$  and  $\epsilon$  are the reflectivity and emissivity, respectively, of the particle cloud,  $\sigma_{t_n}$  is the total cross-section of the  $n^{\text{th}}$  size particle, and  $R_c$  is the distance from  $dA$  to the edge of the cloud. The quantity

$$\left( \vec{n} \cdot \frac{\vec{R}}{R} \right) \frac{dA}{R^2} = d\omega , \quad (478)$$

where  $d\omega$  is the solid angle subtended by  $dA$  from a point on the particle. The quantity  $\vec{n}$  is the normal to the surface  $dA$  which is located a distance  $R$  from the particle of size  $n$ . Using this method, Ohrenberger was able to show only a limited agreement with experiment as he had to make certain geometrical approximations, along with the assumption of an optically thin particle cloud, in order to make simplified integrations over the volumes considered.

The inverse wavelength method of predicting radiation discussed by Fontenot [459] is based upon the Stefan-Boltzmann law for a particle:

$$q_x/A = F \sigma_B \epsilon_{p_x} T_{p_x}^4 . \quad (479)$$

In predicting radiation heating by this method, the particle total emissivity  $\epsilon_{p_x}$  is calculated by equation (434), and the value of  $T_{p_x}$  is found from equation (469). Calculations have been made using this method by Fontenot [576] and Hunt [577] for Minuteman strap-on motors for the S-IC stage and by Mullin and Bender [460], [461] for Saturn ullage and retro motors. In general, it appears that this method gives higher values of radiative heating than does Morizumi's and Carpenter's [463] method or the Aeronutronic method. As stated previously, Fontenot's [459] method makes the assumptions that the particles are all of the same size, that the particle temperature is constant across radial cuts in the plume, and that the effects of scattering may be neglected.

Morizumi's and Carpenter's [463] neutron-scattering analogy was used to predict radiation heating to the base of the Wing VI second stage scale model and full scale Minuteman vehicle and also predict radiation heating to the Vela Nuclear Detection Satellite [578] from its injection rocket exhaust. The basic equation for radiation heating which these investigators used in their numerical technique was

$$q/A = \sigma_B \sum_{i=1}^m \bar{\epsilon}_{a_i}(\tau_i) \bar{T}_i^4 \Delta F_i , \quad (480)$$

where  $\bar{\epsilon}_{a_i}$  and  $\bar{T}_i$  are, respectively, the mean value of apparent emissivity and effective temperature based on equations (436) and (470) for a particular (the  $i^{\text{th}}$ ) isothermal, homogeneous slab through which the radiation is seen. The shape factors  $\Delta F_i$  from the surface to be analyzed to the slabs in the plume are determined by methods of Morizumi [579, 580].

Other investigators have used modifications of Morizumi's and Carpenter's [463] theory to predict radiation from solid propellant plumes. Gulrajani [464] combined Kliegel's [462] two-phase plume and simplified the radiation analysis by segmenting the plume normal to its axis and calculated heating rates from the sub-scale second stage Minuteman rocket fired at AEDC [483]. He also presented a model which was based on an effective length of the plume equal to  $3 d_e$  for purposes of radiation calculation. Hunt [466] programmed Morizumi's and Carpenter's [463] method and used the two-phase plume program of Simons [518] in an attempt to predict heating rates for the first stage Minuteman motor firings discussed by Hunt [581]. Other more simplified analyses of Morizumi's and Carpenter's [463] program were used by Brower [582] to predict heating to the base of the S-IB stage from the exhausts of Minuteman strap-ons, and by Rochelle [465] to predict radiant heating to the S-IC ordnance disconnect caused by the exhaust of the S-II ullage rockets. French [482] also used a modification of Morizumi's and Carpenter's program for a generalized particle radiation problem based on certain velocity and thermal lag assumptions as discussed in the last section.

It is felt that Morizumi's and Carpenter's method is superior to the other methods above; however, it is believed that the particle emissivity,  $\epsilon_p$ , used is not equivalent to the quantity  $m = \sigma_a/\sigma_t$ , and should not be set equal to a constant value of 0.25, which is felt to be more than an order of magnitude too high. The effects of change of index of refraction with phase state (as discussed in the first part of this section), and consequently change of emissivity with phase state, are not considered in their analysis. Also, the assumption of five particle sizes with each size represented by 20 percent (by weight) of the total  $\text{Al}_2\text{O}_3$  weight fraction is not believed to be as valid as an appropriate size distribution function such as equation (427). Finally, although the effects of one-dimensional multiple scattering are included, the effects of anisotropic scattering, in which the phase function  $\gamma(\theta)$  is not equal to unity are not considered, nor is Mie theory used to calculate the appropriate extinction efficiency factor (a value of  $Q_t = 2$  was assumed).

The particle radiation method developed at Aeronutronic under contract to MSFC's Thermal Environment Branch which is based upon the one-dimensional

beam approximation technique described in the previous section and the effective temperature method mentioned in the preceding part of this section, has been described by Kuby [583, 584]. This method, which is based upon one-dimensional multiple anisotropic scattering with appropriate particle size distribution, is believed to be more accurate than any of the methods discussed previously.

The basis of the one-dimensional beam approximation method as originally developed by Schuster [585], modified by Hamaker [586], Churchill et al. [587], and Rossler [484] and further discussed by Klein [588]\* is the writing of the plane-parallel equation of transfer, equation (445), in terms of a forward component  $I_i$  (for  $0^\circ$  or forward scattering) and a backward component  $J_i$  (for  $180^\circ$  or backward scattering). Equation (445) thus reduces to the following two equations in one dimension:

$$\frac{dI_i}{dz} = -N_{p_i} (\sigma_{a_i} + \beta_i \sigma_{s_i}) I_i + N_{p_i} \beta_i \sigma_{s_i} J_i + N_{p_i} \sigma_{a_i} B(T_{\text{eff}_i}) \quad (481)$$

and

$$-\frac{dJ_i}{dz} = N_{p_i} \beta_i \sigma_{s_i} I_i - N_{p_i} (\sigma_{a_i} + \beta_i \sigma_{s_i}) J_i + N_{p_i} \sigma_{a_i} B(T_{\text{eff}_i}), \quad (482)$$

where  $i$  represents the  $i^{\text{th}}$  slab in the direction of the line of sight which has an effective temperature, particle number density, and size distribution, and  $\beta$  represents the back-scattering fraction obtained from equation (452).

A general solution to this set of equations may be found by using the optical thickness  $\tau_i$  and ratio of absorbing to total cross-sections,  $m = \sigma_a/\sigma_t$ , as

$$I = \frac{A}{2} e^{-k'\tau} \left( \frac{k'}{m} + 1 \right) + \frac{C}{2} e^{k'\tau} \left( \frac{k'}{m} - 1 \right) + B(T_{\text{eff}}) \quad (483)$$

and

$$J = \frac{A}{2} e^{-k'\tau} \left( \frac{k'}{m} - 1 \right) + \frac{C}{2} e^{k'\tau} \left( \frac{k'}{m} + 1 \right) + B(T_{\text{eff}}), \quad (484)$$

\*Additional information was obtained from an Aeronutronic unpublished paper of February 1966, by C. D. Bartky, entitled "The Reflectance of Homogeneous, Plane-Parallel Clouds of Dust and Smoke."

where the quantity  $k'$  is defined in equation (459).

If the radiation passes through  $n$  slabs to a surface or detector where it is measured, there would thus be  $2n$  equations ( $I_1, J_1, \dots, I_n, J_n$ ) with  $2n$  constants ( $A_1, C_1, \dots, A_n, C_n$ ) which have to be determined. At the boundaries of the slabs, a set of continuity equations would be written as

$$I_i(\tau_i) = I_{i+1}(\tau_i) \quad \text{and} \quad J_i(\tau_i) = J_{i+1}(\tau_i) \quad . \quad (485)$$

At the two outer boundaries the intensity in the forward direction  $I(\tau = 0)$  would equal  $I_o$ , which would be zero if viewed across a diameter of the plume (incident intensity at the edge of the plume away from the observer would be zero), and if viewed along the axis of the plume (up the nozzle of the motor), the value of  $I_o$  would be

$$I_o = \epsilon_o B \left( T_{\text{eff}_o} \right) + \rho_o J_o(\tau_o) \quad . \quad (486)$$

The  $180^\circ$  scattered intensity at the outer boundary,  $J(\tau = \tau_n)$ , if viewed along the axis would be input as

$$I_{180} = \epsilon_n B \left( T_{\text{eff}_{n+1}} \right) + \rho_n I_n(\tau_n) \quad (487)$$

Equations (483) and (484) would thus be solved to obtain the constants  $A_1, C_1$ , etc., and the intensity at  $\tau_n$ , the position of the surface or detector (if inside the plume) on which the radiation is incident, would thus be determined. The corresponding heating rate would then be the intensity integrated over wavelength and solid angle.

In considering a simplified solution for the intensity for a three-slab case viewed perpendicular to the plume axis near the nozzle exit, Kuby [583] writes the following equation for the radiant intensity to a detector mounted outside the plume. This equation, which considers the reflections and transmissions for all of the slabs as discussed by Bartky and Bauer [34] and by Harrison [310] is

$$I = \left[ I_2 + I_1(1 - \rho_2) t_2 + I_3(1 - \rho_1) t_1(1 - \rho_2) t_2 \right] \quad (488)$$

$$+ \left[ I_2 \rho_1 t_2 + I_1 \rho_3 t_1(1 - \rho_2) t_2 \right] + \left[ I_3(1 - \rho_1) t_1^2 \rho_2 \rho_3(1 - \rho_2) t_2 + \dots \right] + \left[ \dots \right] .$$

The upper ( $\beta = 0$ ) and lower ( $\beta = 1$ ) bounds for the solution of equations (481) and (482) are described by Kuby [583], as well as the "best estimate" obtained by using the correct expression for  $\beta$  as a function of  $\theta$ . Calculations of particle radiation heating using this method are currently being performed by Aeronutronic under the MSFC contract mentioned previously. These calculations will be made to compare with data obtained from both wide- and narrow-view angle radiation detectors as shown in Figure 45, which shows the layout of instrumentation associated with the S-II ullage rocket tests at AEDC, discussed by Rochelle [6, 589]. Comparisons of this theoretical method will be made with the data obtained at AEDC from the narrow (2 in. x 2 in. at 20 ft) view angle FF-1 radiometer presented in Figure 46, together with the wide view angle ( $120^\circ$ ) radiation calorimeter data obtained on the probe shown in Figure 47. Figure 48 shows the theoretical spectrum ( $H_2O$ ,  $CO_2$  and  $CO$  emission) for the S-II ullage rocket calculated by the method described in the previous section entitled "Gaseous Radiation," subsection "Methods of Predicting Gaseous Radiation from Rocket Exhausts," part 3c, as seen by the FF-1 radiometer in Figure 45.

Comparisons will also be made with data from the same FF-1 radiometer and  $150^\circ$  view angle radiation calorimeters for the Centaur retro tests described by Rochelle [590]. It is expected that comparisons will also be made with data obtained from the S-IB retro scale model tests at Cornell discussed by Rochelle [591] and Hendershot and Dennis [592-594]. Calculations of radiation heating to the stagnation point of copper and Teflon hemispherical-cylindrical probes shown in Figure 49, mounted 20 inches from the exit plane during sea level static firings of the S-II ullage rocket, are also expected to be made using this method. This particular test, described by Rochelle [7] and Datis and Fowler [595] resulted in total heating rates at the stagnation point of the order of 3000 to 3200 Btu/ft<sup>2</sup> sec. Finally, calculations of heating caused by 120-in. strap-on motors are expected to be made to the base of the S-IC and S-IB stages. The 120-inch strap-on configuration for the Saturn V vehicle is shown in Figure 50. It is expected that a base heating experimental program will be performed for this configuration (first stage only) at Cornell Aeronautical Laboratory in the spring of 1967, and a combined base heating/Launch Umbilical Tower impingement heating program will be started at MSFC's Test Laboratory early in 1967.

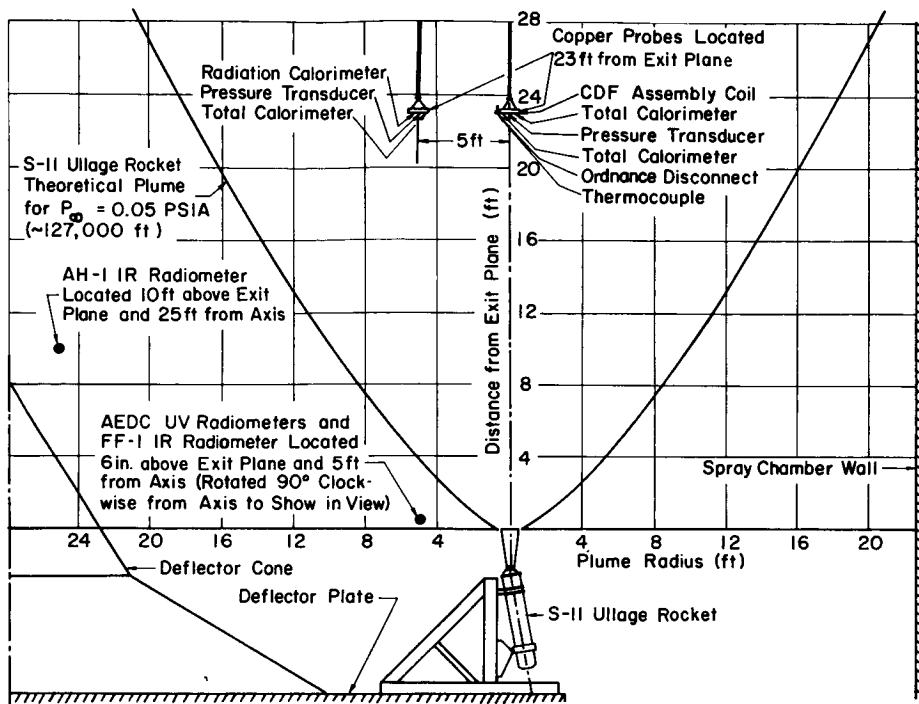


FIGURE 45. SKETCH OF INSIDE OF J-4 TEST CELL SHOWING INSTRUMENTATION LOCATIONS

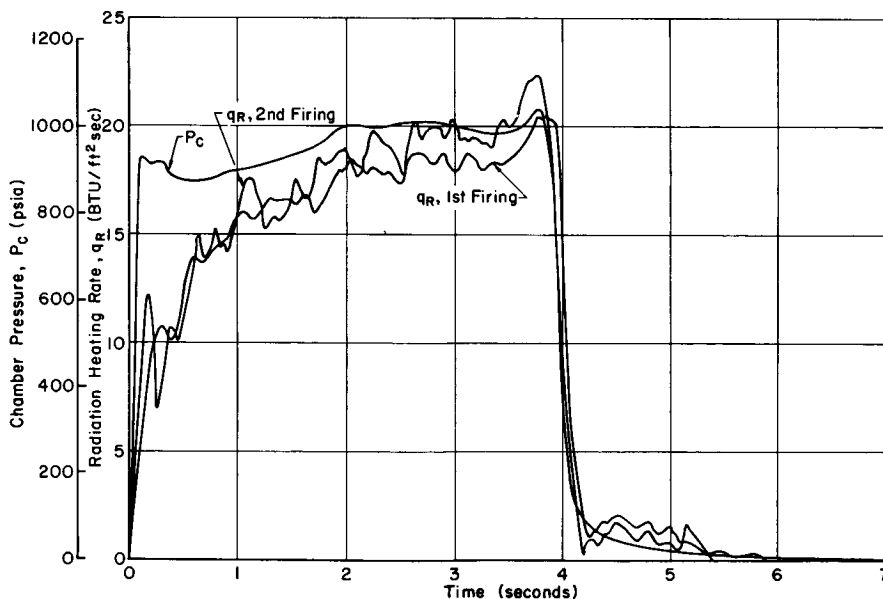


FIGURE 46. RADIATION HEATING RATES FOR S-II ULLAGE ROCKET USING MODEL FF-1 RADIOMETER 6 INCHES FROM EXIT PLANE

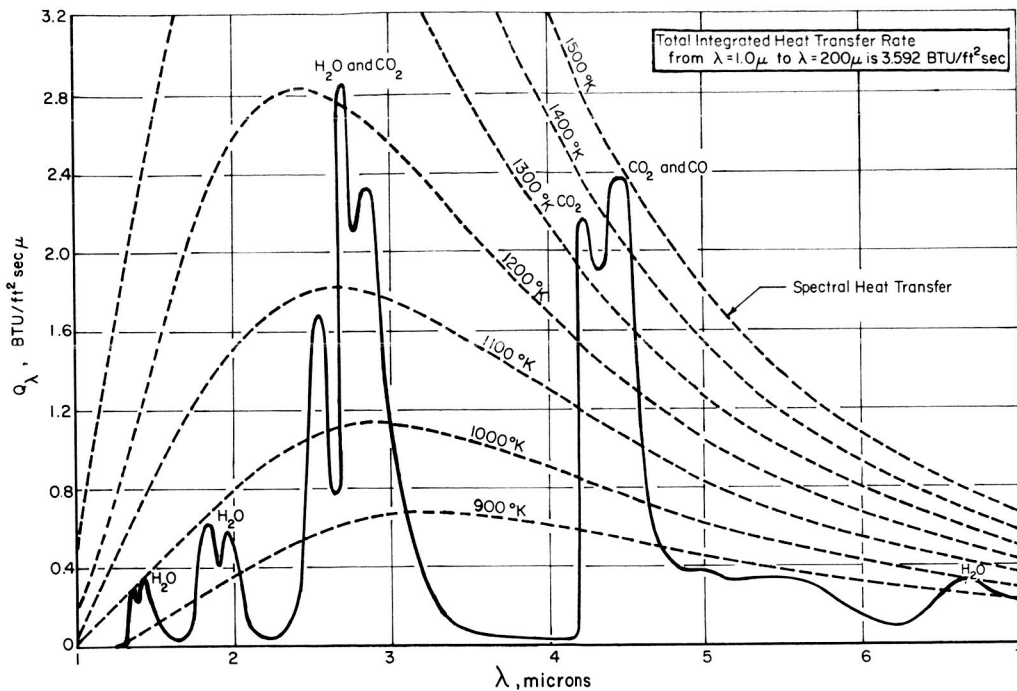


FIGURE 47. S-II ULLAGE ROCKET EXHAUST SPECTRAL HEAT TRANSFER CALCULATIONS AT 120,000 FEET, AT A POSITION 6 INCHES FROM NOZZLE EXIT

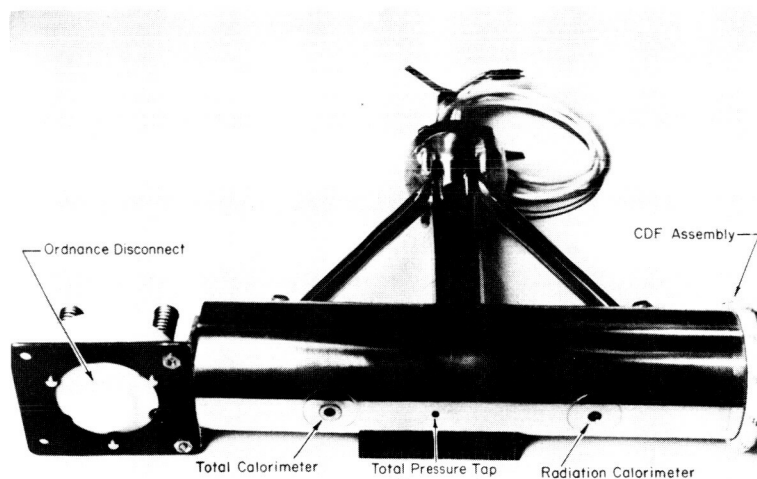


FIGURE 48. HTL COPPER PROBE USED IN AEDC S-II ULLAGE ROCKET TESTS



FIGURE 49. MOUNTING SUPPORT FOR COPPER PROBE USED IN S-II ULLAGE SEA LEVEL TESTS

Besides the radiation analyses of the three major groups (Boeing, TRW, and Aeronutronic) discussed here, it has been recently discovered by the author that another group at Hughes Aircraft has been actively engaged in determining radiation from rocket exhausts which scatter as well as emit and absorb. Edwards and Bobco [596] discuss solutions of the radiation transport equation (51) for an isothermal dispersion which emits, absorbs, and scatters isotropically. Equation (51) is transformed into a second-order differential equation and is solved by using the moment technique to obtain a first-order solution and an iterative procedure to obtain a second-order solution. Bobco [597] describes a closed form solution to obtain directional emissivities from a two-dimensional absorbing and scattering medium. Bobco\* presents an analysis of some of Aeronutronic's alumina measurements and describes calculations of the parameter  $m = \sigma_a / \sigma_t$  for exhausts of the Surveyor main

---

\*R. P. Bobco, "Extinction, Absorption, and Scattering Parameters for Alumina Particles in Exhaust Plumes," Hughes Aircraft Interdepartmental Correspondence, November 22, 1966; also "Some Numerical Results on the Radiant Emission From Particle Exhaust Plumes," Final Report on IR and D Study of Exhaust Plume Radiation, Hughes Aircraft Interdepartmental Correspondence, November 30, 1966.

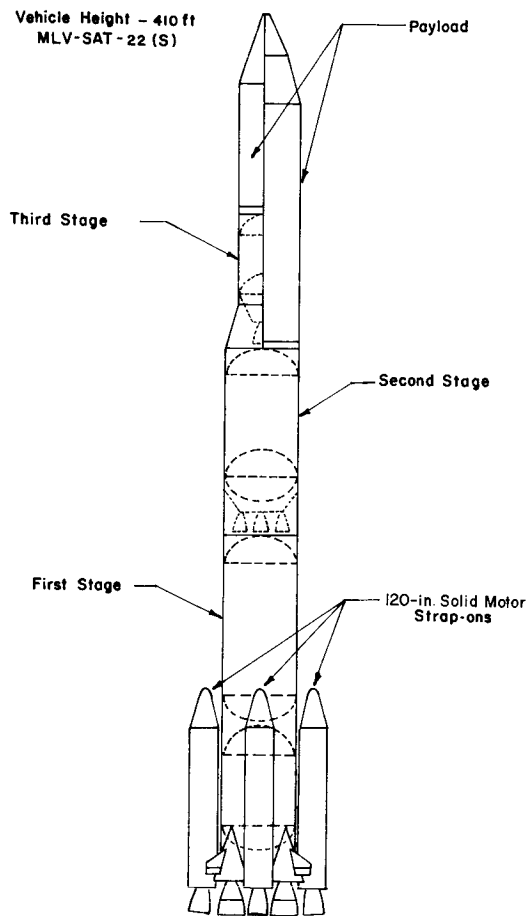


FIGURE 50. PROPOSED SATURN V VEHICLE WITH FOUR 120-INCH STRAP-ONS

Norton Air Force Base, California, on March 15-16, 1967, and the final Aeronutronic report on the NASA contract mentioned previously [599] be consulted.

retro motors engines. Bobco and Edwards [598] describe calculations of directional emissivity from non-uniform axisymmetric dispersions of isotropically scattering particles in which the particle number density,  $N_p$ , is assumed to vary inversely with the square of the distance from the cone vertex.

This concludes the section on radiation from  $Al_2O_3$  particles. It is felt that most of the basic points of radiation from aluminized rocket exhausts were covered. The details of the Mie theory for scattering phenomena, combustion of aluminum to  $Al_2O_3$ , sizes and distributions of  $Al_2O_3$  particles,  $Al_2O_3$  particle cloud emissivities and effective temperatures, and particle radiation programs were discussed. The advantages and disadvantages of several programs of predicting radiation heating from aluminized rocket exhausts were given and it is felt that the one-dimensional beam approximation method of Aeronutronic provides probably the best approach to the particle radiation problem. For additional details and discussion of current problem areas involving particle radiation and 2-phase flow, it is suggested that the proceedings of AFRPL Two-Phase Conference held at

## CONCLUSIONS AND RECOMMENDATIONS

The report has presented a review of the general theory of thermal radiation from liquid and solid propellant rocket exhausts. Discussions of practical programs for predicting gaseous radiation, radiation from carbon particles, and radiation from  $Al_2O_3$  particles were given. The equation of

transfer of radiation for a medium (such as a rocket exhaust) which absorbs, emits, and scatters radiation was derived in detail, and various simplified solutions (such as for a purely absorbing medium or a purely scattering medium) were presented. The gaseous radiation from H<sub>2</sub>O, CO<sub>2</sub> and CO bands in liquid propellant rocket exhausts in which the effects of scattering were neglected was then discussed in detail. Analyses of radiation from an accelerated charge, shape and broadening of spectral lines, band models, and various methods of predicting gaseous radiation from rocket exhausts were then treated. It was concluded that the generalized method with the modified Curtis-Godson approximation, which includes the combined effects of collision and Doppler broadening was best suited for the prediction of gaseous radiation from rocket exhausts. Use is currently being made of the above generalized radiation method by Rocketdyne [266,293] to obtain the radial distribution of temperature, pressure, concentration, and emissivity across various plumes at the nozzle exit. This procedure, termed "zone radiometry," employs the Abel inversion technique and the measured values of transmissivity at the nozzle exit for each zone, together with the calculated values of absorption coefficient as a function of temperature and pressure, to obtain these radial distributions.

Radiation from carbon particles, such as found in the exhausts of H-1 and F-1 engines, was next discussed. It was seen that these carbon particles radiate at near blackbody level, producing a continuous spectrum (except in the regions of atmospheric absorption). One of the main difficulties in analyzing this type of radiation lies in obtaining an accurate mass fraction of carbon present in the exhaust. Recent measurements at Rocketdyne [199,266] have shown that this fraction lies between 0.01 and 0.05 depending upon the position in the plume, the type of hydrocarbon exhaust (gas generator, F-1 engine, etc.) analyzed, and the O/F ratio.

In the section on carbon particle radiation, the formation of carbon particles in luminous flames was discussed, and various theories were presented which suggested possible formation mechanisms for these particles. The determination of carbon particle sizes (an important factor in analyses of scattering by these particles) was discussed briefly, and it was concluded that a mean value for the carbon particle radius, as obtained from luminous flames and both scale model and large (F-1) engine exhausts, could be taken as about 200 Å. The dispersion equation for carbon as it relates to radiation from an oscillating dipole (Rayleigh scattering) was discussed, and equations for the real and imaginary parts of the index of refraction of carbon were developed. The Rayleigh theory of scattering by small particles (such as carbon) in which  $\alpha \ll 1$  was then discussed, various means of predicting carbon absorption

coefficients and emissivities were presented, and subsequently methods of predicting radiation from luminous flames and rocket exhausts were discussed. It was concluded that the experimental methods obtained at General Dynamics/Convair [230,231] were probably the most accurate for predicting carbon absorption coefficients (and consequently radiation), although this method was probably not valid at small wavelengths or for large particle sizes. For these cases the effects of scattering become important, and methods such as used by Stull and Plass [240] and Beheshti [260] should be used to obtain emissivities and radiation. Mention was then made of various means of predicting radiation to the base of the S-I and S-IB stages from the H-1 engine exhausts and to the base of the S-IC from the F-1 engine exhausts as used by MSFC and its associated contractors.

Radiation from  $\text{Al}_2\text{O}_3$  particles, such as those found in the exhausts of solid propellant motors, was then discussed. It was seen that the  $\text{Al}_2\text{O}_3$  particles were larger than the carbon particles and had a lower emissivity, but a higher temperature. Since the  $\text{Al}_2\text{O}_3$  particles are relatively large, scattering effects were seen to be more important than for carbon particles, and the Mie theory of scattering, in which  $\alpha \sim 1$ , was discussed in detail in order to derive expressions for total and scattering cross-sections and efficiency factors. The determination of  $\text{Al}_2\text{O}_3$  particle sizes by various experimental and theoretical methods was then discussed, as well as the combustion of aluminum powder in the propellant to  $\text{Al}_2\text{O}_3$  particles. It was concluded that the  $\text{Al}_2\text{O}_3$  particles were formed by a vapor-phase combustion process, and that the particles were of the general size (radius) of 1 to 3  $\mu$ , although samples obtained from large motors showed sizes larger than this, and particles analyzed by optical techniques showed sizes smaller than this. The particle size distribution equation (427) was concluded to be the best theoretical representation of  $\text{Al}_2\text{O}_3$  particle sizes for use in radiation calculations. Various methods of predicting particle cloud emissivities were presented, and it was believed that the one-dimensional beam approximation method developed at Aeronutronic provided the most realistic analysis. This is because this method considers anisotropic, multiple scattering and uses the most accurate data for  $\text{Al}_2\text{O}_3$  particle emissivity (and consequently index of refraction). A brief discussion of two-phase flow and particle cloud effective temperature was given; it was felt equation (472) should be used for the calculations since it did not depend upon the assumption of five sizes of particles, as did equation (470). Discussions of radiant heating calculated by different methods were then given and various sets of experimental data were listed which are currently being compared with the one-dimensional beam method of predicting  $\text{Al}_2\text{O}_3$  particle radiation.

The ultimate objective of all of these radiation programs is a program which will combine the best methods mentioned above into one single program which can be used with any rocket exhaust. Since a solid propellant exhaust would be the most difficult to analyze theoretically, this ideal program would have the  $\text{Al}_2\text{O}_3$  (and possibly  $\text{Fe}_2\text{O}_3$ ) absorption coefficients tabulated as a function of wavelength and temperature just as the current MSFC radiation programs are being adjusted to have the carbon,  $\text{CO}_2$ ,  $\text{CO}$ ,  $\text{H}_2\text{O}$ , and possibly  $\text{HCl}$  absorption coefficients tabulated. In this combined program the graybody continuum emission of  $\text{Al}_2\text{O}_3$  (or  $\text{Fe}_2\text{O}_3$ ) particles and the near blackbody continuum emission of carbon particles would be superimposed on the bands of the gaseous species whose radiation would be computed by the generalized method with modified Curtis-Godson approximation (with combined collision and Doppler broadening). This is the method currently being used in an attempt to predict radiation heating to the copper and Teflon probes which were immersed in an S-II ullage rocket exhaust 20 inches from the nozzle exit, as discussed by Rochelle [6] and Datis and Fowler [595]. In this particular case, radiation from behind the bow shock in front of the probes will possibly contribute a sizable amount of the total heating and because of the higher temperatures ( $\sim 5500^\circ \text{R}$ ) in this region, absorption coefficients from ionized species might have to be investigated.

Most of the radiation processes discussed in this report have generally been of the equilibrium type, and the temperatures of all of the gaseous species have been assumed to be equal in the same point in the plume. In the afterburning mantle of a plume (especially the plume of a hydrocarbon-fueled engine) where chemiluminescence occurs, it is known that radiation from molecules such as  $\text{OH}$ ,  $\text{CH}$ , and  $\text{C}_2$  may be of the nonequilibrium type (i. e., radiation is emitted when these molecules are in an excited state and the corresponding temperature is higher than the Planck blackbody temperature). Recent studies at Rocketdyne [266] have determined that in the afterburning mantle an effective rotational temperature for  $\text{OH}$  at  $3064 \text{ \AA}$  was about  $8100^\circ \text{R}$  (over  $3000^\circ \text{R}$  higher than  $\text{CO}_2$  gas temperature measured at the same point) and the effective rotational temperature for  $\text{CH}$  at  $4312 \text{ \AA}$  was about  $5400^\circ \text{R}$  (over  $1000^\circ \text{R}$  higher than the  $\text{CO}_2$  gas temperature). It is thus felt that these nonequilibrium effects, including determination of effective vibrational and electronic temperatures, should be investigated further in order to extend the limits of the current radiation programs. Since the next generation in liquid propulsion systems will be hydrogen-fluorine engines, consideration should also be given to nonequilibrium (and equilibrium) radiation from the exhausts of these types of engines. Discussions of the rotational fine structure for the  $\text{HF}$  molecule in the  $2.5$  to  $2.8 \mu$  vibrational band have been given by Simmons and Golden [600], Golden [601], Kuipers, Smith, and Nielson [602], Deeds et al. [603], Benedict et al. [604], Mann [605], and Simmons [606, 607].

Further investigations involving solid propellant plumes might include a practical three-dimensional multiple anisotropic scattering analysis for rocket exhaust radiation. This type of analysis might be applicable for radiant heating to the base of the S-IB and S-IC stages caused by the optically thick exhausts of the 120-inch and Minuteman strap-ons. The problems of searchlight emission from the inside of the combustion chamber possibly should be investigated further, both for solid propellant motors and for hydrocarbon-fueled engines. Since the analysis of radiation from  $\text{Al}_2\text{O}_3$  particles is only as accurate as the particle size distribution assumed, it is felt that additional work in particle size analysis is needed, especially with respect to the larger solid propellant motors and for higher chamber pressures (up to 2000 psia). Experimental measurements to determine the complex part,  $n_2$ , of the index of refraction for liquid alumina should be obtained at wavelengths greater than  $2.3 \mu$ , the limit of current experimental data. Also, values of  $n_2$  for  $\text{Fe}_2\text{O}_3$  should be obtained for temperatures up to and beyond its melting point for a wide range of wavelengths (visible out to 8 to  $10 \mu$ ). According to Kuby [608] current optical measurements show that, at  $\lambda = 1 \mu$  and at room temperature, the value of  $n_2$  for  $\text{Fe}_2\text{O}_3$  is about 15 times that of  $\text{Al}_2\text{O}_3$  at the  $\text{Al}_2\text{O}_3$  melting point and over seven orders of magnitude higher than the room temperature value of  $n_2$  for  $\text{Al}_2\text{O}_3$ . Hence, if the  $\text{Fe}_2\text{O}_3$  value of  $n_2$  is found to increase with temperature as does the  $\text{Al}_2\text{O}_3$  value, the  $\text{Fe}_2\text{O}_3$  will be found to be a stronger radiation emitter than  $\text{Al}_2\text{O}_3$ .

The analysis of scaling effects for radiation measurements obtained from plumes of small motors fired in altitude cells, such as those at Cornell, should be investigated in detail in order to make better comparison with full scale test and flight data. Additional measurements in plumes of velocity, pressure, and temperature such as those performed in the UTC 120 motor plume by Lai [609] and in the Minuteman and larger solid motors by McGee [610] and Johnson et al. [611] should be obtained to correlate with theoretical flow fields which are prerequisites for radiation calculations. Radiation measurements using heat transfer probes which have radiation calorimeters mounted on the stagnation line or point and which are immersed directly in the rocket exhaust, such as those described by Rochelle [6] and [589], should continue to be made for additional correlations of experiment with theory. The analysis of radiation behind normal and oblique shocks, especially for solid propellant plumes, should be investigated further, since this could be a major source of radiative heating to an object inside a plume (especially at low altitudes). Also, thorough investigations should be made of radiation effects of intersecting plumes of solid propellant motors (including effects of clustered nozzles, as well as plumes which intersect some distance downstream). Finally, flow fields

from 120-inch and Minuteman strap-on solid propellant motors which intersect H-1 and F-1 liquid propellant plumes should be analyzed thoroughly so that radiation from these composite flow fields can be predicted for the S-IB and S-IC base regions.

In conclusion, it is felt that this memorandum has provided a detailed review of the various theories of predicting radiation from liquid and solid propellant rocket exhausts, describing what is felt to be the most accurate methods for predicting gaseous radiation, radiation from carbon and  $\text{Al}_2\text{O}_3$  particles, and suggesting possible improvements in these general theories and methods.

George C. Marshall Space Flight Center  
National Aeronautical and Space Administration  
Huntsville, Alabama, April 26, 1967

## REFERENCES

1. Farmer, R. C. ; Prozan, R. J. ; McGimsey, L. R. ; and Ratliff, A. W. : Verification of a Mathematical Model Which Represents Large, Liquid Rocket-Engine Exhaust Plumes. AIAA Paper No. 66-650 presented at AIAA Second Propulsion Joint Specialist Conference, June 13-17, 1966.
2. Chu, C. -W. ; Niemann, A. F. ; and Powers, S. A. : An Inviscid Analysis of the Plume Created by Multiple Rocket Engines and a Comparison with Available Schlieren Data. PART I: Calculation of Multiple Rocket Engine Exhaust Plumes by the Method of Characteristics. AIAA Paper No. 66-651 presented at AIAA Second Propulsion Joint Specialist Conference, June 13-17, 1966.
3. D'Attore, L. ; Nowak, G. ; and Thommen, H. U. : PART II: A Finite Difference Method. AIAA Paper No. 66-651 presented at AIAA Second Propulsion Joint Specialist Conference, June 13-17, 1966.
4. Huffaker, R. M. : Radiation from Rocket Exhaust Plumes. PART I: Inhomogeneous Radiant Heat Transfer from H-1, F-1, and J-2 Rocket Exhaust Plumes. AIAA Paper No. 66-652 presented at AIAA Second Propulsion Joint Specialist Conference, June 13-17, 1966.
5. Carlson, D. J. : PART II: Metallized Solid Propellants. AIAA Paper No. 66-652 presented at AIAA Second Propulsion Joint Specialist Conference, June 13-17, 1966.
6. Rochelle, W. C. : Theoretical and Experimental Investigation of Heating from Saturn Solid Propellant Rocket Exhausts. AIAA Paper No. 66-653 presented at AIAA Second Propulsion Joint Specialist Conference, June 13-17, 1966.
7. Hendershot, K. C. : Some Observations on Exhaust Recirculation from Clustered Rocket Nozzles. AIAA Paper No. 66-681 presented at AIAA Second Propulsion Joint Specialist Conference, June 13-17, 1966.
8. Hopson, G. D. ; and McAnelly, W. B. : Rocket Engine Clustering and Vehicle Integration as Influenced by Base Thermal Environments. AIAA Paper No. 66-563 presented at AIAA Second Propulsion Joint Specialist Conference, June 13-17, 1966.

9. Payne, R. G. ; and Jones, I. P. : Summary of Saturn I Base Thermal Environment. AIAA Journal of Spacecraft and Rockets, vol. 3, 1966, p. 489.
10. Wilson, H. B. : A Short-Duration Technique for Simulated Rocket Exhaust and Wind Tunnel Flow and Its Applications to the Study of Scale Effect of Recirculating Flow Fields. Paper presented at 1966 Heat Transfer and Fluid Mechanics Institute, June 22-24, 1966.
11. Wilson, H. B. : A New Technique for Simulating Rocket Engine Flow for Study of Base Heating Problems. AIAA Paper No. 66-760, presented at the AIAA Aerodynamic Testing Conference, September 21-23, 1966.
12. Beheshti, M. ; and Thibodeaux, D. P. : Radiation from the Saturn IB Rocket Plumes. Chrysler Corporation Space Division TN-AP-66-52, November 1965.
13. Robertson, S. J. ; and Usher, H. : Summary of the Theory of Thermal Radiation Through Non-Grey, Non-Isothermal, Non-Isobaric Gas Medium. Heat Technology Laboratory Report, February 10, 1966.
14. Carpenter, R. L. ; Foreman, W. T. ; and Goldstein, J. S. : Optical Background and Radiation Attenuation in the Early Warning Phase. AFCRC-TR-60-244 (ASTIA No. AD 316801), January 1960 (Confidential).
15. Chandrasekhar, S. : Radiative Transfer. Dover Publications, New York, 1960.
16. Chandrasekhar, S. : An Introduction to the Study of Stellar Structure. Dover Publications, New York, 1957.
17. Busbridge, I. W. : The Mathematics of Radiative Transfer. Cambridge University Press, London, 1960.
18. Kourganoff, V. : Basic Methods in Transfer Problems. Oxford University Press, London, 1960.
19. Ambartsumyan, V. A. : Theoretical Astrophysics. Pergamon Press, New York, 1958.

20. Hopf, E.: *Mathematical Problems of Radiative Equilibrium*. Cambridge University Press, London, 1934.
21. Woolly, R. R.; and Stibbs, D. W.: *The Outer Layers of a Star*. Oxford University Press, 1953.
22. Sobolev, V. V.: *A Treatise on Radiative Transfer*. Van Nostrand, Princeton, New Jersey, 1963.
23. Rosseland, S.: *Theoretical Astrophysics*. Oxford University Press, London, 1936.
24. Pai, S. I.: *Radiation Gas Dynamics*. Springer-Verlag, Inc., New York, 1966.
25. Goody, R. M.: *Atmospheric Radiation*. Vol. I: *Theoretical Basis*. Oxford University Press, London, 1964.
26. Samuelson, R. E.: *Radiative Transfer in a Cloudy Atmosphere*. NASA TR R-215, April 1965.
27. Viskanta, R.: *Heat Transfer in Thermal Radiation Absorbing and Scattering Media*. Argonne National Laboratory ANL-6170, May 1960.
28. Viskanta, R.: *Heat Transfer by Conduction and Radiation in Absorbing and Scattering Materials*. ASME Paper No. 64-HT-33, 1964.
29. Love, T. J.: *An Investigation of Radiant Heat Transfer in Absorbing, Emitting, and Scattering Media*. Aeronautical Research Laboratories ARL 63-3 (ASTIA No. AD 402072), January 1963.
30. Love, T. J.; and Grosh, R. J.: *Radiation and Heat Transfer in Absorbing, Emitting, and Scattering Media*. ASME Paper 64-HT-28, 1964.
31. Viskanta, R.; and Grosh, R. J.: *Heat Transfer in a Thermal Radiation Absorbing and Scattering Medium*. Part IV of *International Developments in Heat Transfer*, ASME, New York, 1961.
32. Seay, J. A.: *Radiation Heat Transfer Through an Absorbing Medium*. Thesis, Univ. of Oklahoma (ASTIA No. AD 298087), 1963.

33. Brown, H. A.: Notes on the Theory of Scattering in the Atmosphere. University of Chicago LAS-TR-199-44, September 1963.
34. Bartky, C. D.; and Bauer, E.: Predicting the Emittance of a Homogeneous Plume Containing Alumina Particles. Aeronutronic U-3232, August 1965. (Also available in AIAA Journal of Spacecraft and Rockets, Vol. 3, 1966. p. 10).
35. Lai, W.; and Purgalis, P.: Abort System Mission Effects for Saturn (Radiation Heat Transfer from Rocket Exhausts). United Technology Center UTC 2105 PFR, August 1965.
36. deSoto, S.: The Radiation from an Axisymmetric, Real Gas System with a Non-Isothermal Temperature Distribution. Paper presented at the AICHE-ASME Seventh National Heat Transfer Conference, August 9-12, 1964.
37. Goulard, R.: Fundamental Equations of Radiation Gas Dynamics, Purdue School of Aeronautical and Engineering Sciences A & ES 62-4, March 1962.
38. Sampson, D. H.: Radiative Contributions to Energy and Momentum Transport in a Gas. General Electric Missile and Space Division R 62SD14, March 1963.
39. Tellep, D. M.; and Edwards, D. K.: Radiant-Energy Transfer in Gaseous Flows, General Research and Flight Science. Lockheed LMSD-288139, vol. 1, part 1, January 1960.
40. Hansen, C. F.: Radiation from Non-Equilibrium, Molecular Gases. General Motors Defense Research Laboratories TR 62-209A, December 1962.
41. Ueno, S.; et al.: Some Mathematical Aspects of Multiple Scattering in a Finite Inhomogeneous Slab with Anisotropic Scattering. Rand Corporation RM-4595-PR, May 1965.
42. Churchill, S. W.; et al.: Exact Solutions for Anisotropic, Multiple Scattering by Parallel Plane Dispersions. DASA-1257 (ASTIA No. AD 272325), September 1961.

43. Garbuny, M.: Optical Physics. Academic Press, New York, 1965.
44. Brown, E. B.: Modern Optics. Rheinhold Publishing Corporation, New York, 1965.
45. Lengyel, B. A.: Lasers. John Wiley and Sons, New York, 1962.
46. Radiative Hydrodynamics and Heat Transfer as Related to Reentry Vehicles, Kaman Nuclear KN-684-64-12 (ASTIA No. AD 444092), July 15, 1964.
47. Milen, E. A.: The Effect of Collisions on Monochromatic Radiative Equilibrium. Monthly Notices of the Royal Astronomical Society, vol. 88, 1928, p. 493.
48. Churchill, S. W.; et al.: The Effect of Anisotropic Scattering on Radiative Transfer. DASA-1184 (ASTIA No. AD 243377), March 1960.
49. Chu, C. -M.; and Churchill, S. W.: Representation of the Angular Distribution of Radiation Scattered by a Spherical Particle. Journal of the Optical Society of America, vol. 45, 1955, p. 958.
50. Yossa, R.: Infrared Spectral Absorption Coefficients. Brown Engineering Company Technical Memorandum AA-10-64-1, March 26, 1965.
51. Huffaker, R. M.: Current Research on Infrared Radiation from Rocket Exhausts. Paper presented at Symposium on Interdisciplinary Aspects of Radiant Energy Transfer, February 24-26, 1966.
52. Ferriso, C. C.; et al.: Study on Exhaust Plume Radiation Predictions. Parts I and II of Interim Progress Report. General Dynamics/Convair GD/C-DBE-66-001, January 1966 and GD/C-DBE-66-001a, February 1966.
53. Thompson, J. A.: Radiative Transfer in Rocket Exhaust Gases. Eighth Symposium (International) on Combustion. Williams and Wilkins Company, Baltimore, 1962.
54. Simmons, F. S.: Spectroscopic Pyrometry of Gases, Flames, and Plasmas. Instrument Society of America Transactions; vol. 2, 1963, p. 168.

55. Ritland, H. N.; Capioux, R.; and Meyerott, R. E.: Radiation Emission Processes in Rocket Plumes. Lockheed LMSC-B007317, December 1962 (Secret).
56. Jackson, J. D.: Classical Electrodynamics. John Wiley and Sons, New York, 1962.
57. Panofsky, W. K.; and Phillips, M.: Classical Electricity and Magnetism. Addison-Wesley Publishing Company, Reading, Massachusetts, 1962.
58. Heitler, W.: The Quantum Theory of Radiation. Oxford University Press, London, 1954.
59. Reitz, J. R.; and Milford, F. J.: Foundations of Electromagnetic Theory. Addison-Wesley Publishing Company, Reading, Massachusetts, 1960.
60. Marion, J. B.: Classical Electromagnetic Radiation. Academic Press, New York, 1965.
61. Sommerfeld, A.: Electrodynamics. Academic Press, New York, 1952.
62. Herzberg, G.: Infrared and Raman Structure of Polyatomic Molecules. D. Van Nostrand Company, New York, 1945.
63. Herzberg, G.: Atomic Spectra and Atomic Structure. Dover Publications, New York, 1944.
64. Herzberg, G.: Spectra of Diatomic Molecules. D. Van Nostrand Company, New York, 1950.
65. Penner, S. S.: Quantitative Molecular Spectroscopy and Gas Emissivities. Addison-Wesley Publishing Company, Reading Massachusetts, 1959.
66. Griem, H. R.: Plasma Spectroscopy. McGraw-Hill Book Company, New York, 1964.
67. Bauman, R. P.: Absorption Spectroscopy. John Wiley and Sons, New York, 1962.
68. Barrow, G. M.: Molecular Spectroscopy. McGraw-Hill Book Company, New York, 1962.

69. Bond, J. W.; Watson, K. M.; and Welch, J. A.: Atomic Theory of Gas Dynamics. Addison-Wesley, Reading, Massachusetts, 1965.
70. Harrison, G. R.; Lord, R. C.; and Loofbourow, J. R.: Practical Spectroscopy. Prentice-Hall, New York, 1948.
71. Baker, H. D.; Ryder, E. A.; and Baker, N. H.: Temperature Measurement in Engineering. Vol. II. John Wiley and Sons, New York, 1961.
72. Marganeau, H.: Pressure Shift and Broadening of Spectral Lines. Physical Review, vol. 40, 1932, p. 387.
73. Marganeau, H.: Pressure Broadening of Spectral Lines, II. Physical Review, vol. 43, 1933, p. 129.
74. Marganeau, H.; and Watson, W. W.: Pressure Effects on Spectral Lines. Reviews of Modern Physics, vol. 8, 1936, p. 22.
75. Marganeau, H.; and Lewis, M.: Structure of Spectral Lines from Plasmas. Reviews of Modern Physics, vol. 31, 1959, p. 569.
76. Ch'en, S. Y.; and Takeo, M.: Broadening and Shift of Spectral Lines Due to the Presence of Foreign Gases. Reviews of Modern Physics, vol. 29, 1957, p. 20.
77. Breene, R. G.: Line Shape. Reviews of Modern Physics, vol. 29, 1957, p. 94.
78. Breene, R. G.: The Shift and Shape of Spectral Lines. Pergamon Press, New York, 1961.
79. Aller, L. H.: Astrophysics. The Atmospheres of the Sun and Stars. Ronald Press Company, New York, 1963.
80. Thompson, H. W.: Advances in Spectroscopy. Vol. II. Interscience Publishers, New York, 1961.
81. Mitchell, A. C.; and Zemansky, M. W.: Resonance Radiation and Excited Atoms. The MacMillan Company, New York, 1934.
82. Seshadri, K. S.; and Jones, R. N.: The Shapes and Intensities of Infrared Absorption Bands - A Review. Spectrochimica Acta, vol. 19, 1963, p. 1013.

83. Benedict, W. S.; et al.: The Strengths, Widths, and Shapes of Infrared Lines, I - General Consideration. Canadian Journal of Physics, vol. 34, 1956, p. 830.
84. Robertson, S. J.; Datis, A.; and Yen, H. Y.: Determination of Velocities in a Turbulent Gas Stream by Measuring Optical Doppler Shift and Broadening of a Monochromatic Light Beam. Heat Technology Laboratory HTL-TM-67, September 25, 1965.
85. Foreman, J. W.; George, E. W.; and Jetton, J. L.: Gas Velocity Measurement Using Scattering Techniques. Brown Engineering Company Technical Note R-178, January 1966.
86. James, R. N.; Seifert, H. S.; and Babcock, W. R.: A Laser-Doppler Technique for the Measurement of Particle Velocity in a Gas-Particle Two-Phase Flow. AIAA Paper No. 66-522 presented at AIAA Fourth Aerospace Sciences Meeting, June 27-29, 1966. (Also available as AFRPL-TR-66-119, June 1966.)
87. Lorentz, H. A.: Proceedings of the Academy of Science of Amsterdam, vol. 18, 1915, p. 134.
88. Stark, J.: Elektrische Spektralanalyse Chemischer Atome. Hirzel, Leipzig, 1914.
89. Holtsmark, J.: Annalen der Physik, vol. 4, 1919, pp. 58 and 577.
90. Jamieson, J. A.; et al.: Infrared Physics and Engineering. McGraw-Hill Book Company, New York, 1963.
91. Plass, G. N.: Useful Representations for Measurements of Spectral Band Absorption. Journal of the Optical Society of America, vol. 50, 1960, p. 9.
92. Plass, G. N.: Spectral Band Absorptance of Radiation Traversing Two or More Cells in Series. Applied Optics, vol. 4, 1965, p. 69.
93. Plass, G. N.: The Influence of Numerous Low-Intensity Spectral Lines on Band Absorptance. Applied Optics, vol. 3, 1964, p. 859.
94. Plass, G. N.: Models for Spectral Band Absorption. Journal of the Optical Society of America, vol. 48, 1958, p. 690.

95. Plass, G. N.: The Theory of the Absorption of Flame Radiation by Molecular Bands. *Applied Optics*, vol. 4, 1965, p. 161.
96. Plass, G. N.: Spectral Emissivity of Carbon Dioxide from 1800-2500  $\text{cm}^{-1}$ . *Journal of the Optical Society of America*, vol. 49, 1959, p. 821.
97. Oppenheim, U. P.; and Ben-Aryeh, Y.: A General Method for the Use of Band Models, with Applications to Infrared Atmospheric Absorption. *Journal of Quantitative Spectroscopy and Radiative Transfer*, vol. 4, 1964, p. 559.
98. Oppenheim, U. P.; and Ben-Aryeh, Y.: Statistical Model Applied to the Region of the  $\nu_3$  Fundamental of  $\text{CO}_2$  at 1200° K. *Journal of the Optical Society of America*, vol. 53, 1963, p. 344.
99. Kaplan, L. D.: Regions of Validity of Various Absorption-Coefficient Approximations. *Journal of Meteorology*, vol. 10, 1953, p. 100.
100. Kaplan, L. D.: A Method for Calculation of Infrared Flux for Use in Numerical Models of Atmospheric Motion. Article contained in the *General Circulation of the Atmosphere*. Rockefeller Institute Press, New York, 1959.
101. Simmons, F. S.: An Analytical and Experimental Study of Molecular Radiative Transfer in Non-Isothermal Gases. Tenth Symposium (International) on Combustion. The Combustion Institute, Pittsburgh, 1965.
102. Penzias, G. J.; and Maclay, G. J.: Analysis of High Temperature Gases in Situ by Means of Infrared Band Models. NASA CR-54002, December 1963.
103. Maclay, G. J.; and Brabov, H. H.: Predicting Infrared Absorptances of Hot Gases: Methods and Applications. Warner and Swasey TR-32, June 1964.
104. Green, A. E.; and Wyatt, P. J.: *Atomic and Space Physics*. Addison-Wesley Publishing Company, Reading, Massachusetts, 1965.
105. Wyatt, P. J.; Stull, V. R.; and Plass, G. N.: Quasi-Random Model of Band Absorption. *Journal of the Optical Society of America*. vol. 52, 1962, p. 1209.

106. Wyatt, P. J.; Stull, V. R.; and Plass, G. N.: Infrared Transmission Studies. Vol. II of The Infrared Absorption of Water Vapor. SSD-TDR-62-127, vol. II (ASTIA No. AD 297458), September 1962.
107. Elsasser, W. M.: Heat Transfer by Infrared Radiation in the Atmosphere. Harvard Meteorological Studies, no. 6, Harvard University, 1942.
108. Godson, W. L.: The Computation of Infrared Transmission by Atmospheric Water Vapor. Journal of Meteorology, vol. 12, 1955, p. 272.
109. Greif, R.: Review of Emissivity Calculations for Diatomic Gases. First Quarterly Progress Report (NASA/MSFC Contract No. NAS8-11468), October 13, 1964.
110. Ladenberg, R.; and Reiche, F.: Annalen der Physik, vol. 42, 1913, p. 181.
111. Howard, J. N.; Burch, D. E.; and Williams, D.: Infrared Transmission of Synthetic Atmospheres, IV: Application of Theoretical Band Models. Journal of the Optical Society of America, vol. 46, 1956, p. 334.
112. Howard, J. N.; Burch, D. E.; and Williams, D.: Infrared Transmission of Synthetic Atmospheres. Vol. II of Absorption by Carbon Dioxide. Journal of the Optical Society of America, vol. 46, 1956, p. 237.
113. Plass, G. N.; and Fivel, D. I.: Influence of Doppler Effect and Damping on Line-Absorption Coefficient and Atmospheric Radiation Transfer. Astrophysics Journal, vol. 117, 1953, p. 225.
114. Struve, O.; and Elvey, C. T.: The Intensities of Stellar Absorption Lines. Astrophysics Journal, vol. 79, 1934, p. 409.
115. Elsasser, W. M.: Mean Absorption and Equivalent Absorption Coefficient of a Band Spectrum. Physical Review, vol. 54, 1938, p. 126.
116. Mayer, H.: Methods of Opacity Calculations. AECD-1870, LA-647, October 1947.
117. Goody, R. M.: A Statistical Model for Water-Vapor Absorption. Quarterly Journal of the Royal Meteorological Society, vol. 78, 1952, p. 165.

118. Malkmus, W.: Random Lorentz Band Model With Exponential-Tailed  $S^{-1}$  Line Intensity Distribution Function. General Dynamics/Convair GD/C-DBE 65-020, November 1965.
119. Stull, V. R.; and Plass, G. N.: Spectral Emissivity of Hydrogen Chloride from 1000-3400  $\text{cm}^{-1}$ . Journal of the Optical Society of America, vol. 50, 1960, p. 1279.
120. Malkmus, W.; Maclay, G. J.; and Brabov, H. J.: Interpretation of Infrared Spectral Absorptance Measurements and Calculations for HCl. Journal of the Optical Society of America, vol. 54, 1964, p. 422.
121. Heatherly, E. R.; and Dash, M. J.: An Estimate of Radiation Heating Environment on the S-II Stage Thrust Structure and Heat Shield. NASA/MSFC Memorandum R-AERO-AT-64-27, September 9, 1964.
122. Heatherly, E. R.; and Dash, M. J.: A Fortran Program to Calculate An Engineering Estimate of the Thermal Radiation to the Base of a Multi-Engine Space Vehicle at High Altitudes. NASA TM X-53148, October 5, 1964.
123. Hottel, H. C.: Radiant-Heat Transmission. Chapter 4 of Heat Transmission. McGraw-Hill Book Company, New York, 1954.
124. Tien, C. L.; and Abu-Romia, M. M.: A Method of Calculating Rocket Plume Radiation to the Base Region. AIAA Journal of Spacecraft and Rockets, vol. 1, 1964, p. 433.
125. Tien, C. L.; and Abu-Romia, M. M.: Radiative Energy Transfer to Outer Base Regions of Cylindrical and Conical Gas Bodies. University of California Institute of Engineering Research AS-63-4, October 1963.
126. Tien, C. L.; and Abu-Romia, M.M.: Radiative Energy Transfer to the Outer Base Region of a Semi-Infinite Cylindrical Gas Body. AIAA Paper No. 64-60, presented at AIAA Aerospace Sciences Meeting, January 20-22, 1964.
127. Giedt, W. H.; et al.: The Study of Base Heating by Radiation from Exhaust Gases. Final Report (NASA/MSFC Contract No. NAS8-850), October 20, 1964.

128. deSoto, S. ; Suarez-Alfonso, E. ; and Vok, C. A. : Final Report: Radiant Heat Transfer Study. Vol. I of Analytical Program. Rocketdyne R-5371-4, August 26, 1964 (Confidential).
129. deSoto, S. : Quarterly Report: Radiant Heat Transfer Study. Rocketdyne R-5371-1, September 30, 1963.
130. deSoto, S. : Quarterly Report: Radiant Heat Transfer Study. Rocketdyne R-5371-3, March 30, 1964.
131. Eckert, E. R. ; and Drake, R. M. : Heat and Mass Transfer. McGraw-Hill Book Company, New York, 1959.
132. Tien, C. L. ; and Abu-Romia, M. M. : Radiation from Rocket Engine Exhaust Gases. Vol. II: Apparent Emissivities of a Semi-Infinite Cylindrical Gas Body. Seventh Quarterly Report (NASA/MSFC Contract No. NAS8-850), November 1962.
133. Tien, C. L. ; and Abu-Romia, M. M. : Radiation from Rocket Engine Exhaust Gases. Vol. III: Apparent Emissivities of a Conic Gas Body. Eighth Quarterly Progress Report (NASA/MSFC Contract No. NAS8-850), February, 1963.
134. Pivonsky, N. : Tables of Blackbody Radiation Functions. The MacMillan Company, New York, 1961.
135. Howard, J. N. ; Burch, D. E. ; and Williams, D. : Infrared Transmission of Synthetic Atmospheres. Vol. III: Absorption by Water Vapor. Journal of the Optical Society of America, vol. 46, 1956, p. 242.
136. Tien, C. L. ; and Wang, L. S. : On the Calculation of Mean Beam Length for a Radiating Gas. Journal of Quantitative Spectroscopy and Radiative Transfer, 1965.
137. Burch, D. E. ; Singleton, E. B. ; and Williams, D. : Applied Optics. Vol. 1, 1962, p. 359.
138. Rolfe, D. B. : Mean Length Calculations for Radiation from Non-Transparent Gases. Journal of Quantitative Spectroscopy and Radiative Transfer, vol. 1, 1961, p. 169.

139. Dash, M. J.: Thermal Radiative Design Criteria for the S-IVB Stage. NASA/MSFC Memorandum R-AERO-AT-65-20, August 25, 1965.
140. Tarbell, D. W.; and Alligood, B. E.: A Method for Calculating the Radiation Heating Rate to the Base of Large Space Vehicles. Brown Engineering Company Technical Memorandum AA-3-65-5, March 18, 1965.
141. Alligood, B. E.: Program to Calculate Radiative Heat Transfer Utilizing Weak-Line or Exact Absorption Coefficients. Brown Engineering Company Interim Progress Report (NASA/MSFC Contract No. NAS8-20169), November 3, 1965.
142. Krakow, B.; et al.: Use of the Curtis-Godson Approximation in Calculations of Radiant Heating by Inhomogeneous Hot Gases. NASA TM X-53411, March 15, 1966.
143. Krakow, B.: Determination of Hot Gas Temperature Profiles from Infrared Emission and Absorption Spectra. AIAA Paper No. 65-105, presented at AIAA Second Aerospace Sciences Meeting, January 25-27, 1965.
144. Tourin, R. H.; and Krakow, B.: Applicability of Infrared Emission and Absorption Spectra to Determination of Hot Gas Temperature Profiles. Applied Optics. Vol. 4, 1965, p. 237.
145. Ferriso, C. C.; Ludwig, C. B.; and Abeyta, C. N.: Journal of Quantitative Spectroscopy and Radiative Transfer, vol. 5, 1965, p. 281.
146. Alligood, B. E.: Analysis of Generalized Radiative Heat Transfer from Rocket Exhaust Plumes. Brown Engineering Company Interim Progress Report AAL-14483-2, February 25, 1966.
147. Conway, L.; Yossa, R.; and Alligood, B. E.: Analysis and Computer Program for Determining Gaseous Thermal Radiation. Brown Engineering Company Technical Note R-210, August 1966.
148. Ludwig, C. B.; et al.: Study on Exhaust Plumes Radiation Predictions, Final Report. General Dynamics/Convair Report No. GDC-DBE66-017, December 1966.

149. Herget, W. F.; Muirhead, J. S.; and Golden, S. A.: Band Model Parameters for H<sub>2</sub>O. Rocketdyne Report No. R-6916, January 27, 1967.
150. Prozan, R. J.: Development of a Method-of-Characteristics Solution for Supersonic Flow of an Ideal, Frozen, or Equilibrium Reacting Gas Mixture. Lockheed LMSC/HREC A782535, April 1966.
151. Ratliff, A. W.: Comparisons of Experimental Supersonic Flow Fields with Results Obtained by Using a Method-of-Characteristics Solution. Lockheed LMSC/HREC A782592, April 1966.
152. Simmons, F. S.: The Spectral Emissivity of Dispersed Carbon in Rocket Exhaust Gases. Rocketdyne RR-60-14, June 22, 1960 (Secret).
153. DeBell, A. G.; Simmons, F. S.; and Levin, B. P.: Spectral Radiance and Emissivities of Rocket Exhaust Plumes. Rocketdyne R-3216, December 1961 (Secret).
154. Levin, B. P.; Wagner, W. J.; and Thompson, J. D.: Final Report. Radiant Heat Transfer Study. Vol. II: Experimental Program. Rocketdyne R-5371-4, August 26, 1964 (Secret).
155. Anon.: Spectrometer Study of Rocket Engine Exhausts. Aerojet-General 2090 (Also available as ASD-TDR-62-29), January 1962 (Secret).
156. Wagner, W. J.: Close-Proximity Spectral Radiance Measurements of Missile-Sized Rocket Engine Exhaust Plumes. Rocketdyne R-5843, September 18, 1964 (Secret).
157. Gaydon, A. G.: The Spectroscopy of Flames. Chapman and Hall, London, 1957.
158. Gaydon, A. G.; and Wolfhard, H. G.: Flames. Chapman and Hall, London, 1960.
159. Palmer, H. B.; and Cullis, C. F.: The Formation of Carbon From Gases. Chapter 5 of Chemistry and Physics of Carbon. Marcel Decker, Inc., New York, 1965.
160. Parker, W. G.; and Wolfhard, H. G.: Carbon Formation in Flames. Journal of the Chemistry Society, 1950, p. 2038.

161. Porter, G.: The Mechanism of Carbon Formation. Combustion Researches and Reviews (AGARD Report) Butterworths, London, 1955.
162. Porter, G.: Carbon Formation in the Combustion Wave. Fourth Symposium (International) on Combustion. The Williams and Wilkins Company, Baltimore, 1953.
163. Thomas, A.: Carbon Formation in Flames. Combustion and Flames, vol. 6, 1962, p. 46.
164. Street, J. C.; and Thomas, A.: Carbon Formation in Pre-Mixed Flames. Fuel, vol. 34, 1955, p. 4.
165. Daniels, P. H.: Carbon Formation in Pre-Mixed Flames. Combustion and Flame, vol. 4, 1960, p. 54.
166. Singer, J. M.; and Grumer, J.: Carbon Formation in Very Rich Hydrocarbon-Air Flames. Vol. I: Studies of Chemical Content, Temperature, Ionization, and Particulate Matter. Seventh Symposium (International) on Combustion, Butterworths, London, 1959.
167. Tesner, P. A.: Formation of Dispersed Carbon by Thermal Decomposition of Hydrocarbons. Seventh Symposium (International) on Combustion, Butterworths, London, 1959.
168. van der Held, E. F.: Formation and Gasification of Carbon in an Atmosphere of Combustion Products. Seventh Symposium (International) on Combustion, Butterworths, London, 1959.
169. Gaydon, A. G.; and Fairbairn, A. R.: Carbon Formation from  $C_2H_2$  and CO in Discharge Tubes. Fifth Symposium (International) on Combustion, Rheinhold Publishing Company, New York, 1955.
170. Arthur, J. R.; and Napier, D. H.: Formation of Carbon and Related Materials in Diffusion Flames. Fifth Symposium (International) on Combustion, Rheinhold Publishing Company, New York, 1955.
171. Scully, D. B.; and Davies, R. A.: Carbon Formation from Aromatic Hydrocarbons. Combustion and Flame, vol. 9, 1965, p. 185.

172. Fenimore, C. P.; Jones, G. W.; and Moore, G. E.: Carbon Formation in Quenched Flat Flames at 1600° K. Sixth Symposium (International) on Combustion, Rheinhold Publishing Company, New York, 1957.
173. Ferguson, R. E.: An Isotopic Tracer Study of Carbon Formation in Hydrocarbon Flames. *Combustion and Flame*, vol. 1, 1957, p. 431.
174. Lee, K. B.; Thring, M. W.; and Beer, J. M.: On the Rate of Combustion of Soot in a Laminar Soot Flame. *Combustion and Flame*, vol. 6, 1962, p. 137.
175. Stehling, F. C.; Frazee, J. D.; and Anderson, R. C.: Carbon Formation from Acetylene. Sixth Symposium (International) on Combustion, Rheinhold Publishing Company, New York, 1957.
176. Godsave, G. A.: Studies of the Combustion of Drops in a Fuel Spray: The Burning of Single Drops of Fuel. Fourth Symposium (International) on Combustion, Williams and Wilkins Company, Baltimore, 1953.
177. Khitrin, L. N.: Fundamental Principles of Carbon Combustion and Factors Intensifying the Burning of Solid Fuels. Sixth Symposium (International) on Combustion, Rheinhold Publishing Company, New York, 1957.
178. Wicke, E.: Contributions to the Combustion Mechanism of Carbon. Fifth Symposium (International) on Combustion, Rheinhold Publishing Company, New York, 1955.
179. Yagi, S.; and Kunii, D.: Studies on Combustion of Carbon Particles in Flames and Fluidized Beds. Fifth Symposium (International) on Combustion, Rheinhold Publishing Company, New York, 1955.
180. Behrens, H.: Flame Instabilities and Combustion Mechanism. Fourth Symposium (International) on Combustion, the Williams and Wilkins Company, Baltimore, 1953.
181. Paushkin, Ya. M.: The Chemical Composition and Properties of Fuels for Jet Propulsion. Pergamon Press, New York, 1962.
182. Minkoff, G. J.; and Tipper, C. F.: Chemistry of Combustion Reactions. Butterworths, London, 1962.

183. Fristrom, R. M.: The Mechanism of Combustion in Flames. Combustion and Engineering News, October 14, 1963.
184. Penner, S. S.: Combustion and Propulsion Research. Combustion and Engineering News, January 14, 1963.
185. McCafferty, R. J.; and Hibbard, R. P.: Combustion in Aircraft Gas Turbine Engines. Literature of the Combustion of Petroleum. Advances in Chemistry Series, No. 20, American Chemical Society, 1958.
186. Penner, S. S.; and Datner, P. P.: Combustion Problems in Liquid-Fuel Rocket Engines. Fifth Symposium (International) on Combustion, Rheinhold Publishing Company, New York, 1955.
187. Wise, H.; and Agoston, G. A.: Burning of a Liquid Droplet. Literature of the Combustion of Petroleum. Advances in Chemistry Series, No. 20, American Chemical Society, 1958.
188. Spalding, D. B.: Some Fundamentals of Combustion. Academic Press, New York, 1955.
189. Williams, F. A.: Combustion Theory; The Fundamental Theory of Chemically Reacting Flow Systems. Addison-Wesley Publishing Company, Reading, Massachusetts, 1965.
190. Fristrom, R. M.; and Westenberg: Flame Structure. McGraw-Hill Book Company, New York, 1965.
191. Bahn, G. S.: Role of Vaporization Rate in Combustion of Liquid Fuels. Literature of the Combustion of Petroleum. Advances in Chemistry Series, No. 20, American Chemical Society, 1958.
192. Starkman, E. S.; Cattaneo, A. G.; and McAllister, S. H.: Industrial Engineering and Chemistry, vol. 43, 1951, p. 2822.
193. Howard and Essenhigh: Mechanism of Solid Particle Combustion with Simultaneous Gas-Phase Volatiles Combustion. Paper presented at the Eleventh Symposium (International) on Combustion, Berkeley, California, August 14-20, 1966.
194. Smith, E. C.: The Emission Spectrum of Hydrocarbon Flames. Proceedings of the Royal Society, A174, London, 1940, p. 110.

195. Klemenc, A.; Wechsberg, R.; and Wagner, G.: Zeit. Elektrochem, vol. 40, no. 488, 1934, and Zeit. Physikal. Chem. vol. 170, 1934, p. 97.
196. Cabannes, F.: La Formation des Particules de Carbone dans les Flammes et l'Observation de la Molecule C<sub>3</sub>. J. Phys. Radium, vol. 17, 1956, p. 492.
197. Gordon, A. S.: A Review of the Kinetics and Mechanism of the Pyrolysis of Hydrocarbons. Combustion and Propulsion: Fifth AGARD Colloquium, High-Temperature Phenomena. Pergamon Press, London, 1963.
198. Rummel, K.; and Veh, P. O.: Arch. Eisenhüttenwesen, vol. 14, 1941, p. 489.
199. Anon.: Radiation and Structural Characteristics of Rocket Exhaust Plumes. Rocketdyne R-6742, September 29, 1966.
200. Anderson, R. C.: Literature of the Combustion of Petroleum. Advances in Chemistry Series, No. 20, American Chemical Society, 1958.
201. Westbrook, E. A.; Hellwig, K. C.; and Anderson, R. C.: Self-Combustion of Acetylene, II: Reactions in Flame Propagation. Fifth Symposium (International) on Combustion, Rheinhold Publishing Company, New York, 1955.
202. Foster, P. J.: Carbon in Flames. Journal of the Institute of Fuel, vol. 38, 1965, p. 297.
203. Huff, V. N.; Gordon, S.; and Morrell, V. E.: General Method and Thermodynamic Tables for Computation of Equilibrium Composition and Temperature of Chemical Reactions. NACA Rept. 1037, 1951.
204. Penner, S. S.: Chemistry Problems in Jet Propulsion. Pergamon Press, New York, 1957.
205. Dodge, B. F.: Chemical Engineering Thermodynamics. McGraw-Hill Book Company, 1944.
206. Boynton, F. P.: Rocket Plume Radiance, IV: Studies of Carbon Particles Formed by Small, Hydrocarbon-Fueled Rocket Engines. General Dynamics/Convair, ERR-AN-007, April 7, 1960.

207. Boynton, F. P.; and Neu, J. T.: Rocket Plume Radiance, V: Calculation of Adiabatic Flame Temperatures of Afterburning Rocket Exhaust. General Dynamics/Convair, ERR-AN-011, May 16, 1960.
208. Homann and Wagner: Some New Aspects of the Mechanism of Carbon Formation in Pre-Mixed Flames. Paper presented at the Eleventh Symposium (International) on Combustion, Berkeley, California, August 14-20, 1966.
209. Echigo; Nishiwaki; and Hirata: A Study on the Radiation of Luminous Flames. Paper presented at the Eleventh Symposium (International) on Combustion, Berkeley, California, August 14-20, 1966.
210. Tesner, P. A.; Snegyreva; and Soorovikin: Kinetics of Dispersed Carbon Formation. Paper presented at the Eleventh Symposium (International) on Combustion, Berkeley, California, August 14-20, 1966.
211. Cullis, C. F.; Read; and Trimm: The Role of Acetylenic Hydrocarbons in the Formation of Carbon from Gases. Paper presented at the Eleventh Symposium (International) on Combustion, Berkeley, California, August 14-20, 1966.
212. Einbinder, H.: Generalized Equations for the Ionization of Solid Particles. The Journal of Chemical Physics, vol. 26, 1957, p. 948.
213. Schuler, K. E.; and Weber, J.: A Microwave Investigation of the Ionization of Hydrogen-Oxygen and Acetylene-Oxygen Flames. The Journal of Chemical Physics, vol. 22, 1954, p. 491.
214. Smith, F. T.: Ionization and the Structure of Carbon Particles at High Temperatures. Third Biennial Carbon Conference, 1958.
215. Sugden, T. M.; and Thrush, B. A.: A Cavity Resonator Method for Electron Concentration in Flames. Nature, vol. 168, 1951, p. 703.
216. Saha, M. N.: Ionization in the Solar Chromosphere. Philosophy Magazine, vol. 40, 1920, p. 472.
217. Pergament, H. S.: Radar Interference in the Exhaust Plume of an Advanced Missile System. AeroChem Research Laboratories TP-121 (ASTIA No. AD 367422), November 1965 (Confidential).

218. Pergament, H. S.; and Calcote, H. F.: Thermal and Chemi-Ionization Processes in Afterburning Rocket Exhausts. Paper presented at the Eleventh Symposium (International) on Combustion, August 14-20, 1966.
219. Kurzius, S. C.; and Silla, H.: Solid Propellant Exhaust Ionization Studies. AeroChem Research Laboratories TN-65, July 1964 (Confidential).
220. Jacobs, D. B.; et al.: Saturn V Exhaust Effects on Radio Systems Performance: Final Report. Boeing Document D5-15606, October 3, 1966.
221. Brower, E. M.; and McEntire, J. A.: Prediction and Correlation of Radio Interference Effects on Saturn V Vehicle. Paper presented at the Fourth Plume Interference Symposium, June 28, 1966.
222. Edelman, R.: Analytical Investigation of Plume Afterburning. General Applied Science Laboratories Monthly Progress Report No. 1 (NASA/MSFC Contract No. NAS8-20298), April 1966.
223. Slutsky, S.; and Melnick, J. D.: Radiation from Carbon in a Rocket Plume Mixing Region with Coupled Convective and Radiative Energy Fluxes and General Optical Thickness. General Applied Science Laboratories GASL Technical Report No. 625, September 1966.
224. Wolfhard, H. G.; and Parker, W. G.: Temperature Measurements of Flames Containing Incandescent Particles. Proceedings of the Royal Physical Society (London), vol. 62B, 1949, p. 523.
225. Erickson, W. D.; Williams, C. C.; and Hottel, H. C.: Light Scattering Measurements on Soot in a Benzene-Air Flame. Combustion and Flame, vol. 3, 1964, p. 127.
226. Kunugi, M.; and Jinno, H.: Determination of Size and Concentration of Soot Particles in Diffusion Flames by a Light-Scattering Technique. Paper presented at the Eleventh Symposium (International) on Combustion, Berkeley, California, August 14-20, 1966.
227. Millikin, R. C.: Sizes, Optical Properties, and Temperatures of Soot Particles. Temperature - Its Measurement and Control in Science and Industry. Vol. III, part 2. Rheinhold Publishing Company, New York, 1962.

228. Millikin, R. C.: Measurement of Particle and Gas Temperatures in a Slightly Luminous Pre-Mixed Flame. *Journal of the Optical Society of America*, vol. 51, 1961, p. 535.
229. Johnson, G. R.; and Anderson, R. C.: Proceedings of the Fifth Conference on Carbon, (Buffalo, New York), vol. 1, 1962, p. 395.
230. Ferriso, C. C.; et al.: Study on the Spectral Emissivity of Carbon Particles Produced by a Rocket Motor. General Dynamics/Convair, GD/C-DBE66-006, May 1966.
231. Boynton, F. P.; et al.: Radiative Properties of Carbon Particles Produced by a Rocket Motor. AIAA Paper No. 66-133 presented at the AIAA Third Aerospace Sciences Meeting, January 24-26, 1966.
232. Stratton, J. A.: *Electromagnetic Theory*. McGraw-Hill Book Company, New York, 1941.
233. Slater, J. C.; and Frank, N. H.: *Electromagnetism*. McGraw-Hill Book Company, New York, 1947.
234. Slater, J. C.; and Frank, N. H.: *Introduction to Theoretical Physics*. McGraw-Hill Book Company, New York, 1933.
235. Born, M.; and Wolfe, E.: *Principles of Optics*. The MacMillan Company, New York, 1959.
236. Sommerfeld, A.: *Optics*. Academic Press, New York, 1954.
237. Böttcher, C. J.: *Theory of Electric Polarization*. Elsevier Publishing Company, New York, 1952.
238. Fleagle, R. G.; and Businger, J. A.: *An Introduction to Atmospheric Physics*. Academic Press, New York, 1963.
239. Wood, R. W.: *Physical Optics*. The MacMillan Company, New York.
240. Stull, V. R.; and Plass, G. N.: Emissivity of Dispersed Carbon Particles. *Journal of the Optical Society of America*, vol. 50, 1960, p. 121.

241. Halpern, O. ; and Hall, H. : The Ionization Loss of Energy of Fast Charged Particles in Gases and Condensed Bodies. *Physical Review*, vol. 73, 1948, p. 477.
242. Senftleben, H. ; and Benedict, E. : Scattering of Light by Carbon Particles of Luminous Flames. *Annalen der Physik*, 4th Series, vol. 60, 1919, p. 297.
243. Oster, G. : The Scattering of Light and Its Applications to Chemistry. *Chemical Review*, vol. 43, 1948, p. 319.
244. Cadle, R. D. : Particle Size. Rheinhold Publishing Company, New York, 1965.
245. Green, H. L. ; and Lane, W. R. : Particulate Clouds: Dusts, Smokes, and Mists. E. and F. N. Spon Ltd. , London, 1964.
246. van de Hulst, H. C. : Light Scattering by Small Particles. John Wiley and Sons, 1957.
247. Sinclair, D. : Light Scattering by Spherical Particles. *Journal of the Optical Society of America*, vol. 37, 1947, p. 475.
248. Sinclair, D. ; and La Mer, V. K. : Light Scattering as a Measure of Particle Size in Aerosols. *Chemical Review*, vol. 44, 1945, p. 245.
249. Dallavalle, J. M. : Micrometrics, The Technology of Fine Particles. Pitman Publishing Company, New York, 1948.
250. Orr, C. ; and Dallavalle, J. M. : Fine Particle Measurement. The MacMillan Company, New York, 1959.
251. Humphries, W. J. : Physics of the Air. McGraw-Hill Book Company, New York, 1940.
252. Tverskoi, P. N. : Physics of the Atmosphere: A Course in Meteorology. Translated from the Russian by Israel Program for Scientific Translation, Jerusalem, 1965.
253. Bullrich, K. : Scattered Radiation in the Atmosphere and the Natural Aerosol. *Advances in Geophysics*. Vol. 10. Academic Press, New York, 1964.

254. Rayleigh, Lord: On the Electromagnetic Theory of Light. Philosophical Magazine and Journal of Science, vol. 12, 1881, p. 73.
255. Rayleigh, Lord: On the Transmission of Light Through an Atmosphere Containing Small Particles in Suspension, and on the Origin of the Blue of the Sky. Philosophical Magazine and Journal of Science, 1899, p. 375.
256. Rayleigh, Lord: On the Scattering of Light by a Cloud of Similar Small Particles of Any Shape and Oriented at Random. Philosophical Magazine and Journal of Science, vol. 35, 1918, p. 373.
257. Born, M.: Optik. Springer, Berlin, 1933.
258. Main, R. P.; and Bauer, E.: Opacities of Carbon-Air Mixtures at Temperatures from 3000-10,000° K. Journal of Quantitative Spectroscopy and Radiative Transfer, vol. 6, 1966, p. 1.
259. Krascella, N. L.: The Absorption and Scattering of Radiation by Small Solid Particles. Journal of Quantitative Spectroscopy and Radiative Transfer, vol 5, 1966, p. 245. (Also available as NASA CR-210, April 1965.)
260. Beheshti, M.: The Absorption and Scattering of Radiation by Solid Carbon Particles. AIAA Paper No. 66-134 presented at AIAA Third Aerospace Sciences Meeting, January 24-26, 1966.
261. Foster, P. J.: Calculation of the Optical Properties of Dispersed Phases. Combustion and Flame, vol. 7, 1963, p. 277.
262. Howarth, C. R.; Foster, P. J.; and Thring, M. W.: The Effect of Temperature on the Extinction of Radiation by Soot Particles. Paper No. 163 presented at Third International Heat Transfer Conference, Chicago, Illinois, August 7-12, 1966.
263. Yagi, S.: Journal of the Society of Chemical Industries (Japan) vol. 40, 1937, pp. 50 and 144.
264. Ruedy, R.: Absorption of Light and Heat Radiation by Small Spherical Particles. Vol. I of Absorption of Light by Carbon Particles. Canadian Journal of Research, vol. 19A, 1941, p. 117.

265. Mie, G.: *Annalen der Physik*, vol. 25, 1908, p. 377.
266. Thompson, J. D.: *A Study of Radiative Properties and Composition of the Turbine Exhaust Products in the F-1 Engine*. Rocketdyne R-6743, September 20, 1966.
267. Becker, A.: *Annalen der Physik*, vol. 28, 1909, p. 1017.
268. Rossler, H.; and Behrens, F.: *Optik*, vol. 6, 1950, p. 145.
269. Pepperhoff, W.: *Optik*, vol. 8, 1951, p. 354.
270. Naeser, G.; and Pepperhoff, W.: *Kolloid Zeit.*, vol. 125, 1952, p. 33.
271. Pepperhoff, W.; and Bahr, A.: *Archiv. Eisenhütten*, vol. 23, 1952, p. 335.
272. Plyler, E. L.; and Humphreys, C. J.: *Use of Radiation from Incandescent Particles as an Indication of Flame Temperature*. *Journal of Research of the National Bureau of Standards*, vol. 47, 1951, p. 6.
273. Rossler, F.: *Temperature Measurement of Transient Phenomena*. Vol. 3, part 2 of *Temperature, Its Measurement and Control in Science and Industry*. Rheinhold Publishing Corporation, New York, 1962.
274. Heidman, M. F.; and Priem, R. J.: *Application of an Electro-Optical Two-Color Pyrometer to Measurement of Flame Temperature for Liquid Oxygen-Hydrocarbon Propellant Combination*. NACA TN 3033, October 1953.
275. Yagi, S.; and Iino, H.: *Radiation from Soot Particles in Luminous Flames*. Eighth Symposium (International) on Combustion, The Williams and Wilkins Company, Baltimore, 1962.
276. Hottel, H. C.; and Broughton, F. P.: *Determination of True Temperature and Total Radiation from Luminous Gas Flames*. *Industrial and Engineering Chemistry, Analytical Edition*, vol. 4, 1932, p. 166.
277. Schack, A.: *Strahlung von Leuchtenden Flammen*. *Zeitschrift für Technische Physik*, vol. 6, 1925, p. 530.

278. Siddall, R. G.; and McGrath, I. A.: The Emissivity of Luminous Flames. Ninth Symposium (International) on Combustion, Academic Press, New York, 1963.
279. Sato, T.; and Matsumoto, R.: Radiant Heat Transfer from Luminous Flames. International Developments in Heat Transfer, American Society of Mechanical Engineers, New York, 1963.
280. Thring, M. W.; et al.: Prediction of the Emissivity of Hydrocarbon Flames. International Developments in Heat Transfer, American Society of Mechanical Engineers, New York, 1963.
281. Hawksley, P. G.: The Physics of Particle Size Measurement: Part II of Optical Methods and Light Scattering. The British Coal Utilization Research Association Monthly Bulletin, vol. 16, 1952, p. 134.
282. Plunkett, J. D.; and Kingery, W. D.: The Spectral and Integrated Emissivity of Carbon and Graphite. Fourth Carbon Conference, 1959.
283. Rutgers, G. A.: Handbuch der Physik. Vol. 26, Springer-Verlag, Berlin, 1958.
284. MacPherson, H. G.: Journal of the Optical Society of America, vol. 30, 1940, p. 189.
285. Lanzo, C. D.: Experimental Spectral Transmissivity of Carbon Particle Clouds. Paper presented at ARS/ANS/IAS Nuclear Propulsion Conference, August 1962.
286. Lanzo, C. D.; and Ragsdale, R. G.: Experimental Determination of Spectral and Total Transmissivities of Clouds of Small Particles. NASA TN D-1405, September 1962.
287. Marteney, P. J.: Experimental Investigation of the Opacity of Small Particles. NASA CR-211, April 1965.
288. Silverman, S.: The Determination of Flame Temperatures by Infrared Radiation. Journal of the Optical Society of America, vol. 39, 1944, p. 275.

289. Tourin, R. H.: Recent Developments in Gas Pyrometry by Spectroscopic Methods. ASME Paper No. 63-WA-252, presented at Winter Annual Meeting of ASME, November 17-22, 1963. (Also available as ASTIA No. AD 427539.)
290. Simmons, F. S.; and deBell, A. G.: Photographic Technique for Measuring Temperatures in Luminous Rocket Exhaust Flames. Journal of the Optical Society of America, vol. 48, 1958, p. 717.
291. Simmons, F. S.; and deBell, A. G.: Photographic Pyrometry with a Color-Separation Camera. Journal of the Optical Society of America, vol. 49, 1959, p. 735.
292. Simmons, F. S.; and deBell, A. G.: Spectral Radiometry and Two-Path Pyrometry of Rocket Exhaust Jets. Temperature, Its Measurements and Control in Science and Industry. Vol. 3, part 2, Rheinhold Publishing Corporation, New York, 1962.
293. Herget, W. F.; et al.: An Instrumentation System to Study Rocket Exhaust Plume Radiative Processes. Rocketdyne R-6288, August 27, 1965.
294. Hendershot, K. C.; and McCaa, D.: Research on Base Heating of Rocket Motor Vehicles Using Shock Tube Techniques. Cornell Aeronautical Laboratory Monthly Progress Report No. 12 (NASA/MSFC Contract No. NAS8-20027), February 1966.
295. Hendershot, K. C.; and McCaa, D.: Research on Base Heating of Rocket Motor Vehicles Using Shock Tube Techniques. Cornell Aeronautical Laboratory Monthly Progress Report No. 13 (NASA/MSFC Contract No. NAS8-20027), March 1966.
296. Thompson, J. D.: Final Report: Measurements of the Radiant Heat Flux from an F-1 Exhaust. Rocketdyne R-6116, March 23, 1965 (Secret).
297. Simmons, F. S.: Photopyrometry of Luminous Combustion Products in a Rocket Engine. Bulletin of Eighth Meeting of JANAF Rocket Static Test Panel, Johns Hopkins University Publication No. SPSTP/8, December 1959 (Confidential).

298. deBell, A. G.; and Speiser, E. W.: Infrared Spectral Radiance of Large Liquid Propellant Rocket Engine Plumes. Rocketdyne R-2019, August 1960 (Secret).
299. deBell, A. G.; and Simmons, F. S.: Radiation Studies of Atlas Engine Exhaust Jets at the Rocketdyne Propulsion Field Laboratory. Rocketdyne R-1107, September 5, 1958 (Confidential).
300. Herget, W. F.; Schumacher, P. S.; and Enloe, J. D.: Radiative Properties of Rocket Exhausts at Simulated Altitudes. Rocketdyne R-6347, October 1965 (Secret).
301. Tourin, R. H.: Application of Quantitative Infrared Spectroscopy to Problems of Launch Phase Missile Defense. AMRAC Proceedings, vol. 10, part 1, 1964 (Secret).
302. Hecht, G. J.: A Two-Wavelength Near Infrared Pyrometer. Temperature, Its Measurement and Control in Science and Industry. Vol. 3, part 2, Rheinhold Publishing Company, New York, 1962.
303. Hill, W. E.: Two-Color Pyrometry. Temperature, Its Measurement and Control in Science and Industry, vol. 3 part 2, Rheinhold Publishing Company, New York, 1962.
304. Hornbeck, G. A.: A High-Speed Ratio Pyrometer. Temperature, Its Measurement and Control in Science and Industry, vol. 3, part 2, Rheinhold Publishing Company, New York, 1962.
305. Brenden, B. B.: An Infrared Radiation Ratio Pyrometer. Temperature, Its Measurement and Control in Science and Industry, vol. 3, part 2, Rheinhold Publishing Company, New York, 1962.
306. Branstetter, J. R.: Some Practical Aspects of Surface Temperature Measurement by Optical and Ratio Pyrometers. NASA TN D-3604, September 1966.
307. Tourin, R. H.: Monochromatic Radiation Pyrometry of Hot Gases, Plasmas, and Detonations. Temperature, Its Measurement and Control in Science and Industry, vol. 3 part 2, Rheinhold Publishing Company, New York, 1962.

308. Tourin, R. H.: Spectroscopic Gas Temperature Measurement: Pyrometry of Hot Gases and Plasmas. Elsevier Publishing Company, New York, 1966.
309. Brewer, L. E.; and McGregor, W. K.: Experimental Determination of a Rocket Exhaust Gas Temperature at Altitude by Infrared Spectroscopy. AEDC TN-61-94, 1961 (Confidential).
310. Harrison, T. R.: Radiation Pyrometry and Its Underlying Principles of Radiant Heat Transfer. John Wiley and Sons, New York, 1960.
311. Foelsch, K.: The Analytical Design of an Axially Symmetric Laval Nozzle for a Parallel and Uniform Jet. Journal of the Aeronautical Sciences, vol. 16, 1949, p. 161.
312. Malkmus, W.: Infrared Emissivity of Carbon Dioxide (2.7 Micron Band). Journal of the Optical Society of America, vol. 54, 1964, p. 751.
313. Tuttle, S.: Theoretical Determination of the Radiation from the Undisturbed Cone of a LOX/RP-1 Rocket Motor. AMRAC Proceedings RF-IR/Optical Program Development, May 8-10, 1961 (ASTIA No. AD 323781) (Secret).
314. Thring, M. W.; Beer, J. M.; and Foster: The Radiative Properties of Luminous Flames. Paper No. 161 presented at Third International Heat Transfer Conference, Chicago, Illinois, August 7-12, 1966.
315. Wolfhard, H. G.; and Hinck: Elementary Processes in Low-Pressure Flames and Their Relation to Rocket Exhaust Radiation. Paper presented at the Eleventh Symposium (International) on Combustion, Berkeley, California, August 14-20, 1966.
316. Zirkind, R.: Radiation from Rocket Exhaust Plumes. Paper presented at the Eleventh Symposium (International) on Combustion, Berkeley, California, August 14-20, 1966. (Also available as Poly. Inst. of Brooklyn Rpt. No. 984.)
317. Simmons, F. S.; and Spadaro, F. G.: Thermal Lag of Solid Particles in Rocket Nozzle Flow. Rocketdyne Research Report No. 59-27, August 1959.

318. Simmons, F. S.; and Spadaro, F. G.: Thermal Lag of Solid Carbon in Rocket Nozzle Flow. *Pyrodynamics*, vol. 2, 1965, p. 177.
319. Wiedmann, M. L.; and Trumpler, P. R.: Thermal Accommodation Coefficients. *Transactions of the ASME*, 1946, p. 58.
320. Dillon, P. L.; and Line, L. E.: Heat Transfer Between Solid Particles and Gas in a Rocket Nozzle. *Jet Propulsion*, 1956, p. 1091.
321. Jones, I. P.: Summary of Base Thermal Environment Measurements on the Saturn I Block I Flight Vehicles. NASA TM X-53326, September 3, 1965.
322. Hartley, L. L.; and Fricken, B. J.: Thermal Environment for the Base Region of the Saturn S-I and S-IB Stages. Chrysler Corporation Space Division, TN-AE-65-74, March 5, 1965.
323. Francis, W. L.: Development of a Saturn IB Base Heating Model. Vol. I of Exhaust Plume Radiation. Chrysler Corporation Space Division, TN-AE-64-36, June 30, 1964 (Confidential).
324. Fricken, B. J.: Base and Exhaust Plume Heating Environments - SA-205. Chrysler Corporation Space Division, TN-AP-66-67, August 1, 1966.
325. Hartley, L. L.: Preliminary Base Thermal Environment for S-IB Stage, Saturn IB Vehicle. Chrysler Corporation Space Division, TN-AE-64-20, January 17, 1964.
326. Hartley, L. L.; Finley, W. L.; and Martin, A. D.: Flight Evaluation of Saturn SA-9 S-I Stage Base and Aerodynamic Heating Data. Chrysler Corporation Space Division, TN-AE-65-81, April 1, 1965.
327. Hartley, L. L.; and Martin, A. D.: Summary of Saturn I, S-I Stage Base and Aerodynamic Heating Data. Chrysler Corporation Space Division, TN-AE-65-115, November 1, 1965.
328. Fricken, B. J.: Base and Exhaust Plume Heating Environments, SA-204. Chrysler Corporation Space Division, TN-AP-66-43, May 19, 1966.
329. Geraghty, J.: IBM Program for Finding the Geometric Form Factors of Rocket Engine Exhaust Plumes. Chrysler Corporation Space Division, TN-AE-67-24, June 15, 1964.

330. Mullen, C. R.: Analysis of Saturn S-IC Base Heating Environment. Boeing Document No. D5-11287, January 7, 1964.
331. McEntire, J. A.; et al.: Launch Vehicle Final Thermal Design Environment - SA-501 Thru SA-503. Boeing Document D5-15513-1, July 22, 1966.
332. Hughes, A. R.; and Reid, J. L.: Radiation Environment of the Saturn V Base Plate. Hayes International Corporation Engineering Report No. 1155, May 25, 1965.
333. Jacobs, D. B.: Saturn V Model Base Heating (S-IC Stage). Boeing Document D5-15615, vol. 1, August 25, 1966, and vol. 2, October 24, 1966.
334. Wasko, R. A.: Wind-Tunnel Investigation of Thermal and Pressure Environments in the Base of the Saturn S-IC Booster from Mach 0.1 to 3.5. NASA TN D-3612, September 1966.
335. Patrick, D. R.: Final Data Transmitted of Jet Plumes Study Test Program. NASA/MSFC Memorandum R-TEST-CV-112-66, November 1, 1966.
336. Talbert, W. W.; et al.: Spectral Measurements of Ballistic Missile Plumes (1.0-5.5 microns) NAVORD Report 6755 (ASTIA No. AD 332915), December 15, 1959 (Secret).
337. Dimmock, T. H.; and Courtney, W. G.: Rocket Exhaust Studies. Thiokol Chemical Corporation Annual Report A-2 [Contract NONr-3543(00)] (ASTIA No. AD 369336), December 1965 (Secret).
338. Wagner, G. D.; Cramer, F. W.; and Borough, H. C.: Visible and Infrared Radiation Measurements of the Plumes of Thiokol R and D Motors. Boeing Document D2-4439, July 1959 (Confidential).
339. Briscoe, R. D.; Bullara, L. A.; and Bressler, M.: Radiation Characteristics of Statically Fired Rocket Engines. Proceedings of AMRAC, Vol. V, University of Michigan, November 1961 (Secret).
340. Sutton, J. W.: Laboratory Studies of Rocket Plume Radiation at Reduced Pressure. AFCRL 62-235 (ASTIA No. AD 273435), December 1961.

341. Schindler, A.; and Penzias, G. J.: Infrared Radiation and Temperature Measurements in Solid Propellant Flames, vol. II; Study of CYH (77), Warner and Swasey TR-30, June 1964 (Confidential).
342. Miller, T. W.: In-Flight Missile Plume Spectra. Proceedings of AMRAC, vol. II, University of Michigan, July 1960 (Secret).
343. Baker, K. L.; and Allport, J. J.: Spectral Measurement of Rocket Motor Plumes. United Technology Center UTC-2075-FR2 (ASTIA No. AD 369062), January 1966 (Secret).
344. Carlson, D. J.: Emittance of Condensed Oxides in Solid Propellant Combustion Products. Tenth Symposium (International) on Combustion, The Combustion Institute, Pittsburgh, Pennsylvania, 1965.
345. Carlson, D. J.; and DuPuis, R. A.: Alumina Absorption and Emittance. Aeronutronic U-2627, May 1964.
346. Launstein, F.; Lindquist, G.; and Tuttle, S.: Launch-Phase Radiometric Data Compiled for 88 Missiles. BAMIRAC Infrared Laboratory Report 4613-47-T, January 1964 (Secret).
347. Anon.: Project RAMP - Measurement of Ballistic Missile Radiation (AMR Tests 1338 and 1339). Aerojet-General 2436 (ASTIA No. AD 333647), December 1962 (Secret).
348. Miller, T. W.; and Sternchak, R. S.: Final Report: Spectrometric Measurements of Missile Plumes. Geophysics Research Directorate GDR-TR-60-299, July 1960 (Confidential).
349. Anon.: Third Annual Report of BAMIRAC Infrared Laboratory. Report 4613-21-F (1), September 1962 (Secret).
350. Condron, T. P.: Color Temperatures of Atlas and Minuteman Continuum Radiation. AFCRL-65-239, January 1, 1965 (Secret).
351. Carlson, D. J.; et al.: A Study of High Altitude Rocket Plume Phenomena. Aeronutronic S-2380, December 1963 (Secret).
352. Carlson, D. J.; et al.: Solid Propellant Exhaust Radiation Studies: Interim Technical Report No. 3. Aeronutronic U-3044, March 10, 1965.

353. Boudreau, C. A.; and Stone, M. L.: Scattering and Attenuation by Precipitation Particles. MIT Lincoln Laboratory, 26th Reference Bibliography, ESD-TDR-65-598, August 1965.
354. Love, T. J.; and Wheasler, R. A.: An Experimental Study of Infrared Scattering by Clouds of Particles. Aerospace Research Laboratories, ARL-64-109 (ASTIA No. AD 603851), June 1964.
355. Pendorff, R. B.: Research on Aerosol Scattering in the Infrared: Final Report. Air Force Cambridge Research Laboratories AFCRL-63-668 (ASTIA No. AD 414384), June 1963.
356. Havard, J. B.: On the Radiational Characteristics of Water Clouds at Infrared Wave Lengths. Ph.D. Thesis, University of Washington (ASTIA No. AD 238268), 1960.
357. Svaton, E. M.; and Winer, M.: Radiative Transfer from Gas-Particle Systems. Douglas SM-42607, November 1962.
358. Wyatt, P. J.: Scattering of Electromagnetic Plane Waves from Inhomogeneous Spherically Symmetric Objects. Physical Review, vol. 127, 1962, p. 1837.
359. Morse, P. M.; and Feshbach, H.: Methods of Theoretical Physics. McGraw-Hill Book Company, New York 1953.
360. La Mer, V. K.: Verification of Mie Theory - Calculations and Measurements of Light Scattering by Dielectric Spherical Particles. Office of Scientific Research and Development, OSRD Report No. 1857, September 29, 1943.
361. Bromwich, T. J.: The Scattering of Plane Electric Waves by Spheres. Philosophical Transactions of the Royal Society of London, vol. 220A, 1920, p. 175.
362. Nawrocki, P. J.; and Papa, R.: Atmospheric Processes. Prentice-Hall, Inc., Englewood Cliffs, New Jersey, 1963.
363. Newton, R. G.: Scattering Theory of Waves and Particles. McGraw-Hill Book Company, New York, 1966.

364. Infield, L.: Quarterly Journal of Applied Mathematics, vol. 5, 1947, p. 113.
365. Aden, A. L.: Electromagnetic Scattering from Spheres with Sizes Comparable to the Wavelength. Journal of Applied Physics, vol. 22, 1951, p. 601.
366. Smith, P. D.: The Conical Dipole of Wide Angle. Journal of Applied Physics, vol. 19, 1948, p. 11.
367. Debye, P.: Annalen der Physik, vol. 30, 1909, p. 59.
368. Gumprecht, R. O.; and Sliepcevich, C. M.: Scattering of Light by Large Spherical Particles. Journal of Physical Chemistry, vol. 57, 1953, p. 90.
369. Gumprecht, R. O.; and Sliepcevich, C. M.: Measurement of Particle Sizes in Polydispersed Systems of Means of Light Transmission Measurements Combined with Differential Settling. Journal of Physical Chemistry, vol. 57, 1953, p. 95.
370. Gumprecht, R. O.; and Sliepcevich, C. M.: Tables of Light-Scattering Functions for Spherical Particles. University of Michigan Press, Engineering Research Institute, 1951.
371. Boll, R. H.; Leacock, J. A.; Clark, G. C.; and Churchill, S. W.: Tables of Light Scattering Functions. University of Michigan Press, The Engineering Research Institute, 1958.
372. Chu, C.-M.; and Churchill, S. W.: Numerical Solution of Problems in Multiple Scattering of Electromagnetic Radiation. Journal of Physical Chemistry, vol. 59, 1955, p. 855.
373. Boll, R. H.; Gumprecht, R. O.; and Sliepcevich, C. M.: Theoretical Light-Scattering Coefficients for Relative Refractive Indexes Less than Unity and for Totally Reflecting Spheres. Journal of the Optical Society of America, vol. 44, 1954, p. 18.
374. Boll, R. H.; and Sliepcevich, C. M.: Evaluation of Errors of Optical Design Arising in the Size Analysis of a Dispersion by Light Transmission. Journal of the Optical Society of America, vol. 46, 1956, p. 200.

375. Chin, J. H. ; Sliepcevich, C. M. ; and Tribus, M. : Determination of Particle Size Distribution in Polydispersed Systems by Means of Measurements of Angular Variation of Intensity of Forward-Scattered Light at Very Small Angles. *Journal of Physical Chemistry*, vol. 59, 1955, p. 845.
376. Chin, J. H. ; Sliepcevich, C. M. ; and Tribus, M. : Particle Size Distributions from Angular Variation of Intensity of Forward-Scattered Light at Very Small Angles. *Journal of Physical Chemistry*, vol. 59, 1955, p. 841.
377. Clark, G. C. ; Chu, C. -M. ; and Churchill, S. W. : Angular Distribution Coefficients for Radiation Scattered by a Spherical Particle. *Journal of the Optical Society of America*, vol. 47, 1957, p. 81.
378. Gumprecht, R. O. ; Sung, N. -L. ; Chin, J. H. ; and Sliepcevich, C. M. : Angular Distribution of Intensity of Light Scattered by Large Droplets of Water. *Journal of the Optical Society of America*, 1952, p. 226.
379. Deirmendjian, D. : Tables of Mie Scattering Cross Sections and Amplitudes. RAND R-407-PR (ASTIA No. AD 295148), January 1963.
380. Deirmendjian, D. : Scattering and Polarization Properties of Water Clouds and Hazes in the Visible and Infrared. *Applied Optics*, vol. 3, 1964, p. 187.
381. Deirmendjian, D. : Scattering and Polarization Properties of Polydispersed Suspension with Partial Absorption. RAND RM-3238-PR, July 1967.
382. Deirmendjian, D. ; and Clasen, R. J. : Light Scattering on Partially Absorbing Homogeneous Spheres of Finite Size. RAND R-393-PR, February 1962.
383. Deirmendjian, D. ; Clasen, R. ; and Viezee, W. : Mie Scattering with Complex Index of Refraction. *Journal of the Optical Society of America*, vol. 51, 1961, p. 620. (Also available as RAND P-2079, August 1960).
384. Pendorff, R. B. : Angular Mie Scattering. *Journal of the Optical Society of America*, vol. 52, 1962, p. 402.

385. Pendorff, R. B.: Research on Aerosol Scattering in the Infrared, Scientific Report No. 5, Atlas of Scattering Diagrams for  $n = 1.33$ . Air Force Cambridge Research Laboratories AFCRL-1044 (ASTIA No. AD 267348), October 1961.
386. Pendorff, R. B.: Research on Aerosol Scattering in the Infrared, Scientific Report No. 2, Mie Scattering in the Forward Area. Air Force Cambridge Research Center AFCR-TN-60-285 (ASTIA No. AD 234935) February 1960.
387. Pendorff, R. B.: Research on Aerosol Scattering in the Infrared, Scientific Report No. 10, Atlas of Scattering Diagrams for  $n = 1.5$ . Air Force Cambridge Research Laboratories AFCRL-62-1131, November 1962.
388. Pendorff, R. B.: Research on Aerosol Scattering in the Infrared, Scientific Report No. 3, Scattering Coefficients for Absorbing and Non-Absorbing Aerosols. Air Force Cambridge Research Laboratories AFCRL-TN-60-667, (ASTIA No. AD 247159), October 1960.
389. Pendorff, R. B.: New Tables of Total Mie Scattering Coefficients for Spherical Particles of Real Refractive Indexes ( $1.33 \leq n \leq 1.50$ ). Journal of the Optical Society of America, vol. 47, 1957, p. 1010.
390. Pendorff, R. B.: An Approximation Method to the Mie Theory for Colloidal Spheres. Journal of Physical Chemistry, vol. 62, 1958, p. 1537.
391. Pendorff, R. B.: Research on Aerosol Scattering in the Infrared, Scientific Report No. 1, Results of An Approximation Method to the Mie Theory for Colloidal Spheres. Air Force Cambridge Research Center, AFCRC-TN-59-608 (ASTIA No. AD 227660), September 1959.
392. Pendorff, R. B.: Mie Scattering Coefficients for Selected Aerosol Size Distributions: Final Report. Air Force Cambridge Research Laboratories AFCRL-65-836 (ASTIA No. AD 626228), October 31, 1965.
393. Heller, W.; and Pangonis, W. J.: Theoretical Investigations on the Light Scattering of Colloidal Spheres, Vol. I: The Specific Turbidity. The Journal of Chemical Physics, vol. 26, 1957, p. 498.

394. Heller, W. ; and Pugh, T. L. : Experimental Investigations on the Effect of Light Scattering Upon the Refractive Index of Colloidal Particles. *Journal of Colloid Science*, vol. 12, 1957, p. 294.
395. Heller, W. ; and Tabibian, R. : Experimental Investigations on the Light Scattering of Colloidal Spheres. Vol. IV: Scattering Ratio. *Journal of Physical Chemistry*, vol. 66, 1962, p. 2059.
396. Heller, W. ; Nakagaki, M. ; and Wallach, M. L. : Theoretical Investigations on the Light Scattering of Colloidal Spheres. Vol. V: Forward Scattering. *The Journal of Chemical Physics*, vol. 30, 1959, p. 444.
397. Heller, W. : Theoretical Investigations on the Light Scattering of Colloidal Spheres. Vol. III: Analytical Expressions for Turbidity Approximating the Performance of the Mie Equations Prior to the First Maximum. *The Journal of Chemical Physics*, vol. 26, 1957, p. 1258.
398. Heller, W. ; and Nakagaki, M. : Theoretical Investigations on the Light Scattering of Colloidal Spheres. Vol. VII: Dissymmetry in Unpolarized and Polarized Light. *The Journal of Chemical Physics*, vol. 31, 1959, p. 1188.
399. Nakagaki, M. ; and Heller, W. : Theoretical Investigations on the Light Scattering of Colloidal Spheres. Vol. VI: Backward Scattering. *The Journal of Chemical Physics*, vol. 30, 1959, p. 783.
400. Nakagaki, M. ; and Heller, W. : Theoretical Investigations on the Light Scattering of Colloidal Spheres. Vol. VIII: Angular Location of Intensity Maxima and Minima in the Radiation Diagram of Colloidal Spheres. *The Journal of Chemical Physics*, vol. 32, 1960, p. 835.
401. Pangonis, W. J. ; and Heller, W. : *Angular Scattering Functions for Spherical Particles*. Wayne State University Press, Detroit, Michigan, 1960.
402. Stevenson, A. F. ; Heller, W. ; and Wallach, M. L. : Theoretical Investigations on the Light Scattering of Colloidal Spheres. Vol. XI: Determination of Size Distribution Curves from Spectra of the Scattering Ratio or from Depolarization Spectra. *The Journal of Chemical Physics*, vol. 34, 1961, p. 1789.

403. Tabibian, R. M.; and Heller, W.: Experimental Investigations on the Light Scattering of Colloidal Spheres. Vol. III: The Specific Scattering at 90°. *Journal of Colloid Science*, vol. 13, 1958, p. 6.
404. Kerker, M.: Scattering Functions for Spherical Particles of Refractive Index of 1.46-4.30i. *Journal of the Optical Society of America*, vol. 45, 1955, p. 1081.
405. Kerker, M.; and Matijevic, E.: Mie Scattering Functions for Refractive Index of 2.105. *Journal of the Optical Society of America*, vol. 51, 1961, p. 87.
406. Kerker, J.; and Matijevic, E.: Light Scattering of Monodispersed Polystyrene Latexes. *Journal of the Optical Society of America*, vol. 50, 1960, p. 722.
407. Kerker, M.; Hampton, M. I.: The Use of Unfiltered Light in Determining Particle Radius by the Polarization Ratio of the Scattered Light. *Journal of the Optical Society of America*, vol. 43, 1953, p. 370.
408. Love, T. J.; and Beattie, J. F.: Experimental Determination of Thermal Radiation Scattering by Small Particles. *Aerospace Research Laboratories ARL 65-110 (ASTIA No. AD 619056)*, June 1965.
409. Plass, G. N.: Mie Scattering and Absorption Cross Sections of Aluminum Oxide and Magnesium Oxide. *Space Systems Division SSD-TDR-62-127, Vol. VI (ASTIA No. AD 407053)*, May 27, 1963. (Also available in *Applied Optics*, vol. 3, 1964, p. 867.)
410. Plass, G. N.: Temperature Dependence of the Mie Scattering and Absorption Cross Sections for Aluminum Oxide. *Applied Optics*, vol. 4, 1965, p. 1616.
411. Plass, G. N.: Mie Scattering and Absorption Cross Sections for Absorbing Particles. *Applied Optics*, vol. 5, 1966, p. 279.
412. Bauer, E.: The Scattering of Infrared Radiation from Clouds. *Applied Optics*, vol. 3, 1964, p. 197.
413. Bauer, E.; and Carlson, D. J.: Mie Scattering Calculations for Micron Size Alumina and Magnesia Spheres. *Journal of Quantitative Spectroscopy and Radiative Transfer*, vol. 4, 1964, p. 363.

414. McCarthy, K. A.; Wolfe, W. L.; and Ballard, S. I.: Refractive Index of Special Crystals and Certain Glasses. American Institute of Physics Handbook. McGraw-Hill Book Company, New York, 1963.
415. Malitson, I. H.: Refraction and Dispersion of Synthetic Sapphire. Journal of the Optical Society of America, vol. 52, 1962, p. 1377.
416. Malitson, I. H.; Murphy, F. V.; and Rodney, W. S.: Refractive Index of Synthetic Sapphire. Journal of the Optical Society of America, vol. 48, 1958, p. 72.
417. Mergerian, D.: Optical Properties of Infrared-Transparent Solids at Elevated Temperatures. Proceedings of Infrared Information Symposium. Vol. 4, no. 4, October 1959 (Secret).
418. McAlister, E. D.: High Temperature Properties of Infrared Optical Materials. Proceedings of Infrared Information Symposia, vol. 4, no. 4, October 1959 (Secret).
419. Monroe, J. E.: Infrared Transmission and Radiation Conductivity of Alumina from Room Temperature to 1800° C. Alfred University, Alfred, New York (ASTIA No. AD 134314), April 1957.
420. Oppenheim, U. P.; and Even, U.: Infrared Properties of Sapphire at Elevated Temperatures. Journal of the Optical Society of America, vol. 52, 1962, p. 1078.
421. Lee, D. W.; and Kingery, W. D.: Radiation Energy Transfer and Thermal Conductivity of Ceramic Oxides. Journal of the American Ceramic Society, vol. 43, 1960, p. 594.
422. Gryvnak, D. A.; and Burch, D. E.: Final Technical Report. Vol. II: Optical and Infrared Properties of Al<sub>2</sub>O<sub>3</sub> at Elevated Temperatures. Aeronutronic U-2623 (ASTIA No. AD 606793), May 31, 1964.
423. Gryvnak, D. A.; and Burch, D. E.: Optical and Infrared Properties of Al<sub>2</sub>O<sub>3</sub> at Elevated Temperatures. Journal of the Optical Society of America, vol. 55, 1965, p. 625.

424. Adams, J. M.; and Colucci, S. E.: The Spectroscopic Measurement of Gas and Particle Temperature in Metalized Propellant Combustion. Paper S66-175, presented at ICRPG/AIAA Solid Propulsion Conference, Washington, D. C., July 18-21, 1966. (Also Colucci, S. E.; and Adams, J. M.: Plume Temperature Measurements of Metallized Propellant. AFRPL-TR-66-56 (ASTIA No. AD 479615), March, 1966.)
425. Glassman, I.: Combustion of Metals - Physical Considerations. Paper presented at ARS Solid Propellant Rocket Conference, Princeton, N. J., January 28-29, 1960. (Also available in Solid Propellant Rocket Research, Academic Press, New York, 1960.)
426. Glassman, I.: Metal Combustion Processes. Princeton University Aeronautical Engineering Laboratory Report No. 473, August 1959.
427. Brzustowski, T. A.; and Glassman, I.: Spectroscopic Investigation of Metal Combustion. Princeton University Aeronautical Engineering Report 586, October 1961. (Also available in Canadian Aeronautics and Space Journal, vol. 9, 1963, p. 141.)
428. Fassell, W. M.; et al.: The Experimental Nature of the Combustion of Metallic Powders. Paper presented at ARS Solid Propellant Rocket Conference, Princeton, N. J., January 28-29, 1960. (Also available in Solid Propellant Rocket Research, Academic Press, New York, 1960.)
429. Fassell, W. M.; et al.: The Combustion Process of Metal Particles. Proceedings of Fourth Meeting of JANAF-ARPA-NASA Thermochemical Panel, Publication T-4, October 1961.
430. Fassell, W. M.; et al.: An Experimental Investigation of Propellant Ingredient Combustion Phenomena: Second Quarterly Technical Report. Aeronautic C-1485, December 15, 1961 (Confidential).
431. Gordon, D. A.: Combustion Characteristics of Metal Particles. Paper presented at ARS Solid Propellant Conference, Princeton, New Jersey, January 28-29, 1960. (Also available in Solid Propellant Rocket Research, Academic Press, New York, 1960.)
432. Gordon, D. A.: Photographic Studies of the Combustion Characteristics of Metal Particles. Jet Propulsion Laboratory Technical Report 32-15, May 10, 1960 (Confidential).

433. Gordon, D. A.: Metal Combustion Research at the Space Sciences and Propulsion Laboratory, Stanford Research Institute. Proceedings of the Fourth Meeting of JANAF-ARPA-NASA Thermochemical Panel, Publication T-4, October 1961 (Confidential).
434. Wood, W. A.; et al.: Quarterly Progress Report on Interior Ballistics. Rhom and Haas Company, Report No. P-60-1, October 31, 1960 (Confidential).
435. Wood, W. A.: Metal Combustion in Deflagrating Propellant. Paper presented at ARS Solid Propellant Rocket Conference, Princeton, New Jersey, January 28-29, 1960. (Also available in Solid Propellant Rocket Research, Academic Press, New York, 1960.)
436. Avery, G. W.: Use of Aluminum Powder in Solid Propellants: A State-of-the-Art Survey. Chemical Propulsion Information Agency Publication 20, 1963 (Confidential).
437. Henderson, C. B.; and Bowen, J. S.: Metal Combustion Investigations. Proceedings of the Fourth Meeting of JANAF-ARPA-NASA Thermochemical Panel Publication T-4, October 1961 (Confidential).
438. Friedman, R.; and Maček: Ignition and Combustion of Aluminum Particles in Hot Ambient Gases. Proceedings of the Fourth Meeting of JANAF-ARPA-NASA Thermochemical Panel, Publication T-4, October 1961 (Confidential).
439. Markstein, G. H.: Combustion of Metals. AIAA Journal, vol. 1, 1963, p. 550.
440. Davis, A.: Solid Propellants: The Combustion of Particles of Metal Ingredients. Combustion and Flame, vol. 7, 1963, p. 359.
441. Kurtovich, D. D.; and Pinson, G. T.: How to Find the Exhaust Heat Radiation of Aluminized Solid Rockets. Space/Aeronautics, July 1961.
442. Kurtovich, D. D.; and Pinson, G. T.: Radiation Characteristics of Exhaust Plume from Aluminized Solid Propellant Rocket Engines. Boeing Document D2-6265, January 1961 (Confidential).

443. Watermeier, L. A.; Aungust, W. P.; and Pfaff: An Experimental Study of the Aluminum Additive Role in Unstable Combustion of Solid Rocket Propellants. Ninth Symposium (International) on Combustion, Academic Press, New York, 1963. (Also available as Ballistic Research Laboratory Report 1168, 1962.)
444. McCarty, K. P.: Techniques for Studying the Combustion of Aluminum in Solid Propellants. Paper presented at 1962 Fall Meeting, Western States Section of the Combustion Institute, November 1962.
445. Gibbons, S. G.; and Seigel, B.: Reduction of Aluminum Oxide by Propellant Combustion Gases at High Temperatures. Space Systems Division SSD-TDR-64-160 (ASTIA No. AD 606058), September 1964.
446. Brown, B.; and McCarthy, K. P.: Particle Size of Condensed Oxides from Combustion of Metallized Solid Propellants. Eighth Symposium (International) on Combustion, Williams and Wilkins Company, Baltimore, Maryland, 1962.
447. Sehgal, R.: An Experimental Investigation of a Gas-Particle System. Jet Propulsion Laboratory JPL-TR-32-238, March 16, 1962.
448. Allport, J. J.; et al.: Dynamics of Two-Phase Flow in Rocket Nozzles. United Technology Center 2102-FR, September 24, 1965.
449. Dobbins, R. A.: Particle Size of Aluminum Oxide Produced by a Small Rocket Motor. Brown University Division of Engineering Report, November 1964. (Also paper presented at Eleventh International Symposium on Combustion, Berkeley, California, August 14-20, 1966.)
450. Dobbins, R. A.: An Emission-Scattering Photometer for Measurement of Particle Size. Brown University Division of Engineering Report, September 1964.
451. Dobbins, R. A.; and Jizmagian, G. S.: Optical Scattering Cross Sections for Polydispersions of Dielectric Spheres. Brown University Division of Engineering Report, September 1964. (Also available in Journal of the Optical Society of America, vol. 56, 1966, p. 1345.)
452. Dobbins, R. A.; and Jizmagian, G. S.: Particle Size Measurements Based on the Use of Mean Scattering Cross Sections. Brown University Department of Engineering Report, November 1964. (Also available in Journal of the Optical Society of America, vol. 56, 1966, p. 1351.)

453. Cheung, H. and Cohen, N. S.: On the Performance of Solid Propellants Containing Metal Additives. AIAA Paper No. 64-116 presented at AIAA Solid Propellant Rocket Conference, January 29-31, 1964.
454. Smith, P. W.: Impulse Scaling Predictions. Air Force Rocket Propulsion Laboratory AFRPL-TR-66-297, November 1966 (Confidential). (Also available as CPIA Publication 124, vol. II, December 1966.) (Confidential)
455. Preckel, R. F.; Jacobs, A. M.; and Gibson, J. D.: Optimization of Double-Base Propellants. Allegany Ballistics Laboratory of Hercules Powder Company, ABL/P-46, July 1966 (Confidential).
456. Povenelli, L.; and Rosenstein, R. A.: Alumina Size Distributions from High-Pressure Composite Solid-Propellant Combustion. Preprint No. 64-115, Am. Inst. Aeron. and Astronaut., January 29-31, 1964.
457. Burns, E. A.: Analysis of Minuteman Exhaust Products. Stanford Research Institute SRI Project No. PRD-3753 (ASTIA No. AD 432233), October 25, 1962.
458. McGregor, W.: The Analysis of Solid Propellant Rocket Exhaust Heating Due to Particle Impingement. Boeing Document D5-12213, November 1965.
459. Fontenot, J. E.: Thermal Radiation from Solid Rocket Plumes at High Altitudes. AIAA Journal, vol. 3, 1965, p. 970.
460. Bender, R. L.; and Mullen, C. R.: S-IC/S-II Separation Thermal and Pressure Environmental Analysis. Boeing Coordination Sheet No. FTS-H-114, August 15, 1965.
461. Bender, R. L.; and Mullen, C. R.: Saturn V Aerodynamic Heating Analysis - Configuration 4106. Boeing Document D5-15230-1, February 2, 1965.
462. Kliegel, R.: Gas Particle Nozzle Flows. Ninth Symposium (International) on Combustion, Academic Press, New York, 1963.
463. Morizumi, S. J.; and Carpenter, H. J.: Thermal Radiation from the Exhaust Plume of an Aluminized Composite Propellant Rocket. AIAA Journal of Spacecraft and Rockets, vol. 1, 1964, p. 501.

464. Gulrajani, B. K.: Analysis of Radiant Heat Transfer from Exhaust Plume of a Solid Propellant Rocket. Boeing Document D2-30861-1, 1964.
465. Rochelle, W. C.: Heating to S-IC Ordnance Disconnect from S-II Ullage Motors and J-2 Engines. NASA/MSFC Memorandum R-AERO-AT-65-18, June 30, 1965.
466. Hunt, J. D.: Thermal Radiation from Solid Rocket Exhaust Plumes. Boeing Document D5-12260, 1966.
467. Crowe, C. T.; and Willoughby, P. G.: A Study of Particle Growth in a Rocket Nozzle. AIAA Paper No. 66-639 presented at AIAA Second Propulsion Joint Specialist Conference, June 13-17, 1966.
468. Crowe, C. T.; et al.: Investigation of Particle Growth and Ballistic Effects on Solid Propellant Rockets. United Technology Center UTC 2128-FR, June 1966.
469. Fein, H. L.: A Theoretical Model for Predicting Aluminum Oxide Particle Size Distributions in Rocket Exhausts. AIAA Paper No. 65-10 presented at AIAA Second Aerospace Sciences Meeting, January 25-27, 1965.
470. Dobbins, R. A.: Measurement of Mean Particle Size in a Gas-Particle Flow. AIAA Journal, vol. 1, 1963, p. 1940.
471. Dobbins, R. A.: Measurement of Particle Size in a Gas-Particle Flow by an Optical Transmission Test. Allegany Ballistics Laboratory of Hercules Powder Company ABL/X-84 (ASTIA No. AD 289520), October 1962.
472. Dobbins, R. A.: Further Studies on the Light Scattering Techniques for Determination of Size Distributions in Burning Sprays. Vol. II: Wide Range Photographic Photometry. Air Force Office of Scientific Research AFOSR TN 60-353 (ASTIA No. AD235952), February 10, 1960.
473. Holland, A. C.; and Draper, J. S.: Analytical and Experimental Investigation of Light Scattering from Polydispersions of Mie Particles. Mithras, Inc., MS 65-195-R1, March 1961.

474. Adams, R. H. ; and Holland, A. C. : Wind Tunnel Investigation of the LID Phenomenon. Mithras, Inc. , MC-115-R4, December 1965 (Confidential) .
475. Peterson, A. H. ; et al. : High Energy Solid Propellant Combustion Efficiency Investigation. Air Force Rocket Propulsion Laboratory AFRPL-TR-66-42, April 11, 1966 (Confidential) .
476. Bartky, C. E. : Theoretical Estimates of Cloud Reflection and Transmission in the Infrared. Applied Optics, vol. 4, 1965, p. 847.
477. Carlson, D. J. ; et al. : Study of Thermal Radiation, Particle Impingement Heating and Flow Field Analysis of Solid Propellant Rocket Exhausts. Aeronutronic P-15245 (U) , August 26, 1965.
478. Morizumi, S. J. : Injection Rocket Thermal Analysis - Estimates of Particle Plume Radiation to Spacecraft by Surface Radiator Technique. Space Technology Laboratories (now TRW Systems) 62-9721.4-93, December 7, 1962.
479. Stuart, G. W. : Multiple Scattering of Neutrons. Nuclear Science and Engineering, vol. 2, 1957, p. 617.
480. Stuart, G. W. ; and Woodruff, R. W. : Method of Successive Generations. Nuclear Science and Engineering, vol. 3, 1958, p. 339.
481. Anthony, G. W. : The Average Escape Probabilities for Once and Many-Times Scattered Neutrons for a Slab. Hanford Atomic Products Operation HW-49188, March 22, 1957.
482. French, E. P. : Engineering Method to Predict Saturn V Vehicle and Launch Complex Environments Due to Rocket Jet Impingement. A. Africano, ed. , North American Aviation SID 65-816, July 29, 1965.
483. Byrd, R. J. : Altitude Base Heating and Ballistic Performance Tests of Subscale Second-Stage Minuteman Wing VI Motors. Arnold Engineering Development Center AEDC-TDR-63-265 (ASTIA No. AD 346281) , January 1964 (Confidential) .
484. Rossler, F. : Radiation of Flames with Strongly Scattering Particles. Optica Acta, vol. II, no. 21, 1964. (Translated from the German as Redstone Information Center RSIC-522, March 1966) .

485. Mecke, R.: *Annalen der Physik*, vol. 65, 1921, p. 257.
486. Romanova, L. M.: Radiation Field in Plane Layers of a Turbid Medium with Highly Anisotropic Scattering. *Optics and Spectroscopy*, vol. 14, 1963, p. 135.
487. Goldstein, J. S.: The Infrared Reflectivity of a Planetary Atmosphere. *Astrophysical Journal*, vol. 132, 1960, p. 473.
488. Chin, J. H.; and Churchill, S. W.: Anisotropic, Multiply Scattered Radiation from an Arbitrary, Cylindrical Source in an Infinite Slab. *ASME Journal of Heat Transfer*, May 1965, p. 167.
489. Bellman, R. E.; et al.: Analytical and Computational Techniques for Multiple Scattering in Inhomogeneous Finite Slabs. Rand RM-4438-PR (ASTIA No. AD 610555), January 1965.
490. Bellman, R. E.; et al.: Computational Solution of Radiative Transfer Problems in Cloud Physics. Rand P-3125 (ASTIA No. AD 615423), May 1965.
491. Evans, L. B.; Chu, C. M.; and Churchill, S. W.: The Effect of Anisotropic Scattering on Radiant Transport. *ASME Journal of Heat Transfer*, August 1965, p. 381.
492. Smart, C.; et al.: Experimental Study of Multiple Light Scattering. *Journal of the Optical Society of America*, vol. 55, 1965, p. 947.
493. Twersky, V.: Multiple Scattering of Waves and Optical Phenomena. *Journal of the Optical Society of America*, vol. 52, 1962, p. 145.
494. Twersky, V.: Multiple Scattering of Waves in Dense Distributions of Large Tenuous Scatterers. *Interdisciplinary Conference on Electromagnetic Scattering*. The Macmillan Company, New York, 1963.
495. Grosjean, C. C.: Recent Progress in the Development of a New Approximate General Theory of Multiple Scattering. *Interdisciplinary Conference on Electromagnetic Scattering*. The Macmillan Company, New York, 1963.

496. Chu, C. M.; et al.: A Variable-Order Diffusion Type Approximation for Multiple Scattering (Also Numerical Solutions for Multiple, Anisotropic Scattering). Interdisciplinary Conference on Electromagnetic Scattering. The Macmillan Company, New York, 1963.
497. Sekera, Z.: Multiple Scattering in Media with Anisotropic Scattering. Interdisciplinary Conference on Electromagnetic Scattering. The Macmillan Company, New York, 1963.
498. Mullikin, T. W.: Uniqueness Problems in the Mathematics of Multiple Scattering. Interdisciplinary Conference on Electromagnetic Scattering. The Macmillan Company, New York, 1963.
499. Bauer, E.: Theoretical Radiative Characteristics of Optically Thick Gas-Particle Clouds and Application to the Carbon-Alumina System. Aeronutronic S-2380, Appendix A, December 1963 (Secret).
500. deBary, E.; and Bullrich, K.: Effects of Higher-Order Scattering in a Molecular Atmosphere. Journal of the Optical Society of America, vol. 54, 1964, p. 1413.
501. Herman, B. M.; and Browning, S. R.: A Numerical Solution to the Equation of Radiative Transfer. Journal of the Atmospheric Sciences, vol. 22, 1965, p. 559.
502. Halpern, O.; Lueneburg, R.; and Clark, O.: On Multiple Scattering of Neutrons, vol. I: Theory of the Albedo of a Plane Boundary. Physical Review, vol. 53, 1938, p. 173.
503. Richards, P. I.: Multiple Isotropic Scattering. Physical Review, vol. 100, 1955, p. 517.
504. Høglund, R. F.: Recent Advances in Gas-Particle Nozzle Flows. ARS Journal, vol. 32, 1962, p. 662.
505. Carlson, D. J.; Lewis, C. H.; and Bartky, C. E.: Solid Propellant Rocket Exhaust Plume Study. Paper presented at TABSTONE Symposium, Washington, D. C., September 29-30, 1965.
506. Altman, D.; and Carter, J. M.: Expansion Processes. Combustion Processes. Princeton University Press, Princeton, New Jersey, 1956.

507. Gilbert, M. ; Davis, D. ; and Altman, D. : Velocity Lag of Particles in Linearly Accelerated Combustion Cases. Jet Propulsion, vol. 25, 1955, p. 26.
508. Kliegel, J. R. ; and Nickerson, G. R. : Flow of Gas-Particle Mixtures in Axially Symmetric Nozzles. ARS Paper 1713-61 presented at ARS Propellants, Combustion, and Liquid Rockets Conference, April 26-28, 1961.
509. Nickerson, G. R. ; and Kliegel, J. R. : The Calculation of Supersonic Gas-Particle Flows in Axisymmetric Nozzles by the Method of Characteristics. Space Technology Labs (now TRW Systems) STL-6120-8345-TU000, May 1962.
510. Crowe, C. T. ; et al. : Dynamics of Two-Phase Flow in Rocket Nozzles: Fourth Quarterly Technical Progress Report. United Technology Corporation UTC 2005 QT4, May 26, 1962.
511. Crowe, C. T. ; et al. : Dynamics of Two-Phase Flow in Rocket Nozzles: Fifth Quarterly Technical Progress Report. United Technology Corporation UTC 2005 QT5, August 1962.
512. Crowe, C. T. ; et al. : Dynamics of Two-Phase Flow in Rocket Nozzles: Final Report. United Technology Corporation UTC 2005 FR, August 31, 1964.
513. Bailey, W. S. ; et al. : Gas Particle Flow in an Axisymmetric Nozzle. ARS Journal, vol. 31, 1961, p. 793.
514. Hoffman, J. D. : An Analysis of the Effects of Gas-Particle Mixtures on the Performance of Rocket Nozzles. Jet Propulsion Center, Purdue University JPC 348, TM-63-1, January 1963.
515. Hoffman, J. D. : Analysis of the Flow of Gas-Particle Mixtures in Two-Dimensional and Axisymmetric Nozzles. Aerojet-General Report No. 0162-01TN-16, December 1, 1962.
516. Hoffman, J. D. ; and Lorenc, S. A. : A Study of Gas-Particle Flows in Conical Nozzles. AIAA Journal, vol. 3, 1965, p. 103.

517. Rannie, W. D.: Perturbation Analysis of One-Dimensional Heterogeneous Flow in Rocket Nozzles. ARS Progress in Astronautics and Rocketry: Detonation and Two-Phase Flow. Vol. 6. Academic Press, New York, 1962.
518. Simons, E. D.: Two-Phase Method of Characteristics Computer Program. Boeing Document AS 1671, 1966.
519. Hassan, H. A.: Exact Solutions of Gas-Particle Nozzle Flows. AIAA Journal, vol. 2, 1964, p. 395.
520. Glauz, R. D.: Combined Subsonic-Supersonic Gas-Particle Flow. ARS Paper 1717-61 presented at ARS Propellants, Combustion, and Liquid Rockets Conference, April 26-28, 1961.
521. Morgenthaler, J. H.: Analysis of Two-Phase Flow in Supersonic Exhausts. ARS Paper 1715-61 presented at ARS Propellants, Combustion, and Liquid Rockets Conference, April 26-28, 1961.
522. Travis, L. P.: Heat Transfer and Particle Trajectories in Solid Rocket Nozzles. Aerojet-General Report No. 0162-01 TN-17, October 19, 1962.
523. Rudinger, C.: Dynamics of Gas-Particle Mixtures with Finite Particle Volume. AIAA Paper 65-9 presented at AIAA Second Aerospace Sciences Meeting, January 25-27, 1965.
524. Marble, F. E.: Dynamics of a Gas Containing Small Solid Particles. Fifth AGARD Combustion Colloquium. Pergamon Press, New York, 1962.
525. Torobin, L. B.; and Gauvin, W. H.: Fundamental Aspects of Solids - Gas Flow. Canadian Journal of Chemical Engineering. Part I, August 1959; Part II, October 1959; Part III, December 1959; Part IV, October 1960; Part V, December 1960.
526. Lype, E. F.: One-Dimensional Analysis of Non-Isentropic Two-Phase Flow. ARS Paper 1605-61 presented at ARS Solid Propellant Rocket Conference, February 1-3, 1961.
527. Soo, S. L.: Gas-Solid Flow. Project SQUID, Technical Report ILL-13-P, May 1964.

528. Soo, S. L.: Dynamics of Multi-Phase Flow Systems. Project SQUID Technical Report ILL-18-P, September 1964.
529. Price, F. C.: Internal Environment of Solid Rocket Nozzles. Aeronutronic U-2709, July 30, 1964.
530. Carlson, D. J.: Experimental Determination of Velocity Lag in Gas-Particle Nozzle Flows. AIAA Journal, vol. 3, 1965, p. 354.
531. Carlson, D. J.: Experimental Determination of Thermal Lag in Gas-Particle Nozzle Flow. ARS Journal, vol. 32, 1962, p. 1107.
532. Carlson, D. J.; and Hoglund, R. F.: Particle Drag and Heat Transfer in Rocket Nozzles. AIAA Journal, vol. 2, 1964, p. 1980.
533. Svehla, R. A.: Thermodynamic and Transport Properties for the Hydrogen-Oxygen System. NASA SP-3011, 1964.
534. Zeleznik, F. J.; and Gordon, S.: A General IBM 704 or 7090 Computer Program for Computation of Chemical Equilibrium Composition, Rocket Performance, and Chapman-Jouget Detonations. NASA TN D-1454, 1962.
535. Gordon, S.; Zeleznik, F. J.; and Huff, V. N.: A General Method for Automatic Computation of Equilibrium Compositions and Theoretical Rocket Performance of Propellants. NASA TN D-132, 1959.
536. Liepman, H. P.: Minuteman Base Heating Studies and Preflight Test Results. Ballistic Systems Division BSD-TN-61-9, July 1961 (Confidential).
537. Irvine, T. M.: Minuteman Thermal Environment During Launch as Measured in 1/20-Scale Tests. Boeing Document D2-4567, December 1960 (Confidential).
538. Barnes, R. H.; and Homer, W. R.: Summary Report of Results of Minuteman Model Tests to Investigate In-Flight Base Heating. Boeing Document D2-9719, August 1961 (Confidential).
539. Brunner, D. W.: Launch Thermal Environment, Summary - AMR Flight Test Program, WS-133A (Minuteman). Boeing Document D2-14744, June 1963 (Confidential).

540. Woodward, J. E.: Final Report: Minuteman Full Scale Combined Staging and Skirt Removal Test No. 8 (EWA 3637). Boeing Document D2-13335, October 1962 (Confidential).
541. Barnes, R. H.: Design Heating Data, Minuteman - In-Flight Base Heating. Boeing Document D2-3976-3, December 1960 (Confidential).
542. Suddarth, J. L.; and Kurtovich, D. D.: Minuteman Launch Radiation Heating. Boeing Document D2-5936, February 1961 (Confidential).
543. Anon.: M-55A1 (Minuteman First Stage) Rocket Motor Performance and Engineering Data. Thiokol TW-589-10-64, September 1964 (Confidential).
544. La Rock, R. G.: Final Report: Minuteman Full Scale Combined Staging and Skirt Removal Tests Nos. 6 and 7 - Interstage 1-2. Boeing Document D2-9751, October 1962 (Confidential).
545. Anon.: Flight Test Report, Minuteman Missile FTM 405. Boeing Document D2-4452-405, January 1962 (Confidential).
546. Anon.: Flight Test Report, Minuteman Missile FTM 427. Boeing Document D2-4452-427, July 1963 (Confidential).
547. Anon.: Flight Test Report, Minuteman Missile FTM 428. Boeing Document D2-4452-428, (ASTIA No. AD 338119), July 1963 (Confidential).
548. Anon.: Flight Test Report, Minuteman Missile FTM 429. Boeing Document D2-4452-429, (ASTIA No. AD 339313), August 1964 (Confidential).
549. Anon.: Flight Test Evaluation Report, Minuteman Missile 1141. Boeing Document D2-14294-1141 (ASTIA No. AD 352402), August 1964 (Secret).
550. Cimino, A. A.; and Byrd, R. J.: Simulated Altitude Test of the Second Stage Minuteman Motor. AEDC-TN-61-69, July 1961 (Confidential).
551. Collis, D. R.: Second-Stage Minuteman M56E1 Wing II Motor Data Book. Aerojet-General Report (AF 33(600) - 36610, ASTIA No. AD 331321), August 6, 1962 (Confidential).

552. Burleson, R. D.: Final Report: Flight Test Firing of Second-Stage Minuteman Motor 44 FTM-442. Aerojet-General Report 0162-01TR-44FTM-42, May 4, 1964 (Confidential).
553. Burleson, R. D.: Final Report: Flight-Test Firing of Second Stage Minuteman Motor 44 FTM-443. Aerojet-General Report 0162-01TR-44FTM-43, May 21, 1964 (Confidential).
554. Burleson, R. D.: Final Report: Flight-Test Firing of Second Stage Minuteman Motor 44 FTM-444. Aerojet-General Report 0162-01TR-44FTM-44, June 7, 1964 (Confidential).
555. Nygaard, R. C.; and Byrd, R. J.: Altitude Test of a Hercules Wing I Qualification XM-57 Third Stage Minuteman Motor (Motor Serial Number B1-4-11). AEDC-TDR-62-204, October 1962 (Confidential).
556. Turner, F. E.; and Nygaard, R. C.: Altitude Test of a Hercules XM-57 Third Stage Minuteman Motor (Continued Development Series). AEDC-TN-6-174, June 1961 (Confidential).
557. Turner, F. E.; Byrd, R. J.; and Nygaard, R. C.: Altitude Test of a Hercules XM-57 Third Stage Minuteman Motor (Flight Test Motor Spare 2). AEDC-TDR-62-70, April 1962 (Confidential).
558. Turner, F. E.; and Vetter, N. R.: Tests of Full-Scale Aerojet Third Stage Minuteman ICBM Development Motors in an Altitude Cell. AEDC-TN-60-165, September 1960 (Confidential).
559. Morris, J. A.; and Cannel, A. L.: Preliminary Flight Rating Test of Full-Scale Hercules Third Stage Minuteman ICBM Motors in an Altitude Test Cell. AEDC-TN-61-56, May 1961 (Confidential).
560. Turner, F. E.; and Nygaard, R. C.: Altitude Test of a Hercules XM-57 Third Stage Minuteman Motor (Continued Development Series). AEDC-TN-61-101, September 1961 (Confidential).
561. Bettencourt, H. S.; and Sutphin, D. L.: Polaris A3 Base Heating Thermodynamics Analysis Report. Lockheed Missiles and Space Company LMSC-803299, October 3, 1963 (Confidential).

562. Antonides, G. J.; Hines, F. L.; and Wong, R. C.: Thermodynamics Analysis Report on Polaris A3 Scale Model Base Environment Program (P8/P16). Lockheed Missiles and Space Company, LMSC-802106, December 2, 1962 (Confidential).
563. Anon.: A3 Polaris Preliminary Base Heating Thermodynamics Analysis Report. Lockheed Missiles and Space Company, LMSC-801935, September 21, 1962 (Confidential).
564. Austin, R. F.; and Milillo, J. R.: Polaris Missile Tests at Transonic Speeds in the AEDC 16-foot Transonic Circuit. Phase IV: Solid Propellant Tests of 0.20-Scale Model. AEDC-TN-59-135, November 1959 (Confidential).
565. Barton, D. L.; and Wilson, R. L.: Tests of an ABL 1/3-Scale Second Stage Polaris Rocket Motor at High Altitudes. AEDC-TN-60-151, August 1960 (Confidential).
566. Barkham, J. E.; et al.: Establishment of Thermal Characteristics in Base Area of Polaris Missile. Lockheed Missiles and Space Division LMSD-450955, April 11, 1959 (Confidential).
567. Weeks, R. M.: 624A (Titan IIIC). Phase III: Base Heating and Recirculation Wind Tunnel Test Post-Test Report. Space Systems Division, SSD-CR-64-15, April 1964 (Confidential).
568. Weeks, R. M.: 624A (Titan IIIC). Phases I and II: Base Heating and Recirculation Test Post-Test Report. Space Systems Division SSD-CR-63-217, December 1963 (Confidential).
569. Baker, D. C.: Base Heating and Base Pressure Investigation of a 5.5-Percent-Scale Titan III Booster with Solid-Propellant Booster Motors. AEDC-TDR-63-194, October 1963 (Confidential).
570. Gerke, P. D.: Base Heating and Base Pressure Investigation of a 5.5-Percent-Scale Titan III, Phase III. AEDC-TDR-63-259, January 1964 (Confidential).
571. Olson, D.: 642A (Titan IIIC). Phase IV: Base Heating and Recirculation Wind Tunnel Test, Post-Test Report. Space Systems Division SSD-CR-64-85, June 1964 (Confidential).

572. Harper, R. E.: Variation of Exhaust Plume Radiant Heat Flux with Altitude from 1/33-Scale Titan III Solid Propellant Rocket Motors. AEDC-TDR-63-101, June 1963 (Confidential).
573. Weeks, R. M.: 642A (Titan IIIC). Phase III: Base Heating and Recirculation Wind Tunnel Test Pretest Report. Space Systems Division SSD-CR-63-142, July 1963 (Confidential).
574. Harris, L.: Preparation and Infrared Properties of Aluminum Oxide Films. Journal of the Optical Society of America, vol. 45, 1955, p. 27.
575. Ohrenberger, J. T.: Analysis of Particle Radiation from a Rocket Exhaust Plume. Space Technology Laboratory (now TRW Systems) 62-9721-94, December 7, 1962.
576. Fontenot, J. E.: Preliminary Stage Heating Data for S-IC with Minuteman Strap-Ons. Boeing Coordination Sheet P/M-RC-23-64, September 24, 1964.
577. Hunt, J. D.: Convective and Radiant Heating Environment for Various Positions on the LUT Deck for the S-IC with Four Minuteman Strap-Ons. Boeing Coordination Sheet P/M-RC-33-64, October 19, 1964.
578. Anon.: Spacecraft Final Mission Report: First Launch Vela Satellite Program. Space Technology Laboratories (now TRW Systems) STL 2400-6124-RC-000, September 15, 1964 (Confidential).
579. Morizumi, S. J.: Analytical Determination of Shape Factors from a Surface Element to an Axisymmetric Surface. AIAA Journal, vol. 2, p. 1964, p. 2028.
580. Morizumi, S. J.: Analytical Method of Determining Shape Factor from a Surface Element to a Conical Surface. Space Technology Laboratories (now TRW Systems) 62-9721.4-78, October 31, 1962.
581. Hunt, J. D.: Minuteman Exhaust Plume Impingement Heating Study-Results Obtained from 7 Second Minuteman Static Firings. Boeing Document D5-12211, August 1966.
582. Brower, E. M.: Results of the Preliminary Thermodynamic Analysis of the Saturn IB/Minuteman Vehicle. Chrysler Corporation Space Division TB-AE-65-139, February 17, 1965.

583. Kuby, W. C.: Study of Thermal Radiation, Particle Impingement Heating, and Flow Field Analysis of Solid Propellant Rocket Exhausts. Aeronutronic Second Monthly Progress Report (NASA/MSFC Contract No. NAS8-20276), March 15, 1966.
584. Kuby, W. C.: Study of Thermal Radiation, Particle Impingement Heating, and Flow Field Analysis of Solid Propellant Rocket Exhausts. Aeronutronic Seventh Monthly Progress Report (NASA/MSFC Contract No. NAS8-20276), September 2, 1966.
585. Schuster, A.: Radiation Through a Foggy Atmosphere. The Astrophysical Journal, vol. 21, 1905, p. 1.
586. Hamaker, J. C.: Radiation and Heat Conduction in Light Scattering Material. Phillips Research Report No. 2, 1947.  
Vol. I - Reflection and Transmission, pp. 55-67.  
Vol. II - General Equations Including Heat Conduction, pp. 103-111.  
Vol. III - Application of the Theory, pp. 112-125.  
Vol. IV - Various Extensions and a Generalized Theory, pp. 420-425.
587. Churchill, S. W.; et al.: The Transmission of Thermal Radiation Through Real Atmospheres. The University of Michigan AFSWP 1035, April 1957.
588. Klein, J. D.: Radiation Heat Transfer Through Scattering and Absorbing Nonisothermal Layers. Paper No. 7 presented at NASA Symposium on Radiation from Solids, 1964.
589. Rochelle, W. C.: Modified S-IC Ordnance Disconnect Heating Analysis and S-II Ullage Motor Test Results. NASA/MSFC Memorandum (for File) AT-20-65, November 23, 1965.
590. Rochelle, W. C.: Experimental Determination of Heating Rates and Impingement Pressures from Centaur Retrorocket Exhausts. NASA/MSFC Memorandum R-AERO-AT-66-4, June 28, 1966.
591. Rochelle, W. C.: Preliminary Test Plan for Retrorocket Tests at Cornell Aeronautical Laboratory. NASA/MSFC Memorandum R-AERO-AT-65-29, October 18, 1965.

592. Hendershot, K. C.; and Dennis, R. J.: Research on Base Heating of Rocket Motor Vehicles Using Shock Tube Techniques. Cornell Aeronautical Laboratory Monthly Progress Report No. 17 (NASA/MSFC Contract No. NAS8-20027), June 30, 1966.
593. Hendershot, K. C.; and Dennis, R. J.: Research on Base Heating of Rocket Motor Vehicles Using Shock Tube Techniques. Cornell Aeronautical Laboratory Monthly Progress Report No. 19 (NASA/MSFC Contract No. NAS8-20027), August 31, 1966.
594. Hendershot, K. C.; and Dennis, R. J.: Research on Base Heating of Rocket Motor Vehicles Using Shock Tube Techniques. Cornell Aeronautical Laboratory Monthly Progress Report No. 20 (NASA/MSFC Contract No. NAS8-20027), September 30, 1966.
595. Datis, A.; and Fowler, J.: Heat Transfer and Ablation Rate Measurement in Saturn S-II Ullage Motor Exhaust Plume. Heat Technology Laboratory HTL-TR-31, July 22, 1966.
596. Edwards, R. H.; and Bobco, R. P.: Radiant Heat Transfer from Isothermal Dispersion with Isotropic Scattering. Hughes Aircraft SSD 50134R, Report No. 3, December 1965.
597. Bobco, R. P.: Directional Emissivities from a Two-Dimensional, Absorbing-Scattering Medium: The Semi-Infinite Slab. Hughes Aircraft SSD 60072R, Report No. 5, March 1961.
598. Bobco, R. P.; and Edwards, R. H.: Radiation from an Absorbing, Scattering Conical Dispersion with Non-Uniform Density. Hughes Aircraft SSD 60571R, Report No. 21, December 1966.
599. Laderman, Arnold; et al.: Study of Thermal Radiation, Particle Impingement Heating, and Flow Field Analysis of Solid Propellant Exhausts. Final Report. Aeronutronic U-4045, May 1967.
600. Simmons, F. S.; and Golden, S. A.: Experimental and Theoretical Determinations of the Spectral Emissivities of Hydrogen Fluoride in Rocket Exhaust Gases. Rocketdyne R-3017, 1961.
601. Golden, S. A.: Approximate Spectral Emissivities of HF and HCl Gas Mixtures. Rocketdyne Report R-3017, 1961.
602. Kuipers, G. A.; Smith, D. F.; and Nielson: Infrared Spectrum of Hydrogen Fluoride. Journal of Chemical Physics, vol. 25, 1956, p. 275.

603. Deeds, W. E.; et al.: Line Intensity and Pressure Broadening Studies in Hydrogen Fluoride and Other Problems in Infrared Spectroscopy. Air Force Cambridge Research Laboratories, AFCRL Report No. 465, University of Tennessee, 1961.
604. Benedict, W. S.; et al.: Infrared Emission of the Hydrogen-Fluoride Flame. Journal of the Optical Society of America, vol. 43, 1953, p. 1106.
605. Mann, D. E.; et al.: Spectroscopy of Fluorine Flames, Vol. I: Hydrogen-Fluorine Flame and the Vibration-Rotation Emission Spectrum of HF. Journal of Chemical Physics, vol. 34, 1961, p. 420.
606. Simmons, F. S.; Arnold, C. B.; and Lirette, E. F.: Infrared Spectroscopic Study of Hydrogen-Fluorine Flames. Vol. I: Experimental Data. Institute of Science and Technology, University of Michigan Report No. 4613-122-T, March 1966.
607. Simmons, F. S.: Infrared Spectroscopic Study of Hydrogen Fluorine Flames. Vol. II: Analytical Procedures. Institute of Science and Technology, University of Michigan Report No. 4613-123-T, March 1966.
608. Kuby, W. C.: Study of Thermal Radiation, Particle Impingement Heating, and Flow Field Analysis of Solid Propellant Rocket Exhausts. Aeronutronic Twelfth Monthly Progress Report (NASA/MSFC Contract No. NAS8-20276), January 27, 1967.
609. Lai, W.: Test Report, 1205-6 Jet Plume Measurements. United Technology Center ER-UTC-64-273, December 18, 1964.
610. McGee, R. S.: Interim Progress Report for Prediction and Measurement of Solid Propellant Motor Exhaust Plumes. Datacraft, Inc., Report No. 215, August 1966. (Also available as ISA Preprint No. 16, October 2, 1966.)
611. Johnson, D. G.; et al.: Rocket Exhaust Plume Profiles. Datacraft, Inc., Report No. 216, December 1966.

REVIEW OF THERMAL RADIATION FROM LIQUID  
AND SOLID PROPELLANT ROCKET EXHAUSTS

By William C. Rochelle \*

The information in this report has been reviewed for security classification. Review of any information concerning Department of Defense or Atomic Energy Commission programs has been made by the MSFC Security Classification Officer. This report, in its entirety, has been determined to be unclassified.

This document has also been reviewed and approved for technical accuracy.

\* Captain, U. S. Army



---

Homer B. Wilson, Jr.  
Chief, Thermal Environment Branch



---

Werner K. Dahm  
Chief, Aerophysics Division



---

E. D. Geissler  
Director, Aero-Astrodynamic Laboratory

DISTRIBUTION

INTERNAL

R-TEST-C

Mr. Charles Verschoore  
Mr. Don Patrick  
Mr. J. P. Jones

MS-IL (8)

MS-IP

MS-H

R-P&VE-PT

Mr. James Moses  
Mr. Joseph Cody  
Mr. William McAnelly  
Mr. George Hopson

I-RM-M

CC-P

MS-T (6)

R-P&VE-PP

Mr. David Farrell  
Mr. Richard Sanders  
Mr. Richard Eilerman

R-AERO

Dr. E. D. Geissler  
Mr. H. B. Wilson  
Dr. R. C. Farmer  
Mr. Milton Huffaker  
Mr. W. K. Dahm  
Mr. Oscar Holderer  
Mr. Robert Elkin  
Mr. Ira P. Jones  
Mr. Dennis Gardner  
Mr. Eugene Cooper  
Mr. Terry Greenwood  
Mr. Alan Forney  
Mr. Roger Heatherly  
Mr. Edwin Brewer  
Mrs. Essie Haywood  
Mr. Marcus Dash

R-AERO

Mr. William W. Vaughan  
Dr. J. R. Scoggins  
Mr. Glenn E. Daniels  
Mr. C. D. Baker  
Mr. W. K. Dahm  
Mr. Helmut J. Horn  
Mr. H. Thomae  
Dr. H. Krause  
Mr. J. Lindberg  
Mr. L. McNair

R-RP-P

Mr. John Williams

DISTRIBUTION (Cont'd)

EXTERNAL

The Boeing Company  
Huntsville Industrial Center  
Huntsville, Alabama  
ATTN: Mr. C. R. Mullen  
    Mr. Robert Bender  
    Miss Elayne Brower  
    Mr. Maurice Baker  
    Mr. Harold Mitchell

Lockheed Missiles and Space Company  
Huntsville Research and Engineering Center  
4800 Bradford Drive  
Huntsville, Alabama  
ATTN: Mr. James Gibson  
    Mr. Douglas Kooker  
    Mr. George Reny  
    Mr. Lee McGimsey  
    Dr. John Golden  
    Mr. Robert J. Prozan  
    Dr. Philomena Grodzka  
    Mr. Alan Ratliff  
    Mr. S. J. Robertson

Heat Technology Laboratory  
4308 Governors Drive, N. W.  
Huntsville, Alabama  
ATTN: Mr. D. L. Jones  
    Mr. Ludwig Holtermann  
    Mr. Rex Zerger  
    Mrs. Beverly Audeh

North American (S&ID)  
Downey, California  
ATTN: Mr. Alfred Africano  
    Mr. K. D. Korkan  
    Dr. Galen Etemad

DISTRIBUTION (Cont'd)

EXTERNAL (Cont'd)

Hayes International  
Birmingham, Alabama  
ATTN: Mr. John Reardon  
Mr. H. J. Laney

Cornell Aeronautical Laboratory  
Buffalo, New York  
ATTN: Mr. K. C. Hendershot  
Mr. R. J. Dennis  
Dr. James Llinas  
Dr. David McCaa

Rhom & Haas  
Redstone Arsenal, Alabama  
ATTN: Mr. Joseph Viles  
Dr. Woodward Waesche

AEDC  
Tullahoma, Tennessee  
ATTN: Mr. William Muse  
Mr. F. E. Turner  
Mr. James Neeley

Purdue University  
Lafayette, Indiana  
ATTN: Dr. Richard Hoglund  
Dr. Robert Goulard

Rocketdyne  
Canoga Park, California  
ATTN: Mr. A. G. DeBell

Rocketdyne  
McGregor, Texas  
ATTN: Mr. Clarence Sanders

DISTRIBUTION (Cont'd)

EXTERNAL (Cont'd)

Douglas Aircraft  
Huntington Beach, California  
ATTN: Mr. Paul Mock  
Mr. D. E. Walters

Ling-Temco-Vought  
Dallas, Texas  
ATTN: Mr. James Medford

General Dynamics  
Fort Worth, Texas  
ATTN: Mr. R. A. Stevens

TRW Systems  
Houston Operations  
Space Park Drive  
Houston, Texas 77058  
ATTN: Mr. R. G. Payne  
Captain W. C. Rochelle (25)

TRW Systems  
Redondo Beach, California  
ATTN: Mr. H. J. Carpenter  
Mr. S. J. Morizumi

Philco-Ford (Aeronutronic)  
Newport Beach, California  
ATTN: Mrs. Charlotte Bartky  
Mr. D. J. Carlson  
Dr. Stanley Byron  
Dr. Arnold Laderman

Chrysler Corporation Space Division  
New Orleans, Louisiana  
ATTN: Mr. John Tucker  
Mr. D. Thibbodeaux  
Mr. Ben Elam  
Mr. Gerry Davis

DISTRIBUTION (Cont'd)

EXTERNAL (Cont'd)

Manned Spacecraft Center  
National Aeronautics and Space Administration  
Houston, Texas  
ATTN: Mr. David Greenshields  
      Mr. K. C. Weston  
      Mr. Robert Reid

University of Texas  
(Aerospace Engineering Department)  
Austin, Texas  
ATTN: Dr. John Porter  
      Dr. John Burtin

AeroChem  
Princeton, New Jersey  
ATTN: Hal Pergament

University of Oklahoma  
Norman, Oklahoma  
ATTN: Dr. Tom J. Love

University of California  
Santa Barbara, California  
ATTN: Dr. William C. Kuby

Brown Engineering  
300 Sparkman Drive  
Huntsville, Alabama  
ATTN: Mrs. Beverly Lavender  
      Mr. Robert Yossa

Hughes Aircraft  
Culver City, California  
ATTN: Dr. R. P. Bobco

DISTRIBUTION (Concluded)

EXTERNAL (Cont'd)

University of Sheffield  
Sheffield, England, G. B.  
ATTN: Dr. P. J. Foster  
Dr. M. W. Thring

Scientific and Technical Information Facility (25)  
P. O. Box 33  
College Park, Maryland 20740  
ATTN: NASA Representative, A-AK/RKT

AFRPL  
1/Lt. Palmer W. Smith